Investigating the tectonic evolution of the NE Newfoundland-Porcupine Atlantic conjugate margins using new seismic reflection data and deformable plate modelling

by

© Pei Yang

A Thesis submitted to the School of Graduate Studies

in partial fulfillment of the requirements for the degree of Doctor of Philosophy.

Department of Earth Sciences

Memorial University of Newfoundland

September 2021

St. John's, Newfoundland and Labrador, Canada

Abstract

In recent years, there has been an improved understanding of the multi-episodic extensional processes that were active along the NE Newfoundland-Porcupine Atlantic conjugate margins during the Mesozoic. However, there are still unresolved key issues about this rift system, including unclear structural styles and crustal architecture due to lacking seismic data constraints, uncertainties about the effects of structural inheritance and rift segmentation on margin development, skepticism about the role of extension obliquity, and increased scrutiny about the conjugate relationship between the Flemish Cap and Goban Spur.

In this thesis, an integrated geophysical study, based on newly acquired seismic reflection data, seismic refraction data, borehole data, and potential field data along the rift system, is undertaken to define the crustal architecture. The faults, sedimentary layers, and basement features display distinct 3D characteristics and the crustal architecture is highly variable along the margin. Along-strike variability is associated with changes in extension rates, rift obliquity, and the effect of reactivation of inherited Caledonian and Variscan basement fabrics, indicative of segmentation of the rift system.

In conjunction with constraints from newly acquired seismic data, this study improves upon published deformable plate models in GPlates by introducing segmentation of the Porcupine Bank and transfer faults on the continental crust of the Goban Spur, generating a better fit compared with previous plate reconstruction models. The updated deformable plate model allows us to visualize the crustal thickness evolution through time and further quantify the amount, orientation, and timing of extension events between the NE Newfoundland, Iberia, and

Irish Atlantic margins. This model shows that the NE Newfoundland-Porcupine Atlantic margin pair is highly segmented and obliquely hyperextended. The model also demonstrates the significant role played by continental ribbons/microplates in controlling crustal thickness within the deformable region. The thesis results reshape our understanding of the complex kinematic evolution of the NE Newfoundland-Porcupine Atlantic rift system and of rift compartmentalization across the southern North Atlantic. The conjugate relationships between the Goban Spur, Porcupine Bank, and Flemish Cap are also renewed, which is beneficial to derisk petroleum exploration in the underexplored conjugate margin basins. Finally, these results can potentially offer insights into the evolution of other rifted margins (e.g., the Red Sea) on the Earth.

General Summary

Studies of the NE Newfoundland-Porcupine Atlantic margins have been plentiful. However, the rift-related domains along these margins have remained poorly defined partially due to limited data coverage. Currently, the well-accepted conjugate relationships of these magma-poor margins are increasingly questioned. Furthermore, extension obliquity and segmentation usually fail to be considered during the rifting between the Flemish Cap and the Porcupine Atlantic margin.

In this thesis, more significant structural features are observed from newly acquired seismic reflection data than from vintage data. These structural features are used to map the crustal architecture in terms of rifted margin domains. Observations from seismic reflection data show that the reactivation of pre-existing structural fabrics has influenced the distributions of the crustal domains along the Porcupine Atlantic margin. Building on the framework of the published plate models, a deformable plate model is updated in GPlates software based on seismic reflection data interpretation, and the results of refraction modelling, gravity inversion, and magnetic mapping. In the preferred updated deformable plate model, the Porcupine Bank is subdivided into four blocks and the continental crust of the Goban Spur is displaced by transfer faults. Finally, crustal thicknesses calculated from the preferred updated deformable plate tectonic model are used to see how the Newfoundland, Irish, and Iberia margins evolved over time and to reveal their conjugate relationships. Both the seismic data and updated deformable plate model imply segmentation of the Porcupine Atlantic margin, which is strongly affected by inherited structures. Crustal thickness evolution reveals the time-dependent variations in

extension rate and obliquity between these three margins, leading to an enhanced understanding of the opening of the North Atlantic from a 3D perspective.

Co-Authorship Statement

The research topics in the thesis were initiated by my supervisor, Kim Welford, and then designed by Kim Welford and Pei Yang. Pei Yang identified specific scientific problems with the guidance and inspiration of Kim Welford. Related methodology and software, data analysis, and original manuscript preparation for each chapter listed below were conducted by Pei Yang.

Chapter 2 is published in *Tectonophysics* (doi.org/10.1016/j.tecto.2020.228364.) and co-authored with Kim Welford, Alex Peace, and Richard Hobbs. Kim Welford provided research supervision, assisted in conceptualization, reviewed and edited the manuscript. Alex Peace and Richard Hobbs helped to shape the ideas and edit the manuscript. Tim Minshull and the other anonymous reviewer gave valuable comments. In addition, this work was presented by Pei Yang at the the Geological Association of Canada (GAC) Newfoundland and Labrador Section Annual Meeting (2019) and European Geosciences Union (EGU) 2020 online.

Chapter 3 is published in *Tectonophysics* (doi.org/10.1016/j.tecto.2021.228809.) and co-authored with Kim Welford. Kim Welford helped to supervise the research, shape the ideas, and provide editorial guidance. Michael Nirrengarten and the other anonymous reviewer provided constructive comments. In addition, this work was presented by Pei Yang at the Geological Society of America (GSA) 2020 online.

Chapter 4 is under revision in *Tectonics* and co-authored with Kim Welford and Michael King. Kim Welford supervised the research and helped to edit the manuscript. Michael King assisted in shaping ideas and editing the manuscript. This work was presented by Pei Yang at European Geosciences Union (EGU) 2021 online.

Chapter 5 was submitted to the journal of *Marine and Petroleum* Geology in July, 2021, co-authored with Kim Welford. Kim Welford helped to edit the original draft and shape the ideas.

Acknowledgments

There are many people to whom I would love to say thanks throughout the years in my Ph.D. study. My deep gratitude goes first to my supervisor Dr. J. Kim Welford. I could not have gotten through graduate education without her expertly tireless guidance, encouragement, and patience. She always efficiently provided constructive advice and valuable assistance (e.g. lending me English novels, encouraging me to attend conversation club, recommending talk shows to improve my English, and so on) when I asked some questions or asked for her help. There are so many that I cannot list all of them here. Besides, she is also a mentor life coach, always inspiring me whenever I am not confident myself and emotionally down. The precious moments we had laughter and shared comforting words and uncertainties during the pandemic will permanently live in my head. I am sure that I will forever benefit from what I have learned from her personal and scientific spirits.

I am also grateful to two other supervisory committee members, Dr. Alison Malcolm and Dr. Luke Beranek, for their advice and kindness. I would also like to extend my gratitude to some other people, who were and are group members of MAGRIT, Alex Peace, Larry Sandoval, Michael King, Michael Dunham, Brant Gaetz, Miguel Shano who provided valuable help in this research through group meetings or private discussions. A huge thanks to Peter Bruce, who helped me a lot regarding geophysical and mapping software. I also want to express my thanks to fellow researchers in the Earth Science Department and friends at MUN for your kindness, support, and friendship that give me abundant warmth.

Special thanks to the Department of Environment, Climate and Communications of Ireland for providing the newly acquired seismic reflection data. I am also grateful to Chevron Canada for generously giving me the Chevron Canada Limited Rising Star Award.

Last but not the least, I am indebted to my Mom Jinping Feng, whose love and constant prayers for me give me strength and persistence to finish the journey. I also acknowledge my sister and brother for their care and love.

Contents

List of Tables

List of Figures

Preamble

This thesis is written in a manuscript format, in which the main body consists of peer-reviewed journal papers. Chapter 1 is the introduction. Chapters 2 and 3 have both been published in *Tectonophysics* and Chapter 4 is under review with *Tectonics*, after one round of revision. Chapter 5 was submitted to *Marine and Petroleum Geology* in July, 2021. Chapter 6 links and discusses the results of Chapters 2-5, while also providing the conclusions and suggestions for future work. To provide background context for the four manuscripts, Chapter 1 provides an overview of the tectonic evolution and structural domains of the southern North Atlantic rifted margins and related sedimentary basins. The pre-breakup plate configurations of the southern North Atlantic, restored using plate reconstructions, are introduced to show the role of inherited structures on the formation of the southern North Atlantic margins. The history of plate reconstructions of the North Atlantic region is also described. Finally, the key scientific problems and research objectives are outlined in this chapter.

Chapter 1

1. Introduction

1.1 Background of the southern North Atlantic (NA)

Continental rifting, extension, subsequent breakup, and the eventual creation of new oceanic centers constitute divergent plate tectonics (Merle, 2011). After continental breakup, passive margins subside below sea level in the inactive rift zone (Ebinger, 2005). These processes forming the passive margins represent one stage of the Wilson cycle, in which tectonic plates recurrently diverge and collide during the disintegration and assembly of supercontinents (Wilson, 1966). The passive margin is often classified into two end-member modes according to the time and magnitude of magmatism: magma-rich (volcanic) and magma-poor (non-volcanic) (Franke, 2013; Doré and Lundin, 2015), despite the fact that most rifted margins show transitional features between the end member examples. There are several distinct features of magma-dominated margins: (1) seaward-dipping reflectors (SDRs), which can be observed on seismic data and are composed of thick lava flows and sedimentary layers; (2) high-velocity lower crust restricted to a narrow area, which probably stems from magmatic underplating (White et al., 1987; Geoffroy et al., 2015); (3) a small amount of subsidence during and after lithosphere rupture due to large volumes of magmatic accretion and incorporation into the crust (White and McKenzie, 1989). Likewise, magma-poor passive margins exhibit common characteristics: (1) little or no presence of igneous rocks produced during rifting; (2) exhumation and serpentinization of mantle within the continent-ocean transitional zone (COT); (3) extreme thinning of the crust; (4) slow extension velocity; (5) a wide necking zone, and (6) no Moho in the exhumed mantle zone (Doré and Lundin, 2015).

The North Atlantic region is regarded as an excellent natural laboratory to understand the dynamic tectonic processes from initial rifting to continental breakup and seafloor spreading (Nirrengarten et al., 2018) (Fig. 1.1a). Some passive margins along the North Atlantic are considered magma-poor (e.g., Newfoundland-Iberia and Newfoundland-Irish conjugate margins) (Funck et al., 2003; Hopper et al., 2006; Sibuet et al., 2007; Gerlings et al., 2012), and some others are considered to be magma-rich (e.g., the Rockall-Hatton Bank and Norway–Greenland margin pair) (Franke, 2013; Geoffroy et al., 2015; Stoker et al., 2017). Hydrocarbon potential in the Atlantic rifted margin basins is always one primary driver to understand related tectonic processes.

1.1.1 Tectonic evolution of the southern North Atlantic margins

The relative motions of the Iberia, North America, Eurasian, and Greenland plates during the Late Paleozoic to Mesozoic contributed to the complex tectonic and structural development of the North Atlantic Ocean (Whittaker et al., 2012), forming a series of hyperextended rifted margins, from “failed” rift systems (e.g., Porcupine Basin, Orphan Basin, Rockall Basin) to “successful” rift-to-drift rifted margins (e.g., Newfoundland, Iberian, and Irish Atlantic margins) (Fig. 1.1a). Here, the Irish Atlantic margins extend from the Goban Spur, across the Porcupine Basin and Porcupine Bank region, to the Rockall and Hatton Bank from south to north.

Rifted continental margins along the southern North Atlantic extending from the Newfoundland Azores-Gibraltar Fault Zone to the Charlie-Gibbs Fracture Zone (Fig. 1.1a), with magma-poor continent-ocean-transition (COT) zones, have been extensively studied based on seismic reflection and refraction data, potential field data, and borehole data, specifically focused on the Newfoundland-Iberia conjugate margins (Funck et al., 2003; Hopper et al., 2006; Van Avendonk et al., 2006; Shillington et al., 2006; Reston, 2007; Sibuet et al., 2007; Welford et al., 2010a; Péron-Pinvidic et al., 2013; Sauter et al., 2018), and the Newfoundland-Irish Atlantic conjugate pair (Keen et al., 1989; Bullock and Minshull, 2005; Naylor and Shannon, 2009; Welford et al., 2010b, 20010c, 2012; Gerlings et al., 2012). Initial rifting along the southern North Atlantic occurred during the Triassic period, creating many sedimentary basins overlying the Irish Atlantic margin (e.g., Porcupine Basin) (Naylor and Shannon, 2009; Štolfová and Shannon, 2009), the Galicia Bank margin (Murillas et al., 1990), and the East Orphan Basin (Enachescu et al., 2004). Later, the major rifting progressed northward during the Late Jurassic to Early Cretaceous periods, resulting in the separation of the Newfoundland Basin from the Iberia Abyssal Plain and the SE Flemish Cap from the Galicia Bank (Tucholke et al., 1989), and the opening of the Orphan Basin (Enachescu et al., 2004). Northeast to southwest extension began in the Late Cretaceous period (de Graciansky et al., 1985; Hopper et al., 2006), leading to the separation of the NE Flemish Cap from the Goban Spur and the Orphan Basin from the Porcupine Bank (Welford et al., 2012). Finally, episodic post-rift movements in the Cenozoic have contributed to the distinctive topography of these passive margins (Praeg et al., 2005).

Pre-existing inheritance imparts first-order control on episodic extensional processes, rift segmentation, structural features, and early deposition of margin basins (Manatschal et al., 2015; Schiffer et al., 2020). Although thermal and compositional inheritance can significantly influence the architecture and evolution of rifted margins (Manatschal et al, 2015), the role of pre-existing structural fabrics has been most extensively studied in the North Atlantic (Štolfová and Shannon, 2009; Schiffer et al., 2020). Structural inheritance localizes shearing and results in complex, multi-scale stress distributions in the crust and lithosphere (Petersen and Schiffer, 2016). In the southern North Atlantic, the crustal-scale pre-existing orogenic structures (Caledonian and Variscan deformation fronts) are oblique to the orientation of the rift axis (Fig. 1.2). The Caledonides were formed due to the collision of Laurentia, Baltica, and Avalonia during the Mid Silurian to the Early Devonian, leading to the closure of the Iapetus Ocean (Gee et al., 2008). Caledonian tectonic elements consist of a series of crustal basement terranes bounded by fault zones, in which the Iapetus Suture follows the NE-SW oriented Caledonides fold belt onshore Ireland, likely representing a compositional change in the crust (Norton, 2002). The Avalonia terrane is a peri-Gondwanan terrane that formed during the opening of the Rheic Ocean in the Ordovician and that eventually docked against Laurentia and Baltica by the Devonian (Murphy et al., 2011). The Variscan Orogeny involved a major collision between peri-Gondwanan and Gondwanan terranes and other microcontinents during the Late Paleozoic (Matte, 2001).

Several mechanisms have been proposed to explain the evolutionary mechanism of rifted margins, such as pure shear (McKenzie, 1978), simple shear (Wernicke, 1985), and composite deformation (Lister et al., 1986). The pure shear model proposes that crustal and lithospheric thinning are symmetric, and are accompanied by faulting in the brittle upper crust. The simple shear model supports the presence of a lithosphere-scale low-angle detachment fault that penetrates into the upper mantle, leading to an asymmetric extension of the lithosphere. The composite deformation model combines the two models above. However, they fail to explain some key aspects of margin evolution because the dynamic processes of rifted margins are extremely complicated. Consequently, in recent years, advanced conceptual models have been developed to better understand the evolutionary history of rifted margins. These models involve depth-dependent stretching (Huismans and Beaumont, 2011), oceanward sequential faulting (Brune et al., 2014), and detachment faulting (Pérez-Gussinyé and Reston, 2001). The complex tectonic evolution of hyperextended rifted margins is governed by many factors, including the mechanical, thermal and rheological properties of the lithosphere, the pre-existing inheritance, extension obliquity and velocity, and sedimentation (Praeg et al., 2005; Huismans and Beaumont, 2007; Manatschal et al., 2015; Brune et al., 2017). Numerical models in 2-D have increasingly been used to evaluate key influencing factors, such as pre-existing inheritance in both the crust and the mantle (Chenin and Beaumont, 2013), the extension rate and crustal rheology (Tetreault and Buiter, 2018), and the influence of sedimentation (Pérez-Gussinyé et al., 2020). Furthermore, advanced 3D models have also been proposed to understand oblique extension and interaction of rift segments within a rift system (Zwaan et al., 2016; Jourdan et al., 2020; Neuharth et al., 2021).

1.1.1.1 The Flemish Cap

The Flemish Cap, as a microplate of the North American plate, lies at the eastern edge of the Newfoundland and Labrador margin, to the southeast of the Orphan Basin, and separated from the Grand Banks by the Flemish Pass Basin (Fig. 1.1) (Hopper et al., 2006). King et al. (1985) summarized that the area was a part of the Avalon zone of the Appalachian orogenic belt. Sibuet et al. (2007) proposed that the Flemish Cap experienced a rotation of 43° relative to the Galicia Bank during the Late Jurassic-Early Aptian period, accompanied by an ~200 km SE displacement from its original location, mainly based on gravity data. By combining seismic data and previous gravity anomaly analysis, Enachescu et al. (2005) suggested that the motion of the Flemish Cap began slowly during the Late Jurassic - Early Cretaceous time when the Cap had a linkage with the East Orphan and Porcupine basins, and that the motion accelerated in the late stage of the Early Cretaceous period. Welford et al. (2010b) favored the rotation and displacement of the Flemish Cap with respect to the Orphan Basin based on both extensional and strike-slip deformation along the NE Flemish Cap margin based on seismic reflection data. Most recently, 3-D geodynamic modelling of the lithosphere has successfully reproduced the rotation of the Flemish Cap by simulating the interaction of two propagating rifts (Neuharth et al., 2021).

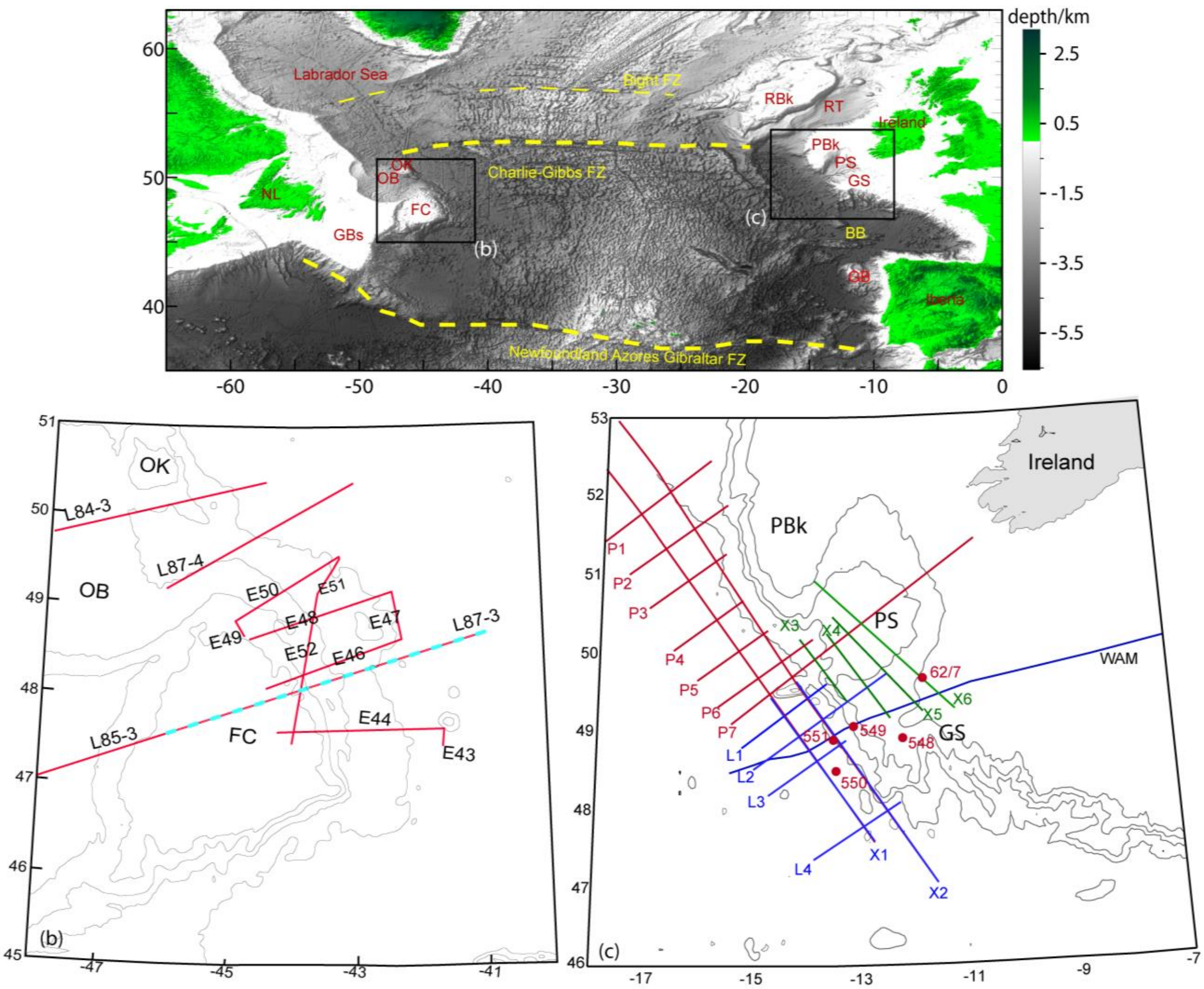

Figure 1.1: (a) Bathymetric map of the southern North Atlantic. (b) Seismic lines overlying the bathymetric contours on the Flemish Cap. The dashed blue line indicates the seismic refraction line (Gerlings et al., 2011). The red seismic reflection lines were interpreted by Welford et al. (2010b) and Gerlings (2013). (c) Newly acquired seismic reflection lines overlying the bathymetric contours on the Porcupine Atlantic margin, plus the Western Approaches Margin (WAM) line (Peddy et al., 1989). The red solid circles in panel c represent the drilling sites. The blue, red, green lines are interpreted in chapters 2, 3, and 5 in detail, respectively. Abbreviations: BB, Bay of Biscay; GB, Galicia Bank; GS, Goban Spur; PS, Porcupine Seabight; PBk, Porcupine Bank; RBk, Rockall Bank; RT, Rockall Trough; FC, Flemish Cap; OK, Orphan Knoll; OB, Orphan Basin; GBs, Grand Banks; FZ, Fracture zone.

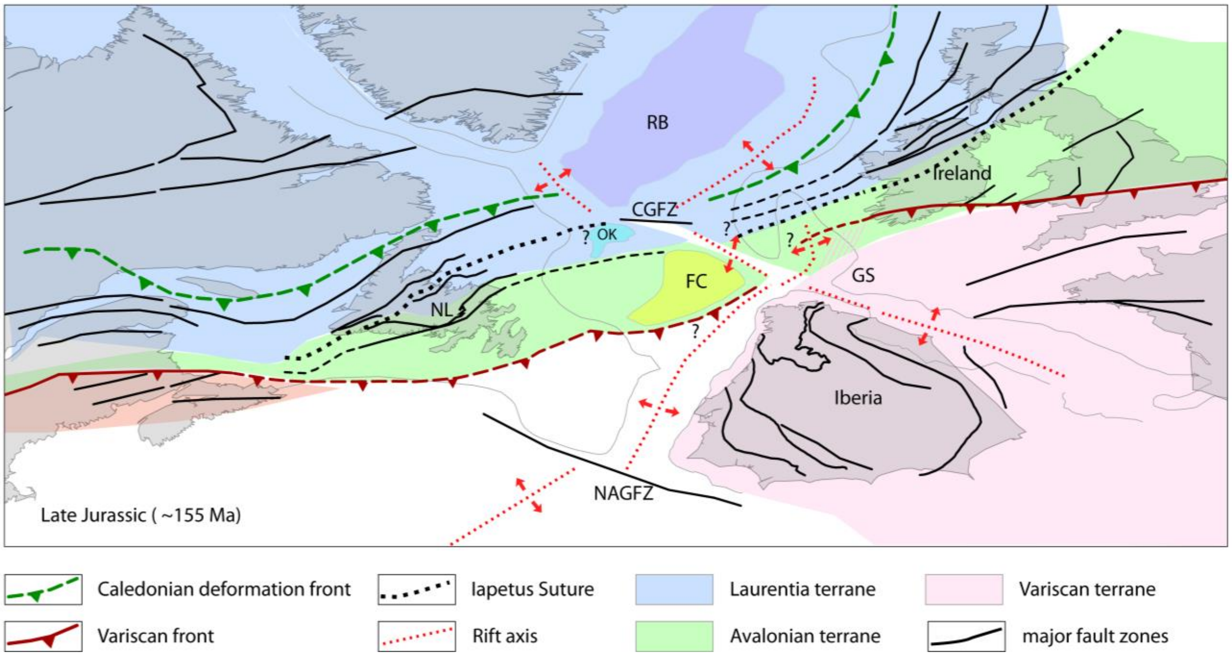

Figure 1.2: Terranes and structure map of the pre-breakup North Atlantic during the Late Jurassic (~ 155 Ma) (compiled from the following work: Chenin et al., 2015; Nirrengarten et al., 2018; Peace et al., 2019; Waldron et al., 2019; Schiffer et al., 2020). Abbreviations: GS, Goban Spur; RB, Rockall Bank; FC, Flemish Cap; OK, Orphan Knoll; CGFZ, Charlie-Gibbs Fracture zone; NAGFZ, Newfoundland Azores Gibraltar Fault Zone.

Gerlings et al. (2011) obtained a P-wave velocity model based on a seismic refraction profile along the NE Flemish Cap (dashed blue line in Fig. 1.1b), suggesting that partially serpentinized mantle underlies the thin continental crust in the transitional zone with velocities ranging from 7.5 km s^{-1} to 7.9 km s^{-1}. In addition, both Welford et al. (2010b) and Gerlings (2013) mapped the crustal architecture of the NE Flemish Cap, mainly based on seismic reflection data in Figure 1.1b. Based on older seismic reflection data analysis, Keen et al. (1989) favored pure shear rifting and an asymmetric lithospheric rupture, accompanied by a narrow necking zone across the NE Flemish Cap-Goban Spur conjugate margins. Gerlings et al. (2012) argued for asymmetric deformation occurring during each stage of the tectonic evolution of the NE Flemish Cap-Goban Spur conjugate margins by combining the seismic refraction and reflection data.

Similar to the Flemish Cap, the Orphan Basin is also underlain by the Avalon terrane (Fig. 1.1). Enachescu (2006) divided the Orphan Basin into two sub-basins: the East Orphan Basin (EOB), related to NE-SW extension of the Tethys rift system during the Late Triassic-Early Jurassic; and the West Orphan Basin (WOB), associated with the North Atlantic opening during the Late Jurassic-Early Cretaceous and the Labrador Sea rifting during the Aptian-Albian. Sibuet et al. (2007) suggested that the West and East Orphan basins had a linkage with the Rockall Basin and the Porcupine Bank, respectively. Lau et al. (2015) found that the crustal thickness was highly variable (4-32 km) across the Orphan Basin from seismic refraction modelling and there was no proof of partially serpentinized mantle in the East Orphan Basin. Also based on seismic refraction modelling, Welford et al. (2020) favored that the Orphan Basin experienced hyperextension and that the crust in the COT zone between the Orphan Knoll and undisputed oceanic crust is either thinned continental crust underlain by serpentinized mantle or embryonic oceanic crust.

1.1.1.2 The Porcupine Atlantic margin

The offshore Porcupine Atlantic margin (Fig. 1.1), extending from the Goban Spur to the Porcupine Bank, includes Late Paleozoic to Mesozoic basins which have been the focus of frontier exploration due to significant hydrocarbon potential in recent years (Shannon, 2018). According to the structural nomenclature of the Irish Petroleum Affairs Division (Naylor et al., 2002), the geological features such as the Porcupine Basin and Porcupine High, offshore Ireland correspond to the bathymetric features known as the Porcupine Seabight and Porcupine Bank. Compared with the Porcupine High and Goban Spur, the Porcupine Basin, a failed rift, is well-studied with denser seismic data coverage. The geologic and geophysical backgrounds for the Porcupine Atlantic margin will be introduced in detail in chapters 2, 3, 4, and 5. Based on the interpretation of newly acquired seismic reflection datasets in this region, the Porcupine Basin is proposed to be highly segmented, associated with the offshore continuation of Caledonian structural lineaments and the Variscan deformation front (Norton, 2002; Whiting et al., 2021). Grow et al. (2019) proposed a shearing and stretching model for the Porcupine Basin based on integrated geophysical analysis, in which the Porcupine Bank also experienced shearing along inherited Caledonian fault zones.

1.1.2 Structural domains of the southern North Atlantic margin basins

Although the crustal architectures of rifted margins vary from one to another, and from one segment to another in the same rifted margin system, they still share some first-order structural components (Osmundsen and Ebbing, 2008; Minshull, 2009; Sutra et al., 2013; Tugend et al., 2015). Péron-Pinvidic et al. (2013) proposed that proximal, necking, hyperextended, exhumed, and outer domains developed along the rifted margins. Each domain displays differences in basin types, faulted features, and crustal thickness. Likewise, lithospheric extension across the North Atlantic (NA) rifted margins has been mapped and characterised by observing various geological and geophysical datasets, particularly along the Newfoundland-Iberia conjugate margins. The NA rifted margins can be divided into distinct structural domains (Fig. 1.3), representative of oceanward migration of progressive extensional deformation in both time and space, following the collapse of inherited Caledonian-Variscan structural fabrics (Sharp et al., 2017).

The proximal domain

The lithosphere undergoes limited stretching in the proximal domain, in which the fault-bounded graben or half-graben basins are formed in the brittle upper crust (McKenzie, 1978).

Faults sole out within the mid-crust without affecting the Moho. Typically, the top basement is sub-parallel to the top mantle at the regional scale.

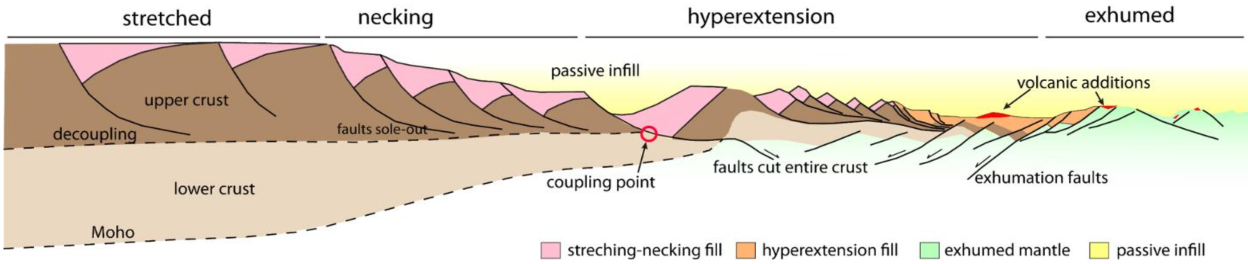

Figure 1.3: Schematic diagram of structural domains within the North Atlantic continental margins, based on observations from a number of marginal basins bordering the North Atlantic (adapted from Sharp et al., 2017).

The necking domain

Within the necking domain, the deformation can extend to the lower crust and the upper mantle, causing a drastic decrease in crustal thickness. Correspondingly, the top basement and the top mantle converge toward each other. The seaward edge of the necking domain indicates the region of coupling between the crust and mantle, where the entire crust becomes brittle and the decoupled deformation transitions into coupled deformation (Reston, 2007). Likewise, faults in the necking domain also sole out at mid-crustal and base-crustal levels.

The hyperextended domain

The continental crust progressively becomes more extended, with rapid accommodation space creation and passive infill. During the hyperextension stage, large-scale detachment faults cut the entire crust and penetrate the mantle, allowing the shallowing of deep crustal or mantle material (Dean et al., 2000; Russell and Whitmarsh, 2003). As the hyperextension continues, multi-phase faults may offset early rift faults that have rotated to very low angles, likely accompanied by rotation of existing fault blocks (McDermott and Reston, 2015).

The exhumed mantle domain

As the progressive seaward migration of deformation continues, low-angle exhumation faults entirely remove the crust. Mantle serpentinisation occurs due to water percolation through the crust to the upper mantle along low-angle normal faults and detachment faults, accompanied by an increasing amount of magma towards the seaward end of this domain. Both sediments and magmatic flows may obscure the top of basement, resulting in the uncertain nature of the reflectivity at the basement (Tugend et al., 2020). Within the exhumed domain, peridotite ridges may be formed due to the uplift of the footwall (Sharp et al., 2017). The seismic expression of this extensional stage has been well observed along the Newfoundland margin (Péron-Pinvidic et al., 2013), Iberian margin (Beslier et al., 1993; Dean et al., 2000), and Australian-Antarctic rifted margins (Gillard et al, 2015).

The oceanic domain

Magmatic activity can trigger eventual lithospheric rupture and the formation of oceanic crust (Zalán, 2015). The lithosphere experiences more gradual breakup in a magma-poor setting.

Rift-related deformation stages can overlap in time and space, thus, the structural units formed during one rifting stage can be reutilized by subsequent rifting stages, leading to complicated crustal architectures (Péron-Pinvidic and Manatschal, 2009). Furthermore, the role of inheritance varies in different evolutionary stages of rifted margin basins (Manatschal et al, 2015). During the stretching stage, the evolution of rift basins is mainly governed by structural inheritance within the brittle upper crust. As lithospheric thinning continues, inheritance in the strong mantle may govern the localization of the necking margin and eventual breakup (Chenin and Beaumont, 2013). During the hyperextension and exhumation phases, although the detachment structures can still be governed by inheritance on a local scale, the crustal architecture is mainly influenced by rift-related processes at the regional scale.

1.1.3 Plate reconstruction of the southern North Atlantic

In the literature, the pre-rift plate configuration of the North Atlantic realm has been restored by many global and regional plate reconstruction models (Srivastava and Verhoef, 1992; Stampfli and Borel, 2002; Seton et al., 2012; Sibuet et al., 2012; Matthews et al., 2016; Müller et al., 2016; Nirrengarten et al., 2018; Peace et al., 2019). Computer software packages are becoming available for plate reconstruction modelling, such as PaleoGIS (www.paleogis.com), and GPlates (www.gplates.org). Generally, traditional rigid plate reconstructions rely on oceanic isochrons, fracture zones observed in ocean basins, and paleomagnetic data (Seton et al., 2012; Müller et al., 2016). They are also mainly dependent on two basic assumptions (Morgan, 1968): 1) tectonic plates are rigid; 2) these plates are separated by narrow borders. These assumptions often result in inaccurate paleo-positions of reconstructed plates because the margins of plates experience either stretching during continental rifting or shortening during continental collision (Ady and Whittaker, 2019). Recently, plate reconstruction modelling packages have improved significantly, evolving from rigid to deformable, allowing for the restoration of continental lithospheric deformation (Gurnis et al., 2018).

Srivastava and Verhoef (1992) first employed the progressive overlap between reconstructed plates to calculate extension amounts and restore the pre-stretched plate configurations in the North Atlantic. Cole and Peachey (1999) incorporated local stretching factors into a rigid plate model to quantify extension in the Rockall Basin. Rotations of microplates or continental blocks/ribbons (i.e., rotation of the Flemish Cap) have been introduced into rigid plate models to obtain a tighter fit (Nirrengarten et al., 2018). Stampfli and Borel (2002) proposed models with dynamically evolving plate boundaries over geologic time, leading to a better fit, despite failing to quantify lithospheric extension. Similarly, the concept of a continuously evolving plate polygon, in which the plate boundary is time-dependent, has been introduced into plate reconstruction modelling to restore global plate reconfigurations in GPlates (Gurnis et al., 2012). Furthermore, in the GPlates context, a continuously deforming field is proposed by Gurnis et al. (2018) to replace the rigid plate polygon for quantifying the change of the deformable region. A grid of points is created in the deformable region with time-dependent geometry. At each point, the time-dependent crustal thickness and stretching factors can be quantitatively calculated.

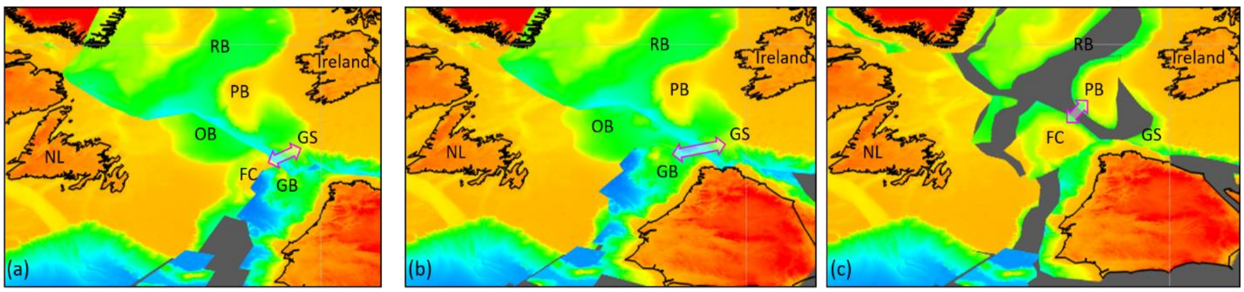

Figure 1.4: Rigid plate reconstructions at the Early Cretaceous (145 Ma) along the southern North Atlantic. The warmer color indicates the shallower bathymetry and elevations. (a) Seton et al. (2012). FC partially overlaps with GB and appears to be conjugate to GS. (b) Matthews et al. (2016). FC overlaps with GB and appears to be conjugate to GS. (c) Nirrengarten et al. (2018). FC appears to connect with PB. Abbreviations: GB, Galicia Bank; GS, Goban Spur; PB, Porcupine Bank; RT, Rockall Basin; FC, Flemish Cap; OB, Orphan Basin.

Ady and Whittaker (2019) proposed a deformable plate kinematic model to examine the impact of inherited structures on the tectonic evolution of the North Atlantic, in which the regional stretching factor, ß, derived from present-day crustal thickness is taken as an essential input parameter. Peace et al. (2019) carried out deformable plate reconstruction in GPlates for the southern North Atlantic region by introducing independent continental fragments, reproducing crustal thicknesses derived from gravity inversion. Based on Peace et al. (2019), King et al. (2020) further improved the deformable plate model for the southern North Atlantic rift system by incorporating the Galicia Bank as an independent continental ribbon. Despite the many existing plate reconstruction models for the southern North Atlantic realm, these models often differ from each other in terms of plate kinematics over geological time due to their various assumptions and their respective limitations (Fig. 1.4).

1.2 Scientific problems & Research objectives

1.2.1 Scientific problems

Even though a detailed understanding of the structure and tectonics of the Flemish Cap-Orphan Basin and the Irish Atlantic margin has been established in recent years, there are still unresolved issues pertaining to this conjugate margin pair:

1) Due to limited data coverage, the rift-related domains along the Goban Spur have remained poorly defined and their architecture has been primarily delineated on the basis of a small number of co-located 2-D seismic profiles (Keen et al., 1989; Bullock and Minshull, 2005). Consequently, knowledge of the rifting evolution of the Goban Spur margin has also been limited by the 2-D nature of previous studies and the sparsity of available geophysical data.
2) The structure and tectonics in the continental domain of the Porcupine Basin have been intensively studied (Naylor et al., 2002; Naylor and Shannon, 2009; Whiting et al., 2021), but the along-strike structural characteristics in the COT and oceanic zones along the western Porcupine region remain unclear due to a lack of seismic constraints.
3) Although both Welford et al. (2010b) and Gerlings (2013) mapped the crustal architecture of the NE Flemish Cap based on seismic interpretation, their interpretations show differing distributions of the serpentinized mantle. Furthermore, Gerlings (2013) has not confirmed the clockwise rotation of the Flemish Cap in spite of interpreting the same seismic data as Welford et al. (2010b).

4) The 2-D velocity structures, crustal thicknesses, and reflectivity patterns across both the Goban Spur and the Flemish Cap are strikingly different (Bullock and Minshull, 2005; Welford et al., 2010b; Welford et al., 2012; Gerlings et al., 2012). These differences call into question the widely-accepted "conjugate" relationship of the two margins. Although some scholars argue against the linkage between the Goban Spur and the Flemish Cap, supporting instead the connectivity between the Flemish Cap and the Porcupine Bank, and the Goban Spur with the Galicia Bank (Nirrengarten et al., 2018; Peace et al., 2019), the models along these margins are mainly dependent on potential field data analysis, lacking seismic constraints, particularly for the Porcupine Atlantic margin.
5) Although the distribution of igneous rocks along the Porcupine Atlantic margin has been derived mainly from magnetic anomalies (Naylor et al., 2002), questions still remain concerning the timing and extent of magmatic activity in the COT zone due to weak magnetic anomaly features (Minshull, 2009).
6) Many researchers assume perpendicular extension in the opening of the southern North Atlantic, without considering extension obliquity (Brune et al., 2017). This assumption may introduce more misunderstanding concerning the evolution of these margins. The northern Newfoundland-Irish Atlantic conjugate margins experienced multiple extensional events with varying stress orientations (Welford et al., 2012; Nirrengarten et al., 2018), but there is still a lack of 3D seismic evidence related to rifting over time and space on both sides.
7) The interaction between the pre-existing structural inheritance (the Caledonian and Variscan orogenic belts) and rift geometry is still poorly understood for the Newfoundland and Irish Atlantic margins. Furthermore, the influence of inheritance on stress partitioning and strain localization for the Porcupine Bank has not been investigated.

8) Since each plate reconstruction model for the southern North Atlantic realm seeks to solve different geophysical issues, it is necessary to build a reliable deformable model to quantify extensional processes of the southern North Atlantic, in which segmentation of the Porcupine Atlantic margin can be incorporated.

1.2.2 Research objectives

New long offset 2D multichannel seismic data, acquired in 2013 and 2014 by Eni Ireland for the Department of Environment, Climate and Communications of Ireland, cover the shelf, slope, and deepwater regions of the offshore Irish Altlantic margin (Fig. 1.1c). Complementary seismic reflection data at the NE Flemish Cap (Fig. 1.1b), seismic refraction data (Bullock and Minshull, 2005; Gerlings et al., 2011), Deep Sea Drilling Project (DSDP) drilling sites (de Graciansky et al., 1985), gravity and magnetic maps (Bonvolot et al., 2012), crustal thickness maps (Welford et al., 2012), and oceanic isochrons (Müller et al., 2016) are all available to be integrated together to achieve the following objectives for the Flemish Cap-Orphan Basin and the Porcupine Atlantic margins:

1) Produce basin and crustal structure descriptions along the Goban Spur and western Porcupine Bank margins, including horizon tracking and fault identification;
2) Delineate the regional rift-related crustal domains across the Porcupine Atlantic margin;
3) Investigate the nature of the COT zone and the role of mantle serpentinization in the evolution of these margins;
4) Investigate the link between the geometry of faults and oceanward migrating deformation;
5) Investigate whether the Porcupine Bank is segmented based on seismic observations and the interplay between inherited structures and progressive deformation during the formation of the NE Newfoundland – Porcupine Atlantic margins;

6) Determine the timing and extent of magmatic activity along the Porcupine Atlantic margin and understand the role of magmatism in the formation of these margins;
7) Investigate whether the Goban Spur and the NE Flemish Cap are conjugate margins from a seismically-constrained viewpoint. If so, how did the extension rate, direction, and asymmetry vary over geologic time, quantified based on plate reconstruction modelling;
8) Perform a deformable plate reconstruction for the NE Newfoundland – Porcupine Atlantic conjugate margins to understand how they interacted, evolved, and finally achieved breakup, leading to an enhanced understanding of the relationship between inherited structures, plate reorganization, and margin evolution during rifting.

1.3 Outline of chapters

Chapter 2 investigates the significant along-strike structural variations along the Goban Spur margin, using a combination of seismic interpretation, gravity inversion results, magnetic and gravity anomaly observations, and constraints from drilling data. Variations in crustal architecture, rift-related magmatism, and the tectonic evolutionary history of the Goban Spur margin are revealed. This chapter has been published as "*Yang, P., Welford, J.K., Peace, A.L., & Hobbs, R., 2020. Investigating the Goban Spur rifted continental margin, offshore Ireland, through integration of new seismic reflection and potential field data. Tectonophysics, 777, 228364. doi.org/10.1016/j.tecto.2020.228364.*"

Chapter 3 investigates the crustal architecture, tectonic history, and rift-related magmatism along the western Porcupine Bank (north of the Goban Spur margin) based on ten newly acquired long-offset multichannel seismic profiles and gravity data. Significant margin-parallel and margin-perpendicular structural variations are observed and described. Ultimately, the reactivation of inherited Caledonian and Variscan structural fabrics is proposed to have influenced the variable geometries of the crustal domains along the Porcupine Atlantic margin. This chapter has been published as "*Yang, P., & Welford, J.K., 2021. Investigating the Porcupine Atlantic margin, through integration of new seismic reflection and gravity data. Tectonophysics, 807, 228809. doi.org/10.1016/j.tecto.2021.228809*."

Chapter 4 proposes five deformable plate tectonic models for the North Atlantic in GPlates with distinct structural inheritance trends. To assess the validity of deformable plate models, crustal thickness estimates obtained from gravity inversion and seismic data modelling are compared with those calculated from deformable plate models. The preferred deformable plate model proposes the subdivision of the Porcupine Bank into four blocks with each block experiencing poly-phased rotation and shearing prior to the final continental breakup, implying strong inheritance and segmentation of the Porcupine Bank and Porcupine Basin. This chapter consists of the manuscript under review in *Tectonics* as "*Yang, P., Welford, J.K., and King, M. Assessing the rotation and segmentation of the Porcupine Bank, Irish Atlantic margin, during oblique rifting using deformable plate reconstruction. Tectonics, 2020TC006665, under review*". This manuscript was assigned major revision and the revised version that constitutes chapter 4 is currently being reviewed.

Chapter 5 was submitted to the journal of *Marine and Petroleum Geology* in July, 2021, with the title of "*Revisiting the Goban Spur margin, offshore Ireland, through integration of seismic reflection data and deformable plate modelling*". It seeks to solve a localized crustal thickness discrepancy of the continental crust of the Goban Spur margin from the deformable plate model proposed in Chapter 4. In this chapter, the model proposed in Chapter 4 is locally updated by incorporating two transfer faults in the Goban Spur with constraints from newly presented seismic reflection data, generating a better match.

Chapter 6 summarizes the overall evolution of hyperextended margins along the southern North Atlantic based on the work from the individual manuscripts and discusses some key factors that affect these extensional events. The chapter also concludes with a brief synthesis and summary of the research and provides suggestions for future work.

Chapter 2

2. Investigating the Goban Spur rifted continental margin, offshore Ireland, through integration of new seismic reflection and potential field data

This chapter is published as "Yang, P., Welford, J.K., Peace, A.L., & Hobbs, R., 2020. Investigating the Goban Spur rifted continental margin, offshore Ireland, through integration of new seismic reflection and potential field data. Tectonophysics, 777, P.228364. doi.org/10.1016/j.tecto.2020.228364." Kim Welford provided research supervision, assisted in conceptualization, reviewed and edited the manuscript. Alex Peace and Richard Hobbs helped to shape the research idea and edit the manuscript.

2.1 Abstract

The Goban Spur, offshore Ireland, is a magma-poor rifted continental margin conjugate to the well-studied Newfoundland margin, offshore Canada. Published studies demonstrated that a 70-km-wide zone of exhumed serpentinized mantle lies between oceanic crust and stretched continental crust at the seaward limit of Goban Spur. However, the along-strike extent of this serpentinized zone has, until now, been unknown due to insufficient data coverage. The crustal architecture of the margin is complicated due to its multi-staged tectonic history. Here, six newly acquired multi-channel seismic reflection lines are processed and interpreted, along with vintage seismic profiles, to characterize its structure and evolution. These seismic profiles reveal significant along-strike structural variations along the Goban Spur margin, and allow us to

delimit five distinct crustal zones related to different rifting stages and their regional extents. The geometries of each crustal domain are variable along the margin strike, suggestive of different extension rates during the evolution of the margin or inherited variations in crustal composition and rheology. The transitional zone between oceanic crust and stretched continental crust consists of both shallow peridotite ridges and deeper exhumed serpentinized mantle, much like the conjugate Iberian and Newfoundland margins. Above the top basement in the exhumed domain, the syn-exhumed sediments show strikingly weak reflectivity, rarely seen at other magma-poor margins. Magmatic events occur coincident with each rifting stage, and the volume of magmatic accretions increases from NW to SE, more than previously interpreted. Plate reconstruction of the Goban Spur and its possible conjugate – the Flemish Cap, shows asymmetry in the crustal architectures, likely due to rift evolution involving more 3-D complexity than can be explained by simple 2-D extensional kinematics.

2.2 Introduction

Studies of magma-poor rifted continental margins around the southern North Atlantic Ocean have been plentiful, particularly for the Newfoundland-Iberia and Flemish Cap-Galicia Bank conjugate margin pairs (e.g., Reston, 2007; Sibuet et al., 2007; Péron-Pinvidic et al., 2013; Sauter et al., 2018). In recent years, attention has increasingly focused on the Newfoundland-Irish and Flemish Cap-Goban Spur conjugate rifted continental margins (Figure 2.1a) (Welford et al., 2010a; Gerlings et al., 2012). Rifting along these margins occurred to the north of the Biscay Triple Junction (BTJ), which formed due to divergent movement between Iberia, North America, and Europe during the breakup of Pangaea (Sibuet and Collette, 1991). Rifting proceeded until the initiation of seafloor spreading between them, beginning in the Cretaceous at magnetic Chron 34 (Figure 2.1a) (Sibuet and Collette, 1991). By studying the continent-ocean transitional zones (COTZ) across these margin pairs, the geodynamic processes that contributed to rifting can be deduced. While early studies of the Goban Spur originally interpreted a sharp continent-ocean boundary (COB) (e.g., Masson et al., 1985; Keen and de Voogd, 1988; Horsefield et al., 1994; Peddy et al., 1989), a 70-km-wide transitional zone of exhumed serpentinized subcontinental mantle has since been interpreted for the COTZ of the Goban Spur based on seismic refraction modelling (Bullock and Minshull, 2005). Similar transitional zones have also been interpreted along the Newfoundland and Flemish Cap, Iberia and Galicia Bank margins (e.g., Boillot et al., 1987; Whitmarsh et al., 1998; Dean et al., 2000; Welford et al., 2010b; Gerlings et al., 2011; Dean et al., 2015; Davy et al., 2016).

Due to limited data coverage, the rift-related domains along the Goban Spur margin have remained poorly defined and their architecture has been primarily delineated on the basis of a small number of co-located 2-D seismic profiles (Figure 2.1b), including CM lines (Montadert et al., 1979), the WAM line (Peddy et al., 1989), and the refraction line (Bullock and Minshull, 2005). Consequently, knowledge of the rifting evolution of the Goban Spur margin has been limited by the 2-D nature of previous studies and the sparsity of available geophysical data.

In order to improve understanding of the offshore Irish Atlantic rifted continental margins, deep long-offset multichannel seismic reflection data were acquired in 2013 by Eni Ireland for the Department of Communications, Climate Action & Environment of Ireland. In this study, six of these newly acquired seismic reflection profiles along the Goban Spur margin are processed and interpreted, providing improved regional coverage (Figure 2.1b). By referring to the structural unit subdivision scheme for magma-poor margins proposed in the literature (Péron-Pinvidic et al., 2013; Tugend et al., 2014), distinct crustal domains are identified and regionally extrapolated across the Goban Spur margin. This is achieved using a combination of seismic interpretation, gravity inversion results, magnetic and gravity anomaly observations, and constraints from drilling data. The improved data coverage allows for better characterization of the variations in rifting mode, rift-related magmatism, and insights into the tectonic evolutionary history of the Goban Spur margin.

2.3 Geological Setting

The Goban Spur is a magma-poor rifted continental margin, situated offshore Ireland, south of the Porcupine Basin and Porcupine Bank, and west of the Fastnet Basin, the Comubian Platform, and the Western Approaches Basin (Figure 2.1) (Auffret et al., 1979; Horsefield et al., 1994; Bullock and Minshull, 2005). To the southeast is the northern Bay of Biscay margin, which experienced rifting from the Jurassic to the Cretaceous (Montadert et al., 1979). The depth, obtained from ETOPO1 Global Relief Model of the National Geophysical Data Center (NGDC) of the National Oceanic and Atmospheric Administration (NOAA), gradually increases from ~1000 m to 2500 m at the southwest edge of the Goban Spur continental shelf, before dropping off abruptly at the Pendragon Escarpment (Figure 2.1b). Farther seaward, the Goban Spur transitions to the Porcupine Abyssal Plain (Figure 2.1b) (de Graciansky & Poag, 1985).

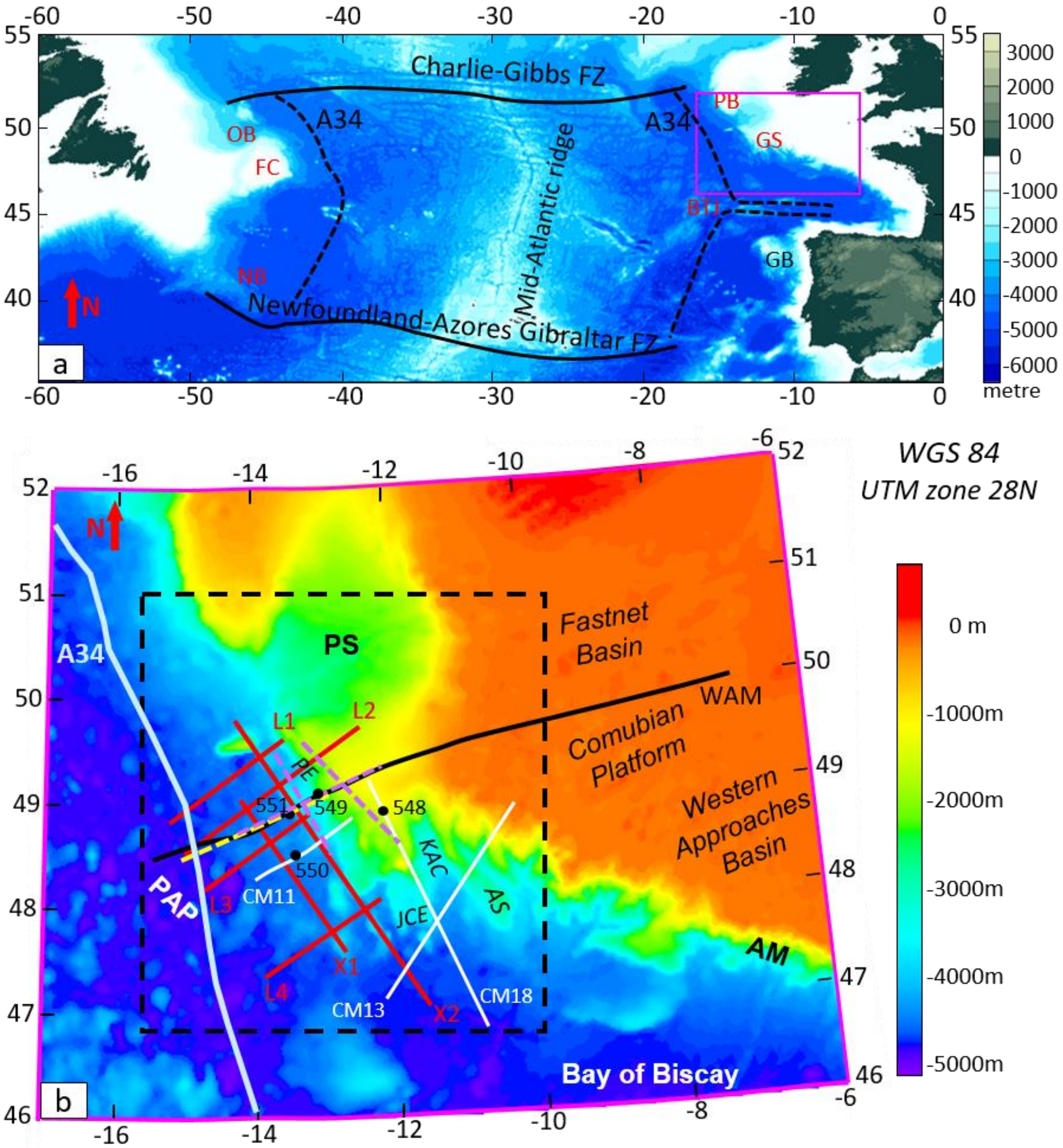

Figure 2.1: (a) Bathymetric map of the North Atlantic. The dashed black line shows magnetic anomaly 34 (Müller et al., 2016). The pink box shows the location of part b. (b) Bathymetry of the Goban Spur. Red lines indicate the newly acquired seismic reflection lines. The black and white lines show the Western Approaches Margin (WAM) line (Peddy et al., 1989) and the CM multichannel seismic profiles (Masson et al., 1985), respectively. The purple and yellow dashed lines indicate the refraction profiles from Horsefield et al. (1994) and Bullock and Minshull (2005), respectively. The black solid circles represent the DSDP Leg 80 drill sites. Crustal domains will be delineated within the dashed black box. Abbreviations: AM: Armorican Margin; AS:Austell Spur; BTJ: Biscay Triple Junction; FC: Flemish Cap; FZ: Fracture zone; GB: Galicia Bank; GS: Goban Spur; JCE: Jean Charcot Escarpment; KAC: King Arthur Canyon; NB: Newfoundland Basin; PAP: Porcupine Abyssal Plain; PE: Pendragon Escarpment; PS: Porcupine Basin; PB: Porcupine Bank.

Generally, the structural features of the Goban Spur can be attributed to the rifting of the European plate from the North American plate, with crustal thinning occurring at the end of the rifting phase during the Early Cretaceous to the Early Albian (Roberts et al., 1981; de Graciansky et al., 1985). However, the formation of the Goban Spur margin has also been influenced by additional interrelated factors, including the formation of the Bay of Biscay (Dingle and Scrutton, 1979), its interaction with the hypothesized conjugate Flemish Cap margin prior to breakup (Cande and Kristoffersen, 1977), and the presence of pre-existing discontinuities in the crustal basement (Dingle and Scrutton, 1977; Sibuet et al., 1985). The interaction between the margin-parallel NW- trending faults due to rifting and the pre-existing NE- trending fault system primarily controls the structure of the Goban Spur continental crust, with the northern Goban province likely an extension of the Fastnet Basin rather than the Cormubian Platform (Naylor et al., 2002). At the northern limit of the Goban Spur, the ENE-trending Porcupine Fault separates the Spur from the Porcupine Basin (Dingle and Scrutton, 1979) while the southern margin may be associated with faults developed in the northern Western Approaches Basin (Naylor et al., 2002). Based on seismic evidence, the NW-trending faults become more complicated and less continuous with more varied orientations towards the southeastward limit of the Goban Spur margin (Naylor et al., 2002). This complexity may be due to the influence of variable basement structure, interactions between the NW-trending fault systems and E-trending faults close to the Jean Charcot Escarpment (Sibuet et al., 1985), and transfer faults that segment the Goban Spur margin (Naylor et al., 2002).

During the Deep Sea Drilling Project (DSDP) Leg 80, four sites (548, 549, 550, and 551) were drilled on the Goban Spur (Figure 2.1b and 2.2) (de Graciansky et al., 1985). Site 548 was drilled near the edge of a half-graben with Devonian basement, and site 549 penetrated the

Variscan basement on the crest of the Pendragon Escarpment at 2335.5 m water depth. In addition, the earliest syn-rift sediments from the Barremian (possibly late Hauterivian) and oldest post-rift sediments from the early Albian were recovered at site 549, which revealed that the rifting phase lasted about 15 Myrs (de Graciansky et al., 1985; Masson et al., 1985). Site 550, at 4432 m water depth, was located in the abyssal plain southwest of the margin and drilled Devonian basement composed of basaltic rocks, overlain by late Albian chalks. The site was ~135 km inboard of magnetic anomaly 34, which represents the first undisputed oceanic crust from seafloor spreading (Srivastava et al., 1988). Site 551 penetrated the basaltic basement imbedded with mudstone, overlain by late Cenomanian chalks (de Graciansky et al., 1985).

Due to the interpreted differential extension between the upper crust and the lower lithosphere at the Goban Spur, Masson et al. (1985) suggested that a uniform-stretching model was not applicable to the margin. Keen et al. (1989) favoured pure shear rifting and asymmetric lithosphere rupture based on the interpretation of seismic reflection data acquired across the NE Flemish Cap-Goban Spur conjugate margins. Since full lithospheric thinning is estimated to have been considerably greater than the observed thinning of the upper crust in the transitional zone across Goban Spur, Healy and Kusznir (2007) have argued for depth-dependent stretching, precluding a pure shear mechanism for the major deformation processes. Gerlings et al. (2012) argued for asymmetric deformation occurring during each stage of the tectonic evolution of the NE Flemish Cap-Goban Spur conjugate margins. Based on similarities in the inferred tectonic processes at the Goban Spur margin and those across the Iberia-Newfoundland margins (Sibuet and Tucholke, 2012), depth-dependent stretching of lithosphere, with crustal rupture preceding lithospheric mantle breakup, has been argued for the Goban Spur margin, just as it has for the Iberia-Newfoundland margins (Huismans and Beaumont, 2011). The geological and tectonic characteristics of the Goban Spur are complex and both time and depth dependent, introducing challenges for geophysical characterization.

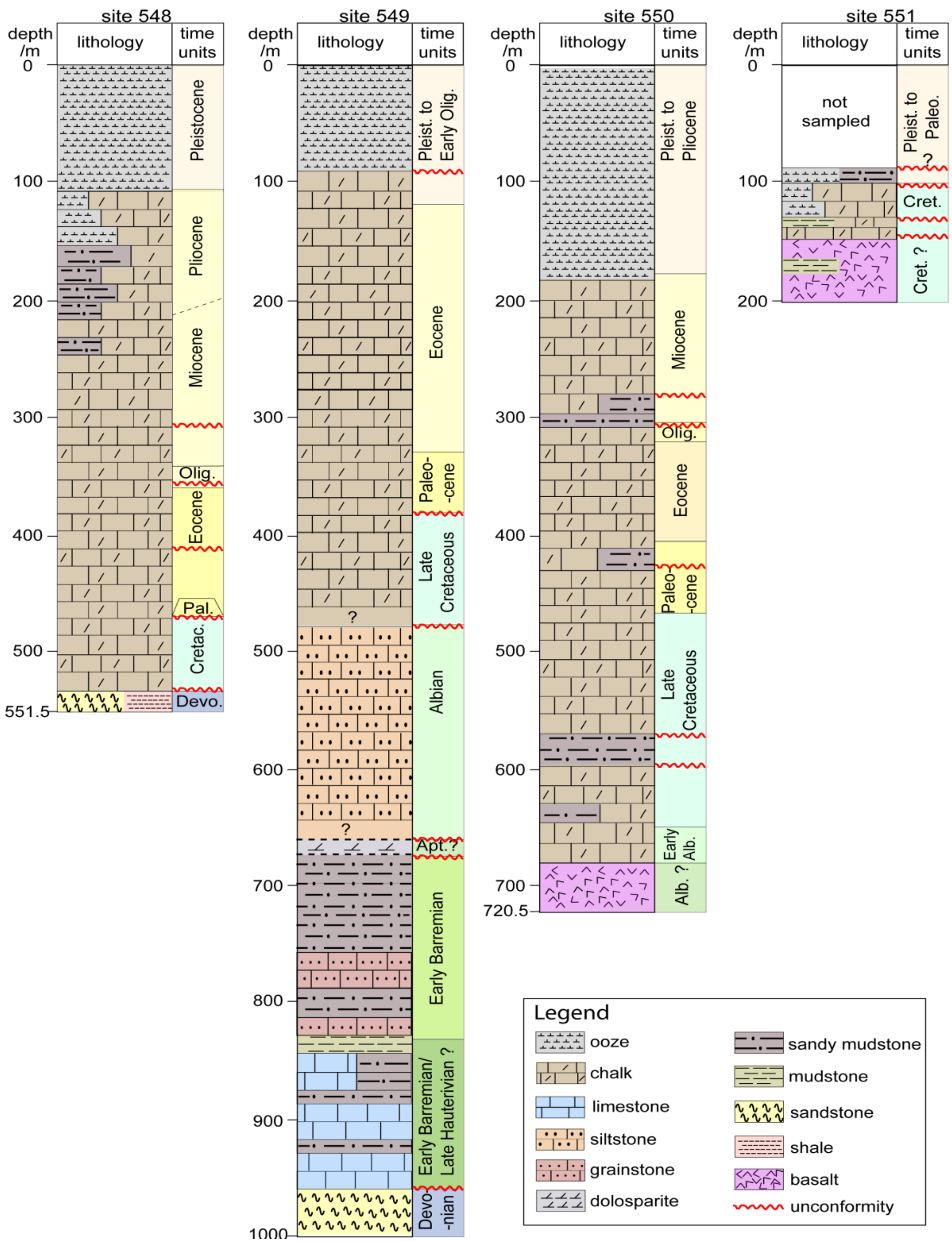

Figure 2.2: Lithological columns for drilling sites 548, 549, 550, and 551 at the Goban Spur margin (modified from De Graciansky et al., 1985; De Graciansky and Poag, 1985).

2.4 Geophysical background

A number of single-channel and multi-channel seismic reflection profiles were acquired during the 1970s, including the CM profiles (white lines in Figure 2.1b) (Montadert et al., 1979; Masson et al., 1985; Sibuet et al., 1985). Although these vintage seismic profiles did not extend into the undisputed oceanic crust defined seaward of magnetic anomaly Chron 34, they provided a good understanding of fault characteristics in the continental portion of the Goban Spur (Masson et al., 1985; Naylor et al., 2002). In 1985, the WAM line (black line in Figure 2.1b) was acquired across the continental and oceanic crust of the Goban Spur, from which faults, half-grabens, crustal types, volcanic features, and a relatively clear continent-ocean boundary were inferred (Peddy et al., 1989; Louvel et al., 1997). To complement the WAM line and quantitatively characterize the structure of the margin, including the presence and extent of igneous rocks, co-located seismic refraction experiments were acquired in 1987 (dashed purple lines in Figure 2.1b; Horsefield et al., 1994) and 2000 (dashed yellow line in Figure 2.1b; Bullock and Minshull, 2005), respectively. Based on the velocity model from the most recent seismic refraction profile (yellow dashed line in Figure 2.1b), continental, transitional, and oceanic domains were defined for the Goban Spur margin, with velocities ranging from 5.2 to 5.8 km s^{-1} and from 6.6 to 6.9 km s^{-1} in upper and lower continental crust, respectively (Bullock and Minshull, 2005). In the transitional and oceanic zones, P-wave velocity in the crust displays a relatively high gradient (4.5 - 6.8 km s^{-1} within 4 km beneath basement). In addition, P-wave velocities are high (> 7.1 km s^{-1}) at depths of 5-7 km beneath the basement of the 70-km-wide transitional region and Poisson's ratio at top basement of this region is higher than 0.34, indicating serpentinized exhumed mantle (Bullock and Minshull, 2005). Furthermore, a 1-km magnetized layer is modelled in the transitional zone, which can be attributed to the formation of magnetite during serpentinization (Bullock and Minshull, 2005).

Free-air gravity data from the Goban Spur margin are shown in Figure 2.3a. The transition from negative to positive gravity anomalies lies parallel to the strike of the margin and coincides with inferred crustal thinning (Bullock and Minshull, 2005). To complement qualitative descriptions of the observed gravity data, gravity forward modelling and inversion have been applied to the margin (Bullock and Minshull, 2005; Welford et al., 2010c). Figure 2.3b shows crustal thickness derived from gravity inversion (Welford et al., 2010c). Welford et al. (2010c) used the GRAV3D algorithm, developed by Li and Oldenburg (1996; 1998), to carry out the gravity inversion. Briefly, a reference density model (relative to a background density of 2850 kg m^{-3}), depth-weighting function and suitable smoothing parameters are all prescribed. Bathymetric data and sediment thickness data, obtained from the NOAA sediment thickness compilation and adjusted in Welford et al. (2010c), are used to constrain the reference density model. The inversion is performed in the least-square sense and the free air gravity data are the observed data. Through multiple iterations, the predicted density model is obtained. Then, Moho structure and crustal thickness are extracted from the recovered density model by assuming that a density anomaly isosurface of 170 kg m^{-3} corresponds to the base of the crust and represents an appropriate Moho proxy. Note that in the reference density model, the region above the bathymetric depths is assumed to have a constant density anomaly of -1820 kg m^{-3}, corresponding to a seawater density of 1030 kg m^{-3}. Below the bathymetry, the sedimentary layer within the reference model is assigned depth-increasing densities with strict bounds that conform to sandstone and shale trends on similar passive margins (Jackson and Talbot; 1986; Sclater and Christie 1980; Albertz et al., 2010). Beneath the sedimentary layer, the inversion algorithm is given greater freedom to assign densities for the crust and mantle in order to reproduce the observations.

The inferred crustal thickness from the gravity inversion reveals that, oceanward, the crust of the Goban Spur margin thins from ~29 km to ~5 km over a distance of ~250 km (Figure 2.3b). Along the northern portion of the margin, the gradient in crustal thickness is larger, consistent with a relatively sharp necking zone. Along the southern portion of the margin, the crustal thickness varies slowly over a wider region, indicating a smoother necking profile. This also suggests that the distribution of continental, oceanic and transitional zones will likely vary from north to south.

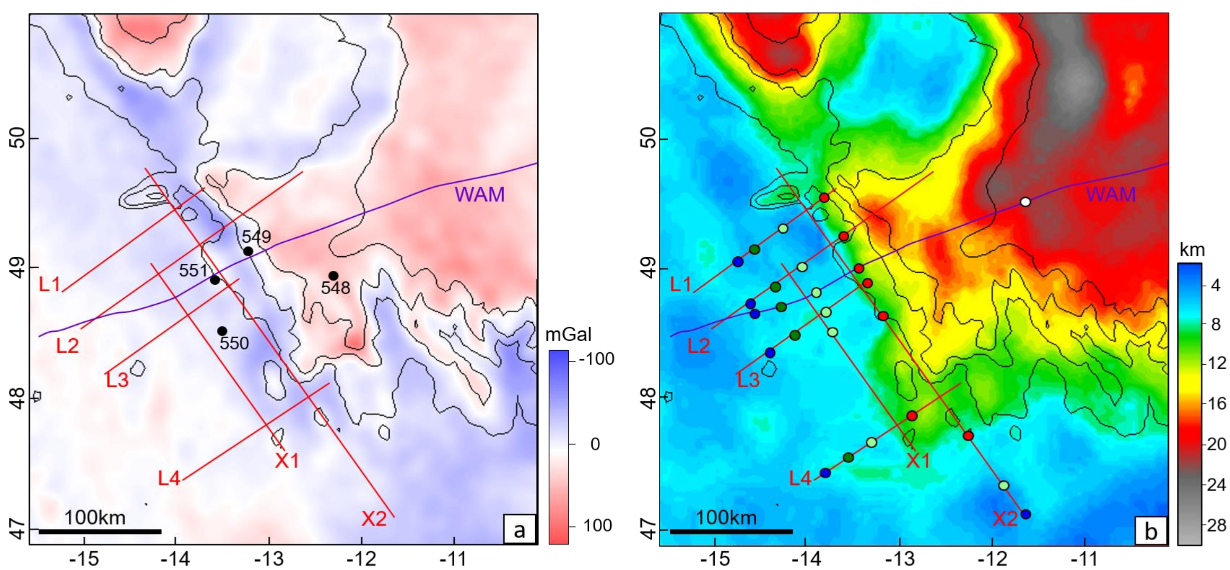

Figure 2.3: (a) The free air gravity anomaly with overlying bathymetric contours (Bonvalot et al., 2012). The black circles represent the DSDP Leg 80 drill sites. (b) Crustal thickness derived from gravity inversion (Welford et al., 2010c) with overlying bathymetric contours. Present-day bathymetric contours (black lines) are displayed with a contour interval of 1000 m. The six red lines indicate the new seismic lines in this study; the purple line represents the WAM line. The blue, dark green, light green, red, and white circles respectively mark the landward limits of the oceanic, exhumed subdomain T2, exhumed subdomain T1, hyperextended, necking, and/or proximal domains along each seismic line (Note: these terminologies will be introduced in section 2.6).

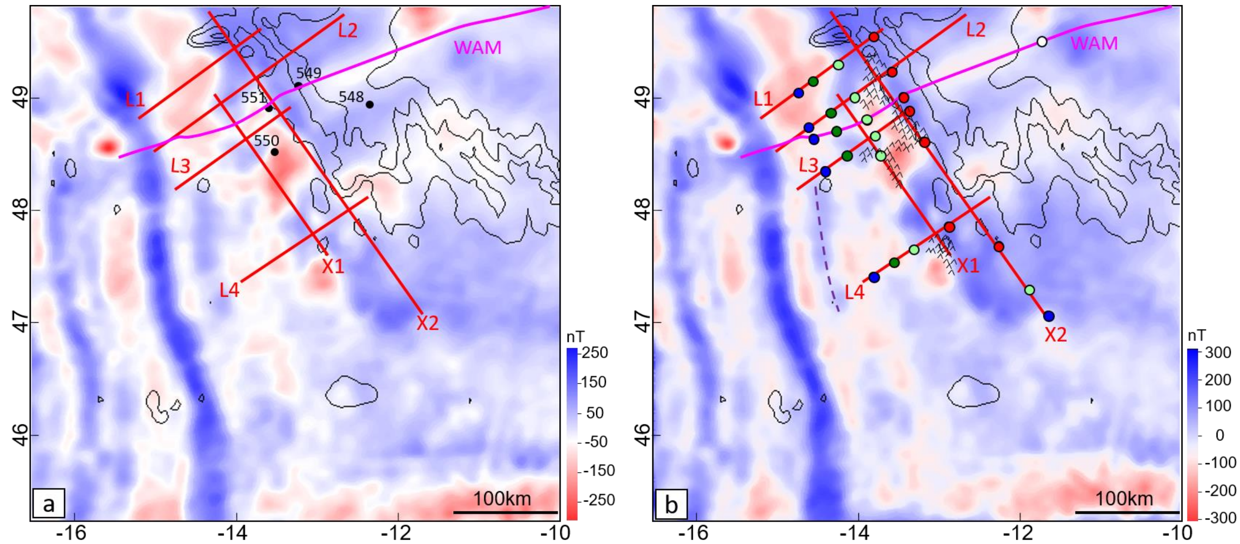

Figure 2.4: (a) Magnetic anomaly map across the Goban Spur margin. The black circles represent the DSDP Leg 80 drill sites. (b) Magnetic anomaly data reduced to pole for the Goban Spur margin. Bathymetric contours (black lines) are displayed with a contour interval of 1000 m. The black clusters of open triangles in part b indicate sill distribution from the Petroleum Affairs Division (PAD) of the Department of Communications, Climate Action & Environment, Ireland (http://www.pad.ie). The dashed purple line indicates a relatively linear magnetic anomaly. The six red lines indicate the new seismic profiles; the pink line is the WAM line. The blue, dark green, light green, red, and white circles are defined in Fig. 2.3b.

The magnetic anomaly data in Figure 2.4 are obtained from the Earth Magnetic Anomaly Grid at 2-arc-minute resolution from NOAA - http://www.ngdc.noaa.gov/geomag/emag2/ (EMAG 2). Magnetic Chron 34 (A34) lies along the linear blue band of high magnetization (Müller et al., 2016). There also exists a relatively linear magnetic anomaly with a southeastern trend, approximately parallel to magnetic Chron 34 between seismic profiles L3 and L4 (purple dashed line in Figure 2.4b). Generally, the further landward from magnetic Chron 34, the weaker the magnetic anomaly becomes, which might be associated with minor magmatic addition during rifting, in contrast to increasing magmatism during the initiation of seafloor spreading (Bullock and Minshull, 2005). The magnetic characteristics in the region between the continental slope and magnetic Chron 34 vary dramatically from north to south. Along the northern portion of the Goban Spur margin, a region (between X1 and X2) of negative magnetic anomalies is very prominent (Figure 2.4b), where DSDP Sites 550 and 551 encounter basaltic rocks (de

Graciansky et al., 1985). Magnetic modelling along the WAM line also demonstrates that a basalt sill located at the foot of the continental slope produces a relatively prominent magnetic anomaly, with the causative body extending into the basement (Louvel et al., 1997; Bullock and Minshull, 2005).

2.5 Seismic acquisition and Methodology

In this study, six new multichannel seismic (MCS) reflection lines (L1, L2, L3, L4, X1, and X2) are processed and interpreted (Figure 2.1b). Seismic profiles L1, L2, L3, and L4 are oriented southwest-northeast, and profiles X1 and X2 cross these four lines, with a northwest-southeast orientation (Figure 2.1b). During acquisition, the survey vessel BGP Explorer towed an array of 48 air guns that were fired with a total volume of 85 L and a shotpoint interval of 25 m for water depths less than 3000 m and 37.5 m for water depths over 3000 m. The seismic data were acquired with a sampling interval of 2 ms and a trace length of 12 s. Data were recorded using a 10 km-long hydrophone streamer with a 12.5 m receiver group spacing, generating 804 traces per shot.

The seismic data processing workflow involves geometry definition with a common-midpoint (CMP) interval of 6.25 m, amplitude compensation, bandpass filtering, predictive deconvolution, multiple attenuation, velocity analysis, pre-stack Kirchoff time migration, and coherency filtering. Next, the time migrated stacked sections are converted from the time domain to the depth domain by using the stacking velocity obtained from velocity analysis. It is worth mentioning that the velocities at and above the basement are primarily picked according to the seismic reflection data, while the velocities beneath the basement are less well constrained and are picked to conform to regional trends derived from seismic refraction data. It should also be noted that the re-processed profiles did not show a significant improvement compared to those provided by Eni Ireland for the Department of Communications, Climate Action & Environment of Ireland (see the comparison of reprocessed lines and those provided from Ireland in Figures A.1-A.6 in Appendix A). The profiles provided from Ireland are used in this study. As for the WAM line, it was not reprocessed in this study, and so the stacking velocities are unavailable. Thus, we interpret the WAM line in the time domain only. Finally, the depth-converted seismic reflection profiles across the Goban Spur rifted margin are interpreted by incorporating insights from seismic refraction data, the complementary WAM line, gravity and magnetic data, crustal thickness estimates from seismic refraction surveys and gravity inversion, and borehole data from DSDP Leg 80.

Since seismic profiles L1, L2, L3, and L4 are subparallel to each other (Figure 2.1b) and the distance between L1, L2 and L3 is relatively small, with ~ 36 km, and ~42 km between L1 and L2, and L2 and L3 respectively, they share numerous features (Figure 2.1b). Furthermore, since lines L1, L2, the WAM line, and the Bullock and Minshull (2005) refraction line extend into the oceanic domain and cross magnetic anomaly 34 (Figure 2.1b), the data coverage is sufficient for investigating the range of tectonic processes from rifting and extension, to the subsequent breakup, and the eventual creation of new oceanic crust. The primary classification standard used for the crustal domains is briefly reviewed in the next section, before discussing the interpreted sections in detail.

2.6 Interpretation

2.6.1 Terminology

Although the crustal architecture of rifted margins can vary significantly from one margin to another, they still share some first-order structural components (Osmundsen and Ebbing, 2008; Minshull, 2009; Sutra et al., 2013; Tugend et al., 2014). Péron-Pinvidic et al. (2013) recommend five structural units to describe the transition from unstretched continental crust to oceanic crust; these include: 1) proximal, 2) necking, 3) hyperextended, 4) exhumed, and 5) outer domains. These structural units show contrasting characteristics in terms of basin types, faulted features, and crustal thickness variations, but also correspond to four evolutionary phases of rifted margins: 1) the stretching phase, 2) the thinning phase, 3) the hyperextension and exhumation phase, and 4) the initiation of seafloor spreading and magmatism phase. Using the structural unit division of rifted margins proposed in the literature (Péron-Pinvidic et al., 2013; Tugend et al., 2014), the corresponding interpretations laterally divide each seismic line into different crustal domains in this study.

2.6.1.1 Proximal domain

The proximal domain undergoes stretching with low extensional values and is commonly characterized by grabens or half-grabens containing syn-rift sediments (Mohn et al., 2012; Péron-Pinvidic et al., 2013). Tilted blocks bounded by listric faults are often observed at the top basement of proximal basins (Whitmarsh et al., 2001). These faults generally terminate in the middle crust without affecting the Moho (Péron-Pinvidic et al., 2013). In addition, the crustal thickness is generally greater than 30 km in the proximal setting (Péron-Pinvidic et al., 2013).

2.6.1.2 Necking domain

The lithospheric thickness dramatically decreases in the necking zone, which gives the crust a wedged structure (Mohn et al., 2012). Within the wedged region, the Moho drastically shallows due to crustal thinning from ~30 km to less than 10 km (Péron-Pinvidic and Manatschal, 2009).

2.6.1.3 Hyperextended domain

Hyper-thinning of the crust is often observed in both hyperextended and exhumed zones (Péron-Pinvidic et al., 2013). The hyper-thinned crust is characterized by hyperextended sag basins and half-grabens and the corresponding crustal thickness is generally less than 10 to 15 km (Tugend et al., 2015). The hyperextension stage is important in the evolution of magma-poor margins, and it often, but not always, leads to serpentinization and mantle exhumation (Pérez-Gussinyé and Reston, 2001). Currently, understanding of the nature of the basement in the hyperextended and exhumed domains still lacks consensus. Nonetheless, we still try to interpret both the hyperextended and exhumed domains separately to distinguish the hyperextension stage and the exhumation stage in this study.

2.6.1.4 Exhumed domain

In the exhumed serpentinized mantle domain, the crust experiences such intense hyper-extension and embrittlement that the extensional faults that provide the conduits for serpentinizing the mantle become detachment faults along which the serpentinized mantle was ultimately exhumed (Pérez-Gussinyé and Reston, 2001; Reston, 2007). P-wave velocities in the crust of this domain gradually range from ~ 4 km s^{-1} at the seafloor to ~ 8 km s^{-1} at depth (Dean et al., 2000; Bullock and Minshull, 2005; Grevemeyer et al., 2018). The Moho interface is usually unidentifiable in this region (Minshull et al., 1998; Gillard et al., 2016). At some magma-poor rifted margins, the exhumation zone is subdivided into a region of deeper exhumed serpentinized mantle with more subdued topography and a region of shallower peridotite ridges according to seismic basement relief. By specifically following the subdivision from Welford et al. (2010a), labelled subdomains T1 and T2 are used to differentiate between the transitional crust characterized by smooth basement relief (subdomain T1) and peridotite ridges (subdomain T2) in the exhumed mantle domain, respectively (Figure 2.5). This does not mean that the shallower peridotite ridges (subdomain T2) are identified on all of the seismic profiles in the study area. It is worthwhile noting that the outer domain mentioned in Péron-Pinvidic et al. (2013) is not interpreted on the seismic profiles in this study, as it cannot be definitively observed.

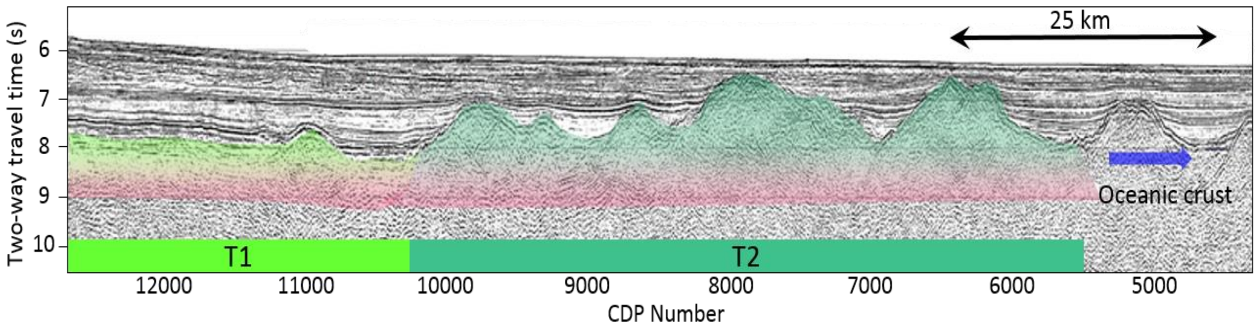

Figure 2.5: Portion of the interpreted seismic profile Erable 56 along the Flemish Cap margin showing the exhumed domain and the transition to oceanic crust (Welford et al., 2010a). Labelled subdomain T1 represents the exhumed serpentinized mantle with relatively deep basement. Labelled subdomain T2 represents the shallower exhumed peridotite ridges.

2.6.1.5 Oceanic domain

In the oceanic domain, geophysical patterns can be highly variable, from the linear magnetic anomalies of the Norway Basin, to the disorganized oceanic magnetic anomalies of the Iberian margin (Péron-Pinvidic et al., 2013). Crustal thickness ranges from 6 km to 7 km for normal oceanic crust formed at low to fast spreading rates (White, 2001; Christeson et al., 2010), while thin oceanic crust (< 5 km) can also be developed in ultra-slow spreading environments (van Avendonk et al., 2017).

2.6.2 WAM line interpretation

In this study, although the WAM line is interpreted in the time domain, it is the only line with approximately coincident constraints from seismic refraction modelling (Figure 2.1b andFigure 2.6d) (Bullock and Minshull, 2005). The relatively comprehensive constraints from seismic reflection and refraction data, Moho variations and crustal thickness along the WAM line ensure the robustness of the interpretation of different crustal domains, considered as the baseline. It is worthwhile noting that as sediments deposited on continental margins record rifting and final lithospheric rupture, pre-, syn-, and post-rift sequences are used to describe the stratigraphic successions at rifted continental margins (Franke, 2013). Pre-rift sequences are commonly onlapped by syn-rift infills in the wedge-shaped half-graben basins bounded by faults, recognized by angular unconformities on seismic data (Franke, 2013). Post-rift and syn-rift sediments are also interpreted along the WAM line (Figure 2.6c). The post-rift section directly overlies the crustal domains, while the sediments gradually pinchout towards the oceanic domain, displaying highly variable sedimentary thicknesses from NE to SW (Figure 2.6c).

The Bullock and Minshull (2005) velocity model interpretation (Figure 2.6d), when projected to the WAM line, helps constrain the landward limit of the oceanic domain (Figure 2.6b and 2.6c). It is consistent with the crustal domain interpretation of some magma-poor margins (e.g., the Iberia margin and Flemish Cap margin), where the oceanic crust is interpreted to be adjacent to peridotite ridges (Welford et al., 2010a; Davy et al., 2016). From the velocity model (Figure 2.6d) (it does not extend to the oceanward limit of the WAM reflection line), the slow-spreading oceanic domain spans ~45 km with an average crustal density of 2740 kg m^{-3} based on gravity forward modelling (Bullock and Minshull, 2005). Correspondingly, the interpreted oceanic domain along the WAM line spans ~70 km and its landward limit lies to the northeast of magnetic Chron 34 (Figure 2.6c). The basement relief of the oceanic domain between distances of 44 km and 70 km is more subdued than that of the normal oceanic zone seaward of magnetic Chron 34 (Figure 2.6b and 2.6c).

Although the zone between the thinned continental crust and the oceanic crust is interpreted as exhumed serpentinized mantle along the WAM line based on the velocity-depth structure (Figure 2.6d) (Bullock and Minshull, 2005), a further subdivision into three parts is warranted based on the basement morphology and seismic character (Figure 2.6c). These three parts are the hyperextended zone (shaded brown), and the exhumed mantle zone, further subdivided into a section with deeper basement displaying smooth basement morphology (subdomain T1, shaded light green in Figure 2.6e), and a section of serpentinized peridotite ridges with relatively shallower basement with rougher relief (subdomain T2, shaded dark green in Figure 2.6e). It is relatively easy to delimit the boundary (marked by the bold dashed dark green line at the distance of ~95 km in Figure 2.6c) between subdomain T1 and T2 due to the apparently different basement morphology, where the top basement deepens landward by ~ 0.5 s and becomes relatively smoother (Figure 2.6e). Transitional subdomain T2 spans ~23 km and its basement is deeper than that of the adjacent oceanic domain (Figure 2.6c). The geometry of the subdomain T2 also appears similar to the ridges imaged on the Iberia/Galicia margin (Pickup et al., 1996) and the conjugate Newfoundland/Flemish Cap margin (Figure 2.5) (Welford et al., 2010a). Several Ocean Drilling Program (ODP) drill sites on both the Iberia margin and the Newfoundland margin have revealed that the equivalently interpreted ridges are composed of exhumed serpentinized mantle material (Sawyer et al., 1994; Whitmarsh et al., 1998; Tucholke et al. 2004), which has been also supported by seismic refraction and reflection data (Pickup et al., 1996; Dean et al., 2000; Shillington et al. 2006; Van Avendonk et al., 2006). At the Goban Spur margin, both Poisson's ratio values (0.34-0.36) and velocities (> 7 km s^{-1} at depths of 5-7 km beneath top basement) obtained from seismic refraction modelling support the presence of serpentinized exhumed mantle in the subdomains T1 and T2 (Bullock and Minshull, 2005). However, the velocities ranging from 7.2 km s^{-1} to 7.6 km s^{-1} within ~ 1.5 km of the top basement in the subdomain T1 at the Goban Spur margin are different from those at the Iberia margin (7.3-7.9 km s^{-1} within 2-6 km below basement) (Dean et al., 2000).

The border (marked by the bold dashed light green line in Figure 2.6b and 2.6f) between the subdomain T1 and the hyperextended domain is determined based on the contrasting seismic patterns at the top basement. The geometry of the top basement is convex downwards in the subdomain T1 and become concave downwards in the hyperextended zone (Figure 2.6f). In addition, within the sedimentary formations above the top basement (indicated by the blue arrow in Figure 2.6f), the reflective events are relatively weak and continuous above the hyperextended crust, while reflection amplitudes typically appear much weaker (or transparent) and discontinuous above the subdomain T1 (Figure 2.6f). The change of seismic facies often occurs during the transition from stretched crust to exhumed mantle at magma-poor rifted margins (Nirrengarten et al., 2018; Gillard et al., 2019). In this study, we refer to these sedimentary formations in the exhumed domain as syn-exhumation sediments. Furthermore, the reflector below the top basement indicated by the black arrow in Figure 2.6f likely indicates the contact between the hyperextended crust and exhumed serpentinized mantle, similar to the S-reflector at the West Iberia margin (Reston et al., 1996).

The boundary (marked by the bold dashed brown line in Figure 2.6b) between the hyperextended zone and the necking zone is primarily defined by the Moho depth derived from gravity inversion (Figure 2.6a) (Welford et al., 2010c). The Moho depth shallows from ~23 km to ~15 km over a distance of ~ 145 km in the necking domain, while it ranges from ~ 15 km to ~ 12 km in the hyperextended zone with crustal thickness less than ~ 10 km (Figure 2.3b and 2.6a). Additionally, the wedged structure bounded by tilted faults is a typical feature in the necking zone (~ 180 - 200 km in Figure 2.6c), while the “sag” type basin is easily observed in the hyperextended region (~ 155 - 175 km in Figure 2.6c), which is consistent with the classification criteria of crustal domains proposed by Tugend et al. (2014; 2015). A basaltic body at the toe of the hyperextended zone was sampled by DSDP drilling site 551 (Figure 2.6c) and was used to infer the location of initial oceanic crust formation (Horsefield et al., 1994). However, Bullock and Minshull (2005) argued that the emplacement of the basaltic body occurred during lithosphere thinning before the mantle material began to be exhumed. Dean et al. (2009) used the basaltic lava at sites 550 and 551 to calculate a rift duration of 8-13 Myr at the Goban Spur margin, close to 14-22 Myr assumed by Bullock and Minshull (2005).

The boundary (marked by the bold dashed red line in Figure 2.6b) between the necking zone and the proximal zone is mainly dependent on the Moho depth and crustal thickness calculated from gravity inversion (Figure 2.6a) (Welford et al., 2010c). The oceanward shallowing Moho and rapid decreasing crustal thickness are evident in the necking zone (Figure 2.3b and 2.6a), while the crustal thickness is roughly 21 km, and the Moho depth varies from ~ 25 km to ~ 22 km in the proximal zone where the Moho depth is ~ 26 km in the velocity model from Horsefield et al. (1994).

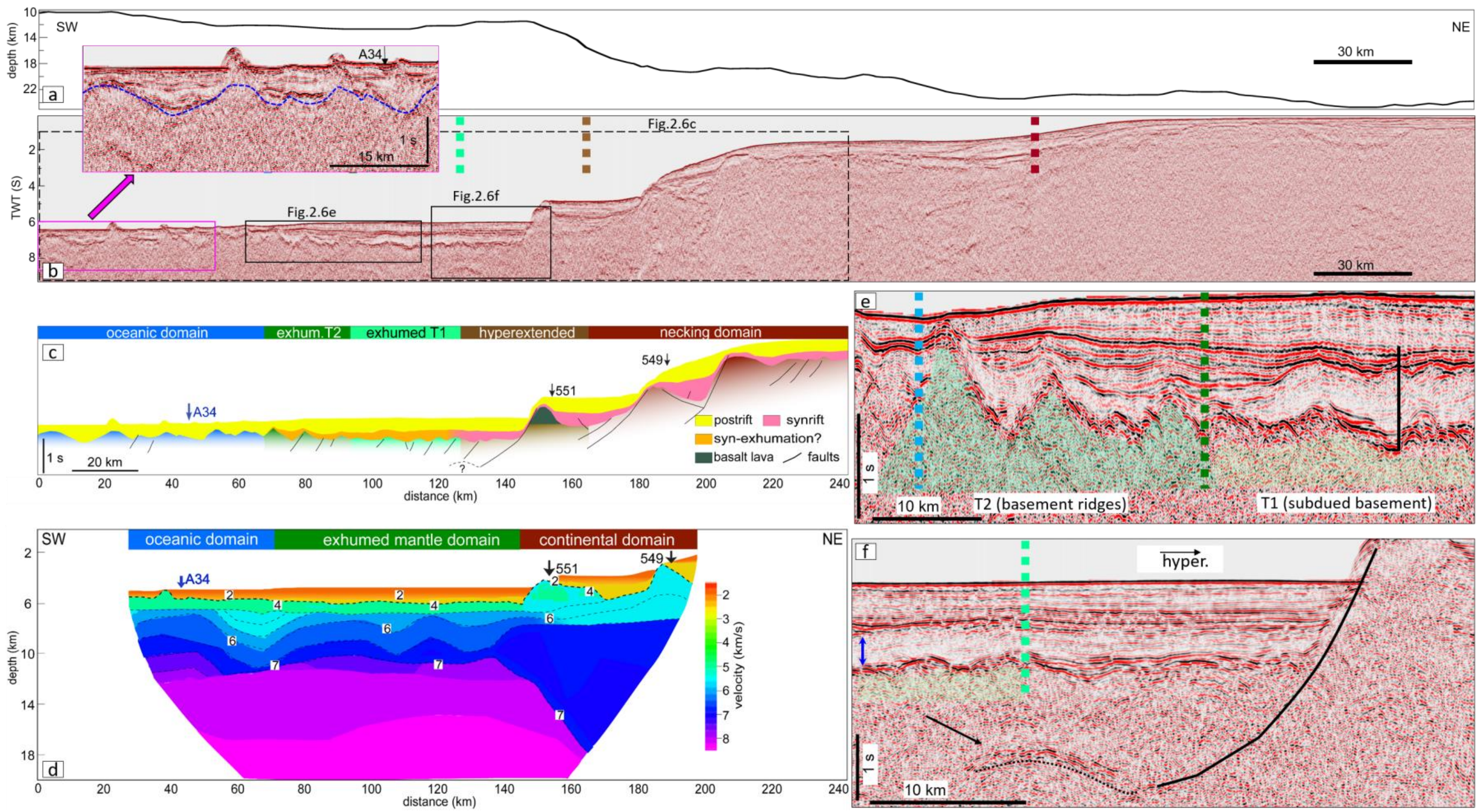

Figure 2.6: (a) Moho depth along the WAM line (from Welford et al., 2010c). (b) A section of the WAM line. The bold dashed coloured lines indicate boundaries between crustal domains. (c) Interpretation of the segment of the WAM line, outlined by the thin dashed black line in part b. Sites 549 and 551 are projected onto the WAM line from ~2.8 km and ~1.5 km away, respectively. (d) Velocity structure derived from seismic refraction modelling (adapted from Bullock and Minshull, 2005). (e) The enlarged portion of the seismic profile in part b. It illustrates the shallower peridotite ridges and the deeper exhumed zone with subdued basement. (f) The expanded portion of the seismic profile in part b. It shows the variation in basement morphology in the exhumed domain and the hyperextended domains.

2.6.3 Crustal domain interpretation

As the WAM line lies within the region intersected by lines L1, L2, and L3, its interpretation is extrapolated to these other profiles. To ease identification of the boundary delineations between transitional subdomains T1 and T2, the WAM line and the four new seismic lines (L1-L4) are truncated to the same length to highlight the seismic reflection character within the transitional zones in Figure 2.7. Lines L1 and L2 cross magnetic Chron 34 and extend ~21 km and ~9 km seaward of magnetic Chron 34, respectively. Meanwhile, the seaward ends of seismic profiles L3 and L4 are ~6 km and ~54 km landward of magnetic Chron 34, respectively.

As introduced above, the boundary between the oceanic crust and the exhumed domain on the WAM line is based on crustal velocity constraints. By comparing the characteristics of basement topography and reflectivity of syn-rift sedimentary layers against the WAM line interpretation, the subdivisions of the exhumed domain along lines L1 and L2 are inferred (Figure 2.7, 2.9 and 2.10). West of the interpreted peridotite ridges (shaded dark green Figure 2.7b and 2.7c) lies the oceanic crust. The serpentinized peridotite ridges exhibit relatively sharp peaks on profiles L1 and L2, spanning ~16 km along L1 (Figure 2.7b and 2.9), and ~25 km along L2 (Figure 2.7c and 2.10). Landward, the peridotite ridges become shorter along both the WAM line and line L2 (Figure 2.7c and 2.7d).

In the exhumed domain on lines L1 and L2, sub-horizontal intra-basement reflectors are observed ~ 2.5 km below the top basement (red lines in Figure 2.9b and 2.10b, indicated by black arrows in expanded solid black boxes in Figure 2.9a and 2.10a, respectively), where the interpreted normal faults appear to root. These discontinuous intra-basement reflections are also visible in the exhumed mantle zone at Iberia-Newfoundland margins and the Armorican margin, and are interpreted as decoupling interfaces (Gillard et al., 2019). These intra-basement reflectors are used to identify the exhumed domain in this study.

Compared with the WAM line, on line L1, and line L2, the basement morphology outboard of the interpreted subdomain T2 on seismic profile L3 is more complicated due to the presence of a seamount and is more uncertain due to the lack of nearby velocity constraints. Nonetheless, since the sub-horizontal and landward-dipping intra-basement reflectors are also observed on the profile L3 (indicated by the black arrow in Figure 2.9a and 2.11b), we define the boundary between the oceanic domain and the subdomain T2 at the oceanward end of the intra-basement reflector, where the normal faults terminate (Figure 2.9a). Since the basement reflection patterns of the intervening T1-T2 transition segment (58-68 km in Figure 2.11) of line L3 fail to be completely consistent with the typical subdomain T1 or T2 described on the WAM line, the border between the two subdomains cannot be accurately defined, but is inferred to lie within the segment (Figure 2.7e and 2.11).

The exhumed domain interpretation of seismic profile L4 is described last because it is the least constrained as it is located 113 km to the south of L3, lying significantly landward of magnetic anomaly 34 (Figure 2.1b). Basement reflectivity along the southwestern half of profile L4 is less continuous and highly faulted, and the depth of the top basement along the segment is ~5.6 km, shallower than the top-basement depth (~6.5 km) of the oceanward northern profiles (L1-L3), possibly due to proximity to the complex stress field near the BTJ. Nonetheless, basement structures and geometry of syn-exhumation formations on both L3 and L4 are similar (Figure 2.8), which helps to constrain the extent of subdomain T2 along L4 (Figure 2.7, 2.8, and 2.12).

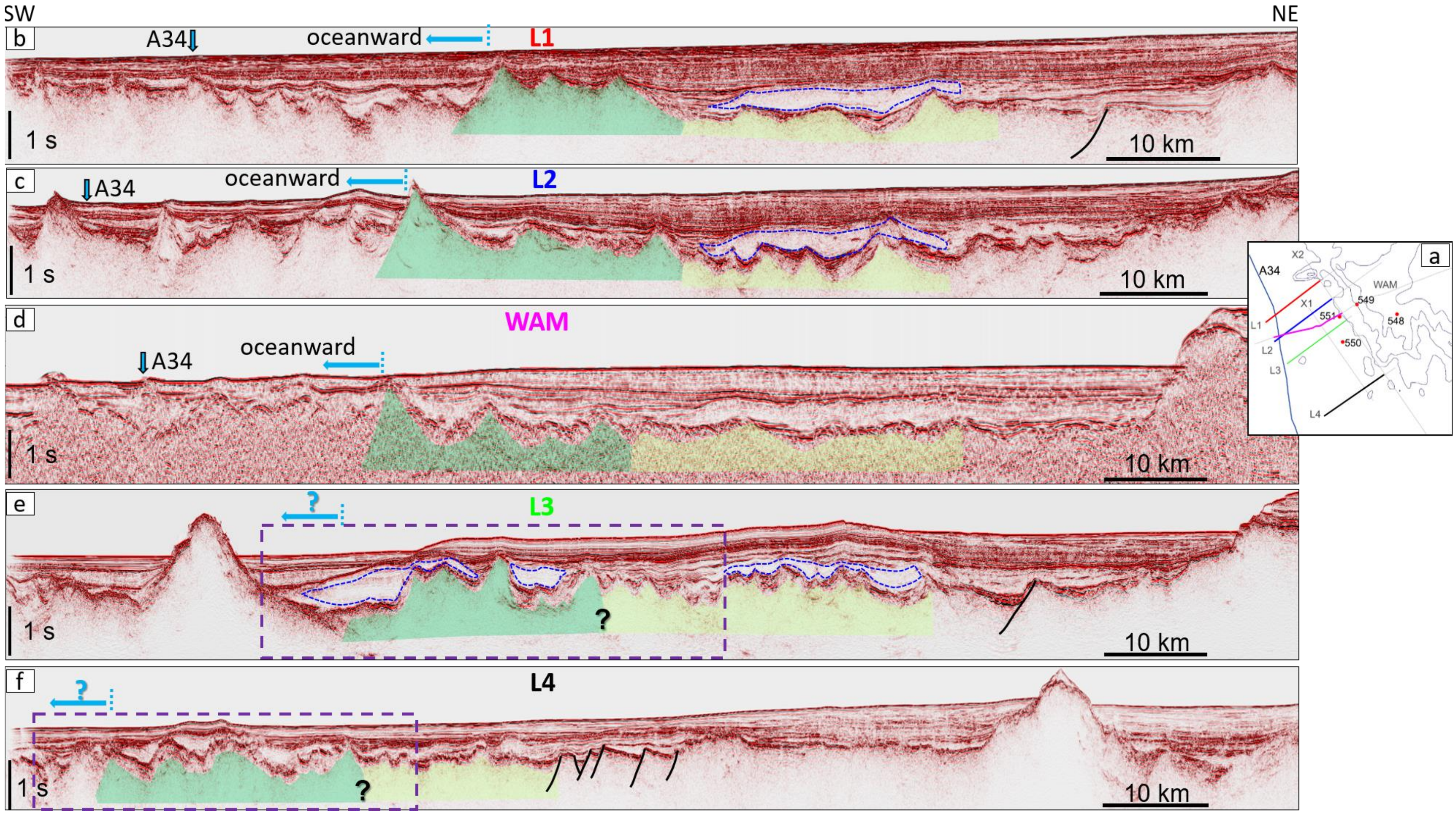

Figure 2.7: (a) The location of the parallel seismic lines as indicated by different line colors. (b)-(f) show the interpreted seismic lines L1, L2, the WAM line, L3, and L4 in the time domain, with label colors matching the line colors in part a. The transparent dark green areas indicate the interpreted serpentinized peridotite ridges with rougher shallow basement (subdomain T2). The light green regions correspond to the interpreted exhumed mantle displaying subdued topography at top-basement (subdomain T1). Faults (black solid lines) are also interpreted on sections L1, L3, and L4. The blue dashed regions roughly indicate geometries of the transparent/weakly reflective syn-exhumation sedimentary layers. The uninterpreted seismic lines are shown in Figure A.7 in Appendix A.

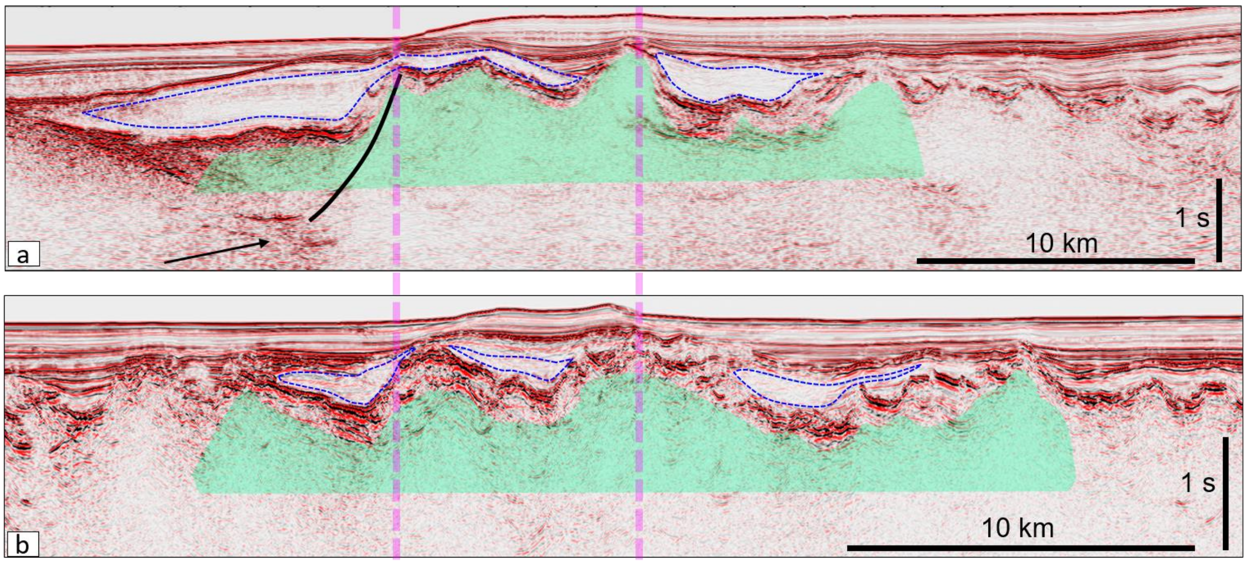

Figure 2.8: The upper and lower panels show the enlarged sections outlined in the dashed purple boxes in Figure 2.7e and 2.7f, respectively. The blue dashed regions roughly indicate geometries of the transparent/weakly reflective syn-exhumation sedimentary packages.

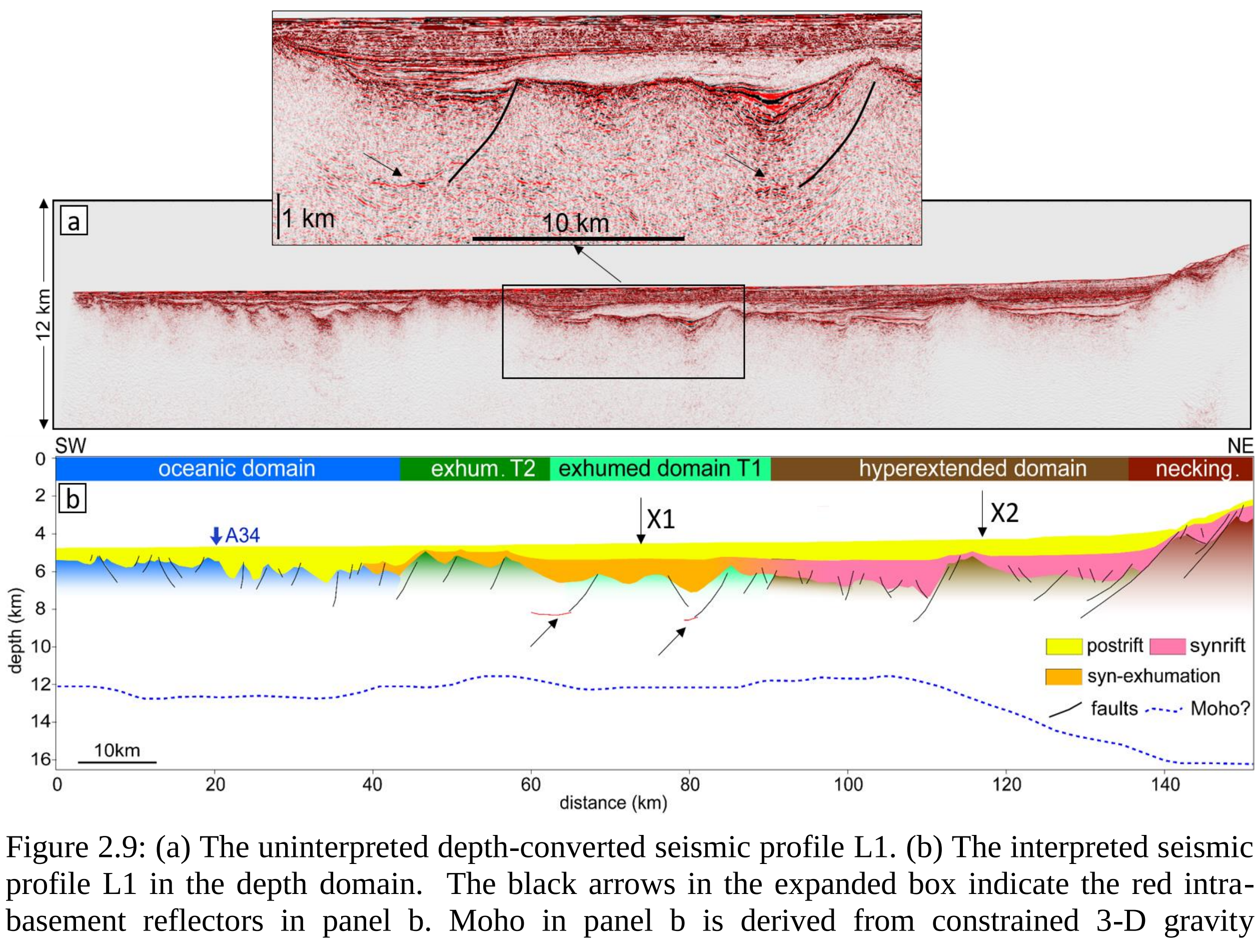

Figure 2.9: (a) The uninterpreted depth-converted seismic profile L1. (b) The interpreted seismic profile L1 in the depth domain. The black arrows in the expanded box indicate the red intra-basement reflectors in panel b. Moho in panel b is derived from constrained 3-D gravity inversion (Welford et al., 2010c).

On lines L1 to L4, the basement relief of transitional subdomain T1 (shaded light green) is generally smoother and deeper than that of transitional subdomain T2 (Figure 2.7). The width of the interpreted transitional subdomain T1 consistently ranges from between ~20 km and ~33 km along each of these seismic lines (Figure 2.7). In the transitional subdomain T1, the reflectivity in the syn-exhumation formations is strikingly weak, especially for lines from L1 to L3 (Figure 2.7).

The boundaries between the exhumed and hyperextended domains are delineated by contrasting basement structure and reflection patterns. The oceanward-dipping listric faults and continuously reflective sedimentary successions in the hyperextended sag basins are clear along lines L1, L3, and L4 (Figure 2.7b, 2.7e, and 2.7f). In addition, the concave downward continuous top-basement reflections transition into rugged disorganized reflections at the border of the two zones along lines L3 and L4 (Figure 2.7e and 2.7f). As for the border between the two domains along line L2, reflectors (indicated by the dash black line in the expanded yellow box in Figure 2.10a) probably also represent the contact between the hyperextended crust and exhumed serpentinized mantle, similar to the deep reflector along the WAM line (Figure 2.6f). Thus, the seaward limit of the reflector is interpreted as the landward edge of the exhumed mantle domain along L2 (Figure 2.7c and 2.10).

In this study, the two seismic crosslines, X1 and X2, are crucial for validating crustal domain subdivisions and ensuring regional consistency in the interpretations. By comparing the reflection patterns along L2 and L3, the region spanning ~ 60 km to the northwest along X1 is certainly defined as the exhumed mantle domain since all three lines show striking transparent syn-exhumation layers (Figure 2.7 and 2.13). In terms of the border between the exhumed and hyperextended domains along X1, it is roughly defined at ~ 70 km by taking two aspects into account. The first is the negative flower structure observed across distances of 80 ~ 90 km (expanded box in Figure 2.13a). The second is the oceanward-dipping reflectors (indicated by the black arrows in the expanded box in Figure 2.13a) that may be similar to those observed along line L2 (expanded in the yellow box in Figure 2.10a), representing the oceanward limit of the hyperextended zone. Since the reflection patterns appear to be consistent and Moho depth shows limited variation (12.5 ~ 14.5 km) to the southeast of X1, the remaining part of the line is interpreted as the hyperextended domain (Figure 2.13).

Along X1, the transparent syn-exhumation layer in the exhumed domain appears to be laterally consistent over a distance of 60 km and gradually pinches out towards the hyperextended domain (Figure 2.13). Towards the southeast, the basement reflectors become shallower and more chaotic in the transitional domain (~ 65-75 km along line X1) from the exhumed domain to the hyperextended domain (expanded box in Figure 2.13). According to the interpretation of sill distribution from PAD (Figure 2.4b), magmatic activities occur in the transitional zone (~ 65-75 km, around the light green circle along line X1 in Figure 2.4b), which may be responsible for the formation of more chaotic basement reflectors. In addition, the magnetic anomalies in the region show the transition from positive to negative (Figure 2.4b).

Compared with seismic profile X1, profile X2 is about 167 km longer and was acquired closer to the continental shelf (Figure 2.1b). Along the southeastern portion of the profile X2, both the hyperextended and exhumed mantle zones span approximately 40 km (Figure 2.14), interpreted on the basis of a northward extrapolation of the crustal domains from the north Bay of Biscay margin interpreted by Tugend et al. (2015).

In addition to relying on seismic characteristics, gravity inversion results from Welford et al. (2010c) are also used to define the boundary between the hyperextended and necking zones.

Along L2, in addition to the shallowing Moho depth in the necking zone, the sag structure (black oval circle in Figure 2.10a) and wedge-shaped blocks (dashed black box in Figure 2.10a) help to roughly define the border between the two zones at ~ 140 km. However, profiles L1 and L3 do not extend landward enough to adequately capture the necking zone, impeding the interpretation of the boundary between the two domains. Conveniently, profile X2 intersects seismic profiles L1, L2, L3, L4, and the WAM line (Figure 2.1b). The necking zone is interpreted based on the decreasing Moho depth, spanning a distance of ~130-250 km along X2 (Figure 2.14b). To the northwest of the necking zone along X2, the reflection patterns at the top basement are laterally consistent and the Moho depth is relatively smooth. Furthermore, the intersection point of L2 and X2 falls into the hyperextended domain from the interpretation of L2 above. Thus, the northwestern portion of X2 is interpreted as the hyperextended domain (Figure 2.14). Then, the landward edges of the hyperextend zones along L1 and L3 are located inboard of X2 since the intersections of L1 and X2, L3 and X2 fall into the hyperextended zone of X2 (Figure 2.9, 2.11, and 2.14). It is found that the Moho depth of the interpreted hyperextended zone of L1 to L3 ranges from ~ 16 km to ~10 km, with crustal thickness less than 10 km (Figure 2.3b and 2.9-2.11). For regional consistency, the border between the hyperextended and necking zones along L4 is placed at ~90 km, where the Moho depth and crustal thickness are approximately 16 km and 10 km, respectively (Figure 2.3b and 2.12). In addition, the prominent continuous high-amplitude reflectors at the top basement within the continental crust along profiles X2 and X1 display similar features (Figure 2.15), and are both interpreted as the hyperextended crust (Figure 2.13 and 2.14).

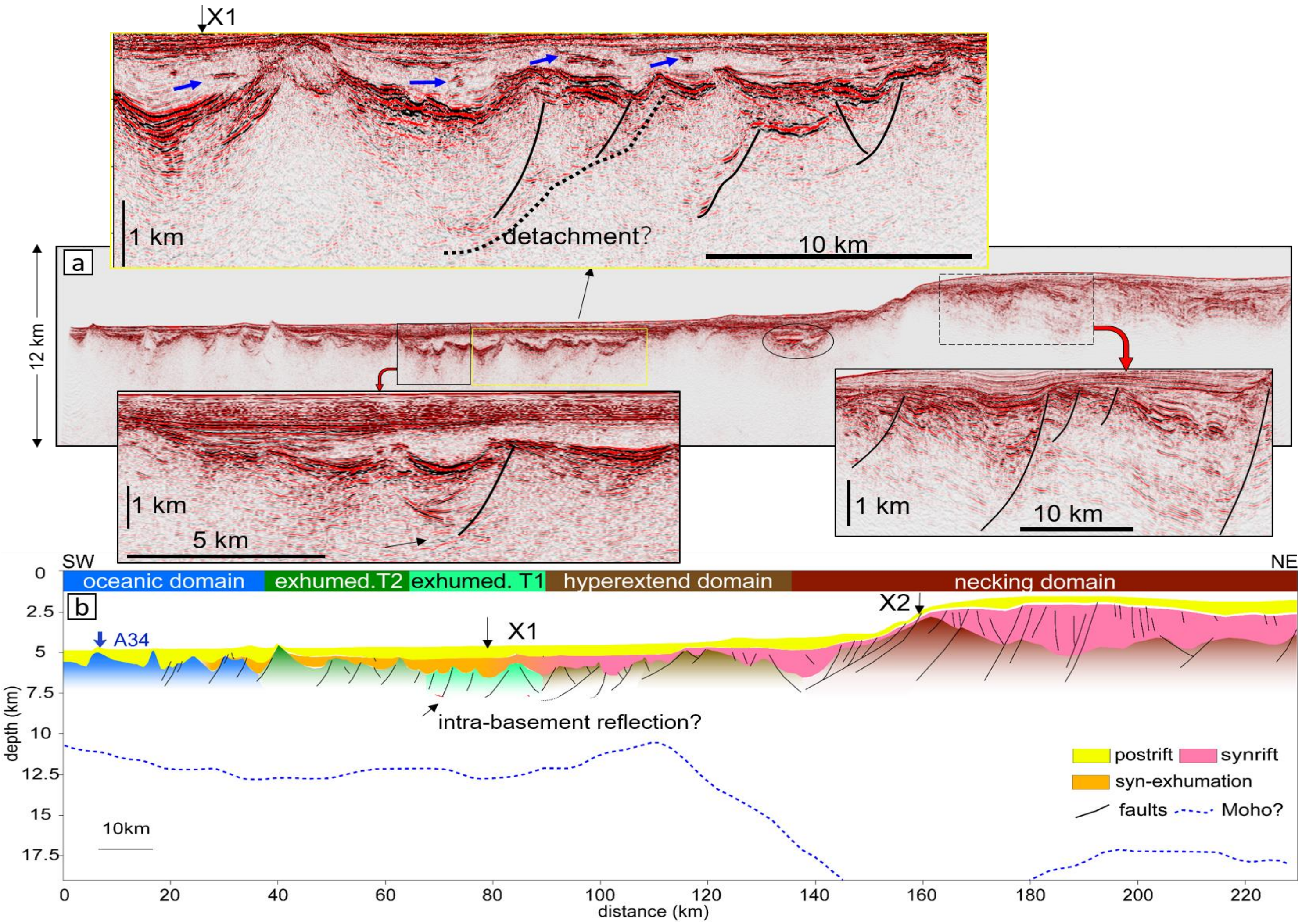

Figure 2.10: (a) The uninterpreted depth-converted profile L2. (b) The interpreted profile L2 in the depth domain. The blue arrows indicate sills (?) in the yellow expanded box. The intra-basement reflection (?) is indicated by the arrow in the expanded solid black box.

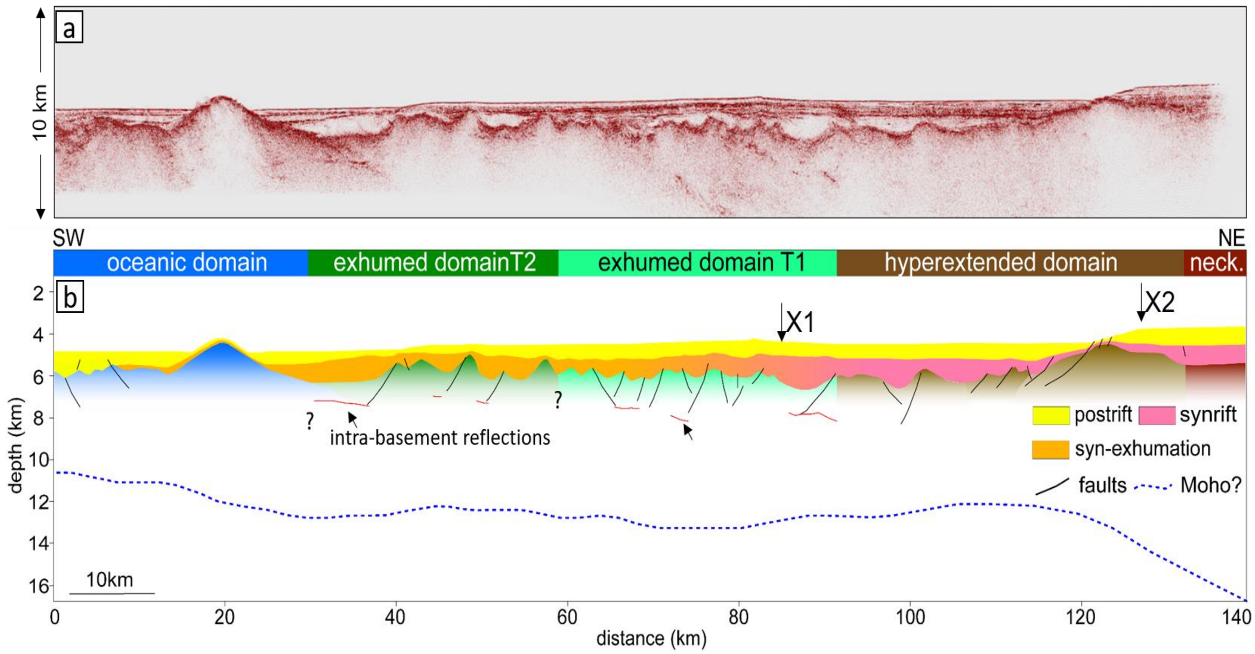

Figure 2.11: (a) The uninterpreted depth-converted seismic profile L3. (b) The interpreted seismic profile L3 in the depth domain.

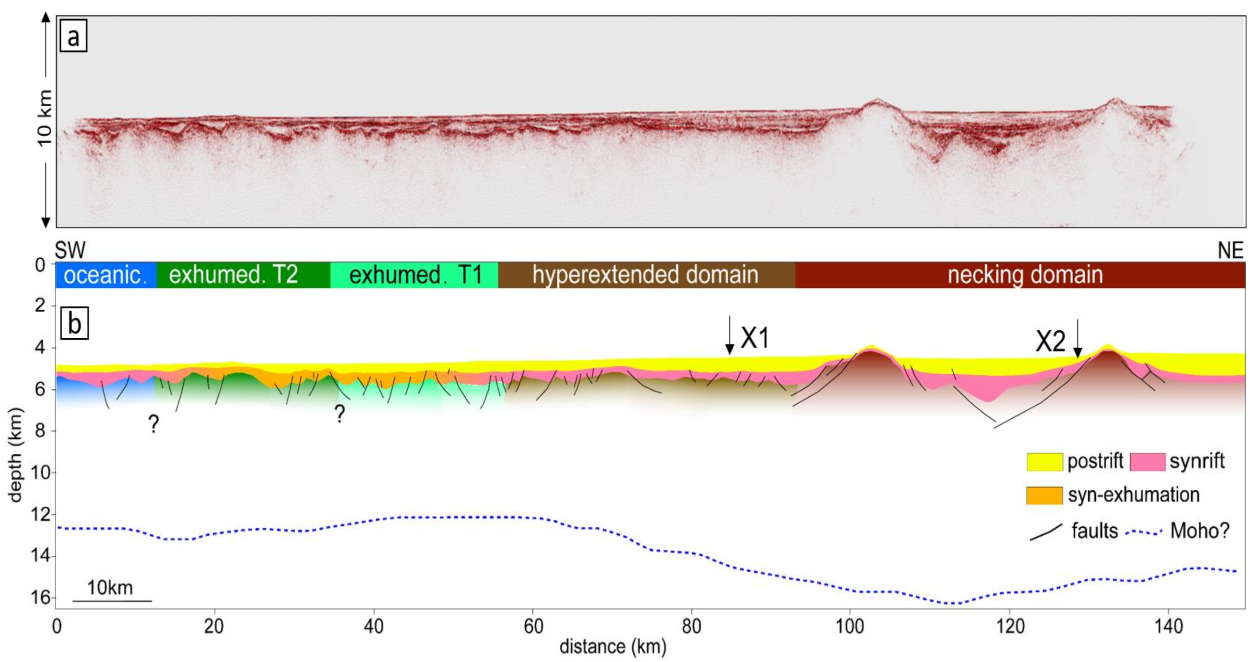

Figure 2.12: (a) The uninterpreted depth-converted seismic profile L4. (b) The interpreted seismic profile L4 in the depth domain.

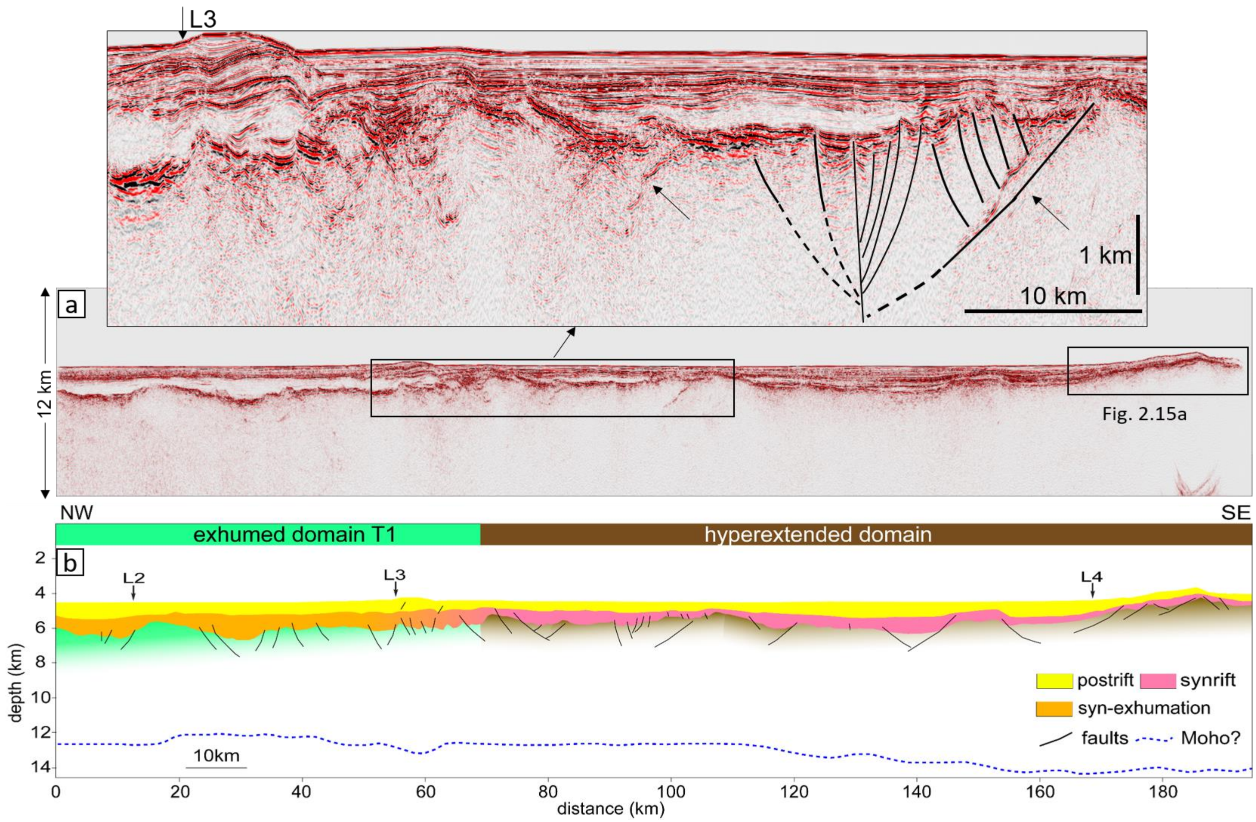

Figure 2.13: (a) The uninterpreted depth-converted seismic profile X1. Expanded box above panel a shows an interpreted flower structure. The arrow indicates the detachment fault (?), similar to that in the expanded yellow box in Figure 2.10. (b) The interpreted seismic profile X1 in the depth domain.

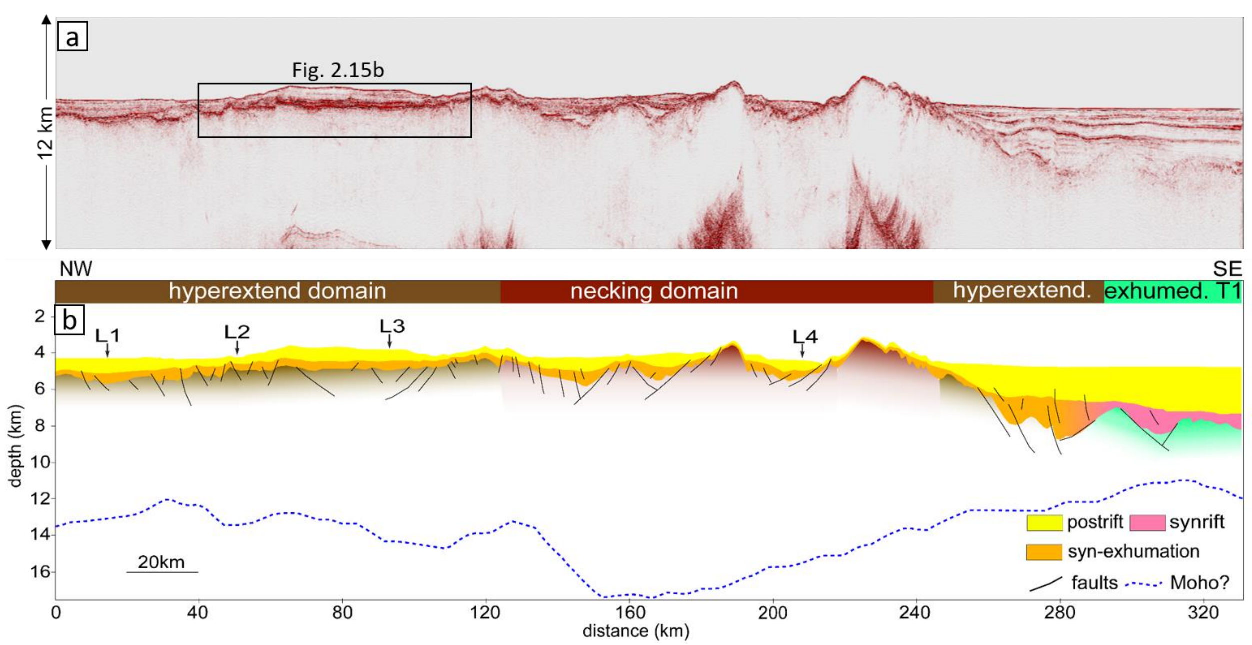

Figure 2.14: (a) The uninterpreted depth-converted seismic profile X2. (b) The interpreted seismic profile X2 in the depth domain.

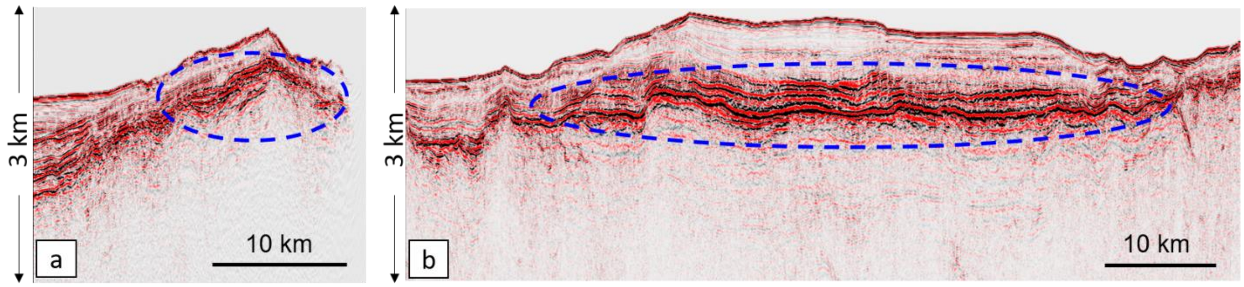

Figure 2.15: (a) The expanded seismic section of the black box shown in Figure 2.13 and (b) the expanded seismic section of the black box shown in Figure 2.14. The blue circles show anomalously strong-amplitude reflectors at the top basement.

2.7 Discussion

2.7.1 Crustal architecture

The interpretations presented for the new seismic profiles (Figure 2.7 to 2.14) have allowed us to map the crustal architecture across the Goban Spur margin (Figure 2.16). The newly constrained crustal domains are complemented by interpreted domains from the surrounding regions derived from gravity inversion (Welford et al., 2010c; Tugend et al., 2015; Sandoval et al., 2019). The landward extent of the new seismic lines into the stretched continental crust is limited, so the rift-related structures (thrusts, normal faults, and transfer faults) from PAD are used to depict structures in the continental domain (Figure 2.16). CM multichannel seismic profiles (white lines shown in Figure 2.1b) are also used to help validate our interpretation (Masson et al., 1985), although the data quality is much poorer. Constraints in the south are fewer than to the north, so many uncertainties remain for understanding the southern part of the margin. It is also noted that the boundaries between the crustal domains are much more diffuse than depicted, as reactivation of structures during subsequent rifting stages has likely happened over the tectonic evolution of the margin (Péron-Pinvidic and Manatschal, 2009). Nonetheless, the crustal architecture map in Figure 2.16 still significantly increases our regional knowledge of the Goban Spur margin structure.

2.7.1.1 Proximal domain

The proximal domain across the Goban Spur margin experienced limited extension, characterized by normal faults (Figure 2.16) (Naylor et al., 2002), which is similar to many other rifted continental margins, such as Iberia-Newfoundland, and the mid-Norway-East Greenland rifted margins (Péron-Pinvidic et al., 2013). The seaward limit of the proximal zone is in agreement with the WAM line interpretation (Peddy et al., 1989), the only seismic line extending into the proximal domain in this study (Figure 2.6). The formation of the proximal zone corresponds to the initial lithosphere stretching during the late Paleozoic and early Mesozoic, accompanied by regional faulting, forming half-grabens and horsts (de Graciansky and Poag, 1985).

2.7.1.2 Necking domain

The necking zone is divided into three subdomains according to their crustal thicknesses (Welford et al., 2010c; Figure 2.3), as defined and color-coded by Sandoval et al. (2019). The crustal thicknesses for necking domains 1, 2, and 3 range from ~21 km to ~16 km, from ~16 km to ~12 km, and from ~12 km to ~ 9 km, respectively. The oceanward boundary of the subdomain necking zone 3 is also constrained by the interpreted hyperextended region. Along strike of the Goban Spur margin, the width of each necking subdomain is highly variable from northwest to southeast. Since the extension rate has an impact on the final structure of passive rifted margins (Tetreault and Buiter, 2018), the highly variable geometry of each subdomain of the necking zone at the Goban Spur may be associated with differential extension rates, the original crustal compositions, and rheology. It has been postulated that the limit of the seaward-thinning continental crust corresponds to a coupling point, separating decoupled deformation between the crust and mantle (continentward) from coupled deformation (oceanward) from a lithospheric rheology perspective, according to Pérez-Gussinyé et al. (2003). The differential stretching in the necking zone may result from rheologically-governed detachment structures overlying the lower crust facilitating greater extension of the upper and middle crust, as has been proposed for the Porcupine Basin (Naylor et al., 2002). Two major orientations of faulting control the structural patterns within the necking zone: NW-SE trending normal faults and NE-SW faults. The former are approximately parallel to the strike of Goban Spur, as shown in the fault interpretation in the necking zone of X2 (Figure 2.14). The latter are approximately perpendicular to the margin strike (Dingle and Scrutton, 1979), aligned with the interpretation of line L2 (Figure 2.10).

2.7.1.3 Hyperextended domain

The parallel-margin hyperextended region is deduced by both seismic data interpretation and gravity inversion results, consisting of a belt of slightly variable width along the strike of the Pendragon Escarpment (Figure 2.1b). Crustal thickness in the hyperextended zone is less than ~ 10 km (Figure 2.3b). From north to south, the magnetic anomaly transitions from negative to positive in this region (Figure 2.4b). Margin-parallel variations in the width of the hyperextended continental crustal domain may have been influenced by an interpreted transfer fault close to Sites 548 and 550, across which the deformation changes from ENE-WSW to NE-SW. The pre-existing Variscan orogenic fabrics may also have contributed to shaping the present-day configuration of the proximal to hyperextended crustal domains (Dingle and Scrutton, 1979). Possible transtensional tectonic movement may also have occurred between the northern and southern portions of the margin based on the presence of interpreted flower structure along X1 (Figure 2.13).

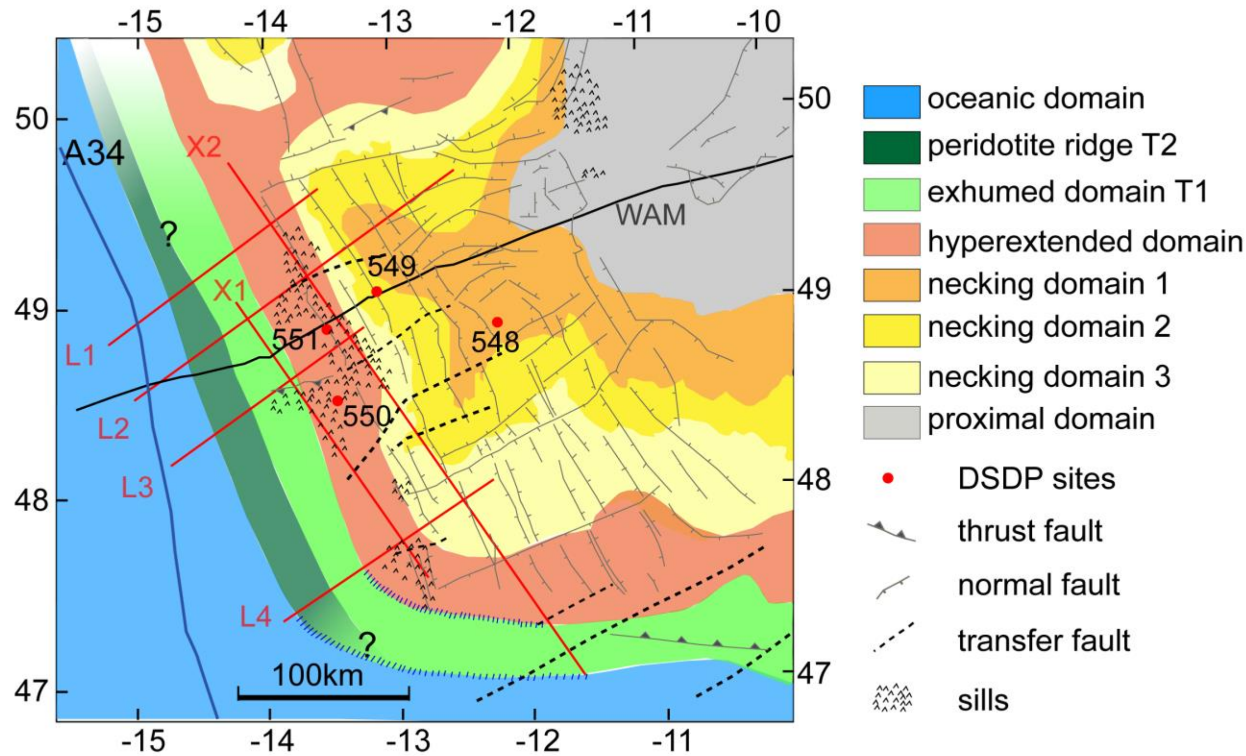

Figure 2.16: Crustal architecture of the Goban Spur margin. The dark blue line indicates magnetic Chron 34 (Müller et al., 2016). Seismic profiles are plotted in red (L1, L2, L3, L4, X1, and X2), and in black (WAM line). Crustal domains interpreted beyond the new seismic coverage are constrained from gravity inversion results (Welford et al., 2010c; Tugend et al., 2015; Sandoval et al., 2019). The hash pattern indicates ill-constrained boundaries between the crustal domains.

2.7.1.4 Exhumed mantle domain

The identification of the exhumed mantle domain across the Goban Spur margin is primarily based on seismic velocity constraints and the reflectivity characteristics on the seismic profiles, and how they compare with seismic reflection data on the southern Flemish Cap margin, as shown in Figure 2.5. This domain is primarily composed of serpentinized mantle peridotite and shows a velocity structure that smoothly increases with depth (Figure 2.6d), suggestive of a decreasing degree of serpentinization with depth (Bullock and Minshull, 2005). Nonetheless, in the seaward portion of the exhumed mantle domain, the basement rocks may have diverse compositions and are generally hypothesized to include: oceanic crust, continental crust, serpentinized mantle peridotite, or hybrid crust composed of any of these (Welford et al., 2010a;

Péron-Pinvidic et al., 2013). In addition, some discontinuous intra-basement reflectors are observed in the region (Figure 2.9-2.11), likely acting as a rheological interface that plays a critical role in localized deformation during exhumation and serpentinization (Gillard et al., 2019). The magnetic anomaly is relatively weak and discontinuous in this domain (Figure 2.4b). Magmatic additions may also occur in this domain, indicated by the observation of sills along L2 and L3 (enlarged sections in Figure 2.10). As introduced previously, we divide the exhumed domain into two subdomains to better characterize the margin (Figure 2.16).

1) Subdomain T1

The transition of top-basement seismic facies from concave downward to convex upward reflections (Figure 2.7), and extensional detachments (expanded boxes in Figure 2.10 and 2.13) helps to define the landward limit of the subdomain T1. This region, juxtaposed landward against the hyperextended domain, shows deep and smooth basement relief (Figure 2.7). The low relief reflective surface at the exhumed basement is interpreted as either a detachment surface allowing for continental crust exhumation (Whitmarsh et al., 2001), or the exhumed serpentinized mantle itself (Sutra et al., 2013). Along strike of the margin, the width of the interpreted subdomain T1 slightly decreases to ~ 22 km to the southeast. At the southeastern limit of the margin, the width of the transitional subdomain T1 averages ~ 40 km, narrower than the equivalent domain along the north Bay of Biscay margin (Tugend et al., 2015).

2) Subdomain T2

Subdomain T2 is characterized by a series of margin-parallel peridotite ridges with shallow and rough basement relief (Figure 2.7). This subdomain lies between the oceanic crust and the transitional subdomain T1. The relief of the basement becomes rougher and higher from the subdomain T1 to the subdomain T2 (Figure 2.7). The change in basement morphology may suggest a time-dependent rheological change during the exhumation stage (Sibuet and Tucholke, 2012). In addition, from Figure 2.7, it can be seen that the basement topography in the T2 subdomain contains three clear serpentinized ridges and shows consistent ridge geometries on the WAM line, L1, and L2. However, the shape of the peridotite ridges becomes more irregular on L3 and L4, with a rougher basement. The diversity of ridge morphologies is probably due to increased igneous addition towards the south portion of the margin due to its proximity to the BTJ. Due to the limitations of 2D seismic data and the absence of borehole data, the geometry, composition, internal structure, and the formation of the basement ridges has been unclear until now.

It is difficult to map the along-strike continuation of the exhumed domain due to the absence of seismic constraints. Since the segments of the subdomain T1 and T2 along L1 are ~ 5 km wider and ~ 9 km narrower than they are along L2, respectively (Figure 2.7), the subdomains T1 and T2 are inferred to become slightly wider and narrower to the north, respectively. The basement ridges of the subdomain T2 are not observed in the exhumed domain to the southeast along X2, thus, we assume that the subdomain T2 gradually diminishes (or disappears?) to the southeast of line L4 (Figure 2.16). Despite the uncertainties in the interpreted geometres of the two exhumation subdomains along the margin, their consistent presence along strike of the margin implies a regionally significant non-uniform exhumation stage.

2.7.1.5 Oceanic domain

Seaward of the interpreted peridotite ridges lies the oceanic crust domain, formed through seafloor spreading. Because of relatively dense constraints (L1, L2, L3, and the WAM line), the interpreted oceanic domain geometry along the northern part of the margin is more robust than it is for the southern part. The border between the exhumed mantle domain and the oceanic domain diverges from magnetic Chron 34 towards the south of the margin. By calculating basement roughness of the initial oceanic zone along both the Flemish Cap and Goban Spur conjugate margins, Sauter et al. (2018) argue that this conjugate pair represents typical slow asymmetric seafloor spreading, consistent with the results from Bullock and Minshull (2005).

2.7.2 Syn-exhumation stratigraphic sequences

In the literature, three main stratigraphic sequences are identified on the Goban Spur: post-rift, syn-rift, and pre-rift sequences (Scrutton, 1979; Masson et al., 1985; de Graciansky and Poag, 1985). Based on the results from drilling site 549 (Figure 2.2), the post-rift sequence spans from present-day to Albian, and the syn-rift ranges from Barremian (Hauterivian?) to Aptian. As for the pre-rift basement, it experienced multiple tectonic events, resulting in not only rough basement relief with rotated and tilted horsts and grabens, but also complex compositionally diverse basement rocks (de Graciansky and Poag, 1985). However, based on the new seismic lines in this study, it is observed that the reflections within the syn-rift formations are relatively continuous and clear for hyperextended domains, while syn-rift sedimentary successions typically appear very weak and often transparent above the top basement of the exhumed domain (Figure 2.6f and 2.7). These sedimentary layers in the exhumed domain are associated with mantle exhumation, so they are termed syn-exhumation sediments as introduced in section 2.6.2. The syn-exhumation sequences are deposited during the transition from the termination of the hyperextended stage to the initiation of seafloor spreading (Péron-Pinvidic et al., 2013). They are still considered syn-rift sequences as mantle exhumation is one of the rifting stages prior to final lithospheric breakup.

Considering the distinctive reflectivity characteristics of sedimentary formations during the evolution of the margin, we have subdivided the sedimentary layers into three parts in this study: syn-rift, syn-exhumation, and post-rift sequences. Due to the lack of drilling data towards the oceanic crust, the three sequences are mainly defined based on reflection characteristics. The post-rift sedimentary layers are parallel or sub-parallel, and have undergone little or no major tectonic movement (Figure 2.7-2.15). The syn-rift sediments deposited in the grabens and the wedge-shaped half-grabens in the continental crust (Figs. 2.7 and 2.10), created from the rotation of faulted blocks in the underlying basement (Scrutton, 1979). The thicknesses of syn- and post-rift sequences are highly variable both along and across the strike of the margin (Figure 2.7-2.15). Likewise, the thicknesses of the transparent syn-exhumation layers show striking variations both parallel and perpendicular to the margin. The syn-exhumation sequences reach about 0.8 s in thickness in the subdomain T1 along L1 and L2 (Figure 2.7b and 2.7c). Along L3, the transparent layer disappears above the transition from subdomain T1 to T2, and reappears above the peridotite ridges (Figure 2.7e). It gradually disappears to the southeast along the X1 profile (Figure 2.13). On lines L1, L2, L3, and the WAM line, sag-type syn-exhumation sequences are observed above the top exhumed basement (Figure 2.7). The formation of this sag architecture may result from a higher sedimentation rate than the exhumation rate, similar to the case for Australian-Antarctic magma-poor rifted margins where the sag geometries of sedimentary layers of above the exhumed basement are also observed (Gillard et al., 2015). The difference is that reflectivity is transparent/weak at the former margin, while it is continuous and clear at the latter margin (Gillard et al., 2015).

Interestingly, the low reflectivity characteristics within the syn-exhumation layers are not readily observed at other magma-poor margins. There is a possibility that automatic gain control (AGC) has been used on the seismic data at some margins to balance amplitudes, whereas the new seismic lines in this study are displayed using true amplitudes as the processing procedures are amplitude-preserving. Magmatic additions are one potential component of syn-exhumation sedimentary packages at the Goban Spur (expanded box in Figure 2.10). However, the compositions and origin of syn-exhumation sediments are still unclear due to the lack of similar observations on other margins and the lack of drilling data.

2.7.3 Magmatism on the non-volcanic/magma-poor Goban Spur margin

Based on an interpreted depth-uniform extension of the lithosphere across the Goban Spur margin (Peddy et al., 1989), Bullock and Minshull (2005) propose that the basaltic material observed along the WAM line in the necking zone was extruded due to decompression melting prior to mantle exhumation. At Site 550, located in the exhumed mantle domain, basaltic pillow lavas were also recovered. According to previous interpretations (Naylor et al., 2002), the areal extent of sills along the northern Goban Spur margin appears much larger than that along the southern margin, and intrusive and extrusive basaltic bodies appear to be distributed across the necking, hyperextended, and mantle exhumation zones (Figure 2.16). This suggests that magmatic events were occurring during rifting, thinning, mantle exhumation, and final continental breakup along the Goban Spur margin. Furthermore, magmatic layers in the exhumed and hyperextended domains along L2 (the blue arrows in the expanded yellow box in Figure 2.10a) illustrate that the region of sills across the Goban Spur may be larger than that previously interpreted by PAD. The distribution of sills across the margin does not appear to correspond to regions with localized high magnetic anomalies (Figure 2.4b), noting that some magnetic anomalies may be associated with serpentinization at the Goban Spur margin (Minshull, 2009). In addition, the igneous bodies appear to be distributed close to the transfer faults that represent tectonic weaknesses in the continental crust (Scrutton et al., 1979) and these faults may provide channels for lava flow migration during margin evolution.

2.7.4 Reconstruction of the Goban Spur and its conjugates

In Figure 2.17, the crustal architecture across the Goban Spur margin from this study and the crustal architecture across the “conjugate” northeastern margin of Flemish Cap from Welford et al. (2010b) are mapped using a rigid plate reconstruction, back to the onset of seafloor spreading using GPlates 2.1 at 83 Ma (Müller et al., 2016). In order to compare the two margins consistently, the stretched crust interpreted along the Flemish Cap margin is assumed to correspond to the necking and hyperextended zones along the Goban Spur margin.

At the Goban Spur, the necking zone is of variable width ranging from ~ 114 km to ~200 km, indicating along-strike variability in lithosphere thinning. In contrast, although the boundary between the necking and hyperextended domains is not clearly defined along the Flemish Cap margin, the width of the necking domain is much narrower (< ~20 km; Welford et al., 2010b), indicating a more abrupt necking of the crust. In addition, the along-strike exhumed serpentinized mantle domain of the Goban Spur margin spans a much wider (~ 42 - 60 km) area while it is much narrower (~25 km) at the northeastern Flemish Cap margin (Welford et al., 2010b). In the exhumed domain, only peridotite ridges are observed at the Flemish Cap (Welford et al., 2010b), while both peridotite ridges (subdomain T2) and a wide region of exhumed mantle with deeper basement (subdomain T1) are observed at the Goban Spur.

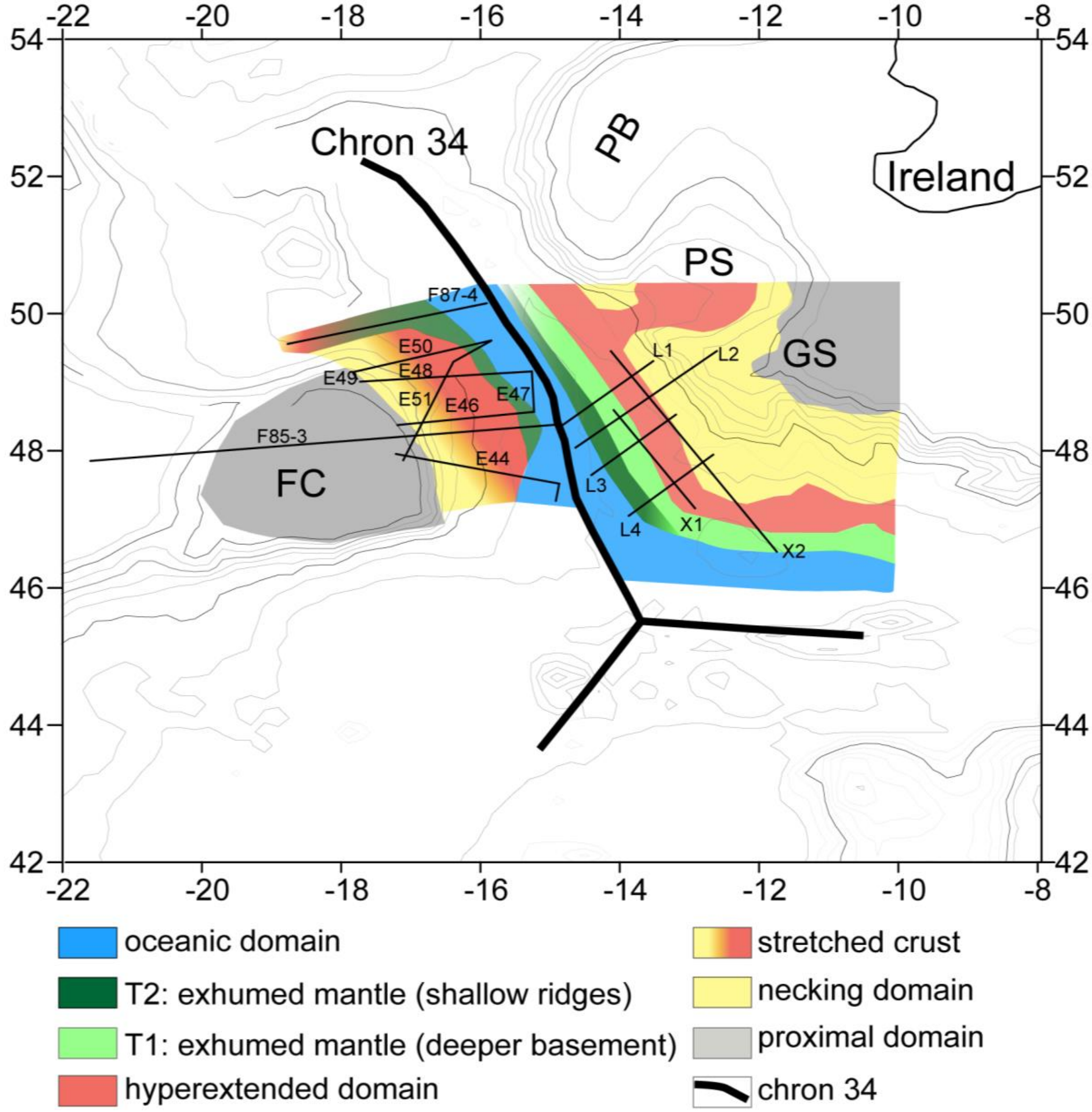

Figure 2.17: Crustal architecture across the northeastern Flemish Cap-Goban Spur margins, reconstructed to magnetic Chron 34 at 83 Ma (thick black line from Müller et al., 2016) using a rigid plate reconstruction in GPlates 2.1 (Müller et al., 2016), overlain by the corresponding bathymetric contours (thin grey lines) at 83 Ma. The crustal domains across Flemish Cap are adapted from Welford et al. (2010b). Labelled thin black straight lines show seismic profiles constraining the crustal architecture interpretations. Abbreviations: FC, Flemish Cap; GS, Goban Spur; PS, Porcupine Seabight Basin; PB, Porcupine Bank.

Overall, the highly variable geometry of each crustal type across the “conjugate” pair is consistent with asymmetric evolutionary mechanisms as hypothesized by Gerlings et al. (2012). However, based on seismic interpretation, Welford et al. (2010b) identified both extensional and strike-slip deformation along the northeastern Flemish Cap margin, consistent with the interpreted rotation and displacement of Flemish Cap with respect to the Orphan Basin during the early Cretaceous period through seismic and potential field data analysis (Sibuet et al., 2007) and more recently deformable plate tectonic reconstructions (Peace et al., 2019). In contrast, the Goban Spur margin experienced mostly margin-perpendicular extension. In addition to the geometric differences in crustal architecture, velocities (> 7 km s^{-1} at depth) in subdomain T2 at the Goban Spur differ from those (7.4-7.9 km s^{-1}) at depth in the serpentinized mantle domain at the northeastern Flemish Cap margin, which may also reflect different degrees of serpentinization (Bullock and Minshull, 2005; Gerlings et al., 2012).

To date, there have been many strikingly different geological and geophysical characteristics (e.g., P-wave velocities, crustal architecture, tectonic deformation mechanism, crustal thickness, etc.) observed across the northeastern Flemish Cap margin and the Goban Spur margin (de Graciansky and Poag, 1985; Keen et al., 1989; Welford et al., 2010b; Gerlings et al., 2012). The mechanism for generating asymmetric features across the two margins is still unclear, suggestive of a more complex model than previously thought for the Goban Spur margin and its possible conjugates. These differences between the two margins also calls into question the widely-accepted "conjugate" relationship since the conjugate margins generally share some common features (Reston, 2009).

As introduced before, the geometries of the peridotite ridges in the serpentinized exhumed domain at the Goban Spur margin are similar to those observed at the west Iberia margin (Dean et al., 2000). The Goban Spur was adjacent to the Iberia margin (specifically, the Galicia Bank) at 200 Ma prior to rifting according to new kinematic evolution models (Nirrengarten et al., 2018; Peace et al., 2019; Sandoval et al., 2019). If so, the prominent asymmetries recorded along both the Goban Spur and Flemish Cap would have resulted from the motion and southward migration of the Flemish Cap (Sibuet et al., 2007; Welford et al., 2010c; Welford et al., 2012; Peace et al., 2019), or, at the least, oblique rifting (Brune et al., 2018). Superimposed on these plate motions, the variable widths of each of the crustal domains across the two margins may also reflect highly variable rifting rates. At the Goban Spur, lower mantle temperatures are supported by geochemical models, suggestive of relatively slower rifting than along other northern Atlantic margins (Dean et al., 2009). Meanwhile, inferred complexities in the tectonic processes along the northeastern Flemish Cap margin also make it difficult to determine the rifting rate. In spite of these discrepancies and uncertainties, the crustal architecture comparison between the two margins provides insightful constraints for unraveling the margin evolution.

2.8 Summary

Six new multichannel seismic reflection profiles, integrated with previous seismic reflection and refraction data, magnetic and gravity data, and DSDP drilling sites, for the Goban Spur magma-poor rifted margin have revealed the following:

(1) Five distinct crustal domains related to different rifting stages are identified and their regional extents are evaluated, significantly increasing knowledge of the crustal architecture of the Goban Spur rifted continental margin.

(2) Along strike, the width of the necking domain on the Goban Spur margin gradually increases from northwest to southeast, suggesting along-strike variations in extension, likely related to the variable pre-existing rheological architecture across the Goban Spur margin.

(3) In the northwest, the exhumed domain consists of shallower peridotite ridges (transitional subdomain T2) and deeper exhumed serpentinized mantle (transitional subdomain T1). The different styles of mantle exhumation are inferred to reflect different exhumation rates. Toward the southeast along the Goban Spur margin, the zone of serpentinized peridotite ridges is tentatively interpreted to diminish or disappear.

(4) During the evolution of the Goban Spur continental margin, localized syn-rift magmatism occurred during lithosphere stretching, thinning, subsequent hyperextension and serpentinized mantle exhumation, and final lithosphere rupture, all prior to seafloor spreading initiation.

(5) The striking asymmetries between the Goban Spur margin and its "conjugate" margin, the northeastern Flemish Cap margin, call into question the conjugate relationship between the two margins.

Future work involving the restoration of the margins using deformable plate reconstructions will help resolve this debate. Such research will help unravel the geological significance of the Goban Spur during opening of the southern North Atlantic Ocean, which led to the separation of the Irish, Newfoundland, and Iberian margins.

Acknowledgement

We are grateful to the Department of Environment, Climate and Communications of Ireland for providing the multichannel seismic reflection data. WAM data were acquired by the UK NERC BIRPS programme in 1985. Great thanks are also given to Schlumberger for donating Petrel software to Memorial University. AP's postdoctoral fellowship at Memorial was funded by the Hibernia Project Geophysics Support Fund and Innovate NL. We would like to thank the members of the Memorial Applied Geophysics for Rift Tectonics (MAGRiT) group for providing suggestions for this research.

Chapter 3

3. Investigating the Porcupine Atlantic margin, offshore Ireland, through integration of new seismic reflection and gravity data

This chapter is published as "Yang, P., & Welford, J.K., 2021. Investigating the Porcupine Atlantic margin, offshore Ireland, through integration of new seismic reflection and gravity data. Tectonophysics, 807, 228809. doi.org/10.1016/j.tecto.2021.228809." Kim Welford helped to supervise the research, shape the ideas, and provide editorial guidance.

3.1 Abstract

While the offshore Irish Atlantic margin and related rift basins have been intensively studied for several decades, the Porcupine Bank, straddling between the well-studied Porcupine and Rockall basins, is a poorly understood region due to lacking sufficient geophysical data coverage. In this study, ten newly acquired long-offset multichannel seismic profiles extending across the western Porcupine Bank margin, combined with potential field data, are used to investigate the crustal architecture, tectonic history, and rift-related magmatism along the margin. Significant margin-parallel and margin-perpendicular structural variations are observed and these are used to map the crustal architecture in terms of rifted margin domains. In the transitional zone between continental and oceanic crust, both peridotite ridges with shallow reflective basement and exhumed serpentinized mantle with deeper and smoother basement are

interpreted, similar to the conjugate Iberian and Newfoundland margins, as well as further south at the Goban Spur margin. In addition to inferred variations in extension rate during poly-phased rifting episodes, the reactivation of pre-existing inherited Caledonian and Variscan structural fabrics are proposed to have influenced the variable geometries and distributions of the crustal domains along the Porcupine Atlantic margin. Northwestward increasing volcanism and related reflectivity patterns support the transition from magma-poor rifting in the southeast to magma-rich rifting in the northwest. Rigid plate reconstructions of the Irish Atlantic and the Newfoundland margins, particularly involving the Flemish Cap, back to the Early Campanian period, show asymmetric rifting and final continental breakup migrating toward the Porcupine Bank region. This asymmetry is possibly due to oblique extension between the two margins, and/or oblique deformation on the Porcupine Bank side due to its rotation during the opening of the Porcupine Basin.

3.2 Introduction

The Irish Atlantic margin has been the focus of geoscientific research for decades as it records the poly-phased rifting episodes from the Paleozoic to the Eocene that led to the opening of the southern North Atlantic, and also hosts many complex sedimentary basins with significant resource potential, such as the Rockall and Porcupine basins (Fig. 3.1) (Shannon et al., 1995; McDonnell and Shannon, 2001; Naylor et al., 2002; Naylor and Shannon, 2005; Sibuet et al., 2007; Kimbell et al., 2010; Welford et al., 2012; Funck et al., 2017; Sandoval et al., 2019; Peace et al., 2019; Peace and Welford, 2020). The structural framework and tectonic evolution of the continental portion of the Irish Atlantic offshore margin have been intensively studied (Croker and Shannon, 1987; Tate, 1993; Naylor et al., 2002; Naylor and Shannon, 2005; Reston et al., 2004; Calvès et al., 2012; Prada et al., 2017; Watremez et al., 2018; Chen et al., 2018); however, the along-strike structural characteristics of the continent-ocean-transition (COT) and oceanic zones still remain unclear due to sparse seismic surveys, particularly north of the Goban Spur margin. With recent plate reconstruction studies of the southern North Atlantic challenging the widely-accepted "conjugate" relationship between the Goban Spur, offshore Ireland, and the Flemish Cap, offshore Newfoundland, and instead supporting a relationship between the Flemish Cap and the Porcupine Bank (Nirrengarten et al., 2018; Sandoval et al., 2019; Peace et al., 2019; Peace and Welford, 2020), additional geophysical constraints are needed to resolve the debate. Furthermore, when analyzing such constraints, increasingly complex rifting models need to be considered in order to account for extension obliquity with varying orientations with respect to the rift axis during multiple extensional events between the Flemish Cap and the Porcupine Bank (Sibuet et al., 2007; Welford et al., 2012; Brune et al., 2018). In addition, questions remain concerning the timing and extent of volcanic activity within the COT zone as it transitions from a magma-poor margin in the south to a magma-rich margin in the north, with few magnetic anomalies available to use as constraints (Minshull et al., 2009).

New long offset 2D multichannel seismic data, acquired in 2013 and 2014 by Eni Ireland for the Department of the Environment, Climate and Communications of Ireland, covering the shelf, slope, and deep-water regions of the western Porcupine and southern Rockall regions (Fig. 3.2), are now available to provide a better understanding of the offshore Irish Atlantic margin. In this study, ten new 2D multichannel seismic lines are interpreted (Fig. 3.2), with support from gravity data (Bonvolot et al., 2012), crustal thicknesses (Welford et al., 2012), and oceanic isochrons (Srivastava et al., 1988; Müller et al., 2016), to map the regional crustal architectural framework and characterize the lithospheric extensional processes from incipient rift to breakup of the Irish Atlantic margin. This work is a northward extension of the Goban Spur study of Yang et al. (2020) and the methodology and nomenclature are kept consistent across the two studies. Additionally, the study also aims to evaluate the influence of pre-existing structures on the distribution of crustal domains along the Irish Atlantic margin. The role of magmatism during margin formation, as interpreted from the seismic data, is also investigated. Finally, seismic evidence supporting whether the Porcupine Bank is conjugate to the NE Flemish Cap, offshore Newfoundland, is also sought to further improve our understanding of the tectonic evolution of the Newfoundland - Irish Atlantic margin pair.

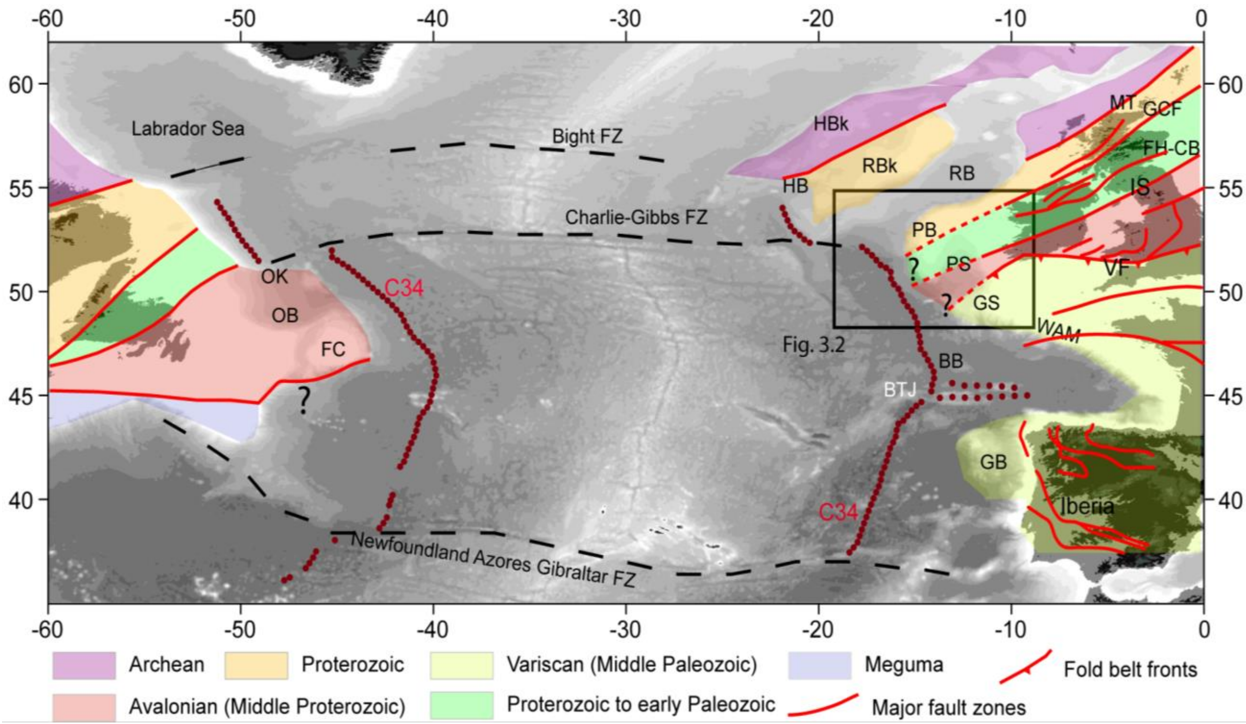

Figure 3.1: Regional map of the North Atlantic (adapted from Tyrrell et al., 2007; 2010; Welford et al., 2012; Ady and Whittaker, 2019; Whiting et al., 2021). The red round-dotted lines show magnetic anomaly 34 (Müller et al., 2016). Abbreviations: BTJ, Biscay Triple Junction; BB, Bay of Biscay; GB, Galicia Bank; GS, Goban Spur; PS, Porcupine Basin; PB, Porcupine Bank; HB, Hatton Basin; HBk, Hatton Bank; RBk, Rockall Bank; RB, Rockall Basin; FC, Flemish Cap; OK, Orphan Knoll; OB, Orphan Basin; FZ, Fracture zone; VF, Variscan Front; IS, Iapetus Suture; MT, Moine Thrust; GCF, Great Glen Fault; FH-CB, Fair Head-Clew Bay Fault Line.

3.3 Geological setting

From south to north, the Irish Atlantic rifted continental margin extends from the Goban Spur, across the Porcupine Bank region, to the Rockall Bank and Hatton Bank regions (Figs. 3.1 and 3.2). Inboard of the Porcupine Bank, the Porcupine Basin is a N-S-trending rift basin that widens to the south toward the Goban Spur (Naylor et al., 2002). The Porcupine Bank is a continental ribbon with steep lateral slopes that separates the Porcupine Basin from the Rockall Basin, the largest deep-water basin on the Irish Atlantic margin (Naylor et al., 2002). The Rockall Bank borders the Rockall Basin to the northwest. Toward the southern part of the Rockall Basin, the Barra Volcanic Ridge System (BVRS) extends from the Charlie Gibbs Fracture Zone (CGFZ) to the Rockall-Hatton Bank region (Bentley and Scrutton, 1987). Isolated, perched sedimentary basins are distributed along the eastern flank of the Rockall Basin and the western flank of the Porcupine Bank (Shannon et al., 1999).

The Caledonian Orogeny formed as a result of the collision of Baltica, Laurentia and Avalonia in the Late Ordovician-Silurian (Torsvik and Rehnstrom, 2003), creating the Laurasia continent that collided with Gondwana-derived terranes during the Carboniferous (Matte, 2001). The primary Caledonian tectonic elements underlying the Porcupine Basin and the Rockall region consist of a series of basement terranes bounded by NE-SW striking sutures and fault zones (e.g., Iapetus Suture and Moine Thrust), while the Variscan deformation front further south reaches the southern limit of the Porcupine Basin (Fig. 3.1) (Tyrrell et al., 2007; 2010). From the Paleozoic to the Eocene, the Irish Atlantic margin experienced multiple rifting episodes with migrating and intersecting rift zones (Shannon, 1991; Tate, 1993; Sinclair et al., 1994; Shannon et al., 1995; Mjelde et al., 2008). The orientations and magnitudes of these extensional deformation events are time-dependent and are reflected in the complexities of the hyper-extended basins offshore Ireland (Shannon et al., 1995; Naylor et al., 2002; Welford et al., 2010a; Nirrengarten et al., 2018). The scale and distribution of these rifted sedimentary basins are influenced by the extensional reactivation of the pre-existing Caledonian and Variscan structural fabrics (Masson et al., 1989; Kimbell et al., 2010; Grow et al., 2019).

The Porcupine Basin, as an important component of the Irish Atlantic margin, experienced multiple rift episodes from the Late Paleozoic to the Cenozoic (Stoker et al., 2017), following the collapse of Variscan and Caledonian orogenic belts (Bulois et al., 2018; Whiting et al., 2021). The timing of key rifting phases that occurred within the Porcupine Basin slightly varies in the literature (Norton, 2002; Štolfová and Shannon, 2009; Jones and Underhill, 2011; Bulois et al., 2018). Generally, in the northern part of the Porcupine Basin (~ 51°50' N), limited extension initiated in the Late Carboniferous, followed by two main rifting episodes during the Late Triassic to Early Jurassic and Late Jurassic to Early Cretaceous (Bulois et al., 2018). The southern part of the Porcupine Basin experienced extreme crustal thinning during the Middle to Late Jurassic (Tate, 1993; Prada et al., 2017; Whiting et al., 2021), and the extensional event continued during the Early Cretaceous (McCann et al., 1995; Johnston et al., 2001). Thereafter, the Porcupine Basin was affected by inversion, volcanism, and local extension during the Cretaceous to the Early Eocene (Jones et al. 2001; McDonnell and Shannon, 2001; Norton, 2002). In addition, vertical tectonic movement, tilting, and sagging (differential subsidence) occurred in the Porcupine region during the Cenozoic (Praeg et al., 2005). To the south, the Goban Spur basins are underlain by Variscan basement that likely started rifting in the Middle Triassic (Cook, 1987; Morgan, 2016). To the west, the Porcupine Bank is inferred to have rotated clockwise as the Porcupine Basin opened during the Jurassic to Early Cretaceous (Fig. 3.3) (Tate, 1993; Peace et al., 2019). Further north of the Porcupine Basin, the main rifting of the NE-SW-oriented Rockall Basin occurred during the Late Jurassic and ended during the Middle-

Late Cretaceous and Tertiary periods (Thomson and McWilliam, 2001). On the conjugate Canadian margin, the clockwise motion of the Flemish Cap continental ribbon likely began during the Late Jurassic-Early Cretaceous (Sibuet et al., 2007; Welford et al., 2010b), and accelerated in the late stage of the Early Cretaceous period (Enachescu et al. 2005; Peace et al., 2019).

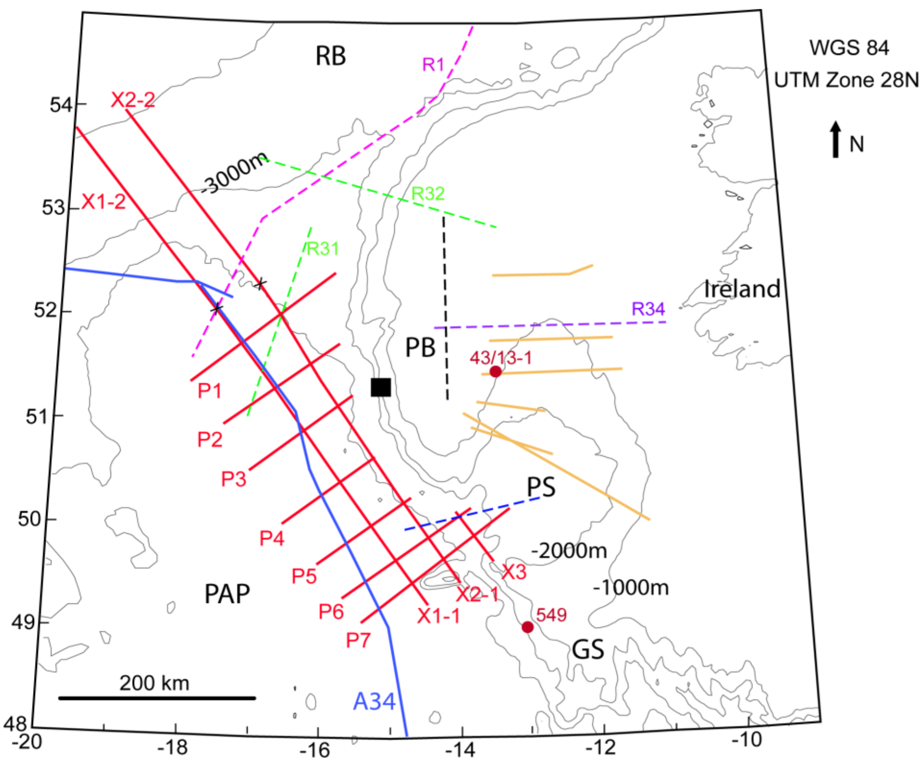

Figure 3.2: Bathymetric contours of the Porcupine Atlantic margin with 1000 m interval (grey lines), expansion of black box in Fig. 3.1. The blue solid line shows magnetic anomaly A34 (Müller et al., 2016). Red lines indicate the newly acquired seismic reflection lines, with NE-SW orientations (P1-P7) and NW-SE orientations (X1-X3). The black square indicates the dredge site from the Cyaporc cruise (Masson et al., 1989). The black dashed line is the IOS seismic refraction profile acquired in 1973 (Whitmarsh et al., 1974), the blue dashed line at the mouth of Porcupine Basin is the COOLE seismic refraction profile from 1985 (Makris et al., 1988). The other dashed lines indicate the Rockall and Porcupine Irish Deep Seismic (RAPIDS) seismic refraction data, in which the pink dashed RAPIDS line 1 was acquired in 1990 (Hauser et al., 1995), the green dashed RAPIDS lines 31and 32 were acquired in 1999 (Morewood et al., 2003), and the purple dashed RAPIDS line 34 in the northern Porcupine Basin was acquired in 2002 (O'Reilly et al., 2006). The orange solid lines indicate seismic reflection data, part of 2-D surveys acquired by Fugro-Geoteam in 1997 (Naylor et al., 2002). Abbreviations: GS: Goban Spur; RB, Rockall Basin; PB: Porcupine Bank; PS: Porcupine Basin; PAP, Porcupine Abyssal Plain.

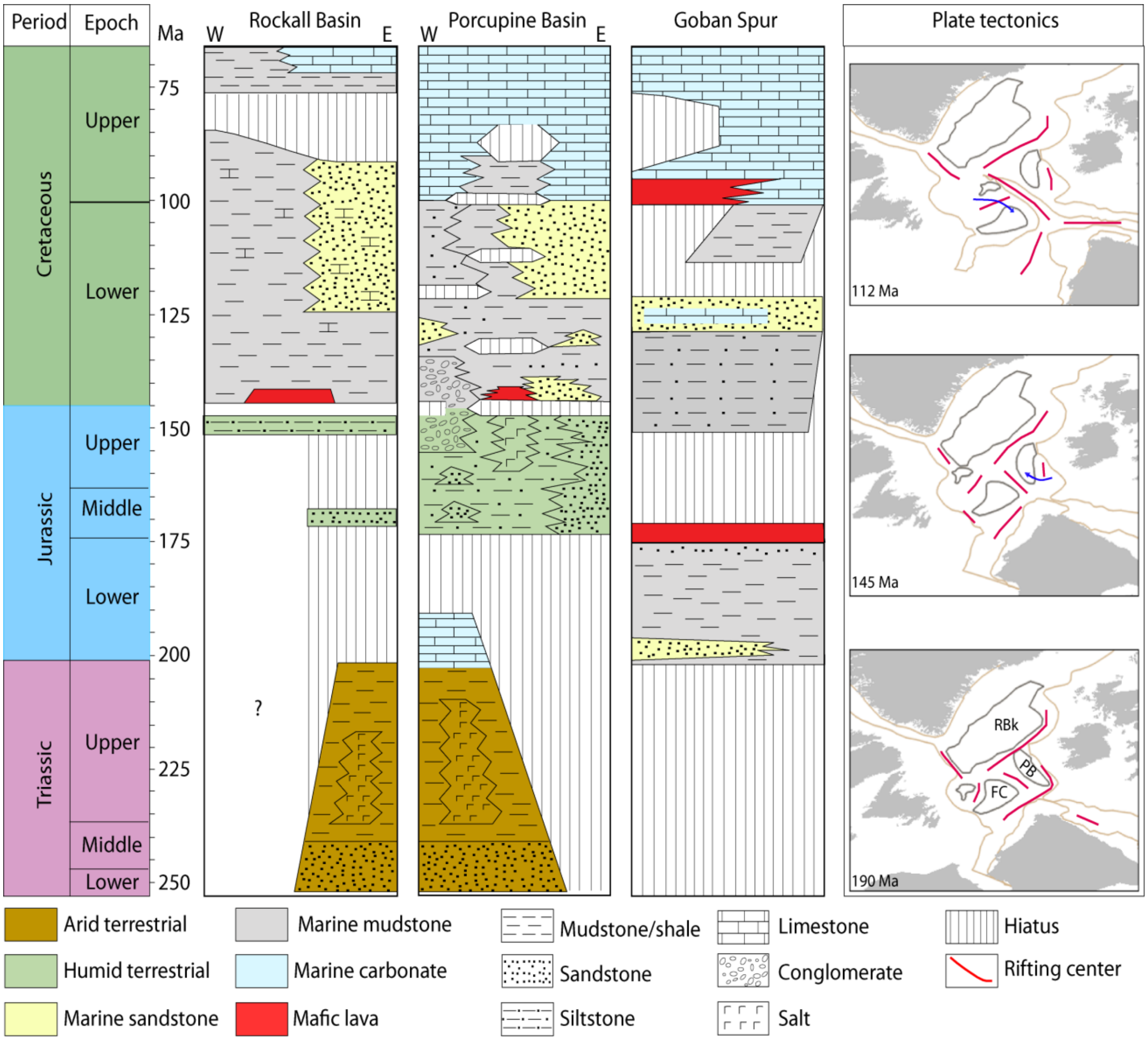

Figure 3.3: Regional stratigraphy showing the generalized Triassic–Cretaceous successions preserved in the Goban Spur–Porcupine Basin–Rockall Basin region (adapted from Stoker et al., 2017). The plate reconstructions with rigid continental blocks (outlined in grey) are modified from Peace et al. (2019). Abbreviations: FC: Flemish Cap; PB: Porcupine Bank; RBk: Rockall Bank.

The Porcupine Bank is a shallow continental block covered by relatively thin sediments, in contrast to the Rockall Basin and the Porcupine Basin to either side (Dingle et al., 1982). Permo-Triassic successions, mainly composed of sandstone and mudstone, are preserved in the North Porcupine Basin, the eastern margin of the southern Rockall Basin, and the western margin of the Porcupine Bank (Naylor et al., 2002; Tyrrell et al. 2010), and these were affected by the reactivation of Caledonian structures (Shannon, 1991). Jurassic sediments, primarily comprised of mudstone, sandstone, and (or) volcanic rocks (Tyrrell et al., 2010), are often preserved in isolated fault-bounded basins in the southern Rockall-Porcupine region (Croker and Shannon, 1987). Late Jurassic-Early Cretaceous limestone and sandstone have been drilled on the western flank of the Porcupine Bank (Haughton et al., 2005). Igneous activity occurred during the Early Cretaceous in the southern Rockall-Porcupine region, epitomized by the Barra Volcanic Ridge System and the Porcupine Volcanic Ridge System (Naylor and Shannon, 2005; Calvès et al., 2012). The Cretaceous unit, mainly composed of sandstone, siltstone, mudstone, and chalk (Tate and Dobson, 1988; Masson et al., 1989; Tyrrell et al., 2010), and interbedded with extrusive basalt lava flows, is often observed in the Rockall-Porcupine region (Stoker et al., 2017). In the Goban Spur region, the Early Cretaceous clastics are overlain by Late Cretaceous carbonates deposited in a marine setting (Fig. 3.3) (Stoker et al., 2017).

3.4 Geophysical background

Numerous geophysical surveys have been carried out across the southern Rockall-Porcupine region (Whitmarsh et al., 1974, Makris et al., 1988; Shannon et al., 1991; Tate, 1993; Morewood et al., 2005; O'Reilly et al., 2006). Whitmarsh et al. (1974) investigate the deep crustal structure beneath the Porcupine Bank and estimate that the Moho depth is ~ 28 km from seismic refraction data (indicated by the black dashed line in Fig. 3.2). The COOLE seismic refraction line, located at the mouth of the Porcupine Basin, reveals that the continental crust abruptly transitions into oceanic crust with a thickness of 9 km seaward (Makris et al., 1988). The transverse RAPIDS line 32 reveals a relatively sharp Moho gradient along the northwestern margin of the Porcupine Bank, and the other RAPIDS profile 31 shows a significant crustal thickness variation across the CGFZ (Morewood et al., 2003; 2005). The RAPIDS seismic refraction lines (R1, R31, and R32 in Fig. 3.2) in the Rockall Basin show that Paleozoic to Cenozoic sedimentary successions, with a thickness of up to ~ 7 km, overlie thin continental crust, which is itself underlain by serpentinized upper mantle (Hauser et al., 1995; Shannon et al., 1995; O'Reilly et al., 1996; Mackenzie et al., 2002; Morewood et al., 2003; 2005). The RAPIDS profile 34 (indicated by the purple dashed line in Fig. 3.2) extends from the Porcupine Bank eastward into the Porcupine Basin and shows asymmetrical basin-fill and crustal velocities consistent with the presence of serpentinized mantle underlying the thin continental crust in the Porcupine Basin (O'Reilly et al., 2006), although there is ongoing debate about the nature of the material of the thin crust in the basin (Johnson et al., 2001; Reston et al., 2004; Calvès et al., 2012; Prada et al., 2017; Watremez et al., 2018; Chen et al., 2018). Seismic reflection profiles (indicated by the orange solid lines in Fig. 3.2) reveal that thick Early/Middle Jurassic sequences developed along the western margin of the Porcupine Basin and that Late Jurassic successions are bounded by basinward-dipping tilted faults along the western and northern borders of the Porcupine Basin (Naylor et al., 2002; Reston et al., 2004; Chen et al., 2018).

Gravity data have been used to identify major structural trends along the Irish Atlantic margin (Readman et al., 1995; McGrane et al., 2001; Kimbell et al., 2010; Welford et al., 2010c; 2012). A NW-SE trending gravity anomaly in the Rockall Basin (the thin dashed white line indicated by the black arrow in Fig. 3.4a) is associated with Caledonian structures and a gravity lineament along the CGFZ shows abrupt gravity gradients (Kimbell et al., 2010). In the southern Rockall Basin, a transverse gravity lineament with a NW-SE trend appears to break the NE-SW trending regional fabric (McGrane et al., 2001). To the east of the CGFZ, the Clare Lineament (indicated by the thin dashed white line labelled CL? in Fig. 3.4a) is observed with a pronounced

NW-SE trending gravity anomaly, which is often interpreted to extend onto the Porcupine Bank and across the Porcupine Basin (Tate, 1992; Johnson et al., 2001; McGrane et al., 2001). The gravity anomaly is large and negative on the Porcupine Bank, whereas it is relatively less pronounced in the Porcupine Basin (Fig. 3.4a). A positive gravity lineament follows the interpreted boundary between continental and oceanic crust west of the Porcupine region (Kimbell et al., 2010). Welford et al. (2012) mapped variations in lithospheric density and crustal thickness across the Irish continental margin using 3D gravity inversion. The resulting crustal thickness gradient along the edge of the Porcupine Bank is steeper than it is along the Goban Spur margin (Fig. 3.4b).

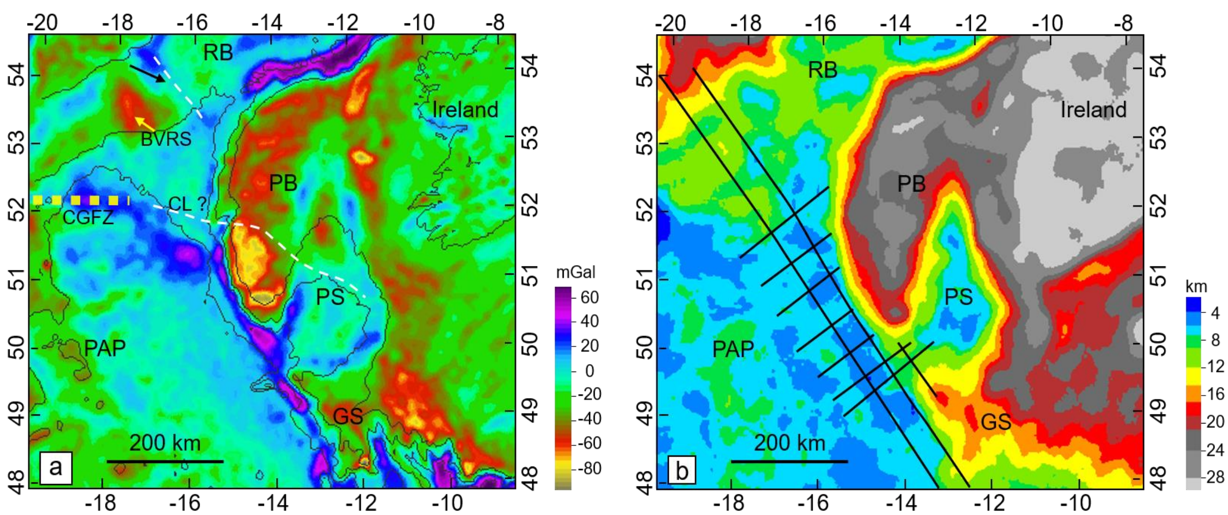

Figure 3.4: (a) The free air gravity anomaly with overlying bathymetric contours (dark grey lines) with an interval of 1000 m (Bonvalot et al., 2012). (b) Crustal thickness derived from gravity inversion (Welford et al., 2012). The black lines indicate the new seismic lines in this study. Abbreviations: RB, Rockall Basin; PB: Porcupine Bank; GS: Goban Spur; PS: Porcupine Basin; PAP, Porcupine Abyssal Plain; CGFZ, Charlie-Gibbs Fracture zone; CL, Clare Lineament; BVRS, Barra Volcanic Ridge System.

3.5 Data and methodology

In this study, ten new multichannel seismic (MCS) reflection lines (P1-P7, and X1-X3) are interpreted (Fig. 3.2). The profiles were acquired in 2013 and 2014 by BGP Explorer, with 25 m and 37.5 m shotpoint intervals for water depths less than 3000 m and greater than 3000 m, respectively. The receiver group spacing is 12.5 m and the sampling interval is 2 ms with 12 s total trace length. Each shot record contains 804 traces. NE-SW oriented seismic lines (P1-P7), located along the southwest limit of the Porcupine Bank, are approximately subparallel and are intersected by three NW-SE oriented seismic lines (X1-X3) (Fig. 3.2). The distances between the NE-SW oriented seismic lines (P1-P7) are variable, with ~ 60 km, ~ 55 km, ~ 67 km, and ~ 54 km between P1 and P2, P2 and P3, P3 and P4, and P4 and P5, respectively. To the southeast, the distances between the other two NE-SW oriented seismic profiles gradually decrease, with ~ 47 km between P5 and P6, and ~ 29 km between P6 and P7. All of these NE-SW oriented seismic profiles cross magnetic Chron 34 (Müller et al., 2016), the location of undisputed oceanic crust (Fig. 3.2). The distance between profile X1 and magnetic Chron 34 gradually decreases from southeast to northwest. At its northernmost extent, profile X1 lies outboard of magnetic Chron 34 and crosses seismic refraction RAPIDS profiles 1 and 31 (Hauser et al., 1995; Morewood et al., 2003), as well as the Charlie-Gibbs Fracture Zone (CGFZ) (Fig. 3.2). All of the seismic profiles were converted to depth using stacking velocities. Next, the depth-converted seismic reflection profiles and their interpretations were re-evaluated using a combination of gravity data (Bonvolot et al., 2012), and crustal thickness estimates from gravity inversion (Welford et al., 2010c; 2012).

Due to the absence of drilling constraints, the stratigraphic framework in the western Porcupine Bank cannot be investigated in detail. Nonetheless, the tectono-stratigraphic sedimentary layers are still grouped into syn-rift and post-rift packages on the basis of seismic observations and the stratigraphic framework from the neighbouring Porcupine and Rockall basins (Gernigon et al., 2006; Tomsett et al., 2017; Sandoval et al., 2019; Whiting et al., 2021). In this study, the proximal, necking, hyperextended, exhumed, and oceanic domains are interpreted to be consistent with the crustal architecture interpretation for the Goban Spur margin (Yang et al., 2020). Briefly, the proximal domain corresponds to continental crust that has experienced only minor stretching, while continental crust within the necking domain becomes wedge-shaped as it thins dramatically from ~30 km to < 10 km (Péron-Pinvidic and Manatschal, 2009). On magma-poor margins, the necking domain typically transitions into the hyperextended domain once the crust is hyper-thinned and crustal embrittlement has been achieved, possibly leading to mantle exhumation (Péron-Pinvidic et al., 2013). Following the subdivision from Welford et al. (2010a), the exhumed mantle zone in this study is subdivided into a section with deeper basement displaying smooth basement morphology (subdomain T1), and a section of serpentinized peridotite ridges with relatively shallower and rougher basement relief (subdomain T2). As rifting ceases and seafloor spreading is initiated, the exhumed domain transitions into the oceanic domain.

The boundary between the necking zone and the proximal zone is mainly dependent on the Moho proxy from gravity inversion (Welford et al., 2012). This is because Moho depth is generally greater than 30 km in the proximal domain, while it can drastically shallow from ~ 30 km to ~ 10-15 km during lithospheric necking (Péron-Pinvidic et al., 2013). The boundary between the hyperextended zone and the necking zone is primarily defined based on Moho geometry and the interpreted fault patterns. The border between the T1 subdomain and the hyperextended domain is defined by the change in top-basement seismic reflectivity characteristics. The top-basement reflective events are concave upwards in the hyperextended domain and become convex upwards in the T1 subdomain. Generally, extensional detachment faults assist in defining the oceanward limit of the hyperextended domain. The boundary between subdomains T1 and T2 mainly relies on the basement morphology, with the former displaying relatively deep and smooth basement relief and the latter composed of inferred serpentinized peridotite ridges displaying shallower and rougher basement relief. The landward edge of the oceanic crust is defined by the seaward edge of the exhumed domain (or the T2 subdomain), mainly based on the top-basement relief. Generally, the top basement in the region between magnetic Chron 34 and the seaward edge of the T2 subdomain is relatively deeper and smoother, compared with the relatively shallow and rough basement in the T2 subdomain (see profile L1 in Yang et al. (2020)). It is also worthwhile noting that the interpretation criteria applicable to seismic profiles in the south (e.g., P1-P3 in Fig. 3.2) may not be suitable for the lines in the north (e.g., P4-P7 in Fig. 3.2) due to the presence of magmatism, and to line-to-line variations in top basement characteristics and fault patterns.

3.6 Interpretations

3.6.1 Seismic interpretation

All of the new seismic lines, except lines X2 and X3, cross magnetic Chron 34, allowing for a comprehensive investigation of extensional tectonic processes for the Porcupine Bank region, from rift to possible mantle exhumation to seafloor spreading. Portions of the NE-SW oriented seismic sections in time (P1-P7) are displayed in Figure 3.5, in order to highlight and compare the reflective characteristics of the transitional and oceanic crustal zones. Interpreted cross-sections in depth are provided for all of the new seismic lines, with the NE-SW oriented profiles (P1-P7) in Figure 3.6, and the NW-SE oriented profiles (X1-X3) in Figure 3.7. All the uninterpreted seismic lines (P1-P7, X1 and X2) are shown in Appendix B. The purpose of these figures is to consistently display the interpreted sedimentary packages, crustal domains, fault patterns, magmatic features, and inferred basement domains across the study area.

Through correlation with the stratigraphic sequence identification over the Hatton-Rockall margin (Gernigon et al., 2006) and the Porcupine Basin (Tomsett et al., 2017; Sandoval et al., 2019; Whiting et al., 2021), several key sequences are interpreted for the Porcupine Atlantic margin (Figs. 3.6 and 3.7). The syn-rift successions range from Early Jurassic to Early Cretaceous (Figs. 3.6 and 3.7) and the post-rift formations mainly consist of the Cenozoic and Upper Cretaceous units (Sandoval et al., 2019).

Both seismic profiles X1 and X2 are key regional tie lines that help illustrate the along-strike structure of the Goban Spur-Porcupine Bank-southern Rockall region (Fig. 3.2). Due to their significant lengths, the profiles are each divided into two sections in proximity to the CGFZ (X1-1 and X1-2, and X2-1 and X2-2, marked by the asterisk in Fig. 3.2) for better display. Further to the northwest of the CGFZ, profiles X1-2 and X2-2 in the southern Rockall Basin transect the area of the Barra Volcanic Ridge System (BVRS), where significant magmatism occurred during the initial spreading of the Porcupine Abyssal Plain (Bentley and Scrutton, 1987). Since profiles X1-2 and X2-2 are far from the Porcupine Bank and are significantly affected by igneous sills, their interpretation is highly uncertain and relegated to the supplemental material. In this study, the region where the crustal thickness from independent gravity inversion is above ~ 20 km is defined as the proximal domain. Since seismic profiles P1-P7 do not extend into the proximal domain (Fig. 3.4b), we mainly interpret the necking, hyperextended, exhumed, and oceanic domains along these profiles in this study.

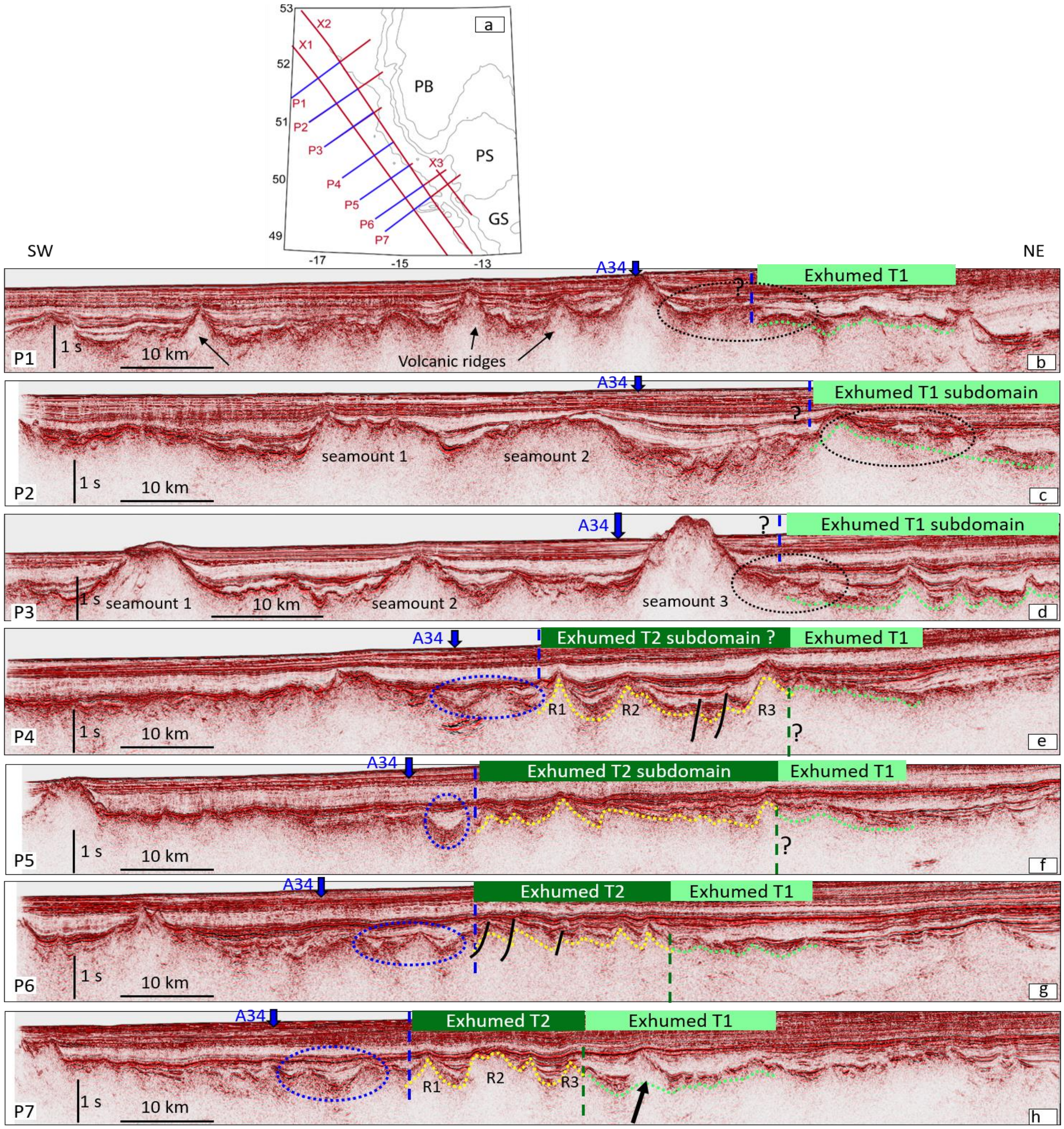

Figure 3.5: (a) Location map for the displayed portions of the parallel seismic profiles, highlighted in blue. (b)-(h) show the portions of the interpreted seismic lines P1- P7 in the time domain from northwest to southeast. The dark green areas indicate the interpreted serpentinized peridotite ridges with rougher and shallower basement (subdomain T2) on profiles P4-P7. The light green regions correspond to the interpreted exhumed mantle displaying subdued topography at top-basement (subdomain T1). The dashed blue line indicates the inferred border between the exhumed domain and oceanic domain. The dashed dark green line represents the inferred boundary between the exhumed subdomain T1 and subdomain T2 on profiles P4-P7. R represents interpreted peridotite ridges. The green and yellow dashed lines illustrate the top basement of the T1 and T2 subdomains, respectively. The blue circles in Figs. 3.5e, 3.5f, 3.5g, and 3.5h indicate concave-up and -down shaped high-amplitude reflectors on seismic profiles

P4-P7. The black dashed circles in Figs. 3.5b, 3.5c, and 3.5d show the similar igneous basement reflection characteristics along profiles P1, P2 and P3. The black arrow in Figure 3.5h indicate the discontinuity of top basement in the exhumed domain along profile P7. The corresponding uninterpreted portions of these sections are shown in Figure B.1 in Appendix B.

3.6.1.1 Necking domain

In this study, only P6 and P7 among the seven NE-SW oriented profiles extend landward into the necking domain based on the crustal thickness map derived from gravity inversion (Fig. 3.4b). It is difficult to define the boundary between the hyperextended zone and the necking zone along profiles P6 and P7 (Fig. 3.6). Both profiles are located at the mouth of the Porcupine Basin, between the Porcupine Bank and the Goban Spur, and intersect seismic profile X3 (Fig. 3.2). Consequently, the boundary between the two zones along profile X3 (Fig. 3.7a) is used to assist in identifying the necking domain along profile P7. Profile X3 transects the mouth of the Porcupine Basin and is close to well-studied seismic surveys along the western flank of the southern Porcupine Basin (Fig. 3.7a). Since the Moho drastically shallows from ~30 km to less than 10 km during the necking stage (Péron-Pinvidic and Manatschal, 2009), the convex upward trend of Moho depths from gravity inversion along profile X3 (dotted blue line in Fig. 3.7a) helps to approximately define the necking zone. Whiting et al. (2021) define the regions of necking and hyperextension of the Porcupine rift system, with the central part of profile X3 interpreted as the hyperextended zone despite the less reflective and chaotic top basement (Fig. 3.7a). Correspondingly, the seaward border of the necking zone along line P7 is roughly defined (Fig. 3.6g). Regarding the seaward limit of the necking zone along profile P6, it is defined based on the interpreted shallowing Moho (Fig. 3.8).

3.6.1.2 Hyperextended domain

The oceanward limit of the hyperextended domain is mainly defined by the limit of interpreted extensional detachment faults and basement reflectivity geometries. The concave-upward continuous reflection amplitudes change into convex-upward chaotic reflectivity from the hyperextended zone to the mantle exhumation zone along profile P6 (Fig. 3.9b). The concave-upward seismic packages bounded by a series of listric faults with SW dips are observed along profiles P6, P5, and P4 (Figs. 3.9b, 3.9c, and 3.9d). These faults detach onto the low-angle faults and penetrate the upper crust (Fig. 3.6). Although the detachment fault is not clearly observed along P7 (Fig. 3.9a), similar basement features along both profiles P6 and P7 help to define the border of the hyperextended zone along P7 (indicated by the blue dashed circle in Figs. 3.9a and 3.9b). In contrast, the border between the hyperextended domain and the exhumed domain along profiles P1-P3 is more uncertain due to the presence of complex sills (Figs. 3.5b-5d). Still, the basement in the hyperextended zone appears to be highly faulted along both lines P1 and P2 (Figs. 3.6a and 3.6b).

The hyperextended domain along X2-1 is based on the interpretation of profile X2 along the Goban Spur margin (Yang et al., 2020). At the boundary between the hyperextended zone and the exhumed domain along X2-1 (indicated by the dashed green line in Fig. 3.10a), the seismic facies change from faulted basement to chaotic basement overlain by transparent, low reflectivity sedimentary layers. It is also noted that the reflection events with strong amplitudes in the sedimentary packages disappear at the oceanward end of the hyperextended zone along both P6 and X2-1 (indicated by blue arrows in Figs. 3.9b & 3.10a). Furthermore, negative flower structures are interpreted in the hyperextended domain along the southeastern part of profile X2-1, crossing the Iapetus Suture and the Variscan Front, respectively (Figs. 3.10 & 3.7b).

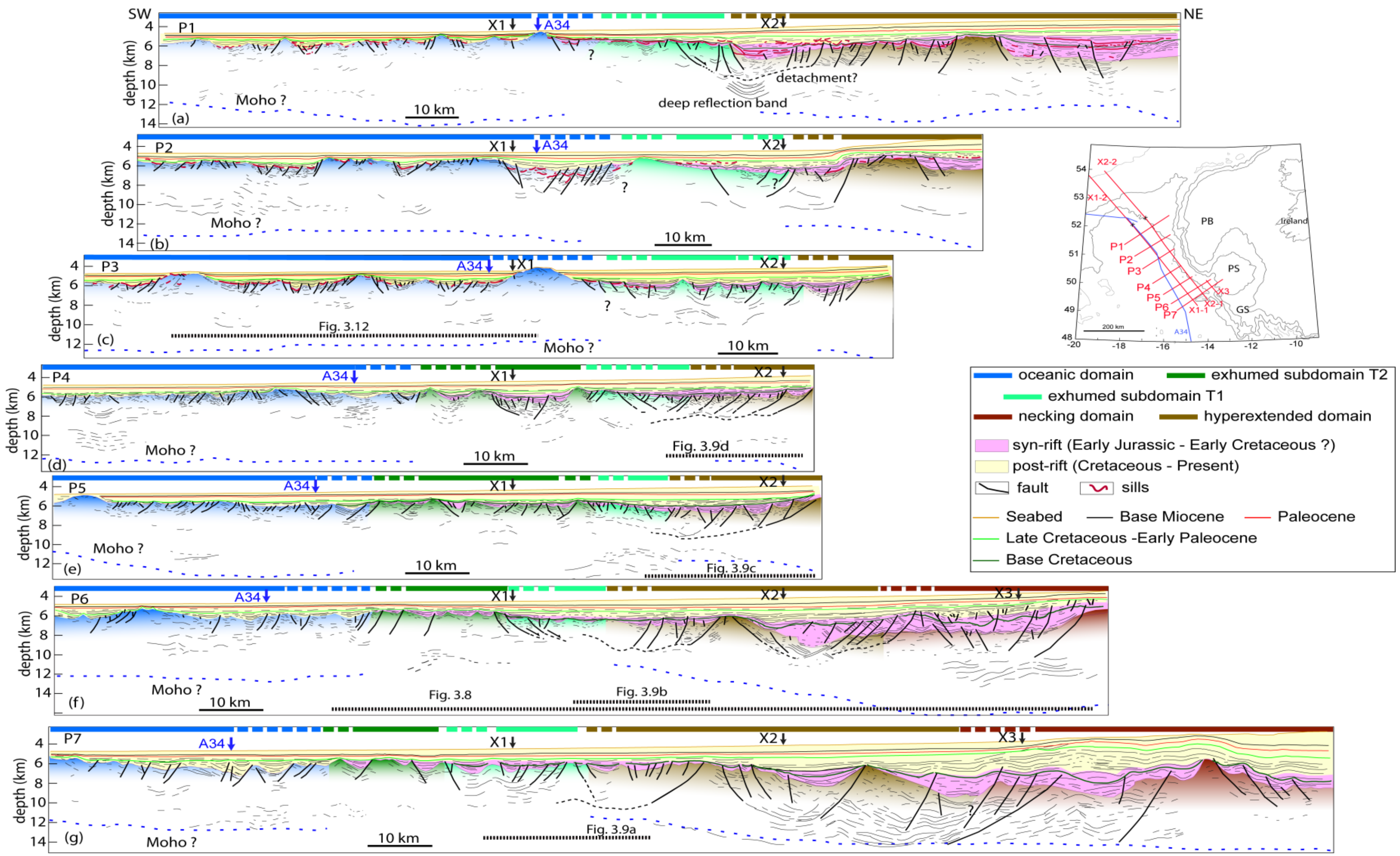

Figure 3.6: The interpreted profiles P1-P7 in the depth domain, aligned according to how they are transected by profiles X1 and X2 (plotted with arrows above the profiles). See location map for the spatial relationship between the lines. The portions of the interpreted profiles for which seismic data enlargements are shown in later figures are highlighted along the base of each profile, with the corresponding figure numbers. The blue dashed line along P1-P7 indicates Moho derived from gravity inversion (Welford et al., 2012). The corresponding uninterpreted seismic lines (except line P6) are shown in Figures B.2-B.8 in Appendix B.

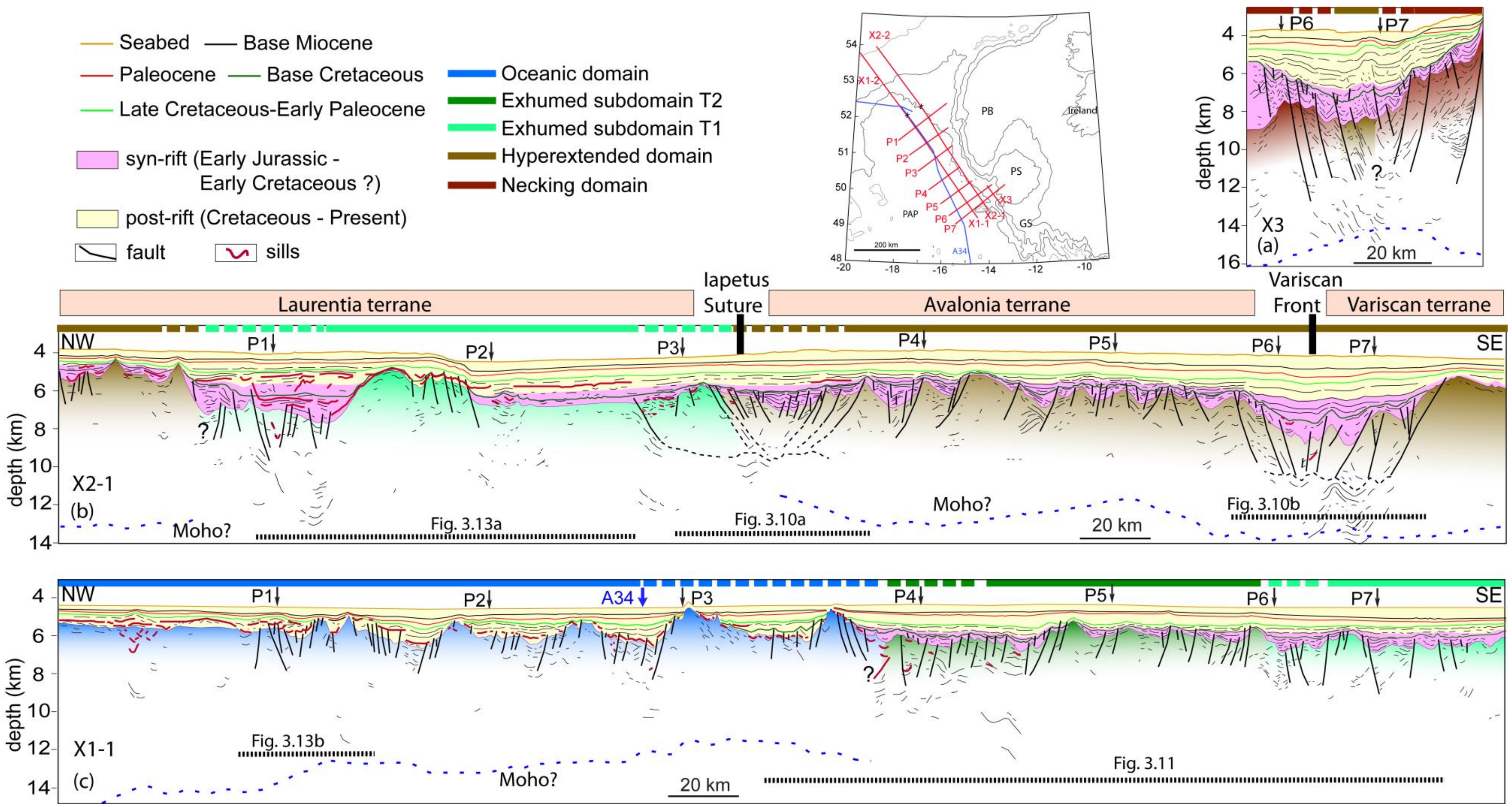

Figure 3.7: The interpreted seismic profiles X3 (a), X2-1 (b), and X1-1 (c) in the depth domain. The locations of the intersecting NE-SW lines (P1 to P7) are plotted with arrows above the profiles. See location map for the spatial relationship between the lines. Above profile X2-1, the inferred basement domains and their boundaries (e.g., Iapetus Suture and Variscan Front) are plotted for reference. The portions of the interpreted profiles for which seismic data enlargements are shown in later figures are highlighted along the base of each profile, with the corresponding figure numbers. The blue dashed line along X1-X3 indicates Moho derived from gravity inversion (Welford et al., 2012). The corresponding uninterpreted seismic lines X2-1 and X1-1are respectively shown in Figures B.9 and B.10 in Appendix B.

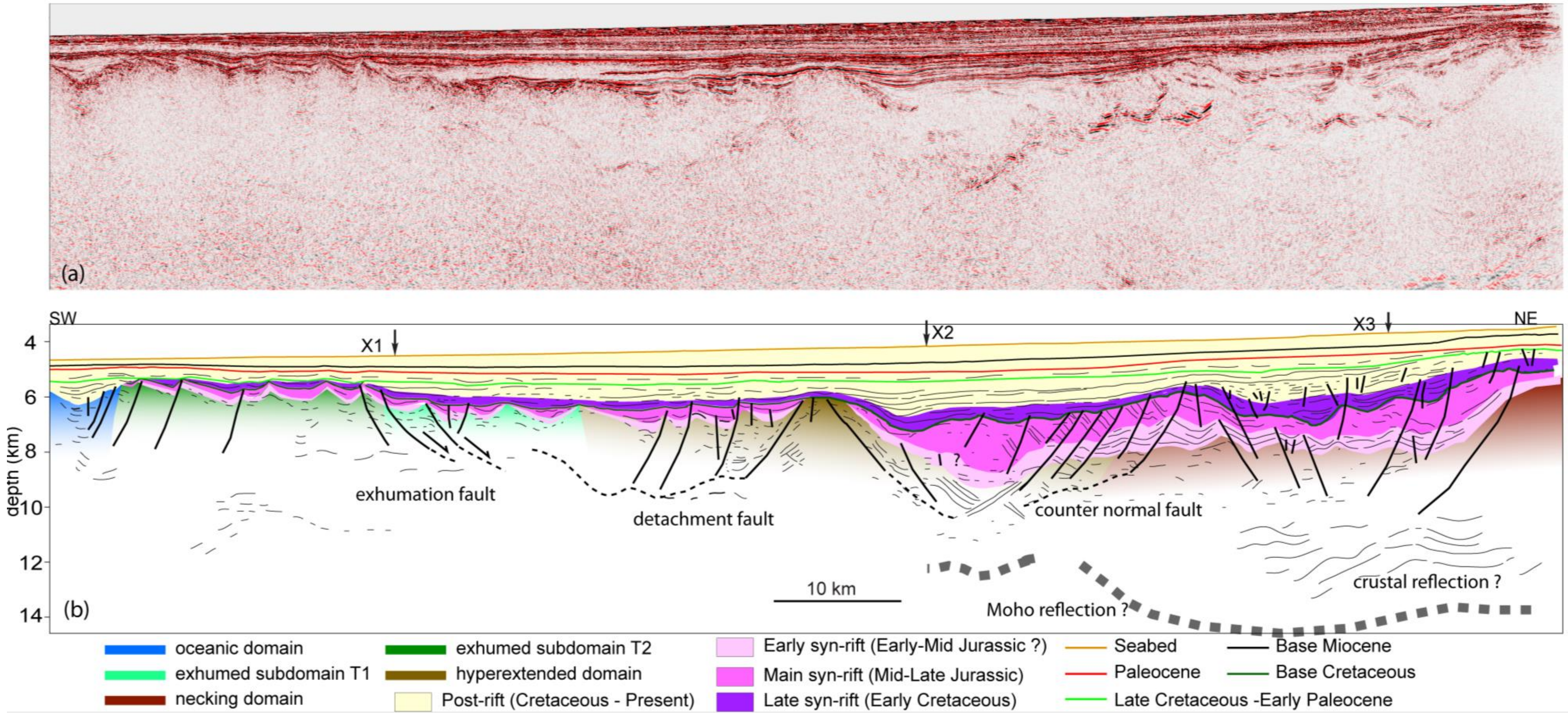

Figure 3.8: Enlargement of seismic profile P6 from Fig. 3.6f. Intersections with profiles X1, X2 and X3 are plotted with arrows above the interpreted profile.

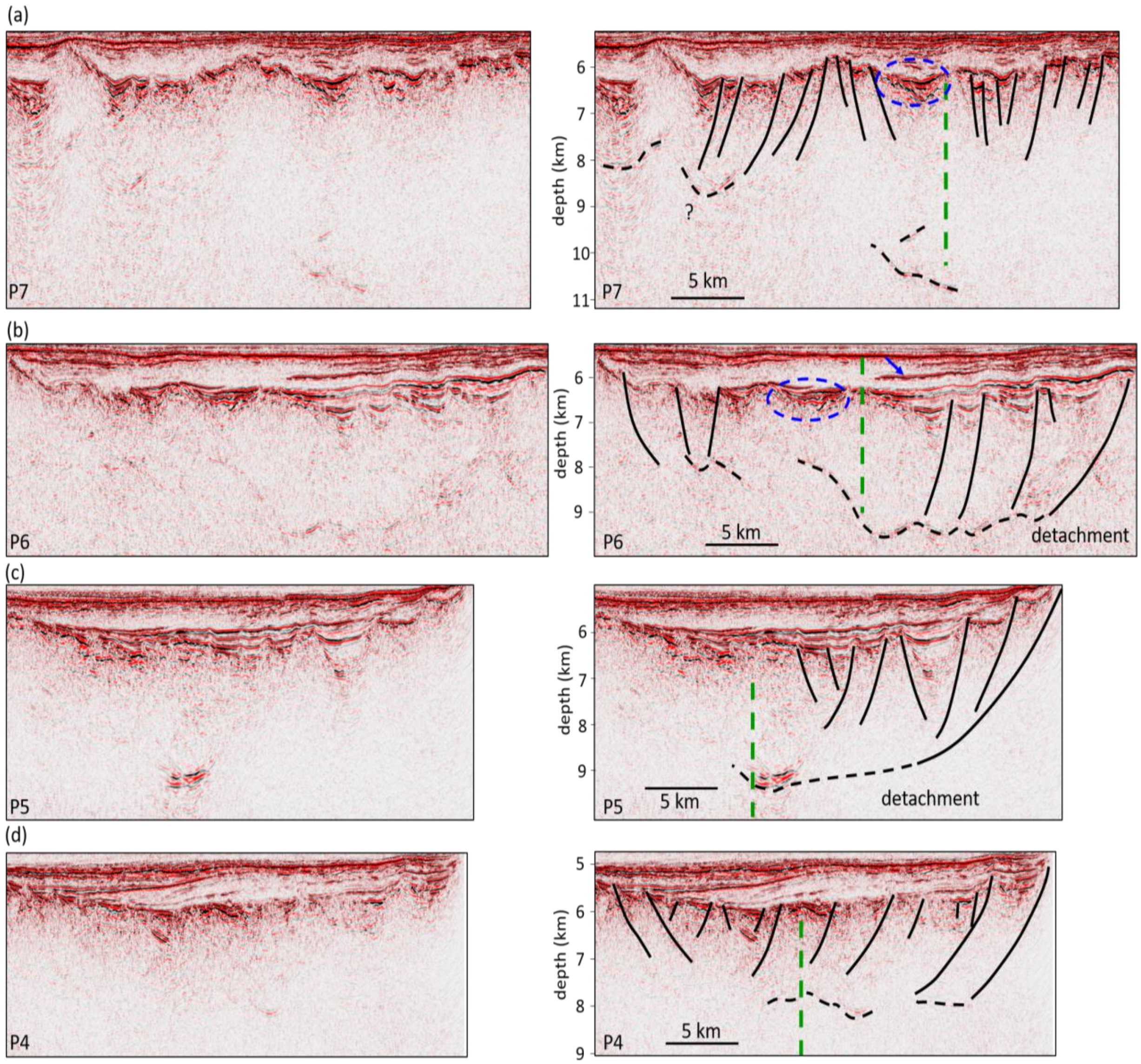

Figure 3.9: Enlargements of profiles P4-P7 from Figure 3.6. The dashed green line represents the inferred border between the hyperextended domain (right) and the exhumed subdomain T1 (left). The blue arrow in Figure 3.9b indicates that the reflection event with strong amplitudes in the sedimentary package disappear at the oceanward end of the hyperextended zone along P6. The blue dashed circles in Figures 3.9a and 3.9b show the similar basement features along both profiles P6 and P7, which help to define the border of the hyperextended zone along P7 since the detachment fault is not clearly observed along P7 (Fig. 3.9a).

3.6.1.3 Exhumed domain

Serpentinized mantle, locally exhumed, has been commonly revealed along most of the margins of the southern North Atlantic Ocean, with the west Iberian margin representing the best studied example based on intense geophysical studies (e.g., seismic surveys and ocean drilling)

(Reston, 2009; Dean et al., 2015; Davy et al., 2016). Compared with the west Iberian margin, the broad zone of interpreted exhumed mantle across the offshore Porcupine region is divided into two exhumed subdomains without the support of oceanic drilling. Since seismic profile P7 is close to profile L1 from the Goban Spur margin (Yang et al., 2020) and supporting seismic refraction constraints (Bullock and Minshull, 2005), the serpentinized peridotite ridges displaying shallower and rougher basement relief (subdomain T2) are defined (dark green region in Fig. 3.5) by comparing the top-basement reflection patterns between both seismic lines. The interpretation of subdomain T2 along seismic profile P7 is then carried over to profiles P6, P5, and P4, progressively, based on observed similarities in basement morphology (dark green regions in Figs. 3.5f, 3.5g, and 3.5h).

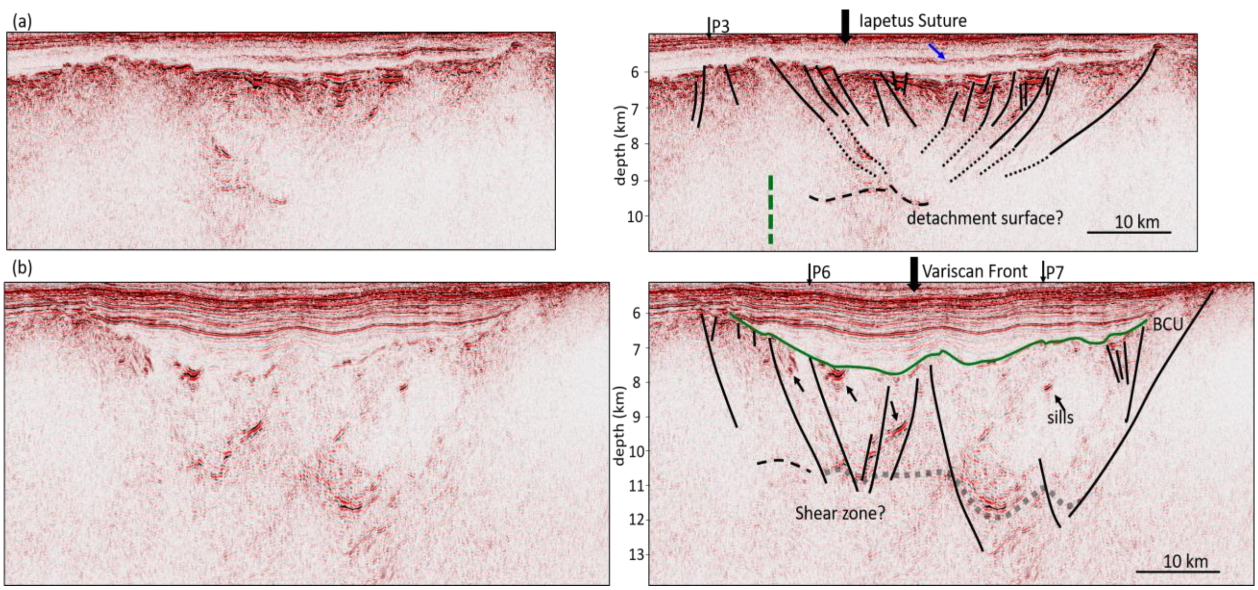

Figure 3.10: (a) Interpreted flower structures in the transition from hyperextended domain to the exhumed domain along line X2-1 from Figure 3.7b. The dashed green line represents the inferred border between the hyperextended domain (right) and the exhumed subdomain T1 (left). The blue arrow indicates the disappearing reflection event in the sedimentary package, similar to that along profile P6 in Figure 3.9b. The deep reflection ~3 km beneath the top basement may be the detachment surface (?), possibly acting as a rheological interface. (b) Interpreted flower structures in the hyperextended domain along line X2-1 from Figure 3.7b. BCU in Figure 3.10b indicates Base Cretaceous Unconformity. The grey thick dashed line may indicate a shear zone, possibly related to the offshore continuation of Variscan structures. The black dashed line represents a deep crustal reflection (?).

The exhumed subdomain T2 for these four seismic profiles (P4-P7) spans different extents and displays highly variable top-basement morphology (Figs. 3.5 and 3.6). Evidently, the top basement in subdomain T2 (yellow dashed line in Fig. 3.5) is shallower and rougher than that in subdomain T1 (green dashed line in Fig. 3.5) along P4-P7. Also, the subdomain T2 along profile P5 is wider than for the other three seismic profiles (Fig. 3.5). In detail, along profile P7, the top basement of ridge 3 is slightly lower than that of ridges 1 and 2 within subdomain T2 (Fig. 3.5h). Along profile P6, the subdomain T2 is composed of small-scale ridges, separated by SW-dipping faults (Fig. 3.5g). Along profile P5, the distance between the basement ridges in subdomain T2 is not uniform and the morphologies of these ridges are different as well (Fig. 3.5f). Along profile P4, basement ridge 2 is relatively deeper than ridges 1 and 3 (Fig. 3.5e). Top basement between ridges 2 and 3 is segmented by faulted blocks (Fig. 3.5e). Although ridge 3 is interpreted to be a serpentinized peridotite ridge, it may also represent an igneous basement high due to its proximity to volcanic features (Figs. 3.6d, 3.7c and 3.11). Along line X1-1, four peridotite ridges are also interpreted, and the top-basement morphology of ridge 4 is more complicated and more poorly imaged than the other three peridotite ridges, which may be due to its location closer to the northern volcanic features (Figs. 3.7c and 3.11). Since the intersection between profiles P4 and X1-1 falls into the interpreted subdomain T2 along profile P4 (Fig. 3.6d), the region between P4 and P5 along profile X1-1 is interpreted as subdomain T2, despite the absence of clear peridotite ridges in the area (Figs. 3.7c and 3.11).

The boundaries between the exhumed subdomains T2 and T1 along P6, P7 and X1-1 are interpreted based on deeper basement for the T1 subdomain and the presence of transparent, reduced reflectivity in the overlying sediments for T1 (Figs. 3.5g, 3.5f, and 3.11), as was observed to the south at the Goban Spur margin (Yang et al., 2020). In this domain, the abrupt disruption of the basement reflection along profile P7 (black arrow in Fig. 3.5h) and the basement high along line X1-1 (white arrow in Fig. 3.11) may be associated with magmatic events during mantle exhumation. Since reduced reflectivity in the sediments overlying subdomain T1 is not observed along P4 and P5, the identification of the boundaries between the subdomains T2 and T1 along both profiles is mainly based on the change in top basement relief, with the former rougher than the latter (Figs. 3.5e and 3.5f). The identification of exhumed subdomain T1 along P1, P2, P3, and X2-1 (Figs. 3.5, 3.6, and 3.7b) is highly uncertain due to the poorly imaged top basement which is masked by sill complexes. Nevertheless, the rugged igneous basement and the presence of transparent, low reflectivity sedimentary layers above the basement help to define the exhumed subdomain T1 along these lines because rugged top basement and transparent layers are also observed in the exhumed domain along P6 and P7.

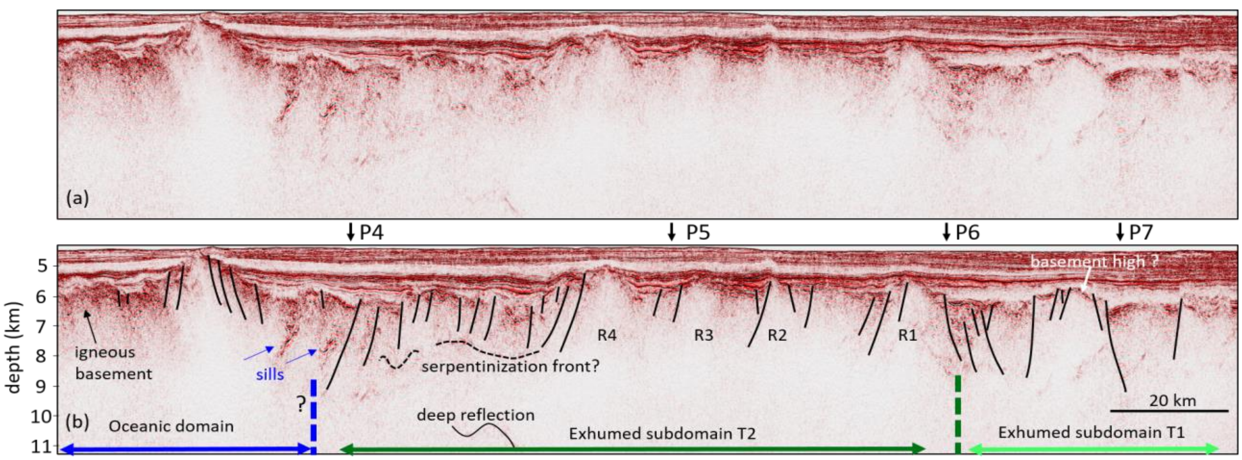

Figure 3.11: Enlargement of seismic profile X1-1 from Fig. 3.7c. The dashed green line represents the inferred border between the exhumed subdomains T1 and T2. The dashed blue line represents the landward border of the oceanic domain. R corresponds to interpreted peridotite ridges.

3.6.1.4 Ocean domain

Although there is a hybrid region involving mantle exhumation and magmatic addition between the peridotite ridges and the steady-state oceanic crust (Gillard et al., 2015), we directly define the seaward limit of peridotite ridges as the oceanic crust zone, mainly due to the subdued seismic character in the hybrid region in this study. In the region between the seaward limit of the peridotite ridges and magnetic Chron 34 (A34), the basement is characterized by one or more concave-down and concave-up shaped high-amplitude reflectors on P4, P5, P6, and P7 (indicated by the blue circles in Figs. 3.5e, 3.5f, 3.5g, and 3.5h). The concave-down basement geometries in this region are relatively deeper, compared with the shallower and rougher basement in the exhumed T2 subdomain. In the region seaward of magnetic Chron 34 (A34) on these four seismic profiles, the reflection amplitudes at the top basement of the normal oceanic crustal domain are continuous, with relatively smooth basement relief (Fig. 3.5). In comparison, the landward limit of the oceanic domain along P1, P2, and P3 is obscured due to the variable character of the volcanic basement, thus the interpretation uncertainty is high (Figs. 3.5b, 3.5c, and 3.5d). Nonetheless, igneous basement reflection characteristics are similar in the region transitioning from the exhumed domain to the oceanic domain along P1, P2 and P3 (indicated by the black dashed circles in Fig. 3.5). Likewise, magmatic events also lead to uncertainty in terms of the border between the exhumed subdomain T2 and the oceanic domain along X1-1. In contrast, further to the northwest of X1-1, the oceanic domain is easily delimited since the northwestern part of X1-1 is almost coincident with magnetic Chron 34 (A34) up until the CGFZ (Fig. 3.7c).

In the undisputed oceanic zone (outboard of magnetic anomaly 34), pronounced basement highs in the oceanic domain along profiles P2 and P3 are consistent with seamounts (Figs. 3.5c and 3.5d), and the rugged oceanic basement along profile P1 is likely related to volcanism as well (Fig. 3.5b). Specifically, along profile P3, the igneous basement between seamounts 1 and 2 is highly faulted with grabens and horsts, while the top basement between seamounts 2 and 3 is intruded by basaltic lava flows, displaying chaotic but strong reflection amplitudes (Fig. 3.12). In addition, sheeted sills outboard of seamount 3 mask the reflectivity at depth (Fig. 3.12). Regarding the two prominent seamounts along profile P2 (Fig. 3.5c), a younger volcano appears to have formed on top of an eroded, older volcanic edifice on the top of seamount 1. The igneous basement of seamount 2 shows subdued relief compared with that of seamount 1 (Fig. 3.5c). On the whole, by observing the seismic profiles from P7 to P1, it is evident that the oceanic basement is much rougher towards the Charlie Gibbs Fracture Zone (CGFZ) than it is along the southwestern limit of the Porcupine Bank region.

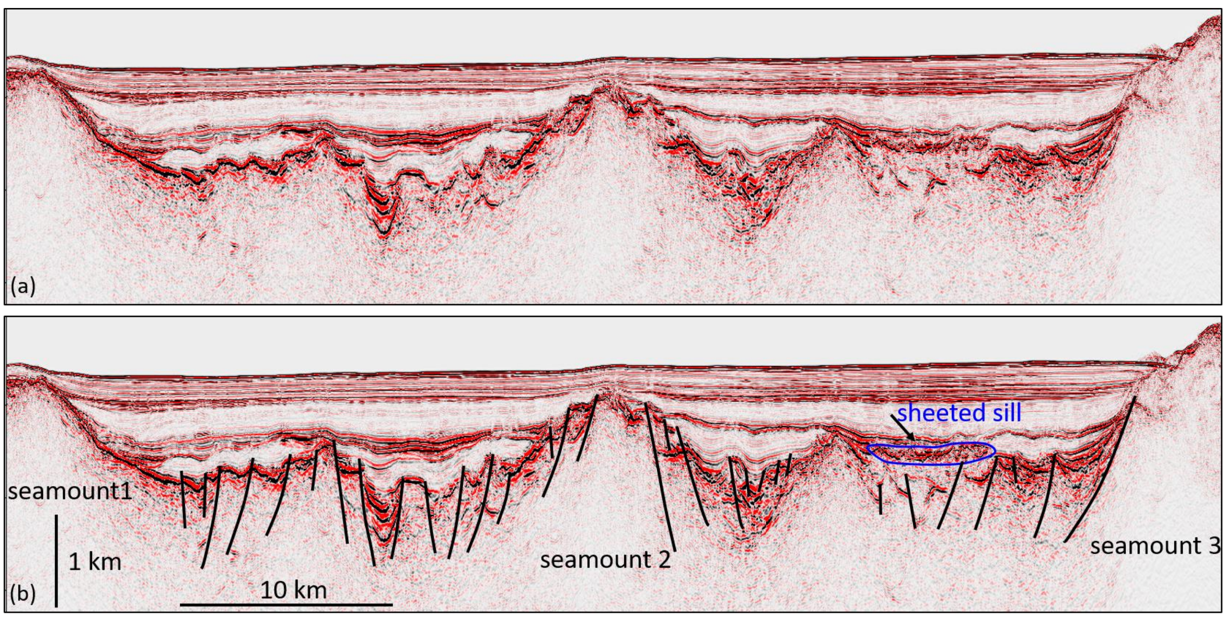

Figure 3.12: Enlargement of seismic profile P3 from Fig. 3.6c.

3.6.1.5 Sills

To the northwest of the study area, magmatic events are significantly enhanced as evidenced by volcanic highs and highly reflective basement along these profiles (Figs. 3.6 and 3.7). For example, in the exhumed region along X2-1, a pronounced basaltic basement high with very-strong-amplitude reflectors is observed (Fig. 3.13a). The sill complexes on the top basement high have a stepping pattern down to the southeast, separated by SE-dipping faults (Fig. 3.13a).

To the northwest of the basement high, the sills hosted in the syn-rift rocks also consist of thick and high-amplitude reflections, similar to the morphology of sills along the northeastern part of profile P1 (Fig. 3.5b). The steeply dipping sill reflections (indicated by dark green arrows in Fig. 3.13a) tend to follow the fault plane, appearing to connect the saucer-shaped sills with concave-upward high-amplitude reflectors in the post-rift layers in the exhumed domain (Fig. 3.13a), which may imply that the deeper sills feed the shallower ones (Thomson and Schofield, 2008). Sub-horizontal sheeted sill complexes intruding the transparent post-rift successions observed along profile X2-1 extend over a distance of up to ~ 38 km (indicated by the dashed blue circle in Fig. 3.13a), obscuring the deeper top basement reflection in the exhumed domain. Along profile X1-1, saucer-shaped sill complexes with variable geometries dominate in the oceanic segment between profile P3 and the CGFZ (Fig. 3.13b). The deeper sheeted sill complexes appear to be separated from the shallower sill complexes by normal faults in the easternmost part of the hyperextended zone along profiles P1 and P2 (Figs. 3.6a and 3.6b).

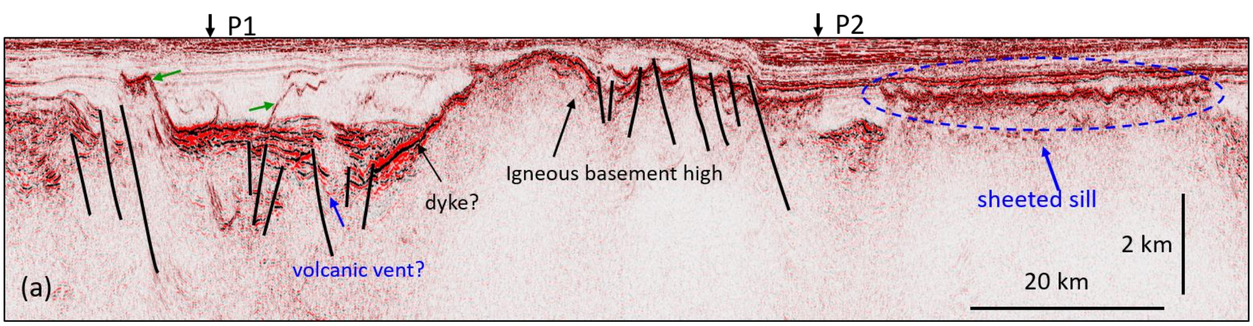

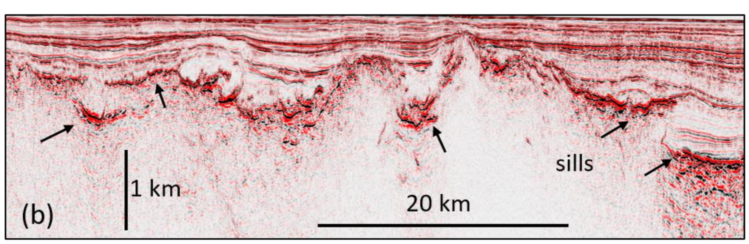

Figure 3.13: (a) Enlargement of a portion of the exhumed domain along profile X2-1 in Figure 3.7b. The dark green arrows show the steeply dipping sill reflections. The pronounced basaltic basement high with very-strong-amplitude reflectors is observed between P1 and P2 along profile X2-1. (b) Enlargement of a portion of the oceanic crustal domain along profile X1-1 in Figure 3.7c. The black arrows in Figure 3.13b indicate sills with various geometries.

3.6.2 Rift domain map description

According to the interpreted boundaries between crustal domains for each seismic line in section 5.1, the boundaries along each line are extrapolated to define the crustal architecture across the western Porcupine Bank-southern Rockall region. This synthesis, combined with the crustal domain distribution across the Goban Spur margin (Yang et al., 2020), results in a map of the crustal architecture across the entire Goban-Porcupine-southern Rockall region, shown in Figure 3.14. The structure and crustal character of the CGFZ, representing the transition between continental and oceanic crust at the mouth of the Rockall Basin, are complicated due to strike-slip movement (Mackenzie et al., 2002). As such, interpretations of the crustal domains in the region close to, and north of, the CGFZ are the least constrained by the new profiles, made more challenging by varying amounts of magmatism and a paucity of other constraints in the area. Nonetheless, the domain interpretations are still supported by previously published seismic refraction data interpretation (Morewood et al., 2003; 2005) and crustal thicknesses (Welford et al., 2012). Overall, the geometry varies for each crustal domain along the western Porcupine Bank-southern Rockall region (Fig. 3.14) and is described in detail in the following.

3.6.2.1 Proximal domain

Since all ten seismic lines do not extend into the proximal domain in the Porcupine Bank region, crustal thicknesses greater than 20 km, determined from gravity inversion (Welford et al., 2012), are interpreted as corresponding to the proximal domain in this study (Fig. 3.4b). From previous work, the proximal domain experiences little thinning of the continental crust, mainly developing normal faults and forming the fault-bounded sedimentary basins on the Porcupine Bank and in the northern Porcupine Basin (Naylor et al., 2002; Bulois et al., 2018; Whiting et al., 2021). Some sill complexes are distributed within the proximal domain of the Porcupine region (indicated by the dashed purple circle in Fig. 3.14), however, they are few or absent in the same domain for the Goban Spur region (Naylor et al., 2002).

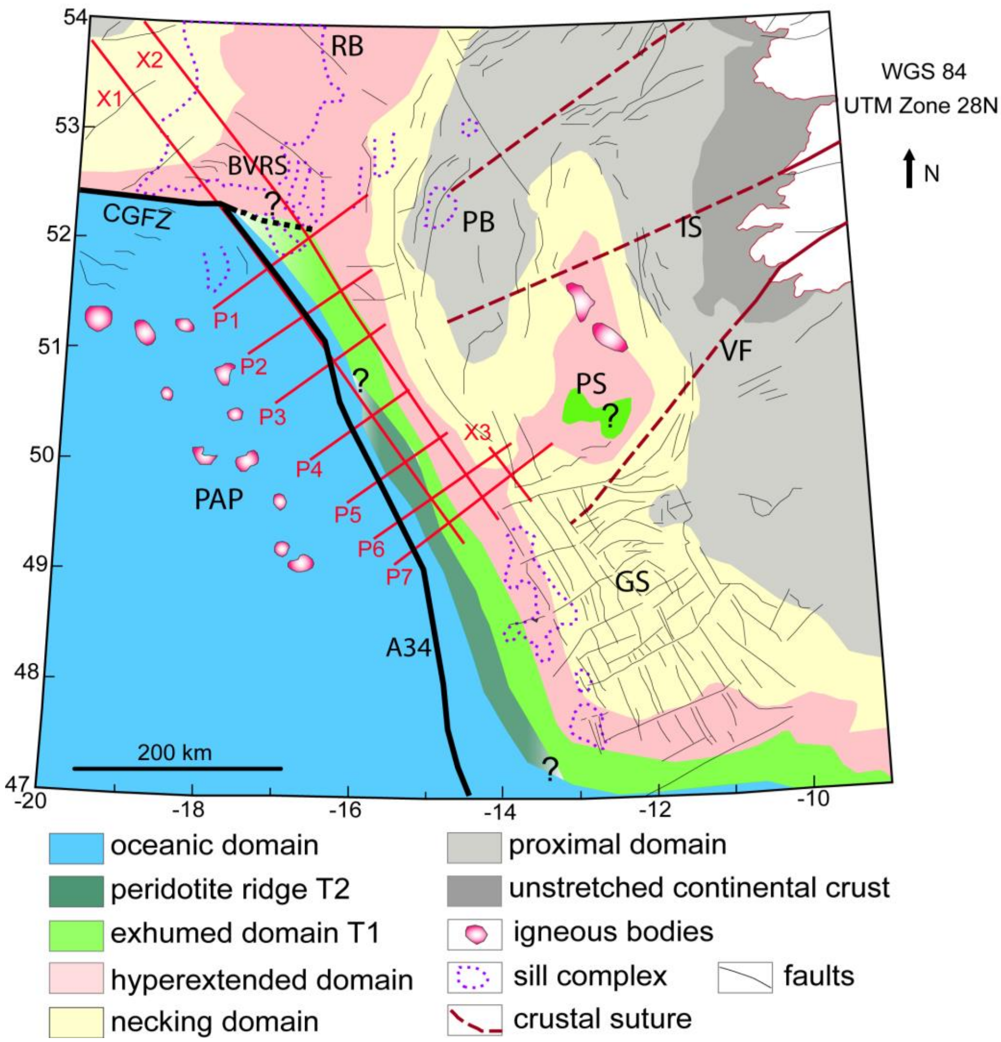

Figure 3.14: Crustal architecture map across the Goban-Porcupine-Southern Rockall region. The black solid line shows magnetic anomaly Chron 34 (A34) (Müller et al., 2016). Red solid lines indicate the new seismic reflection lines in this study. Fault interpretation is from Naylor et al. (2002) and the crustal sutures are adapted from Tyrrell et al. (2007). Igneous bodies and sill complexes are adapted from Naylor et al. (2002) and Gernigon et al. (2006). Abbreviations: GS, Goban Spur; PAP, Porcupine Abyssal Plain; PS, Porcupine Basin; PB, Porcupine Bank; RB, Rockall Basin; CGFZ, Charlie-Gibbs Fracture zone; BVRS, Barra Volcanic Ridge System; VF, Variscan Front; IS, Iapetus Suture.

3.6.2.2 Necking domain

Crustal thicknesses ranging from ~ 9 km to ~ 20 km are defined as the necking zone in regions lacking seismic coverage, consistent with the Goban Spur region (Yang et al., 2020). For the southern Rockall region, the necking domain is mainly delimited according to the shallowing Moho proxy from gravity inversion along both profiles X1-2 and X2-2 (shown in Figs. S-1 and S-2 in the supplemental material). The continental crust experiences localized attenuation in the necking domain, accompanied by the formation of listric faults (Péron-Pinvidic and Manatschal, 2009). From previous study (Naylor et al., 2002; Bulois et al., 2018; Whiting et al., 2021), faults are mainly margin-parallel along the Porcupine Bank and its neighbouring regions, whereas both margin-parallel and margin-perpendicular faults are observed for the Goban Spur region in the inferred necking domain (Naylor et al., 2002). Reverse faults are also observed in the southern Porcupine region, close to the transition from the Caledonian basement domains to the Variscan Front (Naylor et al., 2002). It is evident that the interpreted necking region along the western margin of the Porcupine Bank roughly corresponds to the transitional zone from negative to positive gravity anomalies (Fig. 3.4a). Also, it is narrow and has a steep gradient in crustal thickness based on gravity inversion, while it is wide and has a smooth crustal thickness gradient along the Goban Spur margin (Figs. 3.4b and 3.14).

3.6.2.3 Hyperextended domain

The hyperextended domain forms a narrow band from the Goban Spur region northward to the CGFZ. It is widest at the mouth of the Porcupine Basin, becoming narrower to the southwest of the Porcupine Bank and wider again close to the CGFZ. North of the CGFZ, the domain occupies a larger area in the southern Rockall Basin where the continental crust is highly stretched and underlain by serpentinized upper mantle (Morewood et al., 2003; 2005). Seaward-dipping listric faults and/or extensional detachment faults are observed in the hyperextended zone along these seismic lines (P4-P7), with the oceanward edge of the hyperextended region well constrained by these faults (Figs. 3.5, 3.6 and 3.9). Concave-upward sag basins bounded by

SW-dipping normal faults are generally observed in the hyperextended zone along P3-P7 (Fig. 3.6), consistent with the description in Tugend et al. (2015). Sills are sporadically distributed in the domain along the southwestern Porcupine Bank (Fig. 3.7b). Magmatic activity appears intense in the necking and hyperextended zones in the southern Rockall region (shown in Figs. S-1 and S-2 in the supplemental material).

3.6.2.4 Exhumed mantle domain

The interpreted exhumed serpentinized mantle zone becomes ~ 28 km narrower from the southwest of the Porcupine Bank to the CGFZ, on average. The exhumed subdomain T1 is ~ 13 km wide near the mouth of the Porcupine Basin and becomes ~ 30 km wide northward to the CGFZ. The exhumed subdomain T2 is interpreted to disappear in the region between seismic lines P3 and P4. Locally, the maximum width of the exhumed domain is ~ 32 km between lines P4 and P6, where subdomain T1 is very narrow with a span of ~ 11 km. Subdomain T2 is also interpreted to disappear to the southwest of the Goban Spur region but this is mainly due to the absence of seismic constraints (Yang et al., 2020). The disappearance of subdomain T2 on the western margin of the Porcupine Bank is interpreted based on basement geometry reflectivity characteristics.

Although the region south of the CGFZ along RAPIDS line 31, which intersects with profiles X2 and P1 (Fig. 3.2), is generally interpreted as the oceanic zone (Mackenzie et al., 2002; Morewood et al., 2003), there is also the possibility that a transitional zone between truly oceanic crust south of the CGFZ and thinned continental crust north of the CGFZ may exist (Mackenzie et al., 2002). The faulted basement in the area close to the intersections of profiles P1, X2-1, and RAPIDS line 31 (Figs. 3.7b and 3.13) may support this hypothesis. Stretching factors derived from gravity inversion (Welford et al., 2012) between profiles P1 and P3 range from ~ 3.5 to ~7.5, indicating that complete crustal embrittlement could have occurred (Pérez-Gussinyé and Reston, 2001). The interpreted basement faults along profiles P1, P2, and P3 in this region could have facilitated serpentinization and mantle exhumation when this region experienced extreme hyperextension. Thus, the zone of serpentinized exhumed mantle (subdomain T1) is interpreted in the region spanning the northern profiles P1, P2, and P3, despite a lack of drilling constraints and without evidence for serpentinized peridotite ridges (subdomain T2) along these three profiles (Figs. 3.5 and 3.14). While there is no evidence of exhumed serpentinized mantle in the southern Rockall Basin region (Morewood et al., 2003; 2005), the exhumed subdomain T1 across the Porcupine-southern Rockall Basin region is interpreted to continue northwestward and is assumed to abruptly disappear at the CGFZ. Meanwhile, increasing magmatic additions within the exhumed domain are observed to the north, shown along seismic lines P1 and X2 (Figs. 3.5 and 3.7b).

3.6.2.5 Oceanic domain

The oceanic domain is bounded by the seaward limit of the exhumed mantle domain along most of the margin and the CGFZ in the north, which marks an abrupt transition between continental and oceanic domains in the southern Rockall region (Hauser et al., 1995). The area between magnetic Chron 34 (A34) and the oceanward limit of the exhumed domain becomes gradually narrower from the Goban Spur region in the south to the region between seismic lines P4 and P5 (Fig. 3.14). In contrast, the area northward becomes slightly wider in the region between lines P3 and P4, where exhumed subdomain T2 disappears and magnetic Chron 34 tends to be situated inboard of profile X1. Large volcanic cones are observed between lines P2 and P3, whereas small cones and more volcanic features occur in the region close to line P1 (Fig.

3.5). In the Porcupine Abyssal Plain, igneous bodies and sill complexes have also been identified from potential field data (Gernigon et al., 2006).

3.7 Discussion

3.7.1 The influence of pre-existing inheritance on the western Porcupine Bank

The interpreted crustal domains in this study correspond to a series of rifting stages that capture the life cycle of the rifted continental margin (Péron-Pinvidic et al., 2013; Tugend et al., 2015). Numerous factors such as thermal, rheological, compositional, crustal and/or mantle states of lithosphere, and pre-existing inheritance provide the initial weaknesses that can play an important part in the evolution of rifted margins (Simon et al., 2009; Manatschal et al., 2015; Brune et al., 2017), even varying from one segment to another in the same rift system (Müntener and Manatschal, 2006; Chenin and Beaumont, 2013). Pre-existing orogenic inherited structures are the main focus in this paper since Caledonian and Variscan orogenic structural grains are postulated to have seeded and been reactivated during the rifting of the southern North Atlantic (Masson et al., 1989; Kimbell et al., 2010; Tyrrell et al., 2007; 2010; Chenin et al., 2015). Pre-existing orogenic inheritance is known to have an impact on the crustal geometries and the volume and timing of magmatic events during rifting (Morley et al., 2004; Manatschal et al., 2015; Phillips et al., 2016; Schiffer et al., 2019). In the Porcupine sector, the inherited Caledonian basement is divided into Proterozoic, and Proterozoic to Early Paleozoic terranes, separated by major fault zones (Figs. 3.1 and 3.14) (Tyrrell et al., 2007; 2010). The orientations and locations of these crustal sutures become increasingly uncertain oceanward due to limited constraints and overprinting by later tectonic events. For example, many parts of the Caledonian domain may be eroded because of uplift in the Cenozoic (Gee et al., 2013). Meanwhile, the

Iapetus Suture is interpreted to have a possible connection with the CGFZ, suggestive of reactivation of an inherited Caledonian lithospheric fabric (Shannon et al., 1994; Buiter and Torsvik, 2014), however, it is proposed to extend across the southern Porcupine Bank (Figs. 3.1 and 3.14) (Tyrrell et al., 2010).

By observing profiles X1 and X2 across the western Porcupine region, we can see variable top basement topography (Fig. 3.7). This along-strike variability in top basement relief may be partially due to early and long-lived reactivation of Variscan orogenic trends compared with later rejuvenation of the Caledonian basement terranes (Chenin et al., 2015). Specifically, in the hyperextended domain along X2-1, the top-basement between P6 and P7 is deeper than it is between P4 and P5 (Fig. 3.7b). Also, flower structures are interpreted in the region between profiles P6 and P7 along X2-1, where shear zones (?) are observed beneath the top basement with extensional faults penetrating into the crust (Fig. 3.10b). This could arise in part because this region is close to the offshore continuation of the Variscan Front. Meanwhile, rifting of the southern Porcupine Basin may also have been involved. Likewise, the top-basement between P6 and P7 shallows into peridotite ridges in the exhumed domain along X1-1 (Figs. 3.7c and 3.11). The northwestward change in seismic character from profile P6 to P5 could arise in part because Caledonian-affected regions lie to the north of P6, while regions to the south were progressively influenced by Variscan tectonics (Figs. 3.7 and 3.14). Further to the northwest along X2-1, the negative flower structure observed between P3 and P4 (Figs. 3.7b and 3.10a), further suggests oblique slip between the two pre-existing basement terranes across the Iapetus Suture, which was reactivated during the northward propagation of the North Atlantic rift (Chenin et al., 2015). In this region, the deep reflection ~3 km beneath the top basement may be the detachment surface, possibly acting as a rheological interface (Figs. 3.10a and 3.7b).

Although the interpreted exhumed domain is more speculative close to the CGFZ due to the lack of drilling information and the masking influence of igneous units, both the exhumed T1 and T2 subdomains are interpreted for the Avalonian and Variscan basement terranes along X1-1, whereas only subdomain T1 is interpreted for the Proterozoic to early Paleozoic terrane (or Laurentia terrane) north of the Iapetus Suture along X2-1 (Figs. 3.1, 3.7, and 3.14). The disappearance of the peridotite ridges (subdomain T2) (Fig. 3.14) may illustrate variations in the crustal rifting behavior of the Irish margin from southeast to northwest, due to variations in crustal composition and rheology across the Iapetus Suture (Norton, 2002). Further northwest, although the fault zones separating the Proterozoic basement terrane from the Proterozoic to early Paleozoic basement region appear to extend into the region between profiles P1 and P2 (Figs. 3.1 and 3.14), it is difficult to identify pronounced differences in the basement morphology and reflectivity characteristics between profiles X1-1 and X2-1 (Figs. 3.7 and 3.11). This may be due to enhanced magmatism where profiles X2-1 and X1-1 are, respectively, much closer to, and inboard of, magnetic anomaly 34 (A34) (Fig. 3.2).

This observation appears to be consistent with the idea that extensional deformation, mainly affected by pre-existing inherited structures, gradually transitions into a region of deformation that is primarily influenced by magmatic events from hyperextension-exhumation to steady seafloor spreading (Manatschal et al., 2015; Chenin et al., 2015). This observation is also consistent with the increasingly inferred segmentation of the Porcupine region (Norton, 2002; Grow et al., 2019; Whiting et al., 2021), suggesting that the Porcupine Bank was more structurally complex than a simple uniform continental block, as previously proposed (White et al., 1992; McCann et al., 1995; Peace et al., 2019).

3.7.2 Key tectonic processes of the offshore western Porcupine Atlantic margin

Sedimentary layers are linked to migrating deformation from rift initiation to eventual oceanic crust emplacement during the formation of the Irish Atlantic margin (Péron-Pinvidic et al., 2013). Although we have delimited the structural domains in detail along each of the seismic profiles (Figs. 3.6 and 3.7), the syn-rift sequences are simply shaded pink, with no differentiation of distinct rifting stages. To address the relationship between syn-rift sedimentation and rifting stages, we select profile P6 as a representative profile for the Porcupine Atlantic margin to investigate the link between syn-rift sequences and progressive oceanward migration of deformation in this study in Figure 3.8. At drilling site 43/13-1 on the eastern margin of the Porcupine Bank (Fig. 3.2), which targeted a tilted fault block, Middle Jurassic sequences are interpreted to overlie the rift onset unconformity (Mackay, 2018). With reference to the eastern flank of the Porcupine Bank, the western flank margin is assumed to undergo rifting during the Jurassic, in agreement with the seismic interpretation of the southwestern flank of the Porcupine Basin in Tomsett et al. (2017) and Whiting et al. (2021). It should be noted that although the pre-Jurassic (e.g., Permo-Triassic; Štolfová and Shannon (2009)) syn-rift layers can be observed in the western Porcupine Bank, they are not well constrained. Therefore, in this study, the syn-rift layers are primarily interpreted to be composed of Early Jurassic (?), Mid-Late Jurassic, and earliest Cretaceous sediments (Fig. 3.8). The Early Jurassic sequences are inferred to be related to the stretching-necking stage that initiated from distributed rifting, and the Late Jurassic sedimentary packages are associated with the hyperextension stage. The final syn-rift sequences in the early Cretaceous formed during the mantle exhumation phase. In contrast for the Goban Spur margin, the necking stage began in the post-Barremian and ended before the Late Albian based on drilling site 549 (de Graciansky et al., 1985). Thus, we deduce that while the Goban

Spur was experiencing lithospheric necking, the Porcupine Bank had already entered the hyperextension and exhumation stages. This may have resulted from the longer necking stage of the Goban Spur region with smooth gradients in crustal thickness compared with a shorter necking period for the Porcupine Bank with steep crustal thickness gradients (Figs. 3.4 and 3.14). In addition, the relatively early syn-rift horizons transition into rotated horizons in the main syn-rift stage in the necking and hyperextended domains, probably due to inherited weaknesses associated with the Variscan Front and episodic rifting events of the southwestern Porcupine Basin.

Fault types are proposed to correlate with the rift domains on hyperextended rifted margins (Gillard et al., 2016). In this study, low seismic resolution below basement appears to limit the number of observed faults. The paucity of faults may also reflect the preferential destruction of early faulting evidence due to later faulting from complicated poly-phased extensional episodes (Reston, 2007). Alternatively, the lack of faults may be due to depth-dependent stretching (Kusznir and Karner, 2007). Regardless, faults that sole out in the middle crust are still observed in the necking domain (Fig. 3.8), corresponding to a rapid increase in crustal thinning (Péron-Pinvidic et al., 2013). The top basement and top mantle appear to converge at the SW end of the necking domain based on the shallowing Moho (Fig. 3.8). In the hyperextended domain, in addition to the regional normal faults, which are likely related to N-S and E-W oriented extensional events, a detachment fault is observed at the transition between the hyperextended and exhumed domains, consistent with faults cutting the entire crust. As extension migrates oceanward, the crustal section is entirely replaced by exhumed serpentinized mantle rocks at the seabed through landward-dipping exhumation faults (Fig. 3.8), which appear to connect with the detachment fault. Meanwhile, the post-exhumation faults with footwall uplift (indicated by the fault in the dark green region in Fig. 3.8) help unroof the peridotite ridges and eventually lead to the formation of oceanic crust through decompression melting.

3.7.2.1 The stretching - necking phases

The proximal and necking domains are, respectively, formed during the lithospheric stretching and thinning phases (Péron-Pinvidic et al., 2013). Extensional deformation over the Porcupine Bank during the stretching - necking phase appears to have been less complicated than across the Goban Spur because fault patterns on the former margin appear simpler than over the latter margin (Naylor et al., 2002). As discussed, this may be due to differences in the pre-existing basement terrane compositions and rheologies (Figs. 3.1 and 3.14).

3.7.2.2 The hyperextension-mantle exhumation phases

The hyperextended and exhumed domains correspond to the lithospheric hyperextension and exhumation stages (Péron-Pinvidic et al., 2013). The tectonic processes forming the hyperextension – exhumation domains are still debated. Taking the Iberian margin as an example, seaward migration of sequential faulting (Ranero and Pérez-Gussinyé, 2010), polyphase faulting (Reston, 2005), and detachment deformation (Whitmarsh et al., 2001) have been proposed to explain this rifting stage. At the Porcupine Bank margin, reflectivity is weak beneath basement, but reflective detachment faults at the seaward termination of the hyperextended zone are observed along profiles P4-P6 (Figs. 3.6-3.9). These low-angle detachments, downthrown to the SW in the hyperextended zone (Fig. 3.9), show geometric similarities along P4-P6 (Figs. 3.9b-9d). For example, they terminate in the shallow crust (8-9 km) and can be traced to the exhumed domain. They are also overlain by a series of rotated faulted blocks. This detachment system captures the attenuation of continental crust and the initiation of mantle exhumation. This also suggests a uniform margin-parallel hyperextension phase across profiles P4 to P6. Seaward, the interpreted exhumed domains along profiles P7, P6, P5, and P4, particularly for the serpentinized peridotite ridges, cover different margin-perpendicular extents with variable basement morphologies (Figs. 3.5 and 3.6). These variations suggest that the margin-parallel mantle exhumation was not uniform.

The entire crust becomes brittle when stretching factors are between ~ 3 and ~ 5, and mantle serpentinization follows crustal embrittlement (Reston, 2009). The interpreted hyperextended and exhumed mantle zones along the southwestern Porcupine Bank are consistent with the margin-parallel variations in stretching factors (ranging from ~ 3.5 to ~7.5) derived from gravity inversion (Welford et al., 2012). To date, the formation mechanisms of the interpreted peridotite ridges along the Porcupine Bank margin remain unclear. However, the degree of serpentinization may also be variable along the margin since mantle velocities beneath the southern Rockall Basin are not less than 7.5 km s^{-1} (Shannon et al., 1999), indicative of a low degree of serpentinization, compared with mantle velocities of over 7 km s^{-1} at depth across the Goban Spur margin (Bullock and Minshull, 2005). In addition, there are still relatively strong reflectors ~ 3 km beneath top basement (~ 8-10 km at depth) in the exhumed domain on sections P3, P5, and P6 (Fig. 3.6). These discontinuous intra-basement reflectors (~ 1s TWT beneath top basement in Fig. 3.5) are likely to represent a rheological interface, where localized deformation occurs due to changes in serpentinization degree (Gillard et al., 2019). Increasing extension rates between the Irish and Newfoundland margins may also contribute to forming the serpentinized peridotite ridges by analogy with those on the conjugate Newfoundland margin (Welford et al., 2010a).

3.7.2.3 The breakup and oceanization phases

In this study, we assume breakup is a process involving the late stages of serpentinized mantle exhumation and variable amounts of magmatism, corresponding to the region between the seaward limit of the peridotite ridges and magnetic Chron 34 (A34) (Figs. 3.5 and 3.6). Although the location of the boundary between the oceanic and exhumed domains along the northern part of the western Porcupine Bank margin is uncertain due to the chaotic and unclear basement reflectivity along profiles P1, P2, and P3 (Fig. 3.5) as a result of magmatic intrusions that predate the formation of oceanic crust, the boundary still roughly follows the seaward limit of the exhumed domain (Fig. 3.14). In contrast, the boundary between the two domains is well constrained based on clear reflectivity trends along profiles P4, P5, P6, and P7 (Fig. 3.5). This suggests that breakup-related magmatism becomes more pronounced in the northern part of the western Porcupine Bank margin, particularly close to the CGFZ. In comparison, the breakup of the southwestern Porcupine Bank and the Goban Spur is amagmatic. Post-breakup extensional deformation and volcanism continued to occur on the west Porcupine Bank, clearly illustrated by the normal faults observed at the top basement in the oceanic zone (especially along profile P3, Fig. 3.6c) and volcanoes along profiles P1, P2, and P3 (Figs. 3.5 and 3.6).

On the whole, in spite of the more speculative distributions of the crustal domains further north of the CGFZ due to the influence of magmatism, the crustal domain geometries across the southwestern Porcupine Bank and southern Rockall regions are more complicated than they are for the Goban Spur region. Furthermore, the along-strike variations in crustal architecture along the Porcupine region suggest that it experienced partitioned and localized deformation as a result of complex stress regimes, likely caused by the interplay of Caledonian and Variscan inheritance with Mesozoic rifting.

3.7.3 Magmatism along the Porcupine Atlantic margin

At magma-poor rifted margins, limited volcanism in the crust can still affect the tectonic deformation, and the intrusion of large sills can transport and laterally distribute large volumes of magma from the deep crust (Magee et al., 2016). Understanding the extent and timing of magmatism can provide insights into the structures and overall tectonism of these margins. Major magmatic additions, which may be associated with the pre-, syn-, and post-rift phases, have been mapped over the Rockall and Porcupine basins (Fig. 3.14) (Naylor et al., 2002; Gernigon et al., 2006; Keen et al., 2014; Funck et al., 2017). According to the classification of seismic facies units related to volcanism (Gagnevin et al., 2018), igneous centers (e.g., offshore seamounts and igneous complexes) and sill intrusions are mainly observed across the western Porcupine Bank and the southern Rockall Basin based on regional seismic data. The igneous centers over the southwestern Porcupine Bank from this study are mainly distributed in the oceanic and exhumed domains (Figs. 3.5, 3.6, and 3.7). The volcanic seamounts and complex igneous basement on the seismic data (Figs. 3.5 and 3.6), plus the previously interpreted igneous centers in the oceanic domain (Gernigon et al., 2006), illustrate that magmatism occurred during continental rifting and continued after the breakup between the Newfoundland margin and the Irish Atlantic margin (Figs. 3.5 and 3.14). The basement in the interpreted oceanic domain changes from relatively flat relief (profiles P4-P7) to rugged morphologies (sparse seamounts on profiles P2 and P3, and more narrow volcanic ridges on profile P1) (Fig. 3.5). These indicate that the distribution and magnitude of post-breakup volcanism differed from southeast to northwest. The sill complexes intrude pre-, syn-, and post-rift sedimentary layers and are observed in each crustal domain over a wide range of depths (Figs. 3.6, 3.7, and 3.13). Also, the amount of rift-related magmatism varies from one crustal domain to another based on the interpreted sills.

Overall, the true areal coverage of sills may be greater than the regions outlined in Figure 3.14, due to the relative sparsity of seismic constraints.

The identification of sills based on seismic observation can be complicated by faulted structures and the physical properties (e.g., lithology and pressure) of sedimentary strata (Planke et al., 2005; Gagnevin et al., 2018). Despite the variable geometries of the interpreted sill complexes in this study, sills intruding the post-rift sedimentary layers are mainly observed to be layer-parallel (Figs. 3.7 and 3.13) or saucer-shaped (Fig. 3.13). Regardless of their differing morphologies, deeper sills can be the magma feeders for the shallower sill complexes, and faults can also be exploited by the intruding sills (Thomson and Schofield, 2008). The seismic characteristics of the sill complexes in the study region have also been observed in other rifted sedimentary basins along the NE Atlantic margins (Planke et al., 2005; Thomson and Schofield, 2008; Gagnevin et al., 2018). Models for their emplacement remain topics of active research (Bradley, 1964; Francis, 1982; Thomson and Schofield, 2008).

Based on the distribution of interpreted magmatic features along profiles X1, X2 and from previous studies (Naylor et al., 2002; Gernigon et al., 2006), the magma budget is postulated to increase progressively from the Goban Spur in the south, to the Porcupine-southern Rockall regions in the north (Figs. 3.6 and 3.7). As previously introduced, the southernmost Porcupine Basin and the Goban Spur region are part of the amagmatic Variscan-affected region, while the Porcupine Bank and southern Rockall regions are primarily in the Caledonian-affected regions which experienced more magmatic breakup (Chenin et al., 2015). The variations in the magma budget may also be affected by the interplay between inherited lithospheric features and variations in the degree of decompression melting, as interpreted for other North Atlantic margins (Schiffer et al., 2019; Gouiza and Paton, 2019).

3.7.4 Reconstruction of the Porcupine Atlantic margin and its conjugates

Although there have been many published plate reconstruction models for the rifting and breakup of the North Atlantic for the Mesozoic-Cenozoic eras, the locations of continental fragments and their intervening basins (the Flemish Cap, Orphan Basin, Porcupine Bank, Porcupine Basin, and Goban Spur) have differed through geological time for each plate reconstruction model based on different assumptions and simplifications (Seton et al., 2012; Matthews et al., 2016; Müller et al., 2018; Nirrengarten et al., 2018; Barnett-Moore et al., 2018; Peace et al., 2019). Yang et al. (2020) superimpose the interpreted crustal domains across the Goban Spur margin and the Flemish Cap margin onto the restored plate model from Matthews et al. (2016). However, the model fails to consider the clockwise rotation of the Flemish Cap. In contrast, the reconstructed plate model from Nirrengarten et al. (2018), still based on the rigid plate reconstruction approach, takes the motion of the Flemish Cap into account. Since the rotation of the Flemish Cap has also been supported by gravity data and seismic data analysis (Sibuet et al., 2007; Welford et al., 2010a, 2010b; Welford et al., 2012), the restored plate model from Nirrengarten et al. (2018) is used to compare the crustal geometries along the Porcupine Bank and the Flemish Cap margins in this study (Fig. 3.15).

Compared with the gradual necking zone profile across the Goban Spur, the crustal thickness transitions are steep in the necking domains across both the Flemish Cap and the western Porcupine Bank margins (Welford et al., 2012). Both exhumed subdomains T1 and T2 are mapped along the western Porcupine Bank margin, whereas only subdomain T2 is interpreted on the Flemish Cap margin (Welford et al., 2010b). To the north along both margins, the peridotite ridges (subdomain T2), which display margin-parallel variability, are interpreted to disappear. The crustal domain interpretation on the Flemish Cap margin is primarily based on basement morphologies (Welford et al., 2010b) and on crustal velocities (Gerlings et al., 2011; Welford et al., 2020), which show that either proto-oceanic crust or continental crust underlain by serpentinized upper mantle makes up the continent-ocean transition domain. The reconstructed pre-breakup locations and distributions of interpreted exhumed subdomain T2 on both sides appear misaligned during the mantle exhumation stage (Fig. 3.15), with differing extents of proto-oceanic crust relative to magnetic anomaly 34.

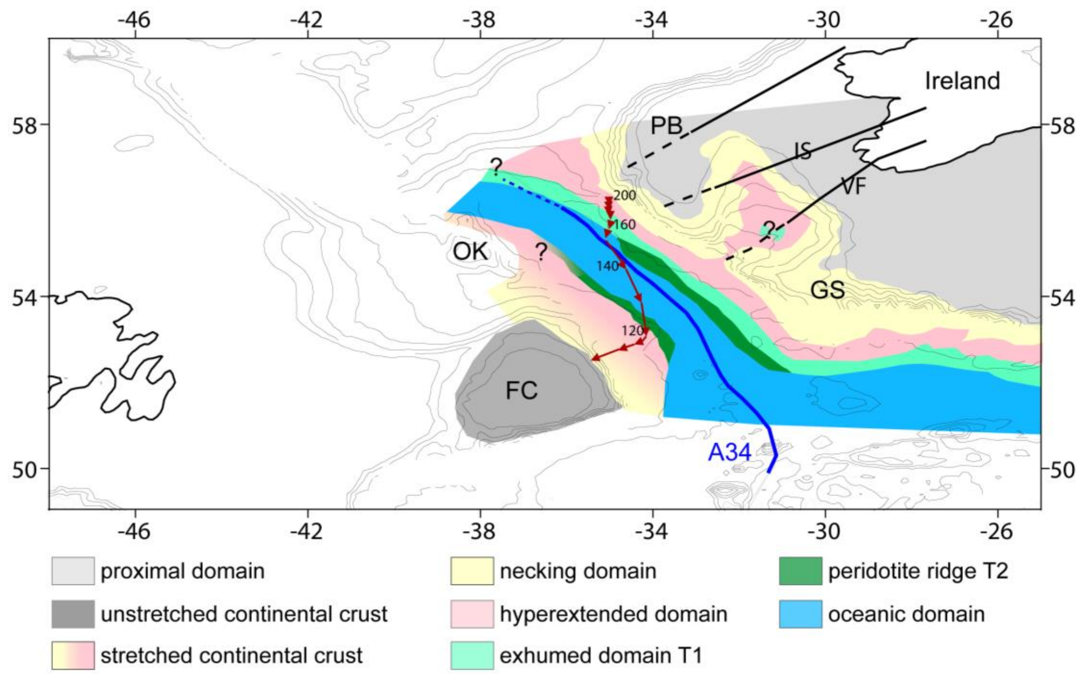

Figure 3.15: Crustal domain map back to the Early Campanian across the Porcupine Atlantic - Flemish Cap margins based on a rigid plate reconstruction in Gplates 2.1 (Nirrengarten et al., 2018), underlain by the corresponding modern-day bathymetric contours replotted at ~ 82 Ma (indicated by the thin grey lines). The blue line shows magnetic anomaly 34 (Srivastava et al., 1988). The dark red arrows indicate the motion path of FC relative to PB from the Early Jurassic to Late Cretaceous (200-82 Ma), with the Greenland plate fixed. The distances between the dark red triangles indicate displacement between FC and PB at 10 Myr increments. The crustal domains on the Flemish Cap margin are adapted from Welford et al. (2010a) and Welford et al. (2020). Abbreviations: VF, Variscan Front; IS, Iapetus Suture; GS, Goban Spur; PB, Porcupine Bank; FC, Flemish Cap; OK, Orphan Knoll.

The seaward edge of the exhumed mantle on the Flemish Cap margin appears to maintain a relatively constant distance from magnetic anomaly 34 in the kinematic restoration model back to the Early Campanian (Fig. 3.15). On the contrary, magnetic anomaly 34 gradually becomes closer to the seaward edge, or even extends northward into the exhumed domain in the western Porcupine region in this reconstruction. Assuming the reconstructed model based on Nirrengarten et al. (2018) is robust and reliable, the paleo-position of the exhumed domain on the western Porcupine Bank should be further away from magnetic anomaly 34 since it represents the first undisputed oceanic region (Srivastava et al., 1988; Müller et al., 2016). Alternatively, the exhumed serpentinized mantle should be interpreted as narrower along the western Porcupine Bank margin. However, so far, the motion of the Porcupine Bank is still under debate. For example, some researchers have suggested independent clockwise rotation of the Porcupine Bank during the rifting of the Porcupine Basin during the Middle to Late Jurassic (Peace et al., 2019), or shearing due to reactivation of pre-existing crustal sutures (Grow et al., 2019), or potential segmentation of the Porcupine region (Whiting et al., 2021). Consequently, the complex rift kinematics of the Porcupine Bank cannot be fully illustrated using the rigid plate reconstruction model from Nirrengarten et al. (2018).

The distributions of crustal domains on both the Porcupine Atlantic and Flemish Cap margins are asymmetric (Fig. 3.15). The motion path of the Flemish Cap relative to the Porcupine Bank from the Early Jurassic to Late Cretaceous (200 - 82 Ma) (the dark red arrows in Fig. 3.15), indicates that the extension rate and orientation vary between the two margins when the Greenland plate is kept fixed. Specifically, during the Jurassic, oblique extension between the two margins occurs with relatively low extension rates. The strike-slip motion appears between both margins in the latest Jurassic to earliest Cretaceous (150-140 Ma), with faster extension rates. As extension continues, rift obliquity resumes until rifting becomes margin perpendicular between the Flemish Cap and Goban Spur during Aptian-Albian time. The asymmetric geometries of crustal domains along both margins were likely influenced by the movement of independent continental blocks accompanied by varying amounts and durations of extension obliquity between the Porcupine Bank and the Flemish Cap during the Jurassic to Early Cretaceous (Brune et al., 2018), and/or the segmentation of the Porcupine Bank. Reactivation of inherited structural fabrics is likely to have played a role as well.

3.8 Summary

New multichannel seismic reflection profiles, combined with potential field data, across the western Porcupine Bank - southern Rockall region, are used to elucidate the crustal architecture and tectonic evolution of the less studied Porcupine Atlantic margin. The discoveries include:

(1) Variable geometries along-strike of the margin for each crustal rift domain from the necking domain, to the hyperextended domain to the exhumed domain and to the oceanic domain, likely related to variations in extension rates during each rifting stage.

(2) Inherited Caledonian and Variscan crustal sutures and fabrics appear to have influenced the different geometries of the crustal domains and can be directly observed on the along-strike seismic profiles.

(3) Zones of exhumed serpentinized mantle, characterized by both deep and subtle topography and shallow peridotite ridges, are interpreted to extend northward from the Goban Spur margin all the way to the southern Rockall region. However, the peridotite ridges disappear to the north, possibly due to changes in composition and rheology of the rifted crustal basement terranes, which controlled their response to rifting.

(4) Considerable along-strike variations in magmatism are revealed, with plentiful and complex saucer-shaped and layer-parallel sill complexes toward the northwest of the margin and

the CGFZ. In contrast, breakup along the southwestern Porcupine Bank and the Goban Spur margins was amagmatic.

(5) Rigid plate restoration of the crustal architecture of the Porcupine Atlantic and Flemish Cap margins indicates asymmetric geometries of crustal domains, and varying extension obliquity and extension rates between the two margins, likely associated with the clockwise rotation of both the Flemish Cap and the Porcupine Bank during the Jurassic to Early Cretaceous. Use of a published rigid kinematic plate restoration to track the interpreted domains through geological time, however, does not account for the segmentation of the Porcupine Bank during the opening of the Porcupine Basin, nor the effect of oblique extension on inherited structural fabrics in the western Porcupine Bank region.

Despite uncertainties due to the sparsity of complementary constraints, this study provides additional insights into the western Porcupine Bank region, contributing to an enhanced understanding of the evolutionary history of the Irish Atlantic margin and its relationship with its conjugate margins. Future work will involve deformable plate modelling in order to better understand the evolving geometries of each crustal domain along both the Irish Atlantic and Newfoundland margins.

3.9 Supplemental material

The supplemental material in this study mainly consists of the interpretations of crustal domains along profiles X1-2 and X2-2. By identifying the boundaries of crustal domains along both profiles, the crustal domains in the northwestern part of the Porcupine Bank can be mapped in Figure 3.14. Specifically, further to the northwest into the Rockall Basin, the border between the hyperextended and necking zones along profiles X1-2 and X2-2 is mainly based on the increased Moho depth from gravity inversion (Welford et al., 2012). In the necking zone along both lines, the normal faults sole out at mid-crustal levels (Figs. 3.S-1 and S-2), suggesting crustal thinning. Saucer shaped and layer-parallel sill reflections are prominent and separated by faults in the necking zone along both profiles. In the hyperextended domain, saucer shaped sills intrude into the sedimentary layers along profile X1-2 (Fig. 3.S-1), while this region along profile X2-2 is characterized by the igneous top basement (Fig. 3.S-2). In total, highly variable geometries of sill complexes are observed along both profiles.

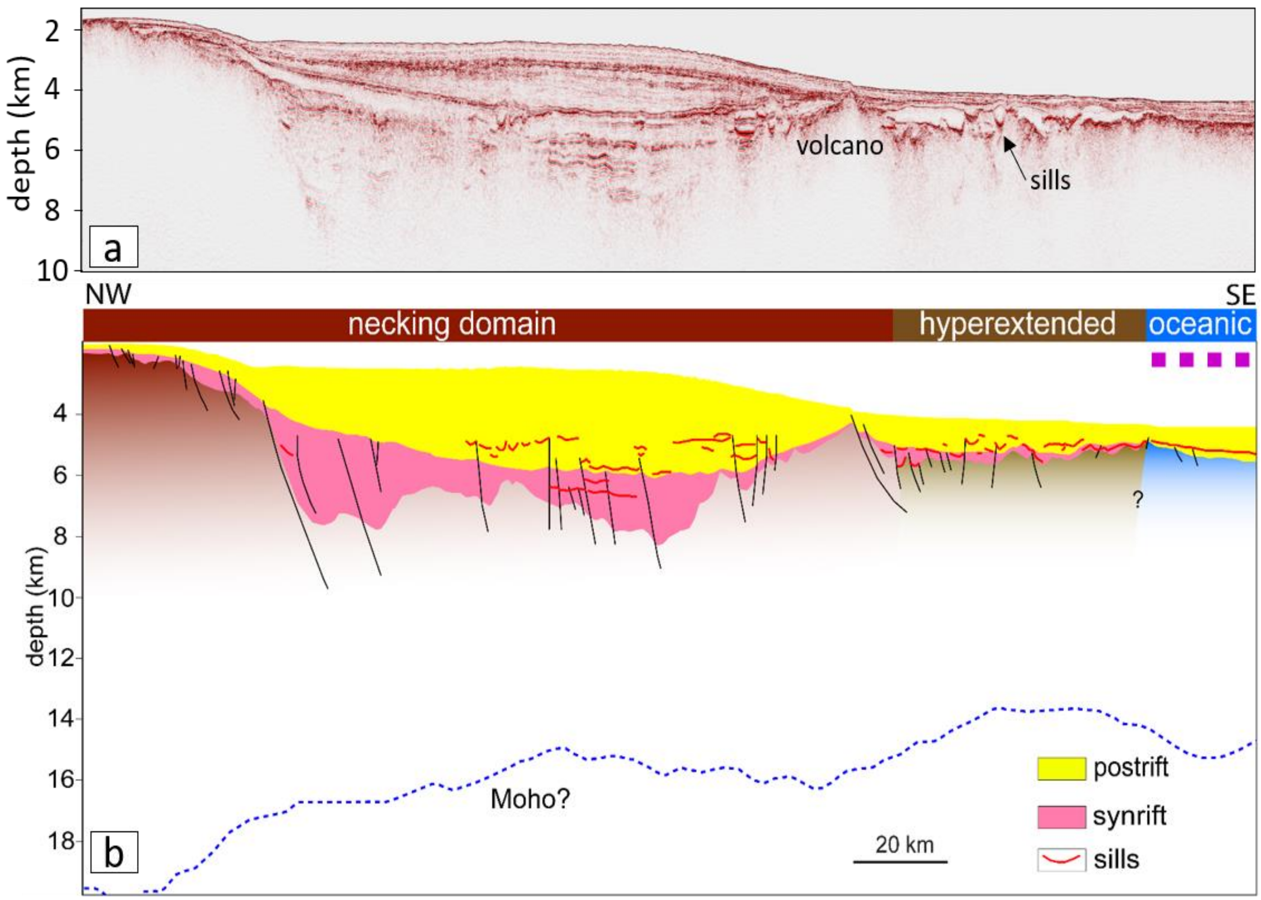

Figure S-1: (a) The uninterpreted section of the northwestern part of seismic profile X1-2 across the CGFZ. (b) The interpreted seismic profile X1-2 in the depth domain. The thick purple dashed line indicates the approximate location of the CGFZ. The blue dashed indicate the Moho (?) from gravity inversion (Welford et al., 2012).

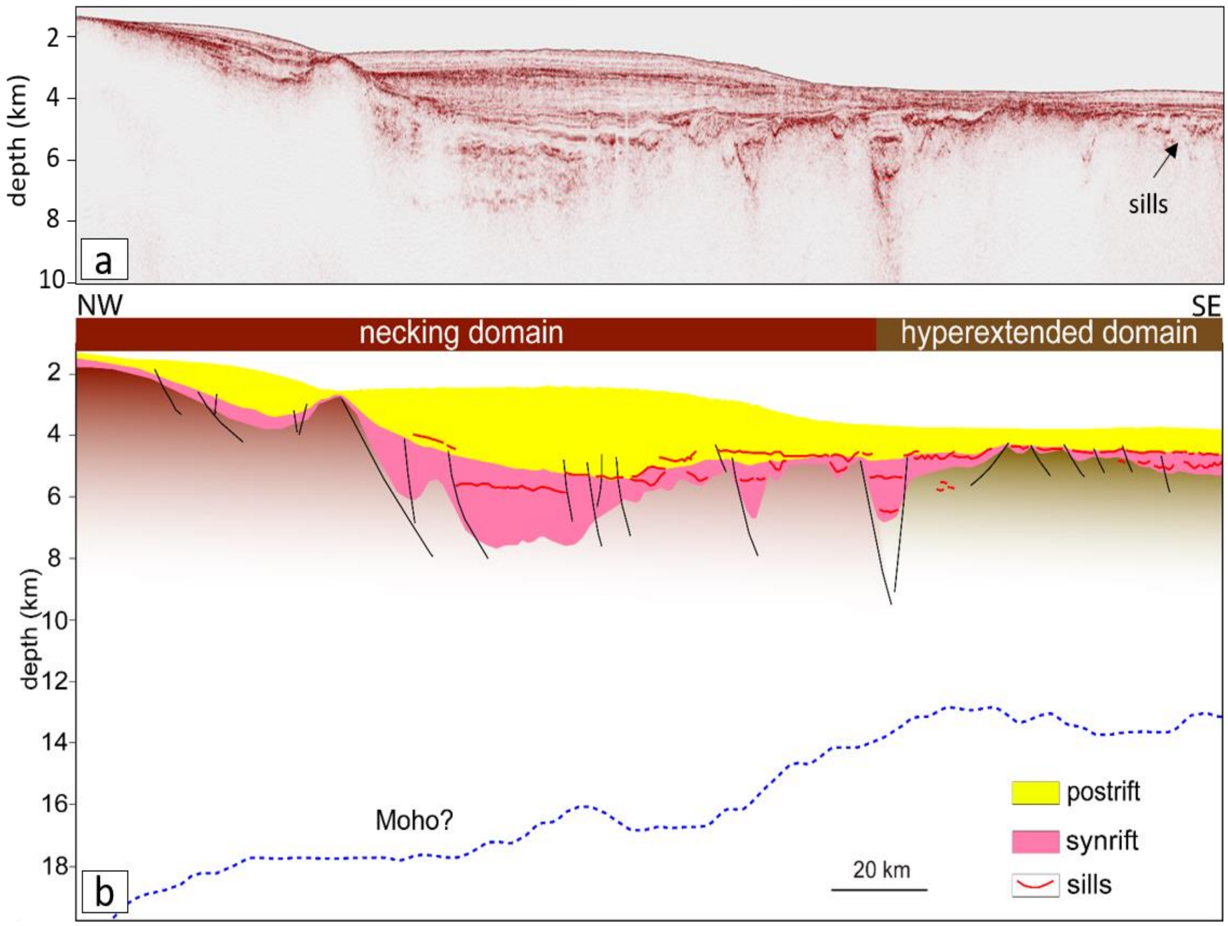

Figure S-2: (a) The uninterpreted depth-converted seismic profile X2-2. (b) The interpreted seismic profile X2-2 in the depth domain. The blue dashed indicate the Moho (?) from gravity inversion (Welford et al., 2012).

Acknowledgement

We are grateful to the Department of the Environment, Climate and Communications of Ireland for providing the multichannel seismic reflection data. We also acknowledge the Petroleum Infrastructure Programme (PIP) in Ireland for access to the technical studies and regional reports. Schlumberger are acknowledged for donating Petrel software to Memorial University of Newfoundland. We would like to thank the members of the Memorial Applied Geophysics for Rift Tectonics (MAGRiT) group for providing suggestions for this research. We appreciated Michael Nirrengarten and the other anonymous reviewer's constructive comments.

Chapter 4

4. Assessing the rotation and segmentation of the Porcupine Bank, Irish Atlantic margin, during oblique rifting using deformable plate reconstruction

This chapter is under review as "*Yang, P., Welford, J.K., and King, M. Assessing the rotation and segmentation of the Porcupine Bank, Irish Atlantic margin, during oblique rifting using deformable plate reconstruction. Tectonics, 2020TC006665*." *Kim Welford supervised the research and helped manuscript preparation. Michael King assisted in shaping ideas and editing the manuscript.*

4.1 Abstract

Published plate reconstructions have provided insights regarding the formation of the North Atlantic, in which the motion of the Porcupine Bank, on the Irish Atlantic margin, underlain by orogenic pre-rift crustal basement terranes, is investigated and restored. However, previous reconstructions of the Porcupine Bank mainly relied on potential field data rather than seismic constraints and failed to reveal the role of inherited crustal terranes during rifting and subsequent crustal deformation. In this study, five deformable plate tectonic models with distinct structural inheritance trends are established in GPlates by adjusting a previously published restoration model for the North Atlantic. For each model, driving factors such as the inclusion of the Orphan Knoll, the Flemish Cap poles of rotation, and the motion of the eastern border of the

Porcupine Basin are also considered. To assess the validity of deformable plate models, crustal thickness estimates obtained from gravity inversion and seismic data modelling are compared with those calculated via deformable plate models. The preferred deformable plate model proposes the subdivision of the Porcupine Bank into four blocks with each block experiencing poly-phased rotation and shearing prior to final continental breakup, implying strong inheritance and segmentation of the Porcupine Bank and Porcupine Basin. The reconstructed paleo-positions of the Flemish Cap and Porcupine Bank within deformable regions reveal evolving conjugate relationships during rifting, which are assessed using regional seismic transects from both margins. Finally, extensional obliquity between both margins is quantitatively restored, showing time-variant orientations due to the rotation and shearing of associated continental blocks.

4.2 Introduction

Previous rigid and deformable plate tectonic reconstruction studies have provided valuable insights regarding the evolution of rifted margins throughout the North Atlantic realm (Srivastava and Verhoef, 1992; Seton et al. 2012; Gurnis et al., 2012, 2018; Matthew et al., 2016; Barnett-Moore et al., 2016; Nirrengarten et al., 2018; Peace et al., 2019; Müller et al., 2018, 2019; Ady and Whittaker, 2019). In several previously published reconstructions (Nirrengarten et al., 2018; Peace et al., 2019), the relative motion of the Porcupine Bank, offshore Ireland (Figs. 4.1 and 4.2), is also restored. However, knowledge concerning the present-day crustal structure of the Porcupine Bank and the tectonic forces responsible for these architectural variations are still limited due to the sparsity of geophysical data coverage over the Porcupine Bank, compared with the well-studied Porcupine Basin to the east, an area proposed to have promising petroleum resources (Shannon, 2018). To date, end-member scenarios have been envisaged for the tectonic evolution of the Porcupine Bank. One proposes that the Porcupine Bank was rigidly connected to the Irish mainland platform and thus, it did not rotate during the formation of the Porcupine Basin in some global plate reconstruction models (Matthew et al., 2016). The second proposes that the Porcupine Bank acted as a uniform continental block, which rotated clockwise relative to Ireland during the formation of the Porcupine Basin (Fig. 4.3) (Tate et al., 1993; Norton, 2002; Peace et al., 2019). Another shearing and stretching model has been presented that assumes a segmentation of the Porcupine Bank along Caledonian major fault zones, which were subsequently reutilized as strike-slip faults during rifting of the Porcupine Basin (Fig. 4.3) (Grow et al., 2019). The segmentation of the Porcupine Bank has also previously been suggested to correspond with a northwestward extension of a transfer zone in the Porcupine Basin (Fig. 4.3), separating a lower degree of extension and subsidence in the northern part of the Porcupine Basin, compared to a higher degree of extension and subsidence in the southern part of the basin (Readman et al., 2005).

Although existing plate tectonic models provide insight into the successive rifting episodes that have affected the Porcupine Atlantic region, they each involve individual assumptions, limitations, and uncertainties; for example, these plate-restored models generally depend on potential field data analysis (Readman et al., 2005; Nirrengarten et al., 2018; Peace et al., 2019; Grow et al., 2019), and lack seismic constraints, particularly for the Porcupine Bank. This leads to increased uncertainty when considering phenomena associated with extensional events such as timing, extension orientations, and the amount of extension during each rifting phase. In addition, although the rotation model of the Porcupine Bank suggested by Peace et al. (2019) is geologically reasonable at the regional scale, the model fails to consider the impact of inherited crustal structures on the episodic rifting phases. In contrast, the stretching and shearing tectonic model proposed by Grow et al. (2019) emphasized the strong influence of tectonic inheritance on extension, however, it fails to take the rotation of the Porcupine Bank into consideration. Although many authors have interpreted the orientations and locations of the inherited Caledonian and Variscan crustal trends on the offshore Irish continental margin based on sparse rock samples or potential field data analysis (Tyrrell et al., 2007, 2010; Štolfová and Shannon, 2009; Chenin et al., 2015; Grow et al., 2019), it is still difficult to accurately map the offshore continuations of the pre-existing crustal terranes in the Porcupine region, offshore Ireland, due to the lack of geophysical constraints and the overprint of subsequent tectonism (von Raumer et al., 2003; Gee et al., 2013). Meanwhile, rift obliquity between the Porcupine Bank and Flemish Cap on the Irish and Newfoundland margins, respectively (Brune et al., 2018), and their interplay with inherited crustal structures and margin evolution, are poorly understood as well. In contrast with the sparse data coverage on the Porcupine Bank, seismic refraction data (O'Reilly et al., 2006; Watremez et al., 2018; Prada et al., 2017; Chen et al., 2018), 2D and 3D seismic reflection data and well data (Norton, 2002; Naylor, 2002; Jones and Underhill, 2011; Bulois et al., 2018; Whiting et al., 2021), and potential field data (Readman et al., 2005; Welford et al., 2012) have been used to investigate the various Paleozoic-Cenozoic extensional events, crustal architecture, and tectono-stratigraphy of the Porcupine Basin. However, the timing of multiple extensional events and the orientations of interpreted transfer zones in the Porcupine Basin are still debated (Norton, 2002; Readman et al., 2005), and the recognition of pre-rift and syn-rift unconformities differs widely in the literature (Norton, 2002; Naylor, 2002; Jones and Underhill, 2011; Bulois et al., 2018; Whiting et al., 2021).

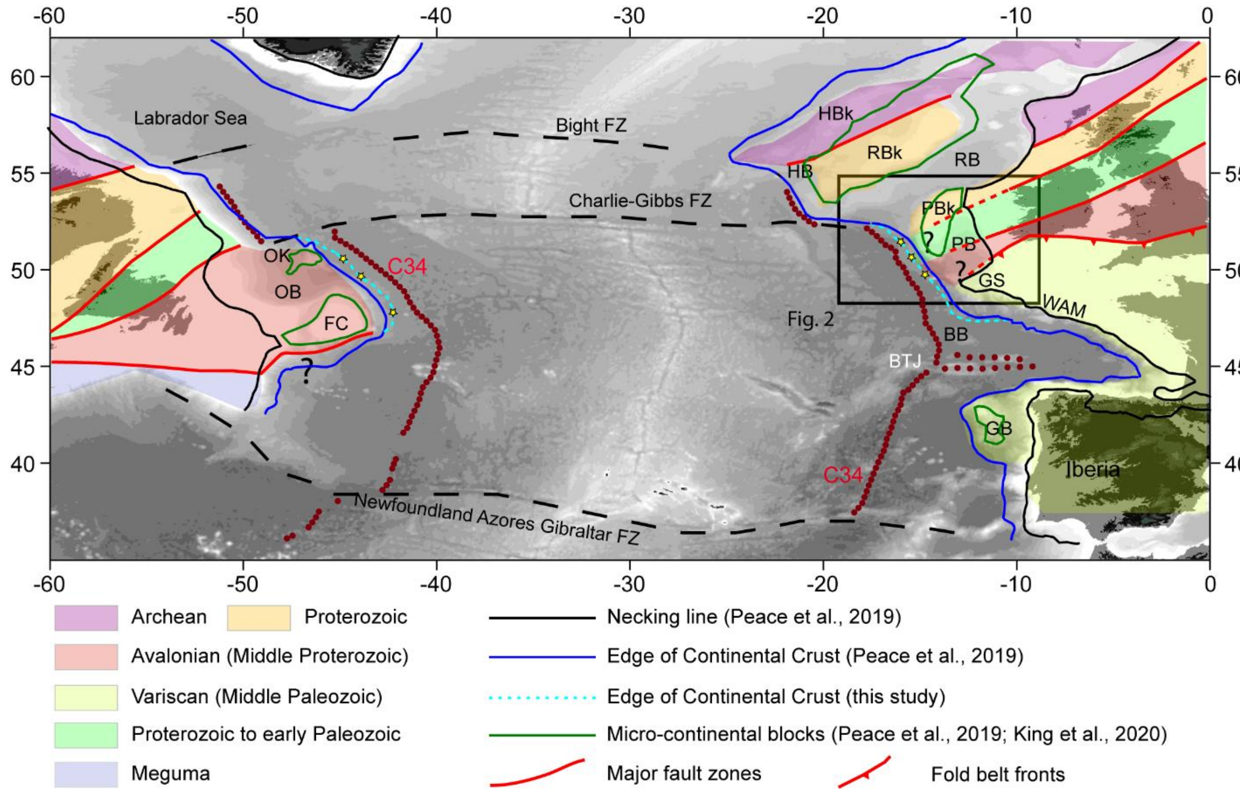

Figure 4.1: Regional map of the southern North Atlantic realm overlain by the different basement terranes (adapted from Tyrrell et al., 2007, 2010; Welford et al., 2012), and the primary boundaries and continental blocks used to build deformable plate tectonic models. The round-dotted lines (red) show magnetic anomaly 34 (Müller et al., 2016). The edge of continental crust (this study) is segmented by the yellow stars, which indicate different appearance times for each segment. Abbreviations: BTJ, Biscay Triple Junction; BB, Bay of Biscay; GB, Galicia Bank; GS, Goban Spur; PB, Porcupine Basin; PBk, Porcupine Bank; WAM, Western Approaches Margin; HB, Hatton Basin; HBk, Hatton Bank; RBk, Rockall Bank; RB, Rockall Basin; FC, Flemish Cap; OK, Orphan Knoll; OB, Orphan Basin; FZ, Fracture zone.

These uncertainties motivate us to build an improved plate tectonic reconstruction model of the Porcupine Bank region. Based on a compilation of geological and geophysical data and published restorations of the North Atlantic opening for the motion of Iberia, Newfoundland, and Europe, this study involves deformable plate tectonic modelling of the Porcupine Bank region. One deformable plate model will consider the Porcupine Bank as a uniform continental block, in contrast to four other models in which the Porcupine Bank is segmented along inferred inherited crustal lineaments. Using GPlates (Gurnis et al., 2012, 2018; Müller et al., 2018), we test the potential orientations and locations of major pre-existing crustal structural boundaries and investigate the role of pre-existing orogenic fabrics in the tectonic evolution and rift geometry of the Porcupine Atlantic region. The preferred deformable plate model is then used to improve the pre-rift continental configuration of the North Atlantic margins and quantitatively explain when and how the Porcupine Bank evolved from the Early Jurassic to the Cretaceous during opening of the modern North Atlantic. Accordingly, the extension timing, magnitude, and orientation between the Porcupine Bank and Flemish Cap regions are quantitatively analyzed to assess rift obliquity between them.

4.3 Geological Background

The Porcupine Bank is situated along the Atlantic margin of western Europe, offshore Ireland (Fig. 4.1), and is bounded by two failed rifted basins with the Porcupine Basin to the east and the Rockall Basin to the northwest (Fig. 4.2). The Goban Spur margin is located to the south of the Porcupine Basin, separated by the Porcupine Fault (Dingle and Scrutton, 1979). During the opening of the southern North Atlantic, rifting began within the Porcupine Basin but the rift axis shifted from within the Porcupine Basin to the west at the Charlie-Gibbs Fracture Zone (CGFZ) and intersected with the rift axis within the Rockall Basin at the northwestern limit of the Porcupine Bank, forming a rift triple junction (Gernigon et al., 2006). The crust that underlies the Porcupine Basin experienced progressive thinning with the amount of extension continuously increasing southward in the basin (Reston et al., 2004), implying a clockwise rotation of the Porcupine Bank relative to the Irish Atlantic continental margin (White et al., 1992; Tate, 1993; Norton, 2002). Stretching factors in the central and southern parts of the Porcupine Basin can be as high as 10, much larger than those in the northern part (5-6) of the basin (Reston, 2009; Prada et al., 2017). These values are consistent with complete embrittlement of the crust, allowing crustal-scale faulting and mantle serpentinization (Prada et al., 2017). The hyper-thinned crust in the Porcupine Basin region is overlain by Late Paleozoic-Cenozoic sedimentary rocks with a thickness of up to 10 km and several Cretaceous-Cenozoic igneous bodies (Fig. 4.2) (Naylor, 2002; Naylor and Shannon, 2005), while the thickness of the unstretched continental crust around the basin is about 25-30 km (Makris et al., 1988; Morewood et al., 2005; O'Reilly et al., 2006; Watremez et al., 2018; Prada et al., 2017; Chen et al., 2018). Some Late Paleozoic to Mesozoic basins are also perched along the western Porcupine Bank (e.g., Macdara Basin in Fig. 4.2).

4.3.1 Inherited structures over the Porcupine region

The multi-phase extensional tectonics that influenced the rift geometry of the Porcupine Atlantic region occurred on pre-existing orogenic-related structural fabrics (Shannon, 1991, 2018; Doré et al., 1999; Norton, 2002; Tyrrell et al., 2007; Chenin et al., 2015; Bulois et al., 2018; Grow et al., 2019). This rift-related deformation within a complex pre-rift template progressively evolved into hyper-thinning of the continental crust, mantle exhumation (O'Reilly et al., 2006; Prada et al., 2017), and/or initial seafloor spreading (Chen et al., 2018). Consequently, the crustal structure and stratigraphy within the Porcupine Basin vary considerably along the basin axis from north to south (Norton, 2002). The crustal pre-rift basement terranes in this region are comprised of distinct basement types from the Palaeoproterozoic to Paleozoic (Fig. 4.1) (Masson et al., 1989; Tyrrell et al., 2007, 2010; Štolfová and Shannon, 2009). The formation of these distinct basement terranes is associated with Phanerozoic orogenies, specifically the Paleozoic Caledonian Orogeny and the Late Paleozoic Variscan Orogeny that record the closure of the pre-Pangean oceans (Bulois et al., 2018; Ady and Whittaker, 2019). The NE-SW trending Fair Head-Clew Bay Fault and Iapetus Suture formed during the Caledonian Orogeny, while the Great Glen Fault was likely affected by the Caledonian, Grenvillian and earlier Laurentian orogenies (Fig. 4.2) (Bulois et al., 2018). Variscan orogenic movement was caused by the closure of the Rheic Ocean during the collision between Gondwana and Laurussia (Kroner and Romer, 2013). Rifting aligned with the Variscan lineaments occurred on the Newfoundland-Iberia conjugate margins, progressing northwards toward the Newfoundland-Ireland conjugate margin pair (Chenin et al., 2015). The impact of Variscan structures on rift-related deformation decreases northward, owing to the predominant influence of the Caledonian Orogen in the north Porcupine region (Chenin et al., 2015; Bulois et al., 2018). The Caledonian structures clearly segment onshore Ireland and the Variscan Orogeny only impacted southern Ireland (Fig. 4.2) These structures are often interpreted to extend to the offshore Porcupine region (Tyrrell et al., 2007, 2010; Grow et al., 2019), despite the challenge of defining their accurate expressions and positions due to subsequent rifting and erosion (von Raumer et al., 2003; Gee et al., 2013).

4.3.2 Tectonic evolution of the Porcupine region

Multiple stages of rifting, with variable stress orientations, occurred in the Porcupine Basin during the Late Paleozoic to the Cenozoic, following the collapse of the pre-existing Variscan and Caledonian orogenic belts (Doré et al., 1999; Norton, 2002; Stoker et al., 2017; Bulois et al., 2018). Although characterization of the extensional events in detail has been possible on a local scale due to increasing numbers of 3D seismic surveys and well data along the flanks of the basin (Jones and Underhill, 2011; Bulois et al., 2018; Saqab et al., 2021; Whiting et al., 2016, 2021), three pronounced rift phases are still used to describe the broad scale evolution (Shannon et al., 1995; Doré et al., 1999; Naylor and Shannon, 2005). Regionally, extension initiated during the Carboniferous (Bulois et al., 2018; Shannon, 2018), followed by the rifting phases during the Permo-Triassic and the Middle to Late Jurassic with the extension rate increasing until the end of the Jurassic (Norton, 2002; Štolfová and Shannon, 2009; Shannon 2018). A subsequent stage of intense rifting during the Late Jurassic to Early Cretaceous influenced most of the Porcupine area (Norton, 2002), creating characteristic rotated fault blocks that were sealed by a major unconformity, the Base Cretaceous Unconformity (Sinclair et al., 1994; Norton, 2002; Jones and Underhill, 2011; Whiting et al., 2021). Both the Porcupine Bank and Basin experienced uplift in the Early Cretaceous, capped by a regional Aptian unconformity (Norton, 2002). Post-rift thermal subsidence during the Late Cretaceous and Paleocene affected most parts of the Porcupine Basin (Norton, 2002). Reactivation of many Middle to Late Jurassic rift-related faults at the end of the Eocene period resulted in relatively minor extension until the end of the Oligocene (Saqab et al., 2021).

Locally, compared with the southern part of the Porcupine Basin, the tectonism and structural features are better understood in the northern Porcupine Basin due to ample seismic data coverage, where several extensional episodes are well constrained by relatively precise syn-rift and post-rift unconformities (Štolfová and Shannon, 2009; Jones and Underhill, 2011; Bulois et al., 2018). In the northern Porcupine Basin, following limited extension in the Late Carboniferous that reactivated Caledonian and Variscan orogenic structures, two main rifting episodes took place during the Rhaetian-Sinemurian (~ 204-190 Ma) and the Oxfordian-Tithonian (~163-145 Ma), controlling the pronounced highly-rotated blocks bounded by normal faults (Bulois et al., 2018). For the entire Porcupine Basin, the Carboniferous and Permo-Triassic sequences are mainly limited to the northern Porcupine Basin. Plus, the Jurassic syn-rift sedimentary sequences are present in most of the Porcupine Basin with many active basinbounding faults (Fig. 4.2) (Norton, 2002; Bulois et al., 2018; Whiting et al., 2021). In the perched basins along the western margin of the Porcupine Bank, thick sequences predating the Late Jurassic syn-rift packages are also interpreted on seismic sections (Norton, 2002; Naylor and Shannon, 2005). Extension continued during the Early Cretaceous in the southern part of the Porcupine Basin, at which time, the Aptian/Albian unconformity is interpreted to be associated with continental breakup at the Goban Spur margin (De Graciansky et al., 1985; Štolfová et al., 2012a). In this study, the timing of key tectonic events that occurred within the Porcupine Basin are constrained from previous literature (Norton, 2002; Naylor and Shannon, 2005; Bulois et al., 2018; Whiting et al., 2021), and are used to define the critical deformation stages of the Porcupine Bank.

The rift-related fault network across the Porcupine Basin (McCann et al., 1995; Norton, 2002; Saqab et al., 2021), and associated syn-rift and post-rift unconformities have been mapped in local areas associated with hydrocarbon potential (Whiting et al., 2016, 2021). Three main extensional fault systems from the Jurassic to Mid Eocene have been interpreted from a 3D seismic survey at the western margin of the Porcupine Basin (Saqab et al., 2021). The tectonically induced faults vary from WNW-trending in the Jurassic to NNW-trending in the Cretaceous. The N-S oriented extensional faults in the Mid Eocene, likely associated with the incipient breakup between Greenland and Europe, are mainly controlled by the pre-existing Jurassic extensional faults (Saqab et al., 2021; Prada et al., 2019). The varying age and orientations of these fault systems within the Porcupine area provide evidence for multiple phases of rifting associated with temporal variations in the orientation of principle stresses (Lymer et al., 2020). In particular, the Porcupine Basin appears to be strongly segmented along the basin axis (Fig. 4.2), which may be controlled by the WSW-ENE oriented transfer zones

(Norton, 2002). These transfer zones are assumed to have accommodated the spatial and/or temporal variations in the extensional tectonics of the basin (Lymer et al., 2020). To the south, the Variscan-affected Goban Spur margin contains NW-SE and NE-SW trending normal fault networks affecting the Barremain-Aptian syn-rift successions (De Graciansky et al., 1985; Naylor et al., 2002). Ultimately, throughout the Irish Atlantic margin and its inboard basins, the interaction between fault reactivation and inherited structures is still poorly understood (Bulois et al., 2018)

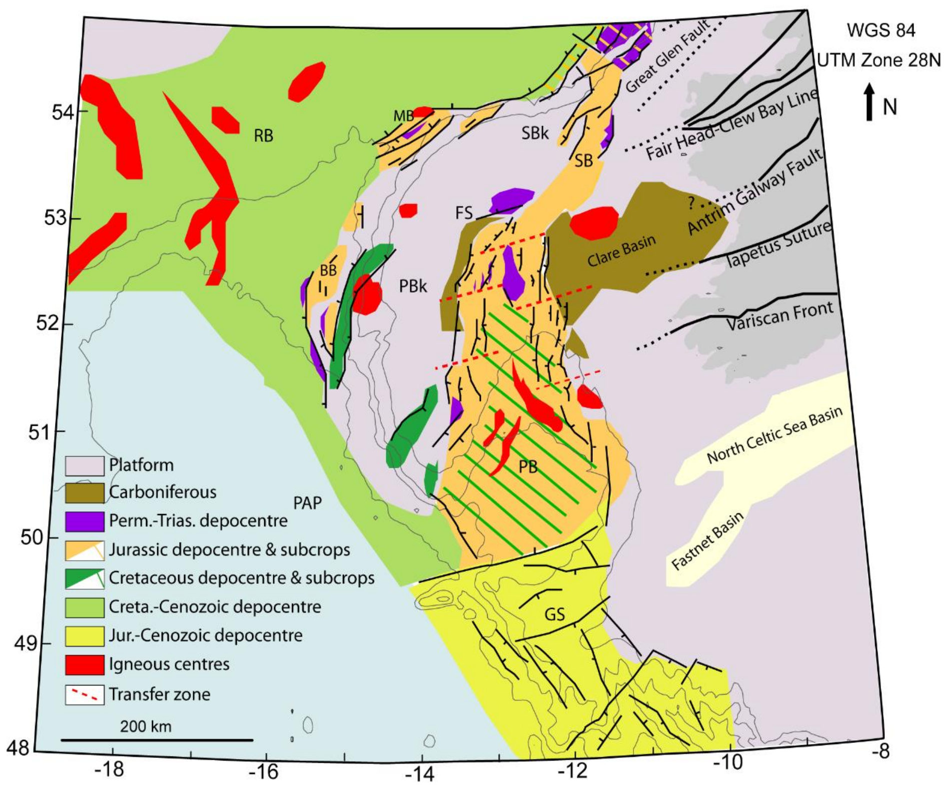

Figure 4.2: A simplified structural map across the Goban Spur-Porcupine region, offshore Ireland, overlain by bathymetric contours with an interval of 1000 m. The basement terranes onshore Ireland are segmented by pre-existing orogenic structural fabrics (e.g., Iapetus Suture, Great Glen Fault, Fair Head-Clew Bay Fault Line, Antrim-Galway Fault) (Bulois et al., 2018). Mesozoic fault trends along the western flank of the Porcupine Bank and the Goban Spur margin are, respectively, adapted from Naylor and Shannon (2005) and Saqab et al. (2017). In the Porcupine Basin, faults at the Base Cretaceous level are segmented by interpreted transfer zones (Norton, 2002). Abbreviations: GS, Goban Spur; PAP, Porcupine Abyssal Plain; PB, Porcupine Basin; PBk, Porcupine Bank; RB, Rockall Basin; SB, Slyne Basin; SBk, Slyne Bank; FS, Finnian's Spur; BB, Bróna Basin; MB, Macdara Basin.

4.4 Methodology

4.4.1 Deformable plate tectonic models

Based on the assumptions of rigid plates and narrow borders between plates (Morgan, 1968), rigid plate tectonic reconstructions generally fail to restore crustal thinning during the formation of hyper-extended rifted margins (Ady and Whittaker, 2019; Peace et al., 2019). In this study, GPlates, an open-source software package (Müller et al., 2018), is used to investigate the plate kinematics of the Porcupine region (Seton et al., 2012; Gurnis et al., 2012; Matthew et al., 2016; Müller et al., 2018; Nirrengarten et al., 2018). Aside from being able to interactively visualize the motion of tectonic plates (Gurnis et al., 2012, 2018), the GPlates software also provides a deformable plate modelling approach which allows users to restore temporal variations in crustal deformation given an initial crustal thickness assumption for a time frame of interest (Gurnis et al., 2018; Peace et al., 2019; Müller et al., 2019). Consequently, the evolution of crustal stretching throughout geological time can be restored and the motion of numerous tectonic plates, microplates or other features of interest can be quantified (Gurnis et al., 2018; Peace et al., 2019).

To build a deformable plate model in GPlates, the region where deformation occurs is defined by vector geometries (points, polylines, and polygons) (Gurnis et al., 2012). These vector geometries specify the geometries of tectonic elements, constrained by geological and geophysical observations (Müller et al., 2018; Welford et al., 2018; Peace et al., 2019; Zhu et al., 2020; King et al., 2020, 2021). In GPlates, each tectonic element is assigned a unique plate ID. Rotation poles are used to govern the relative plate motion of tectonic elements with respect to a fixed rotation axis over geological time. The total reconstruction poles are created by integrating each plate ID with respective rotation poles (Gurnis et al., 2012).

Combinations of vector geometries that delimit the deformable zone are used to create a deforming topological network boundary. Then, within deforming regions, triangulation meshes are created using all points from the network boundary polygon and interior vector geometries. Subsequently, the velocity of each vertex of an individual meshed triangle over time is calculated according to their corresponding rotation poles at the specific time. Next, the velocities of three vertices of each triangle are used to calculate strain rate and velocity at any point within the meshed triangles, by which continuous changes in strain rate within deforming regions throughout geological time can be tracked. Finally, the crustal thickness can be calculated according to its relationship to the strain rate over time (Gurnis et al., 2018). It is worthwhile to note that the deformable plate modelling method does not take the lateral flow of crustal material into consideration.

4.4.2 Boundaries of deformation and timing of crustal breakup

Rigid boundaries are required to define the limits of deforming regions in GPlates (Gurnis et al., 2018). In a deformable plate tectonic reconstruction study of the southern North Atlantic realm proposed by Peace et al. (2019), the necking line (NL) was used as the landward boundary of deformable regions. The oceanward deformable boundary presented the edge of continental crust (ECC) rather than the landward limit of oceanic crust (LaLOC) (Nirrengarten et al., 2018), since the LaLOC includes the exhumed mantle zone (Nirrengarten et al., 2018). The seaward and landward boundaries of deformation implemented by Peace et al. (2019), originally obtained from Nirrengarten et al. (2018), were slightly adapted in regions within proximity to continental blocks (e.g., Orphan Knoll, Porcupine Bank).

Both plate tectonic reconstructions proposed by Nirrengarten et al. (2018) and Peace et al. (2019) argue against the widely-accepted linkage between the Goban Spur and the Flemish

Cap, and support the connectivity of the Flemish Cap with the Porcupine Bank. However, their models along the western Porcupine Bank and Goban Spur margins are mainly dependent on potential field data analysis, lacking sufficient seismic constraints. In this study, the seaward boundary of continental deformation for the southern North Atlantic, other than for the Goban Spur-Porcupine area, is inherited from Peace et al. (2019). Meanwhile, the seaward boundary of deformation in the Goban Spur-Porcupine region corresponds to the oceanward edge of the hyperextended domain interpreted from high quality long-offset seismic reflection data (blue dashed line in Fig. 4.1) (Yang et al., 2020; Yang and Welford, 2021). In addition, the oceanward edge of the continental crust in proximity to the Orphan Knoll and the Flemish Cap is adjusted according to interpretations of seismic reflection and refraction profiles (blue dashed line in Fig. 4.1) (Welford et al., 2010; Welford et al., 2020). Considering the regional geometry for the edge of continental crust (ECC) implemented in this study, the ECC over the NE Newfoundland margin and the Goban Spur-Porcupine region extend farther oceanward in comparison to that used in Peace et al. (2019) (Fig. 4.1). Meanwhile, the landward boundary corresponds to the necking line defined in Nirrengarten et al. (2018), except for the Goban Spur margin where the necking line is slightly modified based on crustal thickness estimates from gravity inversion (Fig. 4.1) (Welford et al., 2012).

Generally, time-dependent tectonic event markers from geological and geophysical observations are used to construct the spatial extent of the deformable meshes throughout geological time (Müller et al., 2019; Peace et al., 2019; Zhu et al., 2020). One crucial marker is the crustal breakup time (i.e., appearance of the ECC in deformable plate models), which has a significant control on crustal thicknesses calculated from deformable plate models in comparison to other model inputs such as the landward deformable boundary (Welford et al., 2018). In Peace et al. (2019), the ECC appears at 120 Ma in the southwestern part of the Porcupine Bank and appears at 115 Ma from the mouth of the Porcupine Basin southeastwards to the Western Approaches Margin. On the conjugate NE Newfoundland margin, the ECC appears at 119 Ma. Since the re-interpreted ECC boundaries along the NE Newfoundland and Porcupine margins are closer to the mid-ocean ridge (MOR) (Fig. 4.1), the corresponding crustal breakup time is inferred to have occurred later than in previous interpretations (Nirrengarten et al., 2018; Peace et al., 2019). Despite uncertainties regarding the timing of crustal breakup along the western margin of the Porcupine Atlantic region, the Aptian/Albian unconformity is interpreted to be associated with continental breakup along the Goban Spur margin based on seismic data and well information (De Graciansky et al., 1985). Since the Porcupine Atlantic region is proposed to be segmented based on seismic data interpretation (Yang and Welford, 2021; Whiting et al., 2021), the edge of continental crust (ECC) in this study is also segmented into four smaller polylines based on the variations in basement characteristics identified from regional seismic transects along the offshore western Porcupine region (e.g., seismic profiles X1 and X2 in Yang and Welford (2021)). The polyline segments are separated by the yellow stars (Fig. 4.1). From previous work, the progressive northward continental breakup of the NE Newfoundland-Irish Atlantic margins occurred between Albian and Santonian time (Whittaker et al., 2012), and the ECC along the Irish Atlantic margin appears between ~ 115 – 83 Ma (Peace et al., 2019). Thus, we assume that the four polylines consisting of the ECC along the NE Newfoundland and Porcupine Atlantic region appear at 112, 100, 95, and 90 Ma from south to north, respectively. The timings of syn-rift phases along the western Porcupine Atlantic region, offshore Ireland, are less constrained. It is worthwhile to note that the appearance time for each polyline segment is non-unique. We just follow the principle that they must appear in the time interval (115-83 Ma), with a decreasing value from south to north.

4.4.3 Model setup

The Porcupine Bank consists of different crustal basement terranes obliquely cut by pre-existing crustal trends (Norton, 2002; Readman et al., 2005; Tyrell et al., 2007, 2010; Chenin et al., 2015; Grow et al., 2019). Similar pre-rift crustal structures are suggested to have played a significant role in the formation of rift segments during continental rifting throughout the Iberian margin (Tugend et al., 2015) and increasingly, segmentation of the Porcupine Basin has been inferred based on fault analysis (Norton, 2002; Whiting et al., 2021). Consequently, it would follow that the Porcupine Bank is likely to have been obliquely segmented in various ways during rifting. To test this hypothesis, variations between deformable plate model components are implemented to investigate the effects of pre-existing inheritance on the tectonic development of the Porcupine Bank and their impact on the temporal variations in crustal deformation experienced within this region. Specifically, five deformable plate tectonic models are established to separately test different parameters, such as the orientations, locations, and numbers of major inherited trends, inclusion of the Orphan Knoll, as well as the Flemish Cap poles of rotation (Fig. 4.3; Tables. 4.1 and 4.2).

In model 1, the Porcupine Bank is defined as a uniform continental block (Fig. 4.3a). The seaward and landward boundaries of the deformable network for the Porcupine region are the same as for the deformable tectonic restoration model proposed by Peace et al. (2019). In model 2, the Porcupine Bank is segmented into two continental blocks (Fig. 4.3b), by including one major ENE-WSW trending orogenic structure (the Iapetus Suture) separating the Caledonian-affected and Variscan-affected areas of the Porcupine region. This abrupt segmentation is prescribed despite the existence of a transitional zone between the Caledonian and Variscan orogenies (Chenin et al., 2015), in which the Iapetus Suture is the eastward extrapolation of the Charlie-Gibbs Fracture Zone (Schiffer et al., 2019).

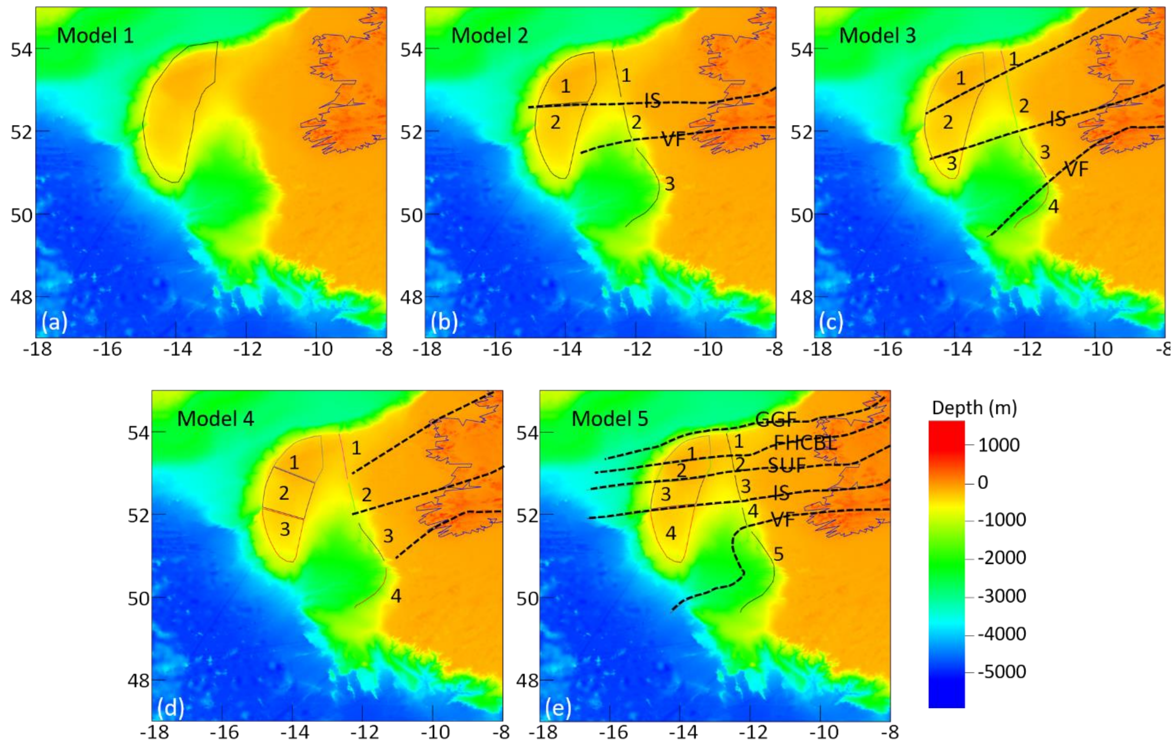

Figure 4.3: The Porcupine Bank segmentation models along the trends of pre-existing structural fabrics, overlying the bathymetry: (a) The rotation model proposed by Peace et al. (2019) without segmentation; (b) the two-block model segmented by the Iapetus Suture extrapolated westward to the Charlie-Gibbs Fracture Zone (Chenin et al., 2015; Schiffer et al., 2019); (c) the three-block model segmented by different crustal terranes proposed in Tyrrell et al. (2007, 2010); (d) the three-block model divided by the interpreted transfer zones in Readman et al. (2005); (e) the four-block model sheared by the inherited crustal lineaments in Grow et al. (2019). In addition to the segmentation over the Porcupine Bank, the eastern border of the Porcupine Basin is also segmented in models 2-5. Abbreviation: IS, Iapetus Suture; GGF, Great Glen Fault; SUF, Southern Upland Fault; FHCBL, Fair Head-Clew Bay Line; VF, Variscan Front. Note that each block of the Porcupine Bank and every segment of the eastern border of the Porcupine Basin are, respectively, labelled with a corresponding number in each model to delineate pairs.

In models 3 and 4, the Porcupine Bank is segmented into three continental blocks (Figs. 4.3c and 3d), with the segmentation being oriented NE-SW in model 3 (Fig. 4.3c), and NW-SE in model 4 (Fig. 4.3d). In model 3, two pronounced NE-SW oriented crustal trends separate the Proterozoic, Proterozoic to Early Paleozoic, and Avalonian terranes beneath the Porcupine Bank from north to south (Fig. 4.1) (Tyrrell et al., 2007, 2010; Štolfová and Shannon, 2009). Model 4 segmentation is based on interpreted NW-SE trending fault structures controlling the extensional deformation of the Porcupine Basin (Fig. 4.3d) (Masson and Myles, 1986; Readman et al., 2005).

The segmentation in model 5 is mainly based on the crustal shearing model with E-W opening of the Porcupine Basin inferred by Grow et al. (2019), in which four onshore Caledonian major fault zones (Fairhead-Clew Bay Fault Line, Southern Upland Fault, Orlock Bridge Fault, and Iapetus Suture, from north to south) extend across the Porcupine region. Since the Iapetus Suture, Antrim-Galway Fault, and Fair Head-Clew Bay Fault Line are the major Caledonian fault zones onshore Ireland (Fig. 4.2) (Norton, 2002; Bulois et al., 2018), we assume that there are two solid blocks between the Fairhead-Clew Bay Fault Line and the Iapetus Suture, rather than there being further subdivision based on the interpreted Southern Upland Fault and Orlock Bridge Fault. Consequently, the Porcupine Bank is segmented into four continental blocks in this scenario (Fig. 4.3e).

In addition to considering the various segmentation scenarios for the Porcupine Bank, the distinct segments along the eastern border of the Porcupine Basin also play an important role on the results produced by deformable plate models since the Caledonian fault zones and Variscan deformation front cut through the entire Porcupine Atlantic region. For clarification, in this study, the components of the Porcupine Bank are described using the term *block*, while the components of the eastern border of the Porcupine Basin are described using the term *segment*. For all models, each block and segment correspond to different Plate IDs (labelled in Fig. 4.3). It should be noted that each modelled block and segment move continuously at a constant extension rate with respect to the fixed plate over a certain geologic interval, yet in reality, the tectonic events are intermittent with variable rates (Saqab et al., 2021). In addition, considering that the scale of the Orphan Knoll is much smaller compared to other continental ribbons previously interpreted throughout the southern North Atlantic (Peace et al., 2019), its presence or absence within the deformable plate models of the southern North Atlantic region is also tested for each model in this work. It should also be noted that since the positions of the inherited crustal trends across the Porcupine Bank are uncertain, the blocks in each model are defined according to the crustal lineament trend being tested in that specific model.

From the preferred model in Peace et al. (2019), anomalously thick crust is observed in local deformable regions along the western Porcupine Bank. In GPlates, the distance between the Porcupine Bank and Flemish Cap over time can affect the topological networks, controlling the variations in crustal thickness. By altering the position of the Flemish Cap at 200 Ma, we make the initial pre-rift distance between the Porcupine Bank and Flemish Cap closer than in previous plate reconstructions (Peace et al., 2019). Then, we progressively increase the distance between the two margins at specific times, relative to previous work (Peace et al., 2019), to generate a reasonable present-day crustal thickness by comparing with that from gravity inversion (Welford et al., 2012). Overall, the adjustments made to the Flemish Cap kinematics present as an important contributing factor in this study (Table. 4.2).

Table 4.1: The parameters used in models 1-5.

Model #	1	2	3	4	5
Seaward border modified ECC of Peace et al. (2019)	Unmodified from Peace et al. (2019)	Yes	Yes	Yes	Yes
Main landward border modified NL of Peace et al. (2019)	Unmodified from Peace et al. (2019)	Yes	Yes	Yes	Yes
Block number of Porcupine Bank	One (Fig. 4.3a)	Two (Fig. 4.3b)	Three (Fig. 4.3c)	Three (Fig. 4.3d)	Four (Fig. 4.3e)
Poles of rotation	Peace et al. (2019)	This study (tables 4.3-4.5)	This study (tables 4.3-4.5)	This study (tables 4.3-4.5)	This study (tables 4.3-4.5)

Note: NL indicates necking line; ECC denotes the edge of continental crust.

Similar to the deformable plate modelling workflow used in Peace et al. (2019), the time frame considered for all models in this study is from 200 Ma to 0 Ma, with an initial crustal thickness assumption of 30 km at 200 Ma, despite the fact that crustal thicknesses are variable, ranging from ~22 – 32 km over the Porcupine Bank from previous studies (Whitmarsh et al., 1974; O'Reilly et al., 2006; Welford et al., 2012; Prada et al., 2017; Watremez et al., 2018; Chen et al., 2018). There are two main reasons why we set the initial crustal thickness as 30 km. On one hand, the deformable region in this study encompasses the southern North Atlantic realm (Fig. 4.1), in which the Porcupine Bank is just one of its continental ribbons. Thus, a uniform and regionally-consistent crustal thickness is better for a regional match. 30 km is a relatively balanced value based on previous studies (Peace et al., 2019). On the other hand, even if the initial crustal thickness is larger or smaller than 30 km, the crust obtained from deformable plate modelling will be proportionally thickened or thinned, which may lead to a larger misfit for the whole deformable region overall. In addition, although crustal extension also occurred prior to 200 Ma in the Porcupine region (Naylor et al., 2002; Norton, 2002; Štolfová and Shannon, 2009; Tyrrell et al., 2010; Shannon, 2018; Bulois et al., 2018), the deformable plate models tested are only restored back to 200 Ma. This is due to poor constraints associated with extensional events prior to 200 Ma as a result of sparse data coverage in the southern Porcupine region. Finally, the density of crustal thickness points within each deformable model is set to be 8 (an interval of 0.15625°) without random offset.

Table 4.2: Four main factors (a-d) considered for each model.

Model #	1	2	3	4	5
a: OK included	Yes	Yes	Yes	Yes	Yes
b: OK included	No	No	No	No	No
c: Location of FC modified from Peace et al. (2019)	Yes	Yes	Yes	Yes	Yes
d: Segments of the edge of eastern flank of PB	One	Three	Four	Four	Five

Note: Orphan Knoll=OK; FC=Flemish Cap; PB=Porcupine Basin. For model 1, model 1c is the same as model 1d.

4.4.4 Rotation file

In GPlates, poles of rotation govern the motion history of each vector geometry or block over time (Gurnis et al., 2012), from which the motion velocity (magnitude and orientation) is calculated to quantitatively track the deformation within a topological network (Gurnis et al., 2018). In this study, other than for the Porcupine Atlantic region, the poles of rotation for other regions of the southern North Atlantic are those from model 6c created by Peace et al. (2019), in which geometries and locations of some independent continental blocks are updated (i.e., Flemish Cap, Orphan Knoll, Porcupine Bank, Hatton-Rockall Bank) based on the work of

Nirrengarten et al. (2018). In addition, the Galicia Bank, along the northwest Iberian margin, is also considered as an independent continental block in the deformable network for the southern North Atlantic (King et al., 2020).

In model 1, the poles of rotation for the Porcupine Bank are from Peace et al. (2019). The introduction of rotation poles for the Porcupine Bank by Peace et al. (2019) was an important improvement for plate reconstructions of the Irish Atlantic margin, yet the definition of these rotation poles lacked support from seismic constraints. For this study, poles of rotation in models 2-5, representing the local kinematics of the Porcupine area, were deduced by using syn-rift and post-rift unconformities from seismic interpretations as inputs to constrain plate motions. That means these key unconformities define when the Porcupine Bank moves and stops over time. The establishment of the rotation poles varies from one block and/or segment to another according to how the Porcupine Bank is segmented for each model (Fig. 4.3). Nonetheless, the rotation parameters for the four models generally follow the constraint that intense rifting occurred from Late Jurassic to Early Cretaceous (Shannon, 1991; Doré et al., 1999; Naylor and Shannon, 2005; Enachescu, 2005). Specifically, in the northern Porcupine Basin, two main rifting episodes took place during the Rhaetian-Sinemurian (~204-190 Ma) and the Oxfordian-Tithonian (~160-145 Ma) (Bulois et al., 2018). Late Jurassic depocenters are distributed along the north, northeast, and southwest flanks of the Porcupine Basin (Whiting et al., 2016, 2021), in which the Tithonian succession is interpreted to document the transition from syn-rift to post-rift events (Moore, 1992). Similarly, the earliest Cretaceous is also interpreted as a transition sequence (Moore, 1992). Despite the Early Cretaceous sequences being interpreted as post-rift from the thermal subsidence stage, normal faults are still observed in the Aptian-Late Cretaceous successions, which may have been caused by a minor extension during this time (Shannon et al., 1993). So, the blocks consisting of the Porcupine Bank in the model are assumed to continue to move during this time interval.

By combining observations from 2D and 3D seismic surveys from previous literature (Norton, 2002; Saqab et al., 2021; Whiting et al., 2016, 2021; Bulois et al., 2018), the poles of rotation for the multiple modelled scenarios follow the assumption that the motion of the northern Porcupine Bank ceases at the end of the Jurassic and the southern part of the margin continues to move during the Early Cretaceous until Albian time. Specifically, block 1 in models 2-5 shares the same poles of rotation. Block 2 in model 2, block 3 in models 3 and 4, and block 4 in model 5 also share the same poles of rotation. Note that block 2 in models 3 and 4 has the same poles of rotation as block 3 in model 5. The same relationships are also applicable for the segments along the eastern border of the Porcupine Basin. For simplicity, the poles of rotation for blocks and segments in model 5 are shown in Tables 4.3 and 4.4, respectively. As mentioned in section 4.4.3, adjustment of poles of rotation of the Flemish Cap can alter the distance between this margin and the Porcupine Bank, which further affects the crustal thickness variations over time. The altered poles of rotation of the Flemish Cap between 190 Ma and 112 Ma are listed in Table 4.5.

Table 4.3: Rotation poles of the Porcupine Bank used in model 5. (EUR = Eurasia)

	Age	Latitude	Longitude	Angle	Fixed plate
Block 1	0	90	0	0	EUR
	140	90	0	0	EUR
	160	55.0975	-11.1153	1.8868	EUR
	180	54.7608	-11.6591	2.6347	EUR
	200	54.8407	-12.4101	3.3828	EUR
Block 2	0	90	0	0	EUR

	140	90	0	0	EUR
	160	55.837	-2.4224	0.967	EUR
	180	54.0947	-11.1377	3.626	EUR
	200	54.461	-11.0028	4.5143	EUR
Block 3	0	90	0	0	EUR
	140	90	0	0	EUR
	160	54.0283	-11.1277	6.4201	EUR
	180	53.3432	-12.3624	12.3928	EUR
	200	53.7918	-11.8974	12.6324	EUR
Block 4	0	90	0	0	EUR
	120	90	0	0	EUR
	130	52.8685	-11.9725	1.0763	EUR
	140	53.0316	-12.0962	4.2508	EUR
	150	53.5561	-12.1529	7.8767	EUR
	160	53.2392	-11.8667	12.1062	EUR
	180	53.327	-11.7628	14.9541	EUR
	200	53.8277	-11.1796	16.2544	EUR

Note: Other poles of rotation that are not listed here are identical to those in Peace et al. (2019), except for the Flemish Cap (Table. 4.5).

Table 4.4: Rotation poles of the segments along the eastern edge of the Porcupine Basin.

	Age	Latitude	Longitude	Angle	Fixed plate
Segment 1	0	90	0	0	EUR
	120	90	0	0	EUR
	140	-25.2504	37.6417	0.0116	EUR
	160	54.6538	-13.4417	-1.9777	EUR
	180	54.7048	-13.3366	-1.8644	EUR
	200	55.0974	-12.8186	-2.1211	EUR

Segment 2	0	90	0	0	EUR
	120	90	0	0	EUR
	140	36.6489	168.5799	-0.0145	EUR
	160	48.7471	-13.4865	0.5766	EUR
	180	73.6359	6.1445	-0.1268	EUR
	200	55.1844	-12.6792	-2.058	EUR
Segment 3	0	90	0	0	EUR
	100	90	0	0	EUR
	120	51.012	-14.3967	0.2392	EUR
	140	29.5314	-25.0247	0.0705	EUR
	160	53.6535	-12.6126	-4.4215	EUR
	180	53.7485	-12.7469	-5.2321	EUR
	200	54.1528	-12.9203	-5.2329	EUR
Segment 4	0	90	0	0	EUR
	100	90	0	0	EUR
	120	65.2891	5.7668	-0.0276	EUR
	140	54.7196	-9.2213	-0.8895	EUR
	160	53.0698	-11.9162	-7.6989	EUR
	180	53.0653	-11.9627	-9.4527	EUR
	200	53.2849	-12.0349	-9.4534	EUR
Segment 5	0	90	0	0	EUR
	100	90	0	0	EUR
	120	49.5983	-14.1544	0.9609	EUR
	140	47.4763	-18.1143	1.2165	EUR
	160	58.3461	-6.8708	-1.8527	EUR
	180	58.8597	-6.3986	-2.0029	EUR
	200	56.6254	-9.3527	-3.2731	EUR

Table 4.5: Adjusted rotation pole for the Flemish Cap. (NAM = North America, IB=Iberia)

Age	Latitude	Longitude	Angle	Fixed plate
0	90	0	0	NAM
112	54.8464	-57.6076	-1.0205	NAM
120	43.0863	-50.7736	5.721	NAM
130	44.4084	-51.2712	12.8582	NAM
140	44.9015	-52.5418	20.0187	NAM
150	44.757	-53.5516	19.4275	NAM
161	44.7481	-55.2164	18.6954	NAM
161	64.0215	-20.9739	69.0218	IB
170	63.5799	-21.7456	70.6225	IB
180	63.1131	-22.1413	72.2219	IB
200	62.1958	-22.973	75.2653	IB

4.5 Results

4.5.1 Crustal thicknesses from deformable plate models

Herein, the crustal thickness evolution and plate kinematic history of deformable plate models between 200-90 Ma are described considering a sampling interval of 10 Ma. In models 2-5, four contributing factors (exclusion and inclusion of the Orphan Knoll, adjustments of poles of rotation of the Flemish Cap, and the motion of the eastern border of the Porcupine Basin) are tested. The first three driving factors are considered in model 1 (Table 4.2). Thus, present-day crustal thickness maps (Figs. 4.4b-4t) are obtained from 19 deformable model scenarios in total. To choose the preferred model, crustal thicknesses from all deformable plate models are compared with those from gravity inversion and results from seismic refraction data modelling in Figure 4. 5. In addition, although the geometry and position of each block in all models at 200 Ma are slightly different, they all produce approximately the same geometrical characteristics for the Porcupine Bank as are observed present day (Fig. 4.4). It should be noted that igneous bodies (Fig. 4.2) are not addressed directly in the gravity inversion process (Welford et al., 2012), although their density contribution, based on their volumes, is not expected to be significant at the regional scale. Likewise, they are of minor importance to, and are omitted from the deformable plate modelling in this study.

First, in model 1(Figs. 4.4b-4d), at the western margin of the Porcupine Bank, there is an apparent discrepancy between the crustal thickness from gravity inversion (Fig. 4.4a) and that calculated from the deformable plate model in Peace et al. (2019) (indicated by the black circle in Fig. 4.4b). When the Orphan Knoll is not included as an independent continental block in the deformable plate model, the discrepancy is slightly reduced at the western margin (Fig. 4.4c). Based on the results in Fig. 4.4c, the motion of the Flemish Cap is adjusted to reduce the anomalous thickness at the western margin (Fig. 4.4d and Table 4.5). Nevertheless, regardless of whether the Orphan Knoll is included or not in the deformable rotation model, the crust in the central and southern Porcupine Basin is extremely thinned from this model (Figs. 4.4b and 4c), ~ 4 km thinner than that from gravity inversion (Fig. 4.4a). In addition, the north end of the V-shaped geometry of the basin from model 4d tends to thin along a northwest trend from deformable modelling, which differs from gravity inversion trends (Figs. 4.4a and 4d).

For the two-block model (indicated by model 2 in Figs. 4.4e-4h), in comparing the crustal thicknesses from gravity inversion, there is still a pronounced thickness anomaly at the western margin of the Porcupine Bank calculated from the deformable plate modelling when the Orphan

Knoll is included as a continental block in the deformable network (Figs. 4.4a and 4e). Still, the area of anomalously thick crust on the western Porcupine Bank is much smaller than that from the Peace et al. (2019) rotation model (Figs. 4.4b and 4e). Although, in general, the crustal thickness calculated from the deformable plate model without the presence of the Orphan Knoll corresponds closely to that from gravity inversion (Figs. 4.4a and 4f), the crust at the western margin is still thicker (indicated by the dashed black circle in Fig. 4.4f) than that from gravity inversion (Fig. 4.4a). After the motion of the Flemish Cap is adjusted (Table 4.5), the thickness of the crust at the western margin is relatively consistent with that from gravity inversion (Figs. 4.4a and 4g). However, the pronounced compression between block 1 and block 2 (~ 52.5° N) in model 2 extends to the northern Porcupine Basin, resulting in anomalously thick crust in the northern portion of the basin (indicated by the black arrow in Fig. 4.4g), which is inconsistent with the imaged gradually decreasing crustal thickness from north to south in this region (Prada et al., 2017; Chen et al., 2018). By moving the eastern edge of the Porcupine Basin in model 2d, the anomalous thickness is dramatically reduced (Fig. 4.4h).

The main difference between model 3 (Figs. 4.4i-4l) and model 4 (Figs. 4.4m-4p) is that the Porcupine Bank is segmented by NE-trending and NW-trending terranes, respectively, at different positions (Figs. 4.3c and 3d). In contrast to model 2, the crustal thickness gradient is smoother from 52.30° N to 51.30° N in the Porcupine Basin in both models 3 and 4, corresponding to the transition from the necking domain to the hyperextended domain (Yang and Welford, 2021). As observed for models 1 and 2, crustal thicknesses at the western flank of the Porcupine Bank in models 3 and 4 show great improvements when the Orphan Knoll is omitted and when the rotation of the Flemish Cap is adjusted, but the crust in the Porcupine Basin is still thicker than resolved from gravity inversion (Figs. 4.4j, 4k, 4n, and 4o). Although the crust becomes thinner when the motion of the eastern edge of the basin is included (Figs. 4. 4l and 4p), the main modelling discrepancies, likely related to orientations and positions of the inherited crustal structural trends, still exist in both models. For instance, for model 3, crustal thickness abruptly changes in the transition zone around block 3 (indicated by the yellow circle in Fig. 4.4l). Also, for model 4, the crust between block 1 and block 2 along the northwestern flank of the Porcupine Bank (~ 53° N) is prominently thick (indicated by the dashed black circle in Fig. 4.4p), which is inconsistent with the gravity inversion results (Fig. 4.4a).

In model 5, the Porcupine Bank is divided into four blocks by ENE-trending Caledonian crustal terranes (Fig. 4.4e). It is evident that by adjusting the paleo-positions of the Flemish Cap and by moving the eastern edge of the Porcupine Basin (Figs. 4.4r and 4s), the crustal thickness of the four-block scenario from the deformable modelling becomes more consistent with that from gravity inversion in the Porcupine Basin, as well as along the western flank of the Porcupine Bank (Fig. 4.4t). In this scenario, variations in the crustal thickness gradient are observed from north to south along the axis of the Porcupine Basin (Fig. 4.4t).

Variations in crustal thickness along the N-S profile (indicated by the north-south white line in Figure 4.4) from gravity inversion, seismic refraction data modelling, and deformable plate modelling show different features (Fig. 4.5a), with the thicknesses from models 1c, 3d, and 4d deviating by ~ 5- 9 km from the thicknesses constrained by seismic refraction and gravity inversion. In comparison, crustal thickness variations of model 2 (dark green color in Fig. 4.5a) and model 5 (dashed red line in Fig. 4.5a) are more consistent. Regarding the W-E profile (indicated by the west-east white line in Figure 4.4), there is a pronounced variation in thickness from west to east in model 1, while the thickness variations from models 2-5 are smaller.

Locally, crustal thicknesses in the central W-E profile calculated from models 2 and 5 are much closer to values from seismic and gravity constraints (Fig. 4.5b).

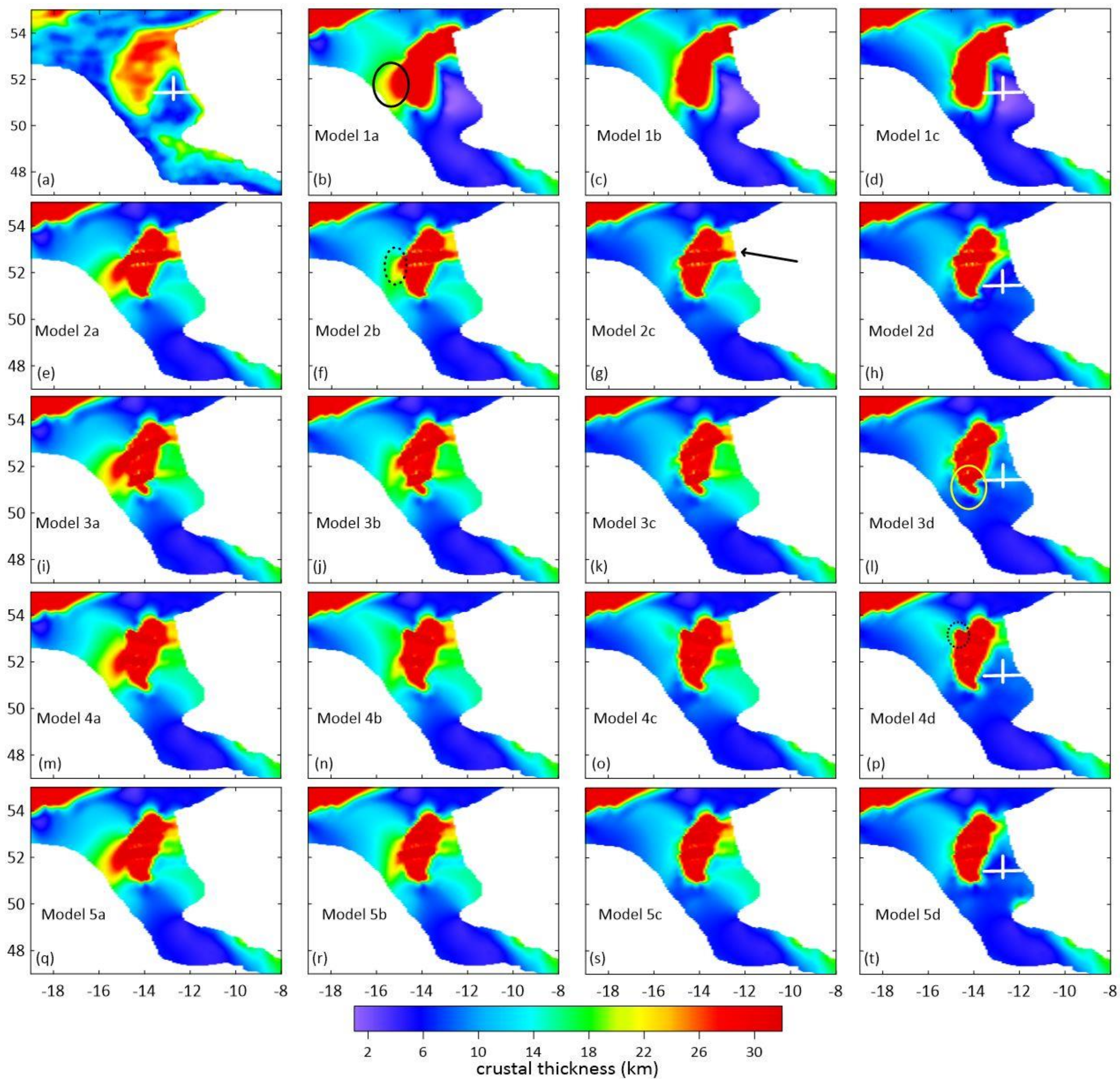

Figure 4.4: (a) Crustal thickness from gravity inversion (Welford et al., 2012), masked to only reveal the extent of the deformable region (Fig. 4.1). (b)-(d): crustal thickness at present day with the Porcupine Bank acting as a uniform continental block in the rotation model (Peace et al., 2019) (Fig. 4.3a), with the Orphan Knoll included as a continental fragment in Fig. 4.4b and omitted in Fig. 4.4c, and the poles of rotation of the Flemish Cap in Fig. 4.4d adjusted. (e)-(h): crustal thickness of the two-block model (model 2) in Fig. 4.3b. (i)-(l): crustal thickness of the three-block model (model 3) in Fig. 4.3c. (m)-(p): crustal thickness of the three-block model (model 4) in Fig. 4.3d. (q)-(t): crustal thickness of the four-block model (model 5) in Fig. 4.3e. For rows 2-5, the first column includes the Orphan Knoll, and the second column omits the

Orphan Knoll. The third column results involve an altered rotation of the Flemish Cap and the omission of the Orphan Knoll. The fourth column results involve the motion of the eastern edge of the Porcupine Basin and the altered motion of the Flemish Cap without including the Orphan Knoll. The white lines in Fig. 4.4a and within each panel of the last column represent locations of the seismic refraction lines used for comparison in Fig. 4.5 (adapted from Chen et al., 2018).

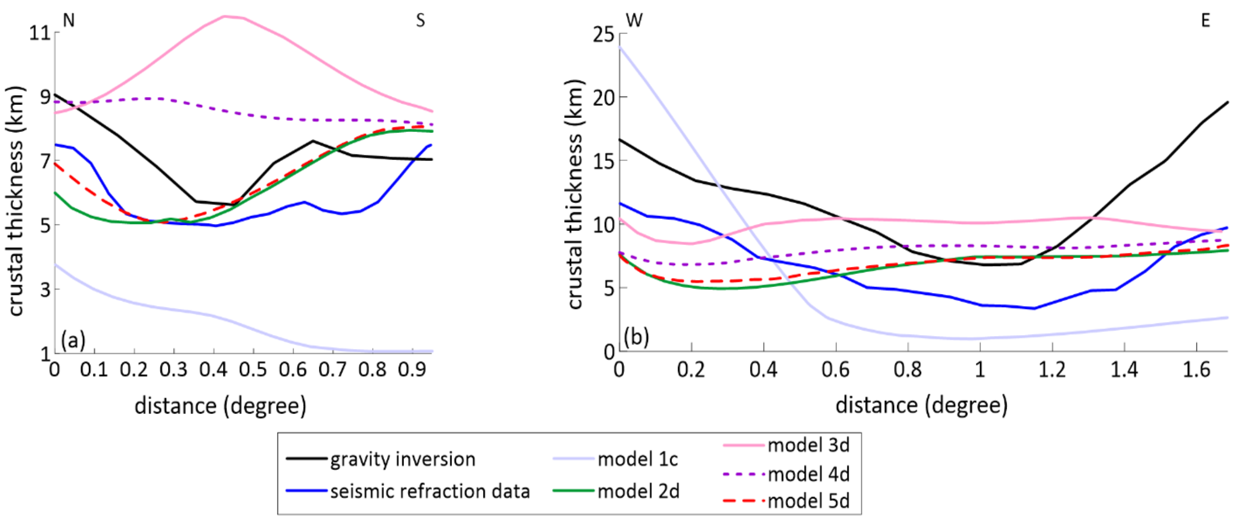

Figure 4.5: Comparison of crustal thickness along two profiles in the Porcupine Basin from gravity inversion (Welford et al., 2012), seismic refraction data (adapted from Chen et al., 2018), and deformable models in this study. (a) the N-S profile indicated by the N-S white line in Figure 4. 4; (b) the W-E profile indicated by the W-E white line in Figure 4. 4.

Based on the deformable models tested above, it is evident that the number and orientations of inherited crustal trends have a significant impact on the present-day crustal thicknesses within the Porcupine Atlantic region. The NNE-trending and NW-trending pre-existing crustal terranes in models 3 and 4 appear to generate less consistent crustal thicknesses compared with the thicknesses from gravity inversion. In contrast, crustal thicknesses from models 2 and 5 with the ENE-trending inherited crustal terranes are more consistent with those calculated by gravity inversion (Fig. 4.6). In addition to differential segmentation of the Porcupine Bank, the kinematic velocities of the blocks and the segmentation of the necking line along the eastern flank of the Porcupine Basin also play key roles in obtaining geologically and geophysically reasonable crustal thicknesses from deformable plate modelling.

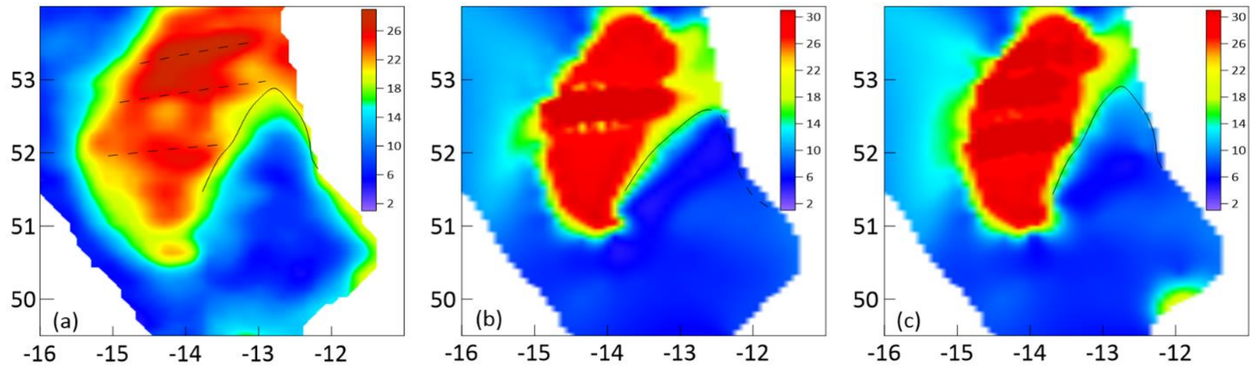

Figure 4.6: Local enlargements of crustal thickness (a) from gravity inversion (Welford et al., 2012), (b) from two-block model 2d, and (c) from four-block model 5d (c). The three dashed black lines in panel a appear to segment the Porcupine Bank. These approximately agree with the segmentation shown in panel c.

In order to better observe the difference between the two scenarios from models 2d and 5d, we enlarge the local region of crustal thicknesses from the gravity inversion (Fig. 4.4a) (Welford et al., 2012), the two-block model 2d (Fig. 4.4h), and the four-block model 5d (Fig. 4.4h), respectively (Fig. 4.6). In both models 2d and 5d, the regions between blocks on the Porcupine Bank experience not only rotation, but also local compression and shearing, leading to local crustal thicknesses larger than 30 km (the initial crustal thickness). We can see that the crustal thickness from gravity inversion appears to also be segmented by the three dashed black lines (Fig. 4.6a), which agree with the compartmentalization in model 5d (Fig. 4.6c), consistent with the offshore continuation of segmentation in the Porcupine Basin based on seismic data interpretation (Norton, 2002; Whiting et al., 2021). Also, the thinned crust at the northern end of the V-shaped Porcupine Basin is asymmetric in model 2d compared with that from the gravity inversion. In comparison, the V-shaped geometry from model 5d agrees well with the crustal thickness map from gravity inversion for the entire basin (indicated by the black solid polyline in Fig. 4.6). Combined with the above analysis and comparison, model 5d appears to be most in agreement with other geophysical observations in this study.

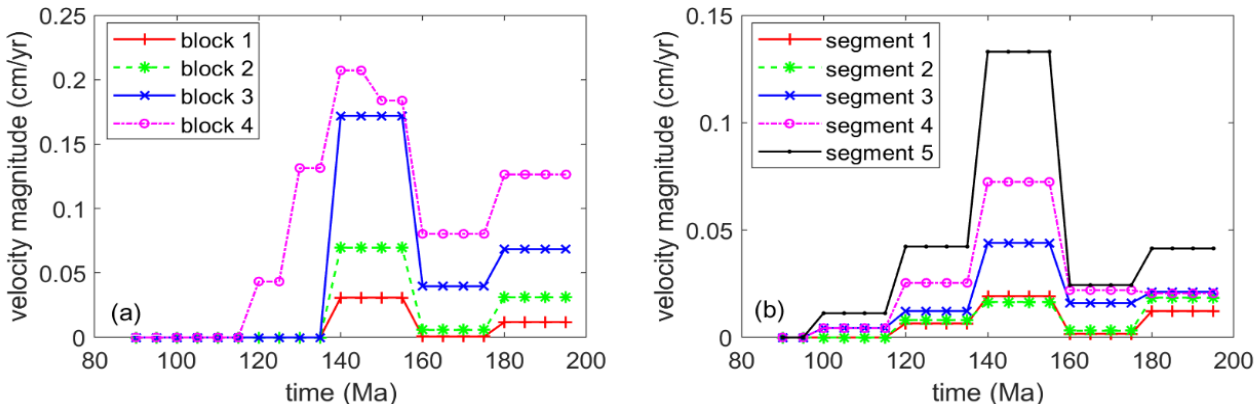

Figure 4.7: (a) The velocity magnitude of the model 5d Porcupine Bank blocks relative to the Irish continental margin between 200-90 Ma. (b) The velocity magnitude of the five segments of the eastern border of the Porcupine Basin relative to the Irish continental margin during the same time interval.

Since scenario 5d provides results that best match complementary geophysical constraints (Figs. 4.4a and 4t), the kinematics of the four blocks making up the Porcupine Bank (model 5) are analyzed in Figure 4.7. All four blocks during the Late Jurassic to Early Cretaceous (160-140 Ma) move approximately two times faster than those during the Early Jurassic (200-180 Ma) (Fig. 4.7a). The onset of rifting from 200-180 Ma is followed by a period of tectonic quiescence (180-160 Ma) for blocks 1 and 2 prior to the major extension stage during the Late Jurassic to the Early Cretaceous. The velocity magnitudes between 180 and 160 Ma are the least among the four blocks during the whole rifting stage (Fig. 4.7a). The first three blocks cease their clockwise rotation away from mainland Ireland at the earliest Cretaceous (140 Ma), while the southernmost block in the model continues to move during the Early Cretaceous, decreasing step-wise in velocity until the Aptian/Albian (Fig. 4.7a). Overall, the velocities of the four blocks during rifting are relatively faster than those of the corresponding four segments along the eastern margin of the basin through geological time (Fig. 4.7). In this study, the motions of the southernmost block (block 4) and the segmented border along the eastern flank of the basin are assumed to continue after 140 Ma, suggesting continued extension of the basin in the Early

Cretaceous, which is likely related to tectonic reactivation during or after continental breakup. In general, velocity magnitudes and crustal thicknesses calculated from model 5d agree with the geophysical observations that suggest the occurrence of lower and higher degrees of stretching in the north and south of the Porcupine Basin, respectively (O'Reilly et al., 2006; Prada et al., 2017; Chen et al., 2018; Watremez et al., 2018), and that the main phase of extension within the Porcupine Basin occurred during the Late Jurassic to Early Cretaceous (Gernigon et al., 2006; Stoker et al., 2017; Bulois et al., 2018; Whiting et al., 2021). It should be noted that paleo-positions and motion of blocks over time in model 5d are not unique, yet they show a geologically reasonable evolution of the Porcupine Atlantic margin.

4.5.2 Quantitative calculation for each rifting event

From the modelled scenarios, it is clear that the present-day crustal thicknesses on the western flank of the Porcupine Bank calculated by deformable plate models are more geologically reasonable when the Orphan Knoll is omitted from the topological network for the southern North Atlantic realm. Although the Orphan Knoll likely played a role in changing local stress directions, its smaller size and present-day crustal thickness suggest that it played a less-critical role in comparison to larger continental blocks such as the Flemish Cap and Porcupine Bank. Plus, there are still many uncertainties concerning its present-day geometry and Mesozoic plate kinematics (Nirrengarten et al., 2018; Peace et al., 2019; Welford et al., 2020). Since this study primarily focuses on the tectonic evolution between the Porcupine Atlantic region and the Flemish Cap, the Orphan Knoll is omitted from the deformable model in this section as its inclusion as a rigid block appears to amplify its contribution and provide unreasonable results.

To justify the adjusted motion of the Flemish Cap in this study, temporal variations in crustal thickness for models 5b and 5d are visualized in Figures 4.8 and 4.9. To aid in contextualizing the results, the interpreted present-day boundaries of different crustal domains (necking, hyperextension, mantle exhumation, and oceanization), primarily based on seismic reflection data along the Irish Atlanic side (Yang and Welford, 2021) and the NE Newfoundland side (Welford et al., 2010), are also projected back to key geological times in Figures 4.8 and 4.9. These crustal domains represent progressive strain localisation during rifting (Péron-Pinvidic et al., 2013). Specifically, we link each crustal boundary (polyline in GPlates) to model 5 by assigning a plate ID for each of them, by which the crustal boundary moves over time in GPlates. When reconstructing these crustal domains back in time, the goal is to avoid overlap between reconstructed geometries of crustal boundaries on both sides during the Jurassic and Cretaceous times. The interpreted crustal domains from seismic reflection data record the complete deformation history since the Carboniferous (Bulois et al., 2018), while the deformable models built in this study consider deformation to initiate at 200 Ma. It is worthwhile to note that the crustal domain mapping between the Flemish Cap and Porcupine Bank at 190 Ma and 170 Ma does not strictly follow the paleo-positions of the interpreted crustal domains during this time interval due to the absence of deformation evidence and little knowledge about the past domain boundary configurations. In section 4.1, velocity magnitudes of four blocks and five segments in model 5d are analyzed to understand the segmentation and motions of the Porcupine Bank relative to the Irish Atlantic continental margin (Fig. 4.7). Similarly, the velocity magnitude and angular velocity between the Flemish Cap and the four-block Porcupine Bank model are also calculated from deformable plate modelling to reveal the extension rate and extension obliquity between the two margins in this section (Fig. 4.10).

During the Jurassic to Early Cretaceous, phases of oblique extension are quantified based on the restored pre-breakup geometries of the Flemish Cap-Porcupine region (Figs. 4.8, 4.9, and

4.10). Models 5b and 5d show minimal change in crustal thickness between the two margins in the earliest Jurassic (200-190 Ma). The crust continues to thin in the Porcupine Basin between 190 Ma and 170 Ma in both models 5b and 5d, but the crustal thickness between the Flemish Cap and the Porcupine Bank does not change significantly during this time interval in model 5b. In contrast, the crust between the two margins thins to ~ 24 km on average at 170 Ma and continues to thin to ~ 16 km at 150 Ma in model 5d (Fig. 4.8). Crustal thickness variations indicate that there is little relative motion between the two margins during the Jurassic in model 5b, in contrast to model 5d, where there is pronounced motion between them during this time interval. Also, the region between block 4 and the Flemish Cap thins faster than the region between block 3 and the Flemish Cap, especially at 170 Ma and 160 Ma. The crust between the two margins continues to thin with variable extension rates during the Cretaceous (140-110 Ma) (Figs. 4.9 and 4.10a), but crustal thicknesses along the western flank of the Porcupine Bank are anomalously thick for the scenario in model 5b (indicated by the first column in Fig. 4.9), as shown in Figure 4.4r. In contrast, the crust gradually becomes thinner and thinner over time in model 5d, with a relatively uniform crust in the region between them (indicated by the middle column in Fig. 4.9). This is mainly attributed to the adjustment of the paleo-location of the Flemish Cap over time (Table 4.5). The adjustment ensures that crustal thicknesses between the two margins remain geologically reasonable, as evidenced by the disappearance of the anomalously thick crust along the western Porcupine Bank.

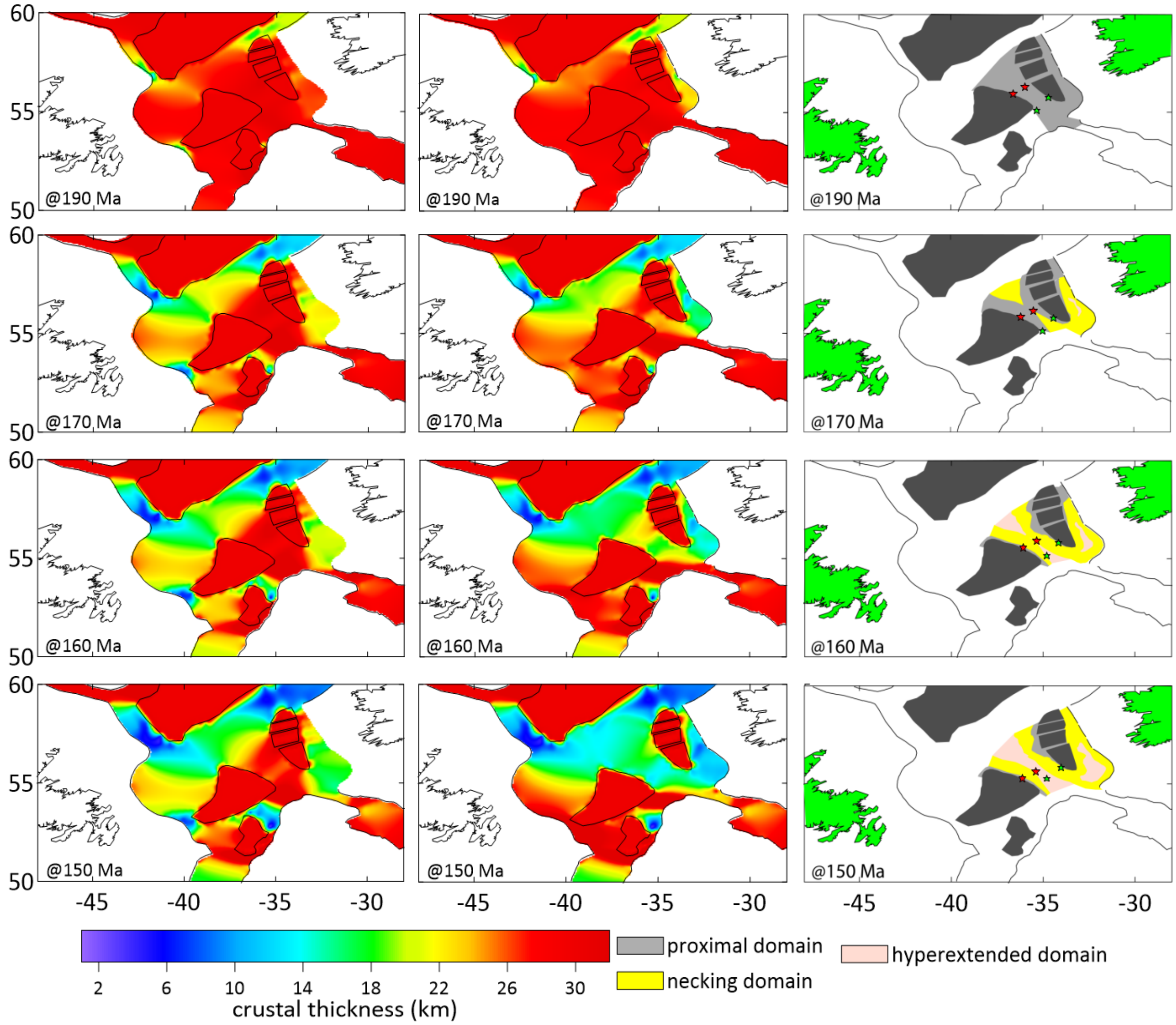

Figure 4.8: Crustal thickness evolution of models 5b and 5d from 190 to 150 Ma. The first two columns show crustal thickness in the Jurassic for models 5b and 5d, respectively. The third column represents the interpreted rift domain map (mainly based on seismic reflection data in Yang and Welford (2021)) reconstructed within the same time interval. The red and green stars in the third column delimit regions of stretched continental crust along reconstructed seismic lines 85-3 on the Flemish Cap margin and PAD 95-13 on the Porcupine Bank margin, respectively.

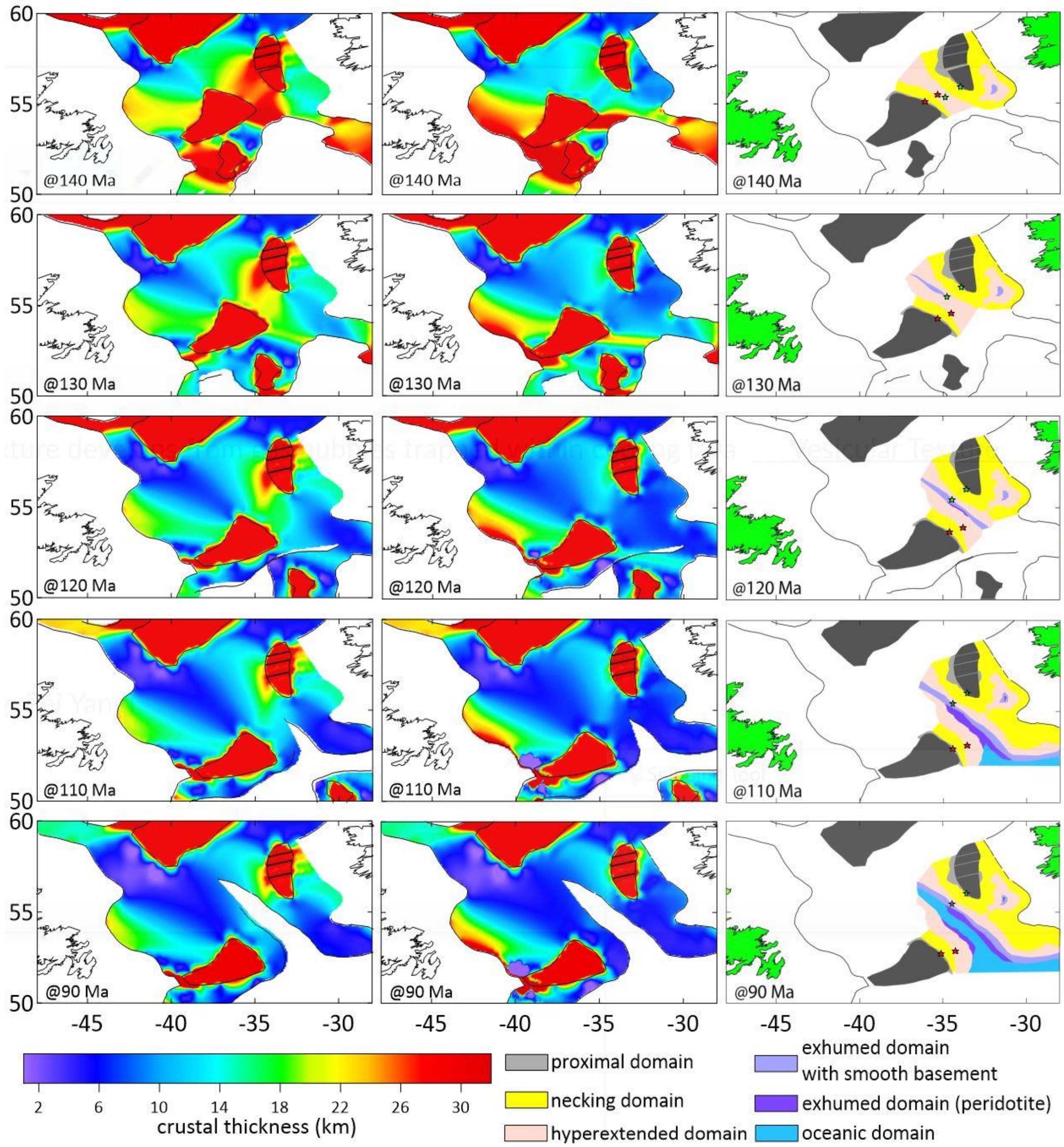

Figure 4.9: Crustal thickness evolution of models 5b and 5d from 140 to 90 Ma. The first two columns display temporal variations in crustal thickness in the Cretaceous for models 5b and 5d, respectively. The third column represents the interpreted rift domain map (based on seismic reflection data in Yang and Welford (2021)) for the same time interval. The red and green stars in the third column delimit regions of stretched continental crust along reconstructed seismic lines 85-3 on the Flemish Cap margin and PAD 95-13 on the Porcupine Bank margin, respectively.

Although crust in the Porcupine Basin thins between 200 -110 Ma and a gradational variation in crustal thickness is clear in model 5b (indicated by the first column in Figs. 4.8 and 4.9), the overall crustal thicknesses are much thinner for model 5d and its variation during this time interval is more geologically meaningful due to the rotation of the segmented borders on the eastern flank of the Porcupine Basin (indicated by the middle column in Figs. 4.8 and 4.9). Specifically, for model 5d, pronounced thickness variations between 200-170 Ma and the minimal change in crustal thickness between 170-160 Ma within the Porcupine Basin are a result of a main extensional event in the Early Jurassic and a later phase of stagnation in the Mid Jurassic (Jones and Underhill, 2011; Stoker et al., 2017; Bulois et al., 2018). The crustal thickness continues to decrease until ~ 120 Ma with variable extension rates (Figs. 4.7-4. 9), mainly caused by another key extensional event during the Late Jurassic-Early Cretaceous in the Porcupine Basin (Jones and Underhill, 2011; Bulois et al., 2018; Lymer et al., 2020; Whiting et al., 2021).

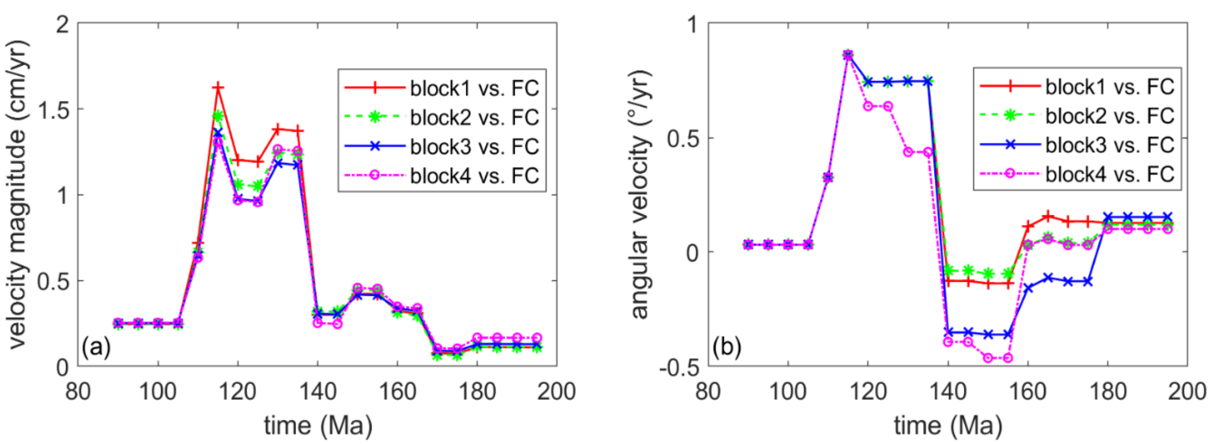

Figure 4.10: Velocity magnitude (a) and angular velocity (b) of the four blocks of the Porcupine Bank with respect to the Flemish Cap, between 200 Ma and 90 Ma, respectively.

From the crustal domain map (indicated by the third column in Figs. 4.8 and 4.9), it is likely that most of the Porcupine Basin transitions from the proximal to the necking phase during the Early Jurassic (190-170 Ma), with an average velocity of ~ 0.2 cm/yr (Figs. 4.8 and 4.10a), while the necking process plays a minor role between the Flemish Cap and Porcupine Bank margins during this time interval. Hyperextension may have started slightly earlier than 170 Ma in the Porcupine Basin while the hyperextension stage between the two conjugate margins starts later at ~ 165 Ma. As rifting proceeds, hyperextension continues with an increased average velocity magnitude of ~ 0.47 cm/yr during the Late Jurassic to earliest Cretaceous (160-140 Ma) between the two conjugate margins (Figs. 4.8 and 4.10a). Mantle exhumation may start from the end of the Jurassic to the earliest Cretaceous (150-140 Ma), although there are still many uncertainties regarding the existence of exhumed serpentinized mantle within the Porcupine Basin (O'Reilly et al., 2006; Prada et al., 2017). Next, mantle exhumation may begin at ~ 135 Ma in the region between blocks 2-3 of the Porcupine Bank margin and the northern Flemish Cap margin, ~ 10 Ma later than when it occurred in the Porcupine Basin (Fig. 4.9). This exhumation continues until ~ 120 Ma. In comparison, the sub-lithospheric mantle between block 4 and the Flemish Cap starts to be exhumed between 130 and 120 Ma, and serpentinized peridotite ridges are formed approximately at 120 Ma. Finally, continental breakup occurs between Goban Spur and Flemish Cap around 110 Ma, possibly ~ 10-15 Ma earlier than between the Porcupine Bank and the Flemish Cap.

In this study, the velocity magnitude of the Flemish Cap relative to the Porcupine Bank is highly variable over time and the variations in angular velocity reflect polyphase oblique extensional events between the two margins (Fig. 4.10). Overall, the velocity magnitude between the two margins from the Early Jurassic through to the end of the Jurassic is much slower than that during the Early Cretaceous (140-112 Ma) (Fig. 4.10a). In contrast, the faster motions of the four blocks and the segmented borders of the eastern margin of the Porcupine Basin in model 5 occur during the Late Jurassic (160-140 Ma) (Fig. 4.7). This suggests that rifting migrates from the Porcupine Basin to the region between the Flemish Cap and the Porcupine Bank. In addition, the timing of the change in motion velocity at ~ 120 Ma coincides with the interpreted formation time of exhumed serpentinized peridotite ridges between the two margins (Fig. 4.9).

While the Porcupine Bank moves northwest relative to the Irish Atlantic continental margin during rifting, seeming to approach the Flemish Cap, the overall Irish offshore margin moves southeast relative to a fixed Greenland between 200 Ma to 140 Ma. Meanwhile, the Flemish Cap also moves in a southeastward direction relative to a fixed Greenland between 200 Ma to 112 Ma such that the relative extension between the Porcupine Bank and the Flemish Cap is much larger than their average motion velocities with respect to the Irish Atlantic continental margin and the Orphan Basin, respectively (Figs. 4.7a and 4.10a). In addition, rift orientation changes from E-W in the Early Jurassic (200-180 Ma) to NNE-SSW in the Early-Mid Cretaceous (Figs. 4.8 and 4.9). In summary, the orientation, magnitude, and duration of lithospheric extension between the Porcupine Bank and the Flemish Cap vary significantly from Jurassic rifting to Cretaceous breakup.

4.5.3 Regional seismic transects

A variety of vintage and new 2D seismic reflection profiles have been acquired along the Porcupine Bank region (e.g., PAD data acquired in 1995, 2013, and 2014) and the Flemish Cap (Erable and FGP seismic data acquired in the 1980s). However, none of the more recently acquired seismic lines along the Porcupine Bank margin extend far enough continent-ward to reach the necking domain (Yang and Welford, 2021). Here, the previously unpublished regional 2D seismic profile PAD95-13, in the southwest region of the Porcupine Bank, which extends landward to the necking region, is interpreted. By comparing seismic line 85-3 from the FGP program over the Flemish Cap (Welford et al., 2010), and PAD95-13 on the Porcupine Bank, some similarities are observed in the necking and initial hyperextended domains along both profiles after reinterpreting line 85-3 (Fig. 4.11). The geometries of the syn-rift basins bounded by seaward dipping faults in the necking domain and the transition zone from necking to hyperextended domains are similar on both profiles (indicated by the red arrows in Figs. 4.11c and 4.11d).

In this study, the positions of portions of both seismic profiles are reconstructed back to where they would have been over geologic time in accordance with the plate tectonic evolution of model 5d (red and green stars in the third column in Figs. 4.8 and 4.9). Evidently, the paleo-positions of the partial transects move relatively toward each other with NW-SE orientations during the Jurassic to earliest Cretaceous (200 - 140 Ma), then become aligned from 140 Ma to 130 Ma based on the rotation parameters in model 5d (red and green stars in the third column of Figs. 4.8 and 4.9). This time interval also corresponds to the transition from hyperextension to mantle exhumation between the Flemish Cap and the Porcupine Bank from the crustal domain map in Figure 4.9. Subsequently, they move farther away from each other in a NE-SW direction prior to final continental breakup (Figs. 4.8 and 4.9). Although the basement is locally uplifted in the hyperextended domain along both profiles (indicated by the black arrows in Fig. 4.11), the basement morphology is rougher and more highly faulted along seismic line 85-3 than PAD 95-13, indicating asymmetric amounts of deformation during the hyperextension stage on both sides. This may be associated with the northwestern motion of the Porcupine Bank gradually bringing it closer to the Charlie-Gibbs Fracture Zone, potentially leading to magma-assisted extension with lava-sealed transitional crust, while the Flemish Cap rotated southeastwardly and amagmatically to the southwest of the Porcupine Bank (Figs. 4.7 and 4.8). Overall, the mapped reconstruction of the two partial seismic profiles (Figs. 4.8 and 4.9) and the direct comparison of both seismic lines provides a qualitative tool for assessing the geological implications of model 5d.

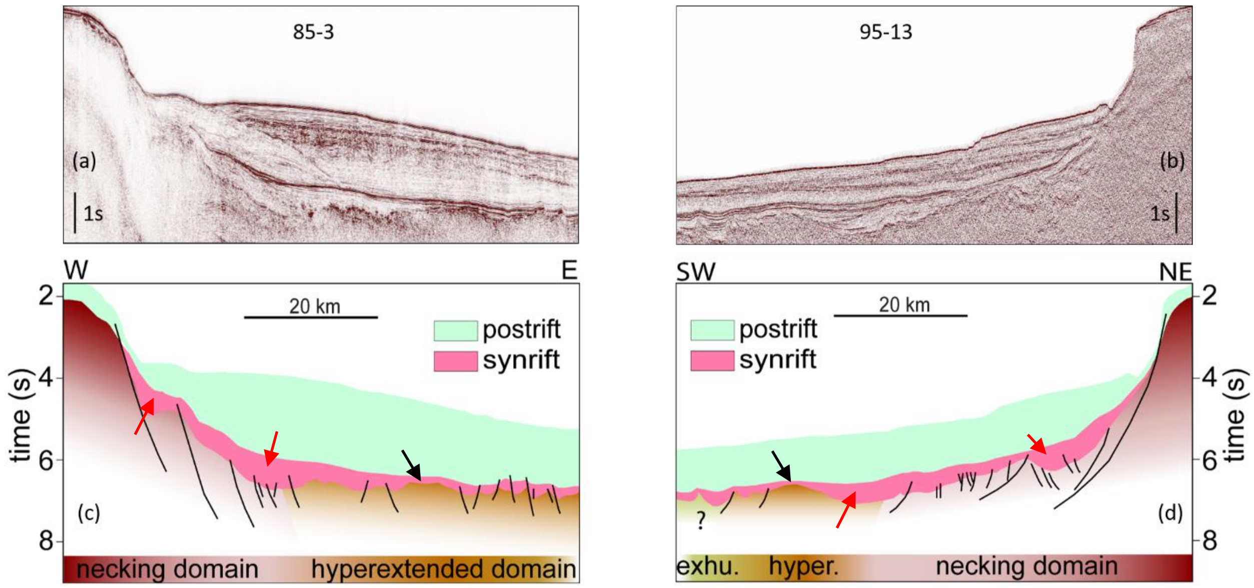

Figure 4.11: Comparison of seismic sections over the Flemish Cap (left panel) and the Porcupine Bank (right panel). The upper and lower panels correspond to uninterpreted and interpreted sections in the time domain, respectively. The locations of the partial profiles 85-3 and 95-13 are delimited by the red and green stars, respectively, in the third column in Figures 4.8 and 4.9.

4.6 Discussion

4.6.1 Strong inheritance across the Porcupine Bank

In this study, deformable plate tectonic reconstructions have been used to simulate the opening of the Porcupine Basin, clockwise rotation of the Flemish Cap away from North America, and the complex protracted and poly-phase oblique extensional events between the Porcupine Bank and the Flemish Cap during the formation of the southern North Atlantic Ocean (Figs. 4.8 and 4.9). The relative motion of individual continental blocks or that between the two margins is highly influenced by the geometries of inherited crustal basement terranes, illustrated by the crustal thickness distributions from the five models considered in this study (Fig. 4.4). The crustal thickness variations from the five models also reveal how the orientations of major fault zones that segment the Porcupine region control the timing and orientations of deformation over geologic time (Figs. 4.4 and 4.6). This may be attributed to considerable variations in rheology and lithology associated with different inherited crustal basement terranes (Johnson et al., 2001; Readman et al., 2005), which have a fundamental effect on the rift geometry from inception to final continental rupture (Phillips and McCaffrey, 2019).

In addition to the orientation of major fault zones (e.g., models 2, 3, and 4 in Fig. 4.4), the number of basement crustal terranes separated by major fault zones also plays an important role in the evolution of the Porcupine Atlantic region based on comparing crustal thicknesses calculated from the five models against complementary geophysical constraints (i.e., gravity inversion and seismic refraction). Model 5d provides the most geologically reasonable deformable plate model, in which the Porcupine Bank is subdivided into four blocks with each experiencing polyphase rotations and shearing prior to final continental breakup. The motion velocity magnitude and orientation for each block vary from one to another (Fig. 4.7). This likely means that the Porcupine Bank experienced partitioned and localized deformation as a result of complex stress regimes caused by the interplay of Caledonian and Variscan inheritance with Mesozoic rifting. This suggests that the Porcupine Bank was more structurally complex than a simple uniform continental block, as previously proposed (White et al., 1992; McCann et al., 1995; Peace et al., 2019). In addition, the Flemish Cap rotates towards the Iberian plate until the Albian (~ 112 Ma), while the motion of the Porcupine Bank ceases during the Aptian (120 Ma), earlier than the Flemish Cap. In model 5d, the Flemish Cap is an independent continental block, while the Porcupine Bank is highly-segmented. Studies show that the mean duration from initial rift to final breakup for passive margins with more inherited structures tends to be shorter compared with margins without pre-existing inheritance due to no reactivation of the inherited structures (Holdsworth et al., 2013). This may be one possible reason why Porcupine Bank stopped moving earlier than the Flemish Cap. Most recently, 3-D geodynamic modelling has reproduced the rotation of the Flemish Cap by simulating the interaction of two propagating rifts (Neuharth et al., 2021). The mechanism of rotation of the Porcupine Bank may be similar.

The Porcupine Bank is obliquely cut by two main crustal terrane boundaries in Figure 4. 3c, in which the NE-SW trending Iapetus Suture (~ 51.3° N) isolates the southern portion of the Porcupine Bank (Tyrrell et al., 2007, 2010). In Figure 4.3b, the Iapetus Suture (~ 52.6° N) with an ENE-trending strike directly connects with the Charlie-Gibbs Fracture Zone, dividing the Porcupine Bank into two blocks (Chenin et al., 2015; Ady and Whittaker, 2019). However, the crustal thicknesses calculated from both modelled configurations (models 2 and 3) do not support the interpreted segmentation from seismic data interpretation (Whiting et al., 2021). According to observations from gravity and magnetic data, the Porcupine Bank appears to be segmented into three main Caledonian crustal terranes, in which the ENE-trending Iapetus Suture (~ 52.1° N) extends further into the oceanic region (Grow et al., 2019) (Fig. 4.3e). Since crustal thicknesses calculated from this model are in general agreement with similar estimates calculated using gravity inversion, the four-block model (model 5d) is preferred relative to the other models. This model can also be used to infer the most probable position for the Iapetus Suture, which may be laterally offset from the Charlie-Gibbs Fracture Zone rather than directly connected with it as shown in model 2 (Fig. 4.3b) or extending to the southern limit of the Porcupine Bank as shown in model 3 (Fig. 4.3c).

In addition to identifying the orientations and number of inherited Caledonian crustal terrane boundaries dividing the Porcupine Atlantic region, the timing of reactivation of these terrane boundaries also contributes to our understanding of the plate kinematic evolution of the

Irish-Newfoundland conjugate margins. In the Early Jurassic, decreasing crustal thicknesses in the Porcupine Basin are related to the motion of individual blocks with respect to the Irish continental margin and the relative motion between each block. Although the motion of the first three blocks in model 5 ceases during the earliest stage of the Cretaceous (140 Ma) (Table 4.3 and Fig. 4.6a), they have distinctive velocity magnitudes, resulting into different motion displacements in the Jurassic. This suggests that the role of inheritance between these blocks diminishes by the Early Cretaceous, possibly accompanied by an increased magma supply along the western portion of the northern Porcupine Bank (Norton, 2002). Meanwhile, block 4 continues to move during the Early Cretaceous, and it moves relatively faster than the other three blocks (Fig. 4.7a) , suggesting that the displacement of block 4 lasts the longest among the four blocks with respect to the Irish continental margin. This also suggests that the role of pre-existing structural inheritance varies during different evolutionary stages of the Irish Atlanic margin. This phenomenon is consistent with previous interpretations that suggest pre-existing inheritance mainly governs the stretching stage, and gradually exerts less control on rift dynamics during the hyperextension and exhumation phases (Manatschal et al, 2015). It is also worthwhile to mention that this study mainly focuses on the structural inheritance from the Caledonian and Variscan orogenies, but pre-existing compositional heterogeneities and thermal inheritance may also play a role in the formation of the Porcupine region (Chenin et al., 2015; Manatschal et al., 2015).

4.6.2 Implications for the formation of the Porcupine Basin

Tectono-stratigraphic features in the Porcupine Basin provide valuable insights regarding the episodic extensional events of the hyperextended basin, as documented from previous seismic studies within the northern Porcupine Basin (Naylor et al., 2002; Whiting et al., 2021; Lymer et al., 2020). However, inherited Caledonian and Variscan crustal terranes are often not considered as key contributors during the formation of the basin. This study bridges that gap and indicates that the formation of the Porcupine Basin is highly influenced by pre-existing structural fabrics, through a combination of compartmentalized shearing and clockwise rotation with respect to the Irish Atlantic continental margin, rather than simply involving pure rotation (McCann et al., 1995; Peace et al., 2019), or a shearing model (Grow et al., 2019), or the inferred strike-slip fault zones in the basin (Readman et al., 2005). This study also restores the evolving paleo-geometry of the Porcupine Basin over time. In model 5d, the motion of each continental block contributes to the direction and rate of extension during multi-phase rifting within the Porcupine Basin during the Jurassic to Early Cretaceous, indicative of differential extension, which is consistent with the variations in age and orientation of observed fault systems (Lymer et al., 2020; Saqab et al., 2021). Shearing between blocks in model 5d also exerts a great impact on segmentation along the basin axis, in agreement with observations of compartmentalised sedimentary depocenters and lineaments orthogonal to tilted blocks along the basin flanks (Gernigon et al., 2006; Lymer et al., 2020). In addition, the locations of individual crustal terrane boundaries that traverse the Porcupine Basin in model 5d are approximately consistent with the rift-segmenting transfer zones identified based on seismic interpretations within the basin (Norton, 2002).

According to model 5d, the motions of block 4 and segment 4 along the eastern border of the Porcupine Basin from the Late Jurassic to Early Cretaceous (160-130 Ma) primarily contribute to the crustal thinning experienced within the southern basin (Figs. 4.8 and 4.9), consistent with the high stretching factor (equal to or larger than 10) (Tate et al., 1993; Prada et al., 2017). Although seismic interpretations suggest that rifting within the Porcupine Basin ceased during the earliest Cretaceous (Whiting et al., 2016, 2021), the pre-existing crustal lineament between block 3 and block 4 may have been reactivated in the Early Cretaceous, leading to a degree of continued extension during the time interval of 130 -115 Ma in the southern Porcupine Basin (Fig. 4.7). This continued minor extensional event may be associated with syn-rift Aptian/Albian sediments in the southern Porcupine Basin and the Goban Spur region (Sinclair et al., 1994; Štolfová et al., 2012a), possibly associated with the interpreted Early Cretaceous transitional stage between the syn-rift and early post-rift phases (Whiting et al., 2021). In addition to the rejuvenation of inherited basement terrane boundaries or Jurassic faults (Saqab et al., 2021), this minor rifting event within the southern basin may be a consequence of the accelerated basin subsidence associated with Mid-Ocean-Ridge push during the North Atlantic opening (Shannon et al, 1993; McCann et al., 1995), or the effect of far-field tectonic forces (e.g., the opening of the Bay of Biscay (Tugend et al., 2015)), or continental breakup of the southwestern Goban Spur margin (Bullock and Minshull, 2005).

4.6.3 Oblique extension between the Porcupine Bank and the Flemish Cap

The interpreted crustal domain maps reveal asymmetric tectonic evolution between the two margins and a gradual proximal-to-oceanic transitional region from highly thinned continental crust to a zone of exhumed serpentinized mantle, intruded by magmatic intrusions prior to, during, and after continental breakup (Gernigon et al., 2006; Yang and Welford, 2021). Evidently, from the segmentation in model 5d, the pre-existing crustal structures play a significant role in the progressive change in structural style during the formation of the NE Flemish Cap - Porcupine Bank conjugate pair, likely related to the variable rheology of individual crustal terranes. The rheological contrasts may cause significant variations in faulting geometries (Phillips and McCaffrey, 2019), affecting extensional orientations and magnitudes.

They also exert strong influence on the width and timing of formation of oblique rifts and passive margins (Duclaux et al., 2020).

Another implication of scenario 5d is that the rotations of the Flemish Cap and the Porcupine Bank may accommodate oblique-slip deformation between the two margins. The extensional obliquity between them is low during the Early-Mid Jurassic (200-160 Ma) and thereafter, the obliquity of NW-SE oriented extension between the Flemish Cap and blocks 3-4 increases during the Late Jurassic (Fig. 4.10b). Extension between the two margins is significantly more oblique during the Early Cretaceous (140-112 Ma) (Fig. 4.10b). Although Brune et al. (2018) show that time-averaged rift obliquity in the Irish Atlantic rift system ranges from moderate to high (~ 30°- 75°) since Pangea fragmentation, the modelled evolution of obliquity over time has no seismic constraints in the study margin area. In this study, oblique extension between both margins throughout geological time is revealed by the variations of crustal thicknesses from the deformable plate models with more seismic constraints.

Oblique divergence between the two margins produces 3-D stress fields, strongly affecting syn-rift tectonics and protracting the duration of hyperextension (Chenin et al., 2015; Brune et al., 2018). In the Porcupine Basin, it also allows more time for the formation of hyperextended crust (Reston et al., 2004; Reston, 2009), or mantle exhumation (O'Reilly et al., 2006), or proto-oceanic crust (Chen et al., 2018). Consequently, simplified 2-D analyses of the rift system are inadequate for capturing the complicated plate kinematic history of the NE Newfoundland-Irish conjugate margin pair.

4.6.4 Conjugate relationship update

The formation of the Newfoundland- Irish Atlantic conjugate margins between two triple junctions (i.e., the Bay of Biscay to the south and the mouth of Rockall Basin to the north (Fig.

4.1)) principally resulted from a series of episodic northward rift propagation events during the Late Paleozoic to Mesozoic (Naylor et al., 2002). However, by failing to account for deformation within continental domains and the lack of consideration for the rotation and segmentation of independent continental blocks within an evolving rift system, the previous literature regarding this conjugate margin pair may be incomplete, leading to false conclusions. For example, many previously published tectonic models show connectivity between the Porcupine Basin and the Orphan Basin during the Late Jurassic - Early Cretaceous (Enachescu et al., 2005; Gerlings et al., 2011; Ady and Whittaker, 2019), whilst the movement of the Orphan Knoll and Flemish Cap, identified as undeformed continental blocks, played an important role regarding the extensive thinning observed within the Orphan Basin (Štolfová et al., 2012b; Nirrengarten et al., 2018; Peace et al., 2019). Similarly, the Goban Spur and the Porcupine Bank on the Irish Atlantic margin have been proposed to link directly with the NE Flemish Cap and the East Orphan Basin, respectively, on the Canadian side (Masson and Miles, 1986; Srivastava and Verhoef, 1992; Sibuet et al., 2007; Gerlings et al., 2012). Meanwhile, the inferred clockwise rotation of the Flemish Cap with respect to the Orphan Basin has been supported by interpretations of gravity anomaly data (Sibuet et al., 2007), crustal thickness estimates from gravity inversion (Welford et al., 2012), and interpretations of seismic data (Enachescu et al., 2005; Štolfová et al., 2012a). This has called into question previous widely-accepted conjugate margin relationships and possible paleo-positions of these rifted continental margins (Sibuet et al., 2007; Welford et al., 2012; Peace et al., 2019). Subsequent rigid and deformable plate reconstruction models, and structural restorations, show that the NE Flemish Cap and the Porcupine Bank are more likely to have been conjugate to each other at the onset of rifting, and that the Porcupine Basin and the

Goban Spur margin might have a potential conjugate relationship with the Galicia Interior Basin on the Iberian margin (Nirrengarten et al., 2018; Peace et al., 2019; Sandoval et al., 2019).

The deformable plate reconstruction model proposed in this study further supports the conjugate relationship between the NE Flemish Cap and the Porcupine Bank during the early rifting. However, due to the rotations of both margins and the segmentation of the Porcupine Bank, the conjugate relationship between the two margins and the time at which different portions of the margins were conjugate to each other during rifting vary along-strike (Figs. 4.9 and 4.10). Specifically, block 1 in model 5d appears to have a link with the Rockall Bank in the earliest Jurassic (190 Ma), while blocks 2, 3, and 4 are conjugate to the NE Flemish Cap during the Jurassic. As rotation of the Flemish Cap and block 4 of the Porcupine Bank (in model 5d) continue into the Early Cretaceous (140-120 Ma), the NE Flemish Cap margin gradually aligns with the region at the mouth of the Porcupine Basin and the Goban Spur margin, which is consistent with the observed serpentinized peridotite ridges on both sides during Aptian time (Fig. 4.9). These results highlight the complicated conjugate relationship between the Irish Atlantic-Newfoundland conjugate margins and the need to incorporate pre-existing inheritance when studying rift systems in regions of prior orogenesis.

4.6.5 Limitations of this work

By incorporating more seismic constraints than previously published plate restorations (Nirrengarten et al., 2018; Peace et al., 2019; Ady and Whittaker, 2019; King et al., 2020), the deformable plate tectonic reconstruction of the NE Newfoundland-Irish Atlantic conjugate margins presented in this study enables an enhanced understanding of detailed plate motions, the duration and extensional orientations of distinct rift episodes, the timing of the final rupture, and the significance of different inherited crustal terranes over geologic time. However, deformable plate tectonic reconstructions built in GPlates still involve many limitations and uncertainties. Many of these have already been described by Peace et al. (2019), such as the oversimplistic assumption of homogeneous initial crustal thickness (30 km), the initial rifting time (200 Ma) failing to record the whole history of tectonic events, and the occurrence of edge effects due to the inability to allow strain to diffuse from deformable regions into undeformable regions. Also, due to the assumption of homogeneous crust, deformable plate models built in GPlates cannot deal with the nature and origin of lower crustal bodies. The temporal overlap of rifting episodes also fails to be considered (Péron-Pinvidic et al., 2013). Although the onset and cessation of extensional events are mainly constrained by interpreted tectono-stratigraphy (Bulois et al., 2018; Saqab et al., 2021; Whiting et al. 2021), timings of rotation poles may still be underestimated or overestimated due to sparse data constraints. Despite of the possible presence of oceanic crust in the Porcupine Basin (Chen et al., 2018), this study mainly supports the result that the Porcupine Basin underwent hyper-extension without the formation of ocean (Whiting et al. 2021). Additional uncertainties also involve interpretations of the edge of continental crust (ECC), and the challenging task of accurately identifying crustal breakup times in the presence of magmatic additions and with little knowledge regarding the extent of lithospheric mantle exhumation during extension between the two margins, especially for the northwestern flank of the Porcupine Bank. Discrepancies in crustal thicknesses between deformable plate modelling and geophysical observations may also result from the inability to model depth-dependent stretching of the crust (Kusznir and Karner, 2007).

It should be noted that the crustal thicknesses modelled for the continental domain of the Goban Spur margin for all of the model setups appears to be much thinner than those derived from gravity inversion. This may be related to uncertainties regarding the seaward boundary

(ECC) and landward limit (NL) of the deformable region in the southwest of the margin due to sparse seismic constraints (Yang et al., 2020). Likewise, the crustal breakup time within the deformable network in the southwest of the margin is not well constrained either. The continental crust of the Goban Spur is highly partitioned by complex fault system with various orientations (Dingle and Scrutton, 1979; Sibuet et al., 1985). However, segmentation of the Goban Spur margin is not considered in this study due to lacking constraints. Furthermore, the geometry and location of the inherited Variscan orogenic front may play an important role in the evolution of crustal thickness over time in the Goban Spur region. Yet, the proposed deformable plate model fails to consider Variscan structural fabrics as a tectonic element due to uncertainties in their geometry and location. Finally, controversy regarding the timing, orientation, and magnitude of rotation of the Iberian plate with respect to the Irish continental margin (Causer et al., 2019) may also contribute to the intrinsic uncertainties of the rotation parameters used in model 5d. For example, in the Nirrengarten et al. (2018) plate reconstruction model, the motion of the northern Iberian plate since the Jurassic is perhaps overestimated (Angrand et al., 2020).

4.7 Conclusions

By testing various parameters for five deformable plate tectonic reconstructions of the Porcupine Bank, offshore Atlantic Ireland, we find that the offshore continuation of inherited Caledonian crustal terrane boundaries across the Porcupine Bank tends to follow an ENE-orientation. Meanwhile, velocity magnitudes and crustal thicknesses calculated for a segmented Porcupine Bank composed of four blocks (model 5d) provide the best correlations with independent geological and geophysical observations. Within the preferred model, the independent plate kinematics for each block vary from one to another, implying that the crustal evolution of the Porcupine Bank is likely controlled by a complex combination of shearing and rotation, coeval with the rejuvenation of inherited Caledonian and Variscan structures and fabrics. Other processes such as enhanced magmatism in the northern Porcupine Bank may have also contributed.

The deformable plate restoration quantifies temporal variations in crustal thickness during rift evolution between the Flemish Cap and Porcupine Bank, revealing poly-phase and oblique crustal deformation between both margins. With considerable variations in extension obliquity between the Flemish Cap and Porcupine Bank from the Jurassic to Cretaceous, the preferred deformable model highlights lithospheric necking and hyperextension at low obliquity during the Early-Mid Jurassic, which transitioned into lithospheric hyperextension/mantle exhumation at higher obliquity during the Early Cretaceous.

Overall, the deformable plate tectonic reconstruction of the Flemish Cap and Porcupine Bank provides a significantly improved understanding of the role of inherited crustal structures, plate reorganization, and the tectonic evolution of the offshore Irish Atlantic margin. The findings of this study also contribute to unraveling the spatial and temporal evolution of southern North Atlantic rifting during the Mesozoic, prior to the initiation of seafloor spreading.

Acknowledgement

We are grateful to the Department of Environment, Climate and Communications of Ireland for providing the multichannel seismic reflection data. We also acknowledge the Petroleum Infrastructure Programme (PIP) in Ireland for access to the technical studies and regional reports. Schlumberger are acknowledged for donating Petrel software to Memorial University. We would like to thank the members of the Memorial Applied Geophysics for Rift Tectonics (MAGRiT) group for providing suggestions for this research. Archiving of GPlates data files used to generate deformable plate models are underway and the Mendeley Data repository will be used. Our gratitude also goes to anonymous reviewers for their valuable comments and suggestions.

Chapter 5

5. Revisiting the Goban Spur margin, offshore Ireland, through integration of seismic reflection data and deformable plate modelling

This chapter is a manuscript paper for Marine and Petroleum Geology, submitted in July, 2021. It revisits the continental crust of the Goban Spur margin and seeks to bridge and address remaining regional knowledge gaps. The manuscript authorship is Yang, P., and Welford, J.K. Kim Welford supervised the research and helped manuscript preparation.

5.1 Abstract

Resource prospectivity offshore Atlantic Ireland remains a topic of interest, particularly with respect to connectivity with conjugate margin basins. However, due to sparse seismic data coverage and limited wells, existing studies have struggled to characterize the structural features and tectonic evolution of the basins on the continental portion of this margin, resulting in a poor understanding of their tectonic evolution. In this study, newly presented long-offset seismic reflection data provide an opportunity to observe the complex architecture of the Goban Spur basins, filled with highly variable sediment thicknesses, which suggest a protracted and polyphased rifting history. Inversion structures, complex compressive structures (folds and reverse faults), and transtensional features (flower structures) are also observed in the pre-rift and syn-rift sedimentary layers that are poorly imaged on vintage seismic data, which implies that

continued reactivation of both the Variscan basement terranes and inherited faults occurred on this margin. This study also locally updates an existing deformable plate model in GPlates by incorporating two transfer faults based on seismic constraints, showing that the faults play a significant role in reshaping the evolution of crustal thickness of the continental crust of the Goban Spur. Crustal thickness evolution from this updated model in the Goban Spur region is affected by the interplay between the rotation of the Flemish Cap, the motion of the Iberia plate, and the opening of the Porcupine Basin during the Mesozoic, following the collapse of the Variscan Orogeny. The updated deformable plate model supports the hypothesis of segmentation of the hyperextended Goban Spur region, highlighting the significant role of inherited structures, and renewing linkages between the Goban Spur and its potential conjugates during oblique rifting. These relationships have important implications for reducing exploration risk in the Goban Spur basins.

5.2 Introduction

The magma-poor Goban Spur continental margin and associated basins (Fig. 5.1), offshore Ireland, are largely underexplored compared with the Porcupine Basin. Recently, source rocks and reservoirs in the Jurassic and Cretaceous strata have been proven in the southern Porcupine Basin (Hawkes et al., 2019). The well drilled on the shelf of the Goban Spur, 62/7-1 (Fig. 1), encountered Cretaceous and Jurassic reservoir and Lower Jurassic source rocks as well (Cook, 1987; Colin et al., 1992; Copestake et al., 2017). The promise of prospectivity in the southern Porcupine Basin-Goban Spur region motivates increased study into the structural and tectonic evolution of basins developed therein.

In this study, we focus on the continental crust of the Goban Spur, bounded by the Fastnet Basin to the east and a NW-SE trending escarpment to the west (inboard of profile X2 in Fig. 5.1). The rift-related crustal architecture on the Goban Spur margin, composed of the proximal, necking, hyperextended, exhumed mantle, and oceanic domains, has been previously mapped (Yang et al., 2020; see chapter 2). Based on this mapping, the region of thinned continental crust interpreted as the necking zone appears to be much wider than other crustal domains based on seismic interpretation and gravity inversion. The mechanism behind the wide necking zone on this Spur is unclear. Plate reconstructions have not reached a consensus in terms of whether the Goban Spur is conjugate to the Flemish Cap or not (Masson and Miles, 1986; Seton et al., 2012; Peace et al., 2019). For example, the Goban Spur basins are proposed to have a linkage with the Flemish Pass Basin (Masson and Miles, 1986), or a connection with the Galicia Interior Basin (Peace et al., 2019; Sandoval et al., 2019). Meanwhile, the crustal thickness of the Goban Spur margin derived from existing deformable plate models is very thin, inconsistent with the results from gravity inversion (Welford et al., 2012; Yang et al., 2021). This discrepancy motivates us to continue to investigate the origin of the deformed continental crust of the Goban Spur.

Structural features and Mesozoic stratigraphic sequences of the Goban Spur basins overlying stretched continental crust have mainly been constrained based on vintage seismic reflection profiles (e.g., Continental Margin (CM) survey in 1975 and WAM line in 1985) (Dingle and Scrutton, 1979; Masson et al., 1985; Peddy et al., 1989) and sparse drilling sites (de Graciansky et al., 1985; Colin et al., 1992). However, thin sediments (Peddy et al., 1989), volcanic sills intruding the Cretaceous succession (de Graciansky et al., 1985), and potential salts (O'Sullivan et al., 2021) degrade the quality of the vintage seismic data, reducing confidence in existing interpretations. Meanwhile, although the continental part of the Goban Spur is highly faulted, with two fault systems with predominant NW-SE and NE-SW trends well developed (Dingle and Scrutton, 1979; Roberts et al., 1981), the timings and origins of these faults are still unclear, including the relationships between pre-existing and more recent faults. In addition, little attention has been paid to the possibility of segmentation of the Goban Spur due to interpreted transfer faults and to how pre-existing Variscan basement structures may have affected the evolution of the continental portion of the Goban Spur.

By interpreting four seismic reflection profiles (X3-X6) acquired in 2013/2014 (Fig. 5.1), this study seeks to build on previous knowledge of structural features and tectono-stratigraphy in the Goban Spur basins and unravel the role of inherited structures in basin development. By incorporating newly interpreted transfer faults from these seismic reflection data, we locally update an existing regional deformable plate model in GPlates. The present-day crustal thicknesses from the updated deformable plate model are compared with those from gravity inversion across the Goban Spur region, to assess the role of transfer faults in the margin development. Finally, the crustal thickness evolution on the Goban Spur during the Mesozoic is visualized to illustrate the effect of segmentation and oblique rifting on the hyperextended basins of the Goban Spur, providing further insights into this largely underexplored region.

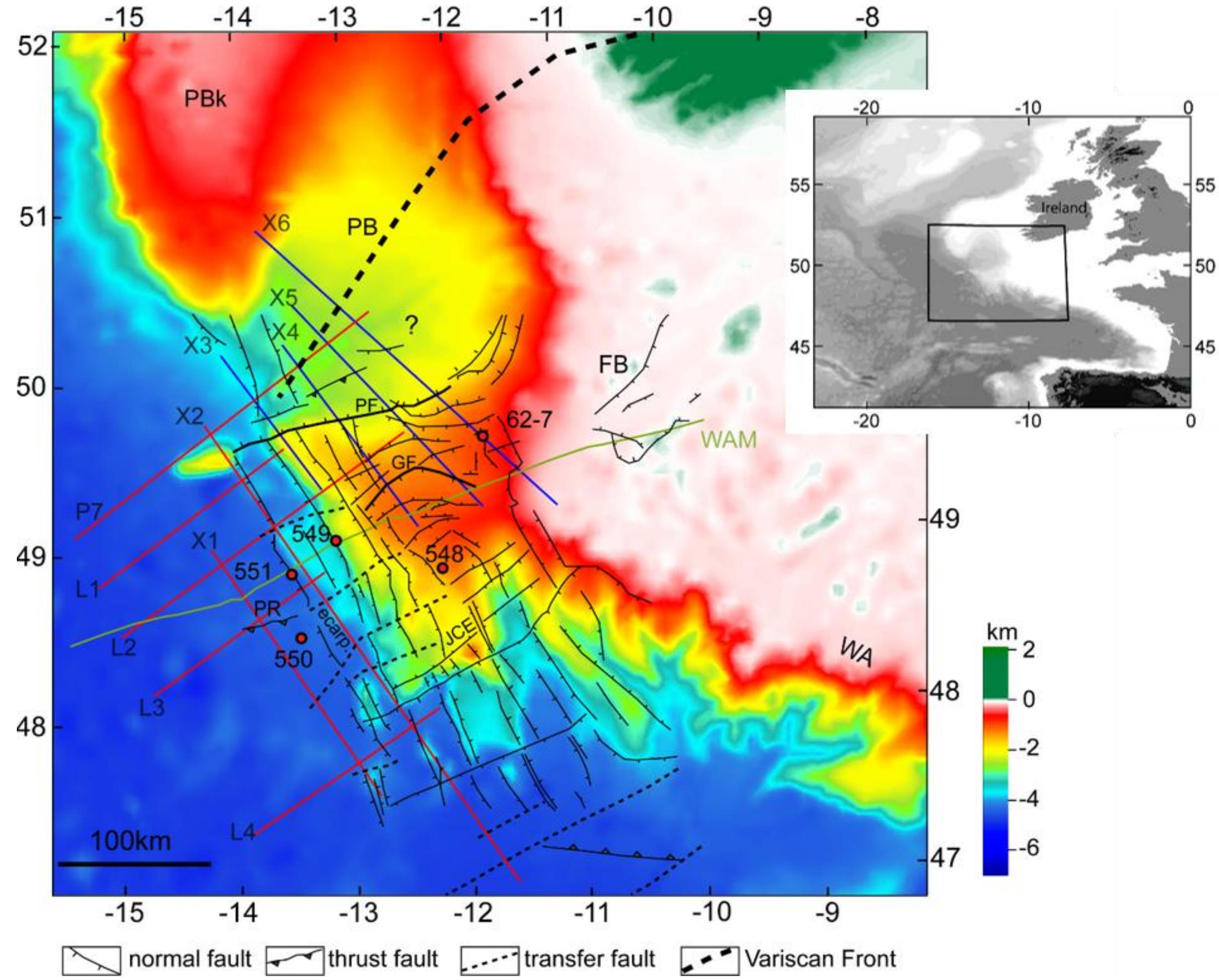

Figure 5.1: The bathymetry of the Goban Spur, offshore south-west Ireland with the tectonic elements. The WAM seismic reflection line (light green) was from Peddy et al. (1989). The red lines (L1-L4, P7, and X1-X2) are interpreted in Yang et al. (2020) and Yang and Welford (2021). The blue lines (X3-X6) are interpreted in this study. The offshore continuation of the Variscan Front is from Tyrrell et al. (2010). The faults are from the Petroleum Affairs Divisions of Ireland (http://gis.dcenr.gov.ie). Four boreholes (sites 548-551) were drilled during Leg 80 of the Deep Sea Drilling Project (DSDP) (de Graciansky et al. 1985). Well 62/7-1 was drilled by Esso E&P Ireland in 1982 (Cook, 1987). PR represents Pastouret Ridge, a local bathymetric high between sites 550 and 551. Abbreviations: GS, Goban Spur; WA, Western Approaches; PB, Porcupine Basin; PBk, Porcupine Bank; PF, Porcupine Fault; GF, Goban Fault; FB, Fastnet Basin, JCE, Jean Charcot Escarpment.

5.3 Background

The Goban Spur is located to the south of the Porcupine Basin and to the north of the Western Approaches margin (Fig. 5.1). To the south of the Goban Spur, the bathymetric morphology is very complex with multiple incised valleys, whereas the seabed relief to the north is relatively smooth (de Graciansky et al. 1985). The lithosphere of the Goban Spur region was affected by the Caledonian and Variscan orogenies before the formation of the rifted margin, which was itself associated with the separation of the Irish and Newfoundland margins, as well as the opening of the Bay of Biscay (Sibuet et al., 1985). Many scholars have attempted to extrapolate the location of the Variscan deformation front from onshore to offshore south-west Ireland by using geophysical data (Sibuet et al., 1985; Tyrrell et al., 2010; Grow et al., 2019). However, the Variscan deformation front has a weak geophysical signature onshore southern Ireland (Jacobi and Kristofferson, 1981; Masson et al., 1998; Landes et al., 2003), giving rise to uncertainty in its location. Nonetheless, there is a general consensus that it is located in the southern Porcupine Basin (Sibuet et al., 1985; Colin et al., 1992). It may lie north of DSDP sites 549 and 551, coincident with the Goban Fault (Sibuet et al., 1985) or further northward (Grow et al., 2019). Correspondingly, the offshore continuation of the Variscan Front remains uncertain.

The pre-rift basement of the continental part of the Goban Spur margin is mainly composed of inhomogeneous Paleozoic rocks, influenced by metamorphism from the formation of the Variscan orogenic belt (Sibuet et al., 1985; Masson et al., 1989) that was mainly caused by the collision between Gondwana and Laurussia (Matte, 2001). Recognition of the overlying syn-rift sedimentary sequences varies in the literature. Masini et al. (2013) proposed that syn-rift packages are composed of Jurassic and Cretaceous units. The four DSDP boreholes helped to only define the Cretaceous and Cenozoic strata on the Goban Spur (de Graciansky et al. 1985) (Fig. 5.1). Well 62/7-1 penetrated Early Jurassic sedimentary rock, as well as 200 m of porphyritic basaltic lavas overlain by Hauterivian sediments (Copestake et al., 2017). However, the age of the basaltic lava remains unclear, probably dated back to the Bathonian (Colin et al., 1981), or the Valanginian (Tate and Dobson, 1988). Although there were no Triassic rocks penetrated in the Goban Spur region, the formation of the Goban Spur basins is proposed to have begun in the Triassic based on a close affinity with the Fastnet Basin to the east (Colin et al., 1992). According to constraints from well 62/7-1, the extensional stage for the Goban Spur basins occurred during the Triassic and Early Jurassic, followed by a quiescent stage during the Middle Jurassic - Early Cretaceous (Colin et al., 1992). Crustal thinning across the Goban Spur margin continued in the Early Cretaceous to Middle Albian (Masson et al., 1985). Then, the post-rift stage started in the Middle Albian over the whole margin, with intraplate deformation occurring in the Eocene (Sibuet et al., 1985). The continental breakup unconformity for the Goban Spur is dated between the Late Barremian or Early Aptian and the Early Albian based on well 62/7-1 and the four DSDP drilling sites (Colin et al., 1992). To the south, there was an important faulting stage along the Western Approaches-Armorican margin during the Early Albian, associated with the initial crustal breakup in the Bay of Biscay (Sibuet et al., 1985).

The Goban Spur margin is structurally complex and has been modified by distinct fault systems (Dingle and Scrutton, 1979), with prospective hydrocarbon potential in rotated fault blocks (Cook, 1987). In the study area, the ENE-WSW trending Jean Charcot Escarpment has been referred to as a “south boundary fault” and another two NW-SE oriented escarpments (Fig. 5.1) are called “outer boundary faults” in Dingle and Scrutton (1979). The two NW-SE-oriented escarpments reveal a discretely abrupt change in bathymetric morphology of the Goban Spur, different from the more gradual change in morphology of both the western Porcupine Bank to the north and the Flemish Cap on the Newfoundland side. The structural map (Fig. 5.1) reveals two major fault systems with NW-SE and NE-SW trends, which mainly control the different structural provinces on this margin (Dingle and Scrutton, 1979). The pronounced NE-SW trending Porcupine Fault separates the Goban Spur from the south Porcupine provinces (Naylor and Shannon, 2005). In addition, transfer faults that offset marginal features are also identified according to the Petroleum Affairs Division (PAD) (Fig. 5.1). The transfer fault north of site 549 may be related to the oceanward limit of the NW-SE trending escarpment. The oceanward portions of transfer faults between L3 and L4 may be caused by the reactivation of the Pastouret Ridge during the Eocene, which is assumed to represent an oceanic fracture zone (Sibuet et al., 1985). Further south, the transfer faults may be related to the onset of spreading between Iberia and Europe (Sibuet et al., 1985). Finally, some reverse faults are also observed at the southern Porcupine Basin and the Pastouret Ridge (Fig. 5.1).

5.4 Seismic interpretation

The presented seismic lines (X3-X6) have the same acquisition parameters as the profiles in Yang et al. (2020) (indicated by red lines in Fig. 5.1). The interpretation criteria of the crustal domains along these four lines are the same as those used in the Porcupine Atlantic region, introduced in Yang et al. (2020) and Yang and Welford (2021). Concisely, the boundary between the proximal and necking domains on the Goban Spur is determined based on the crustal thickness variations from gravity inversion. In this study, it is updated to be further landward based on the WAM line (indicated by the red dashed line in the supplemental Fig. 5.S1). Seismic profiles X4-X6 are located inboard of the updated boundary. Accordingly, the landward portions along these seismic profiles are directly interpreted as the necking zone and the portions further toward the Porcupine Basin are primarily interpreted as the hyperextended domain (Fig. 5.2).

5.4.1 Tectono-stratigraphy overlying the continental crust of the Goban Spur

Since well 62/7-1 intersects seismic profile X6 (Fig. 5.1), the major tectono-stratigraphy along seismic profile X6 is determined based on the seismic well tie at well 62/7-1 (Copestake et al., 2017). The key sequences are then correlated from profile X6 to the other profiles (X3-X5). Previous seismic data interpretations of the southern Porcupine Basin and Goban Spur region (Sibuet et al., 1985; Naylor and Shannon, 2005; Yang et al., 2020; Whiting et al., 2016; 2021; O'Sullivan et al., 2021) are also incorporated to identify major sedimentary layers and their boundaries, including the base Cretaceous unconformity, the base Cenozoic, and the top pre-rift basement (Fig. 5.2). In addition, syn-rift and post-rift sedimentary layers are also interpreted, just as was done across the Porcupine Atlantic region in Yang and Welford (2021). It should be noted that although the Early Jurassic rocks are the oldest rocks that well 62/7-1 encountered (Colin et al., 1992), it does not mean that there are no Triassic (and earlier) rocks in the Goban Spur basins since the development of margin basins in the southwestern part of offshore Ireland is believed to have initiated in the Triassic and/or earlier on the regional scale (Naylor and Shannon, 2005). Triassic and older sequences are interpreted on seismic profiles of Goban Graben bounded by the Goban Fault (Fig. 5.1) (Naylor and Shannon, 2005; Štolfová and Shannon, 2009; O'Sullivan et al., 2021). Consequently, syn-rift sediments in some areas of the Goban Spur basins may contain Triassic and/or earlier rocks. The significant difference between the newly presented data and the vintage seismic data is that more clear reflectors below the top basement are imaged on the former (indicated by the line drawings beneath the top basement in Fig. 5.2).

As with previous interpretations of the stretched continental crust of the Goban Spur area (Sibuet et al., 1985; Masson et al., 1985; Peddy et al., 1989), a series of horsts, grabens (or half-grabens), and tilted fault blocks with thin Cretaceous and Cenozoic cover along the newly presented seismic reflection data profiles (X3-X6) are also observed (Fig. 5.2). A series of disconnected sub-basins are separated by local basement highs formed due to uplift, especially along profiles X3, X4, and X6 (Figs. 5.2, 5.3, and 5.4). The thickness of syn-rift Jurassic-Early Cretaceous successions, overlying the continental crust in the necking zone of the Goban Spur, is highly variable (Fig. 5.2).

Some fault-bounded basins may contain up to ~5 km of syn-rift Mesozoic sediments (see the southeast end of profiles X3 and X4 in Figs. 5.3 and 5.4, respectively). Over local basement highs, syn-rift sedimentary layers are relatively thin (Figs. 5.2 and 5.4). The thick and inclined syn-rift sequences with varying dips in the basin along the southeast end of profile X4 show that deposition occurred during the rotation of fault blocks (indicated by the arrow in Fig. 5.4). Hyperextension in the southern Porcupine Basin (north of the Goban Spur) accommodated thick Jurassic-Early Cretaceous sediments (Fig. 5.2), due to fault-controlled half-graben sedimentation being followed by the deposition of a thick Cretaceous succession during a protracted phase of thermal subsidence (Naylor and Shannon, 2005; Whiting et al., 2016). The Base Cretaceous Unconformity (BCU), extensively developed in the Goban Spur-Porcupine region (Naylor and Shannon, 2005), is pronounced and easily identified on the four seismic sections as well, with reflection truncations from beneath and onlaps from above. Enlargements along profiles X3 and X4 clearly show that fault-bounded Jurassic depocentres are truncated by the overlying BCU (Figs. 5.3 and 5.4). Although basaltic lava was drilled at well 62/7-1, there is little to no syn-rift magmatic addition identified along the four seismic profiles.

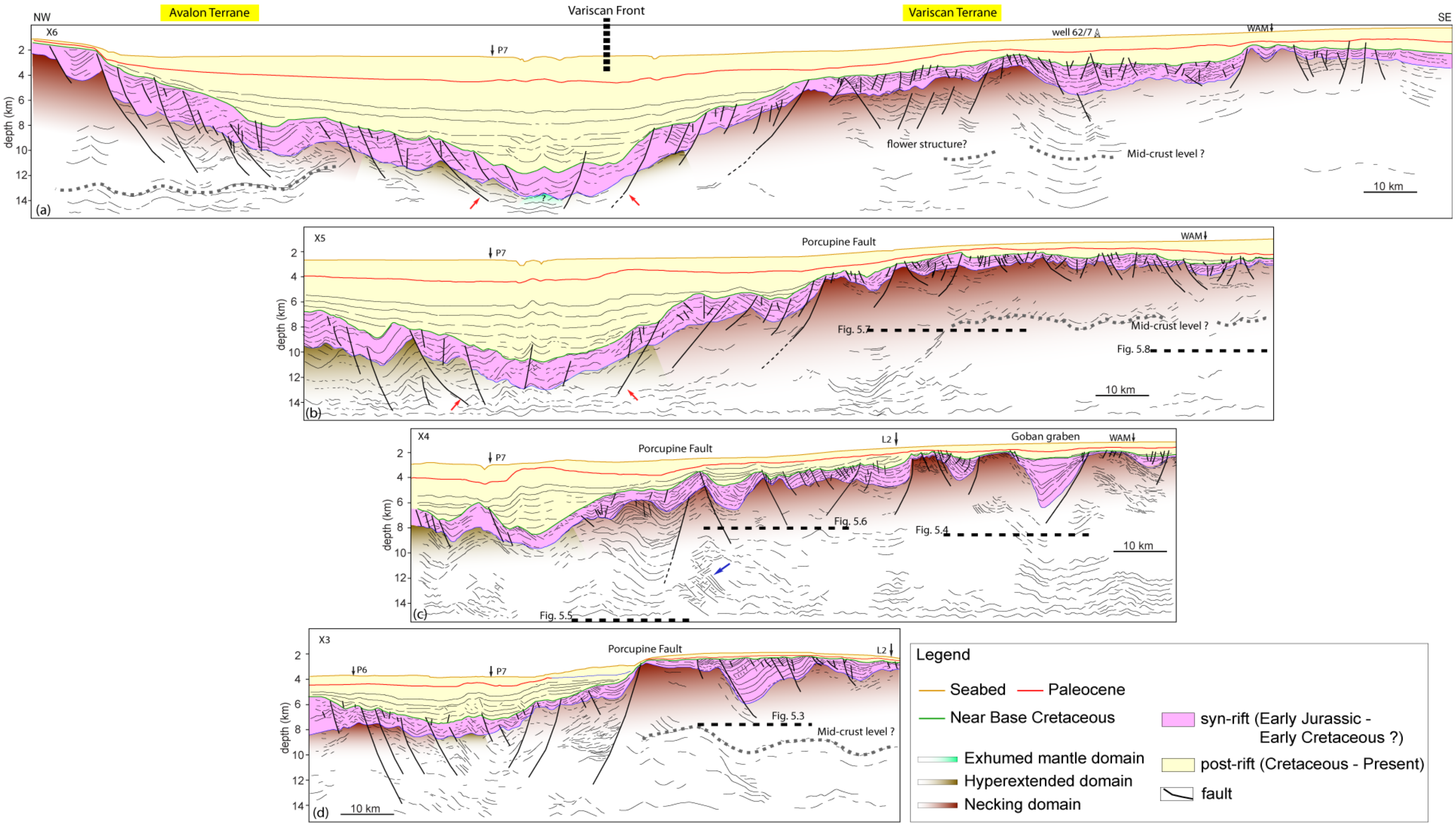

Figure 5.2: Interpreted seismic sections (X3-X6) in the depth domain, oriented NW-SE through the northern Goban Spur. Line P7 interpreted in Yang and Welford (2021) crosses profiles X3-X6, and the WAM line intersects with lines X4-X6. The thick dashed grey curved line may indicate the middle crust (?). The Variscan Front is projected to line X6, separating the Variscan and Avalon basement terranes (Tyrrell et al., 2010). The uninterpreted seismic lines are shown in Appendix C.

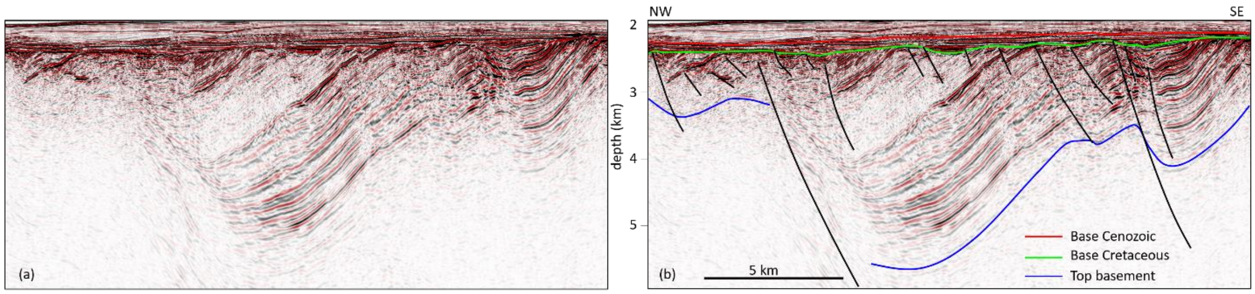

Figure 5.3: Enlargement of a portion of profile X3 shown in Figure 5.2. (a) uninterpreted seismic profile; (b) interpreted seismic profile.

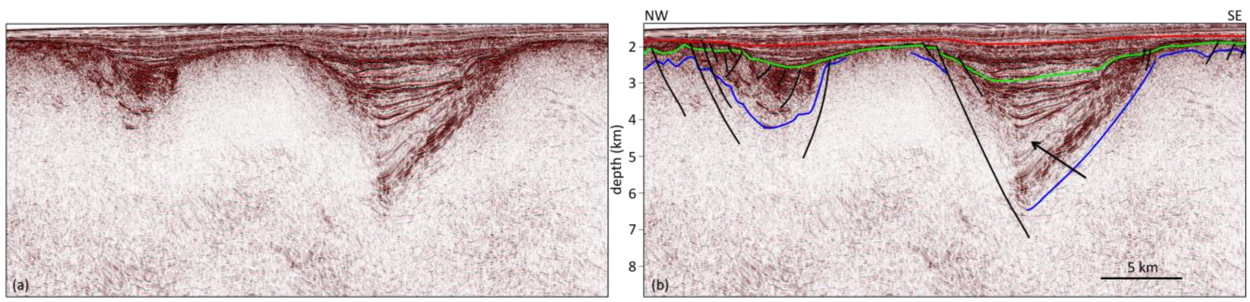

Figure 5.4: Enlargement of a portion of profile X4 shown in Figure 5.2. (a) uninterpreted seismic profile. (b) interpreted seismic profile. The red, green, and blue lines, respectively, indicate the base Cenozoic, base Cretaceous, and top basement.

5.4.2 Structural features of the continental crust of the Goban Spur

In this study, the pre-rift to syn-rift faults along profiles X3-X6 are the main focus of the interpretation (Figs. 5.2-5.8), despite the presence of post-rift faults. Rifting throughout the Jurassic to Early Cretaceous created rotated fault block trapping structures in the southwestern Porcupine Basin (Tomsett et al., 2017). Likewise, basinward rotated fault structures are also observed along profiles X5 and X6 at the southern end of the Porcupine Basin (Fig. 5.2). Along profile X6, the hyperextension and/or exhumed mantle domain is interpreted to be spatially correlated with the Variscan deformation front (Fig. 5.2a). In addition, pre-rift fault blocks are observed along profile X6 with different dips from syn-rift faults. Further toward the center of the Porcupine Basin, some weak and wavy reflectors beneath the top basement are still observed, which are bounded by faults with opposite dips (indicated by red rows in Figs. 5.2a and 5.2b), especially along profiles X5 and X6. These wavy reflectors (beneath ~ 14 km) may reflect compressive events associated with Variscan thrusting.

Westward (toward profiles X3 and X4), the reflectors beneath the top basement in the Porcupine Basin become tilted and disordered, possibly suggesting shearing (?) since shearing occurred in a pre-existing Triassic graben in the southern Porcupine Basin (Grow et al., 2019). However, toward the northern Goban Spur, thick reflector packages beneath the basement next to the Porcupine Fault along X3 and X4 close to the NW-SE trending escarpment are evident but distinctly different. The former appears to be chaotic in a pre-Jurassic rotated faulted block (Fig. 5.2d), while the latter indicates compression related to a rejuvenated inherited Variscan structure (Fig. 5.2c and related enlargement in Fig. 5.5). These reflections can be laterally traced for over 15 km distance and are vertically detectable to ~ 15 km depth (Fig. 5.5), possibly continuing to greater depth despite failing to be observed due to the limited sample length of seismic data. Their origin is still enigmatic, yet they may represent the rift-attenuated remnants of original thick reflection packages, emplaced before extension according to the analysis of the WAM line by Peddy et al. (1989). Further to the southeast of profile X4, the cross-cutting reflectors (indicated by the blue arrow in Fig. 5.2c) suggest two pre-Jurassic extensional events with orthogonal stress fields, assuming that the seismic data have been correctly processed.

Southeastward within the continental crust of the Goban Spur region, discontinuous intra-crustal reflectivity patterns (indicated by the thick dashed grey curved lines in Fig. 5.2) may represent a detachment surface or the mid-crustal level. The normal faults sole out on this surface for the northwest portion of profile X6 (Fig. 5.2a). Considering the crustal thickness (~ 14-20 km) in this region from gravity inversion (Welford et al., 2012), we tentatively interpret this surface as the mid-crustal boundary, ranging ~ 10-12 km in the Goban Spur region. Pervasive reflective fabrics in the lower continental crust are observed on these reflection profiles, with varying seismic character from one line to another. Although the origin of these reflections remains unclear, they capture significant crustal processes, possibly corresponding to lithological changes and/or rheological changes. The highly faulted basement, possible middle crust boundary, and wavy reflectors at depth in the continental part of the Goban Spur may imply delamination of the lower crust, assuming thin brittle upper crust and ductile lower crust in this region.

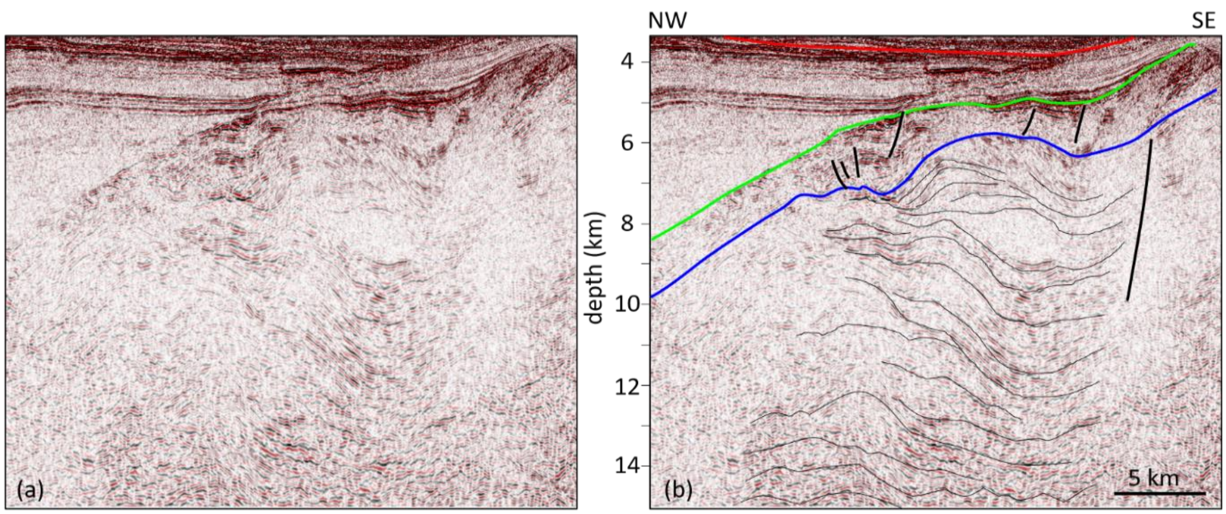

Figure 5.5: Enlargement of the portion of seismic line X4 in Figure 5.2. (a) uninterpreted seismic profile. (b) interpreted seismic profile. The red, green, and blue lines, respectively, indicate the base Cenozoic, base Cretaceous, and top basement.

In the northern Porcupine Basin, inherited Jurassic faults exert major control on the style, distribution, and segmentation of the younger stages of faulting (Saqab et al., 2021). Likewise, the Cretaceous and Cenozoic faults along the Goban Spur continental margin may also be a result of the reactivation of inherited Jurassic and pre-Jurassic faults. In addition to the tectonically-induced extensional faults during distinct stages of rifting recognized in this region, classic compressive structures (inversion structures, reverse faults, and folds) are also observed in the continental crust of the Goban Spur (Figs. 5.6 and 5.7). In Figure 5.6, the syn-rift Jurassic and/or older succession is erosionally trimmed. Compression occurs locally while regional extension dominates during the Jurassic and/or earlier periods, which may be associated with reverse reactivation of the nearby normal fault. O'Sullivan et al. (2021) tentatively interpreted the presence of the Late Triassic salt pillow (indicated by the polygon in transparent green color in Figure 5.6) within the pronounced fold structure based on analogs with seismic reflection data in the Slyne-Erris basins. In Figure 5.7, there is an inversion structure beneath the top basement and reverse faults are observed in the syn-rift successions. A negative flower structure, indicative of transtension between two basement structural fabrics, is interpreted in the local enlarged section along profile X5 (Fig. 5.7). Flower structures are also observed along profile X4 (Fig. 5.6), profile X6 (Fig. 5.2), and the southeastern end of profile X5 (Fig. 5.8). Along profile X6, the flower structure is below the top basement, suggesting that transtension occurred before the onset of rifting. The negative flower structures along profiles X4 and X5 are not symmetrical and extend upward into the Cretaceous succession, indicating that transtension continued during the Mesozoic rifting of the Goban Spur. These flower structures are the result of intraplate oblique motion between basement terranes with different fabrics. This oblique motion likely led to the reactivation of inherited pre-Jurassic faults and the formation of younger faults.

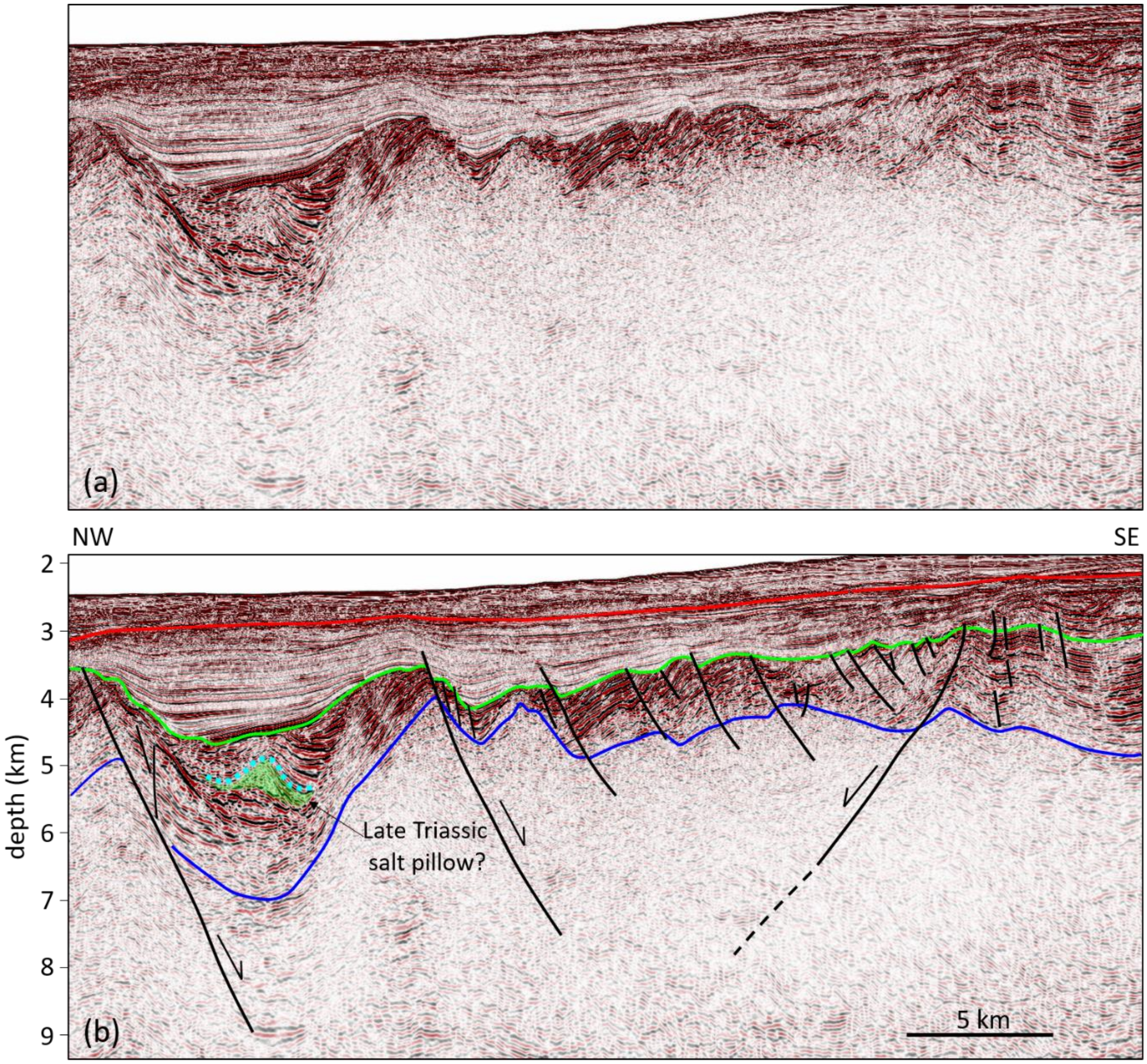

Figure 5.6: Flower structure shown in the local enlargement along seismic profile X4 indicated in Figure 5.2. (a) uninterpreted seismic profile. (b) interpreted seismic profile. The dashed turquoise line indicates evidence of local compression during the Jurassic. The red, green, and blue lines, respectively, indicate the base Cenozoic, base Cretaceous, and top basement.

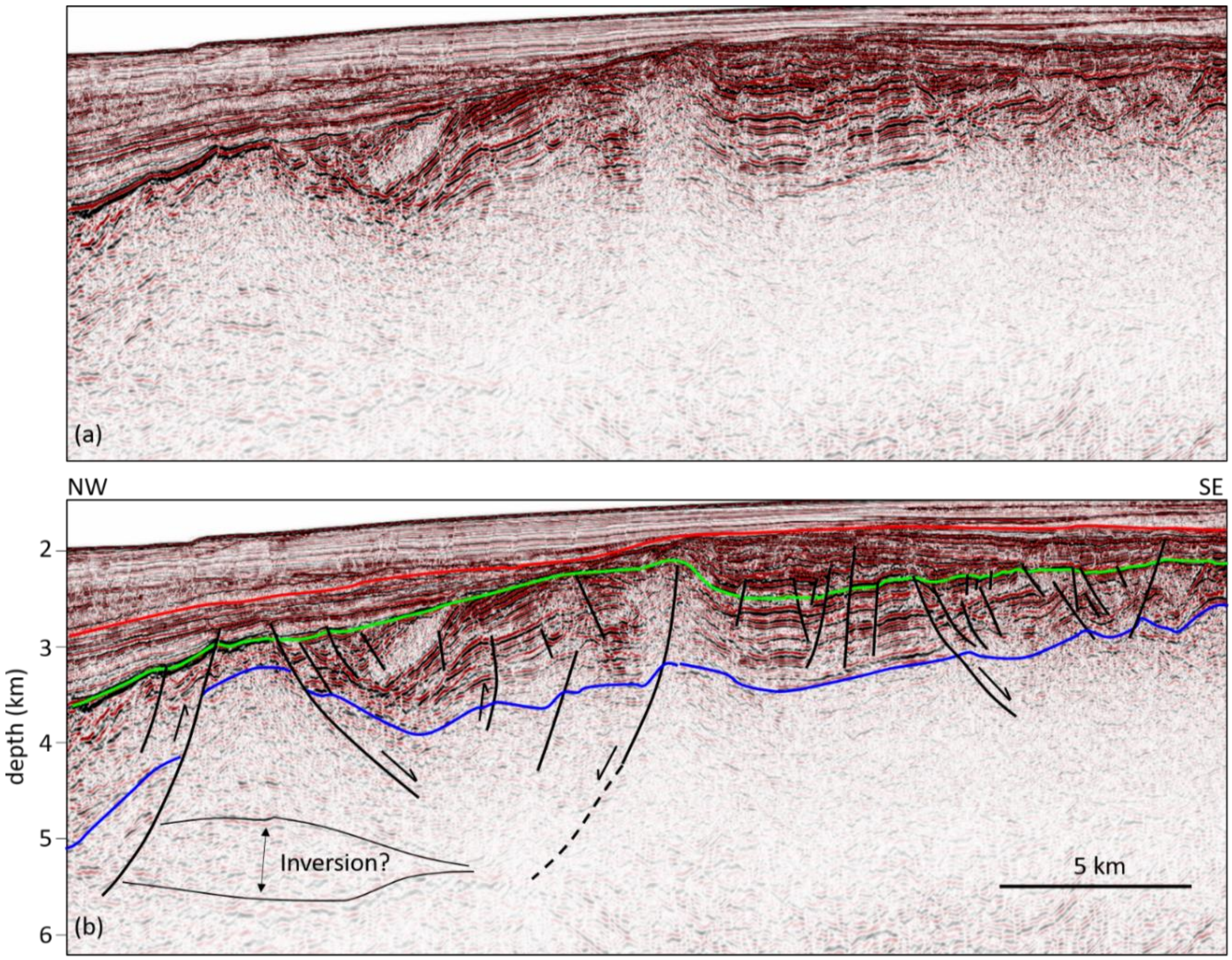

Figure 5.7: Local enlargement along seismic profile X5 indicated in Figure 5.2. (a) uninterpreted seismic profile. (b) interpreted seismic profile. Reverse faults are locally observed in this region. The red, green, and blue lines, respectively, indicate the base Cenozoic, base Cretaceous, and top basement.

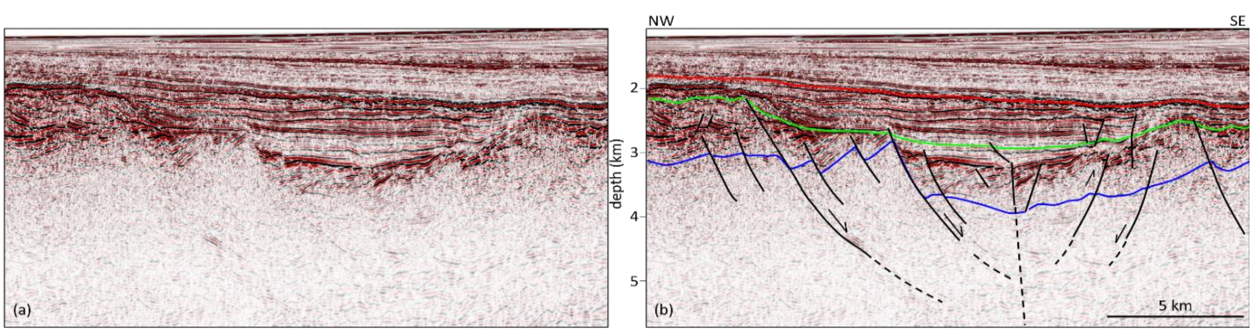

Figure 5.8: Enlargement of the southeastern part of profile X5 indicated in Figure 5.2. (a) uninterpreted seismic profile. (b) interpreted seismic profile, in which the flower structure is evident. The red, green, and blue lines, respectively, indicate the base Cenozoic, base Cretaceous, and top basement.

On the whole, these four seismic profiles across the northern Goban Spur margin-southern Porcupine Basin illustrate the complexity and variability in structural and sedimentary architecture that developed during the Mesozoic. Basinward faulting or detachment controlled the evolution of the northern margin of the Goban Spur, especially along profiles X5 and X6 (Fig. 5.2a and 5.2b). Further to the west, pre-rift compressive events played an important role in the formation of the northern part of this margin (shown in Fig. 5.2c along profile X4). Further to the west along profile X3 (Fig. 5.2d), the formation of this region appears to have involved shearing (?), inherited from Variscan deformation and the opening of the Porcupine Basin. This interpreted E-W lateral variability in deformation style along the northern Goban Spur margin can be also supported using gravity inversion results as the region across profiles X5 and X6 in the Porcupine Basin has a higher stretching factor than that at the mouth of the Porcupine Basin (Welford et al., 2012). The Variscan deformation front is farther away from the northern Goban Spur margin in the region between profiles X5 and X6. We propose that the compressive structures observed along profile X5 may be a result of the reverse reactivation of pre-existing faults. In contrast, the compressive events that occur along X4 may be associated with the continuous reactivation of Variscan deformation.

5.5 The locally updated deformable plate model

As mentioned in the introduction, this study also seeks to solve the inconsistency in crustal thickness over the continental part of the Goban Spur margin between gravity inversion and deformable plate modelling. The deformable plate modelling methodology in GPlates has been described in the literature (Gurnis et al., 2018; Peace et al., 2019; King et al., 2020; Yang et al., 2021). Concisely, in GPlates, vector geometries of tectonic elements represented by points, polylines, and polygons are assigned by a specific plate ID. Trees of rotation poles indicating the relative motion of tectonic elements with respect to a fixed rotation pole over time are established (Gurnis et al., 2012). The vector geometries of tectonic elements consisting of the boundary of the deformable zone connect and form a closed polygon for the topology, in which the continuous deformation of the deformation region over time is represented by triangular meshes (Gurnis et al., 2018). The locally updated deformable plate model allows us to visualize the crustal thickness evolution through time and further quantify the orientation and timing of extension events between the Flemish Cap, Iberia, and Goban Spur margins.

5.5.1 Model setups and rotation poles

Generally, a previously published plate model is the starting point for developing regional/local models with greater detail. In this study, we mainly update the proposed model 5d in Yang et al. (2021), in which the deformable zone is defined by the necking line and the edge of continental crust, just as in the Nirregarten et al. (2018) and Peace et al. (2019) models. In the updated model, the initial rifting time is set at 200 Ma and the initial crustal thickness is set at 28 km. There are two main aspects updated from the previous model 5d in Yang et al. (2021). One is that the necking line along the Goban Spur margin is pushed landward (indicated by the green dashed line in Fig. 5.9), mainly based on the reinterpretation of the WAM seismic line (shown in the supplemental Fig. 5.S1). The other aspect is that two sets of transfer faults in the Goban Spur area (F1 and F2 shown in Fig. 5.9), which are inferred to represent major crustal discontinuities and to accommodate lateral displacements of different amounts within the thinned continental crust of the Goban Spur region, are incorporated into the preferred model (model 5d) from Yang et al. (2021). The key components tested in this section are summarized in Table 5.1.

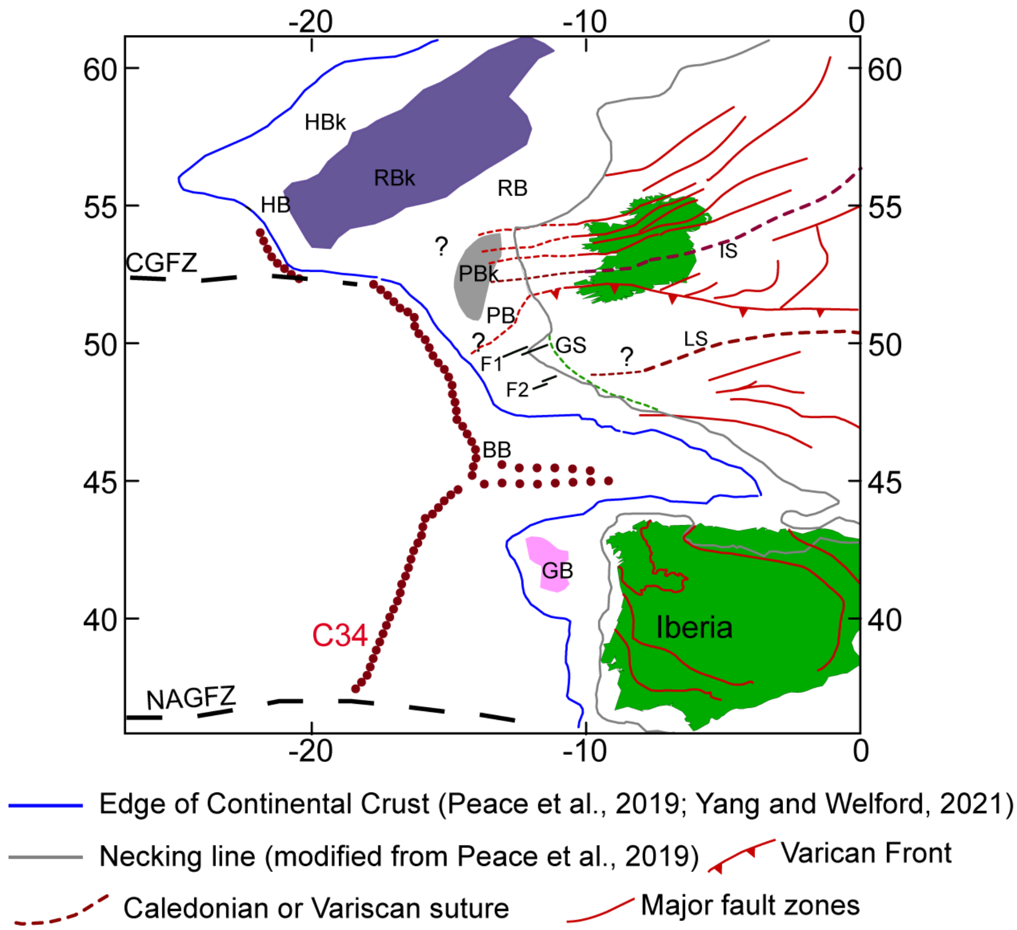

Figure 5.9: Deformable region in the Goban Spur-Porcupine Atlantic region bounded by the necking line and the edge of continental crust in GPlates. Within the deformable region, the micro-continental blocks (PBk, RBk, and GB) are from Peace et al. (2019) and King et al. (2020). The fault zones and crustal sutures are compiled from the literature (Bois et al., 1990; Grow et al., 2019; Schiffer et al., 2020). F1 and F2 on the Goban Spur margin indicate the new faults incorporated into the deformable plate model (model 5d) proposed in Yang et al. (2021). The big and solid dark red dots represent the magnetic Chron 34 (Müller et al., 2016). Abbreviations: BB, Bay of Biscay; GB, Galicia Bank; GS, Goban Spur; PB, Porcupine Basin; PBk, Porcupine Bank; HB, Hatton Basin; HBk, Hatton Bank; RBk, Rockall Bank; RB, Rockall Basin; IS, Iapetus suture; LS, Lizard suture; CGFZ, Charlie-Gibbs Fracture zone; NAGFZ, Newfoundland Azores Gibraltar Fracture Zone.

Table 5.1: Parameters tested in the four models adapted from model 5d in Yang et al. (2021).

# Model	1 (model 5d)	2	3	4
Updated NL	×	√	√	√
F1 incorporated	×	×	√	√
F2 incorporated	×	×	×	√

Note: NL indicates the necking line. F indicates transfer fault.

The key steps are to define the locations and rotation poles of both faults. In this study, the transfer faults are introduced in GPlates to represent oblique-slip movement between different crustal components. The flower structures observed along profiles X4-X6 suggest oblique-slip between basement terranes, and these are used to help to define the approximate locations of the NE-SW transfer fault (Fault 1) in the northern Goban Spur (F1 in Fig. 5.9). Tectono-stratigraphy interpreted along profiles X3 to X6 helps to identify the timings of tectonic events, further constraining the rotation poles of introduced faults in the model. To the south of the Goban Spur, the morphology is very complicated due to the presence of several canyons (Fig. 5.1) and poor seismic data constraints. Nonetheless, the second fault (F2) is introduced to the updated deformable plate model to generate more reasonable crustal thicknesses. Both faults are incorporated into model 4 since the deformable model with only one introduced fault (model 3) produces a poorer match compared to crustal thicknesses from gravity inversion. Fault F2 is possibly related to the offshore continuation of the Lizard Suture (Bois et al., 1990). The simple distribution of faults considered in the deformable models is intended to demonstrate that the present-day crustal structure of the Goban Spur can be achieved with minimal large-scale complexity. The results do not mean that there are no more sets of faults developed in the continental part of the Goban Spur and that more faults could not be introduced into the original plate model (model 5d in Yang et al. (2021)). We simply follow the principle that the simpler, the better, provided that the crustal thicknesses from the tested models can be consistent with those from gravity inversion (Welford et al., 2012). It is noted that there are some transfer faults interpreted in the oceanic portion of the Goban Spur margin (Fig. 5.1), which are related to the oceanic fracture zones and the onset of seafloor spreading between Iberia and Europe (Sibuet et al., 1985). Thus, these interpreted transfer faults from the Petroleum Affairs Division (PAD) are not incorporated into the deformable plate models since the models are meant to mainly consider the crustal thinning during rifting. In GPlates, a transfer fault is represented by two dynamic polylines that move relative to each other over time. In this study, two transfer faults are introduced (F1 and F2) as mentioned before. The polylines moving toward the ocean are referred to as F11 and F21, while the polylines with the landward motion are referred to as F12 and F22. The rotation poles of these polylines are listed in Table 5.2

Table 5.2: Rotation poles of two sets of faults. (EUR=European plate)

	Time	Latitude	Longitude	Angle	Fix plate
F21	0	4.2877	-106.5366	0.4915	EUR
	90	0.4215	-102.447	0.4487	EUR
	100	-4.4362	73.3059	-0.5035	EUR
	120	47.918	-44.8265	1.4745	EUR
	140	-10.4944	65.099	-0.6261	EUR
	150	-13.3944	61.6596	-0.6763	EUR
	180	-15.4882	59.1036	-0.7335	EUR
	200	-15.4882	59.1036	-0.7335	EUR
F22	0	90	0	0	EUR
	90	-28.6969	41.0914	-0.0147	EUR
	120	48.6714	-9.867	-0.4283	EUR
	140	40.597	70.1952	-0.0126	EUR
	150	66.3318	62.1889	-0.0098	EUR
	180	73.1849	83.0514	-0.0118	EUR
	200	77.8923	76.9337	-0.0121	EUR
F11	0	74.3189	82.0005	19.7053	EUR
	90	71.8414	92.9655	18.3958	EUR

	120	71.9045	93.3376	18.4309	EUR
	140	68.5561	102.4527	17.2936	EUR
	150	74.8177	81.0129	20.0729	EUR
	180	72.4583	93.1654	18.7904	EUR
	200	73.6656	88.6675	19.3794	EUR
F12	0	51.284	-13.314	10.8672	EUR
	90	52.3169	-13.899	6.8412	EUR
	120	51.541	-13.5254	8.1447	EUR
	140	50.5151	-12.8328	8.5665	EUR
	150	50.4134	-13.2106	11.3064	EUR
	180	50.4692	-13.2277	9.712	EUR
	200	50.5259	-13.291	10.5034	EUR

5.5.2 Present-day crustal thickness for the Goban Spur

By only updating the necking line from model 5d in Yang et al. (2021) (the original necking line in grey and the updated necking line in dashed green in Fig. 5.9), the present-day crustal thickness over the Goban Spur from the updated model (Fig. 5.10c) is not as thin as that from model 5d in Yang et al. (2021) (Fig. 5.10b). Yet, it is still not in agreement with that from gravity inversion (Fig. 5.10a). When one fault (F1) is incorporated into the deformable model with the updated necking line (Fig. 5.10d), the crustal thickness does not match with that from gravity inversion either, despite some improvements in crustal thickness on the western edge of the necking line over the Goban Spur. The crustal thickness from the deformable plate model with two faults (F1 and F2) and the updated necking line over the Spur (Fig. 5.10e), is most consistent with that from gravity inversion (Fig. 5.10a). From Figure 5.10(e), the crust is still very thin towards the edge of the continental crust on the Goban Spur margin, but the gradient in crustal thickness is smoother from east to west. Thus, model 4 is the preferred deformable model in this study.

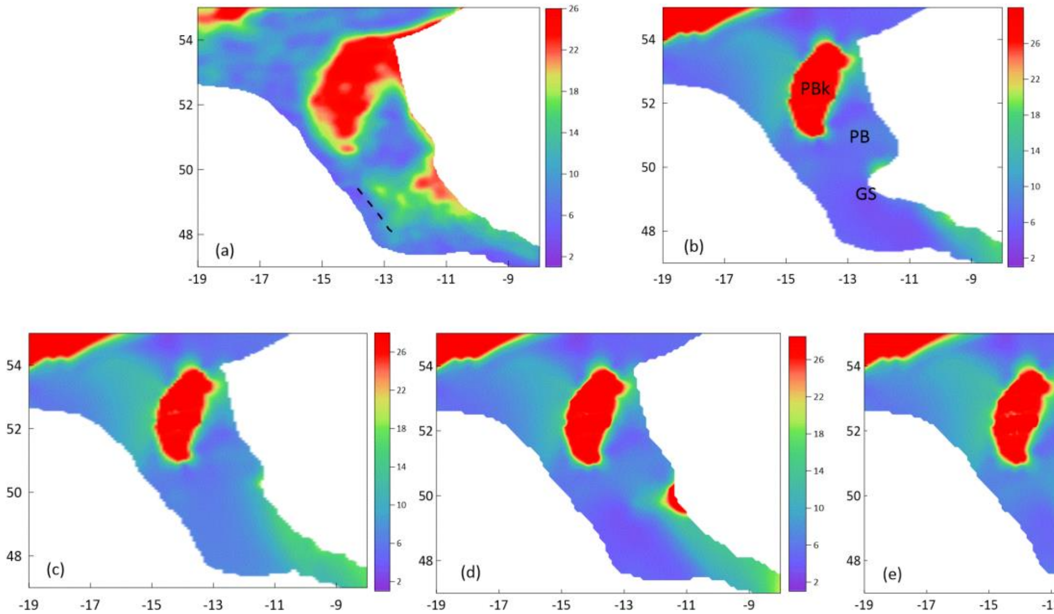

Figure 5.10: Comparison of the present-day crustal thicknesses over the Goban Spur-Porcupine region. (a) from gravity inversion (Welford et al., 2012); (b) from the deformable plate model 5d in Yang et al. (2021); (c) from the deformable plate model with updated necking line over the Goban Spur margin (indicated by the dashed green line in Figure 5.9); (d) from the deformable plate model with the updated necking line and one transfer fault on the Goban Spur, in which the fault (F1) is mainly defined by the seismic data interpretation in section 5.4; (e) from the deformable plate model with the updated necking line, as well as the incorporation of two transfer faults (F1 and F2) over the Goban Spur area shown in Figure 5.9. Abbreviations: GS, Goban Spur; PB, Porcupine Basin; PBk, Porcupine Bank

Although the present-day crustal thicknesses from model 4 are much improved in the eastern part of the Goban Spur, the crustal thicknesses towards the NW-SE-trending escarpment (see the black dashed line in Fig. 5.10a) remain very thin (Fig. 5.10e). The results from model 4 in this study generate a relatively sharp crustal thickness gradient (Fig. 5.10e), indicating a narrow necking zone for the Goban Spur, while crustal thicknesses from gravity inversion display a more gradual decrease oceanward (Fig. 5.10a), resulting in a wide areal extent of the necking zone. The necking zone usually spans a relatively narrow distance compared with the hyperextended domain along magma-poor rifted margins (Doré and Lundin, 2015), but the necking zone of the Goban Spur is still interpreted to be relatively wide (seen in the interpretation of the seismic lines in Yang et al. (2020) and the WAM line in Figure 5.S1 in the supplemental section).

5.5.3 Crustal thickness evolution for the Goban Spur

Here, the crustal thickness variations for the Goban Spur over geologic time from model 5d in Yang et al. (2021) and the locally updated model in this study are compared (see the first two columns in Figs. 5.11 and 5.12). Meanwhile, an interpreted crustal domain map is also projected through geologic time to improve our understanding of the architectural evolution of the region (see the third column Figs. 5.11 and 5.12). Inherited structures are reconstructed back through geologic time by assigning them corresponding plate IDs. Motion velocities (velocity magnitude and angular velocity) of the Goban Spur relative to the Iberian margin and the Flemish Cap, respectively during the Jurassic to Cretaceous are also calculated (Fig. 5.13) These allow the time-variant extensional obliquity between margins to be quantitatively restored.

In the Early Jurassic (200-170 Ma), there is limited change in crustal thickness over the Goban Spur in the original model (indicated by the first column in Fig. 5.11), whereas crustal thinning is segmented due to the presence of the two faults during the same period in the model proposed in this study (indicated by the middle column in Fig. 5.11). Later, crust rapidly thins over the Goban Spur during the Late Jurassic to the earliest Cretaceous (160-140 Ma) in the original model (see the first column in Figs. 5.11 and 5.12). In comparison, the crustal thickness over the Goban Spur in the updated model gradually continues to be segmented by a thin crustal region between the two introduced transfer faults during this time in the updated model (see the middle column in Figs. 5.11 and 5.12). Next, the Goban Spur crust continues to thin in the Early Cretaceous in the updated model, in response to the interplay of continued hyperextension between the NE Newfoundland margin and the Porcupine Atlantic margin (see the third column in Fig. 5.12) and transtension between the Iberian margin and the Goban Spur (see the angular velocity variation between 140 Ma and 110 Ma in Fig. 5.13a)

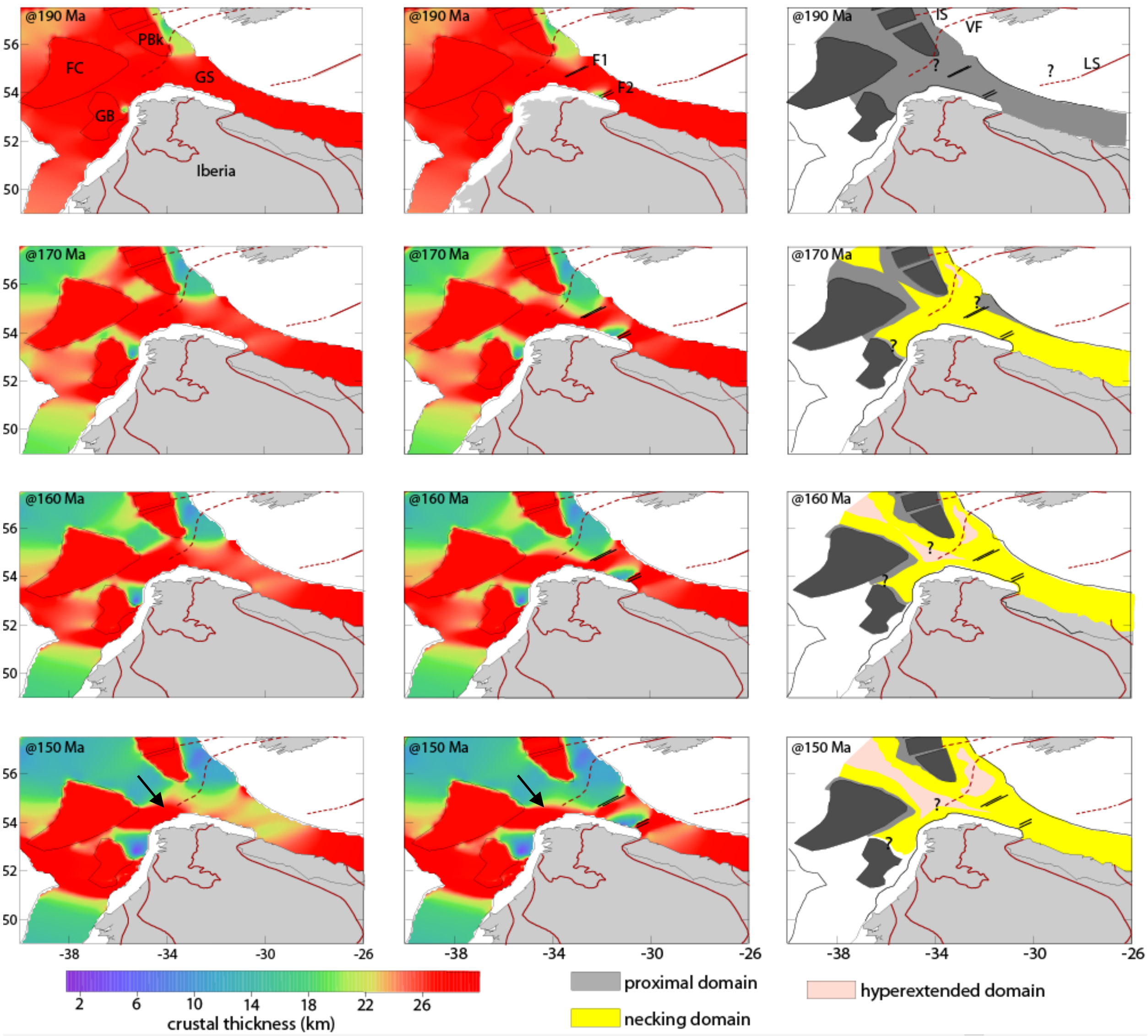

Figure 5.11: Evolution of crustal thickness (left two columns) and rift domain map (right column) during the Jurassic (190 to 150 Ma), overlain by the major pre-existing fault zones (indicated by the red lines). The first column indicates the results from model 5d in Yang et al. (2021). The middle column shows the results from the locally updated model in this study. F1 and F2 indicate the new introduced faults in the Goban Spur. The interpreted rift domain map is mainly based on seismic reflection data interpretation in Yang et al. (2020) and Yang and Welford (2021). Abbreviations: FC, Flemish Cap; GB, Galicia Bank; GS, Goban Spur; PBk, Porcupine Bank; VF, Variscan Front; IS, Iapetus suture; LS, Lizard suture.

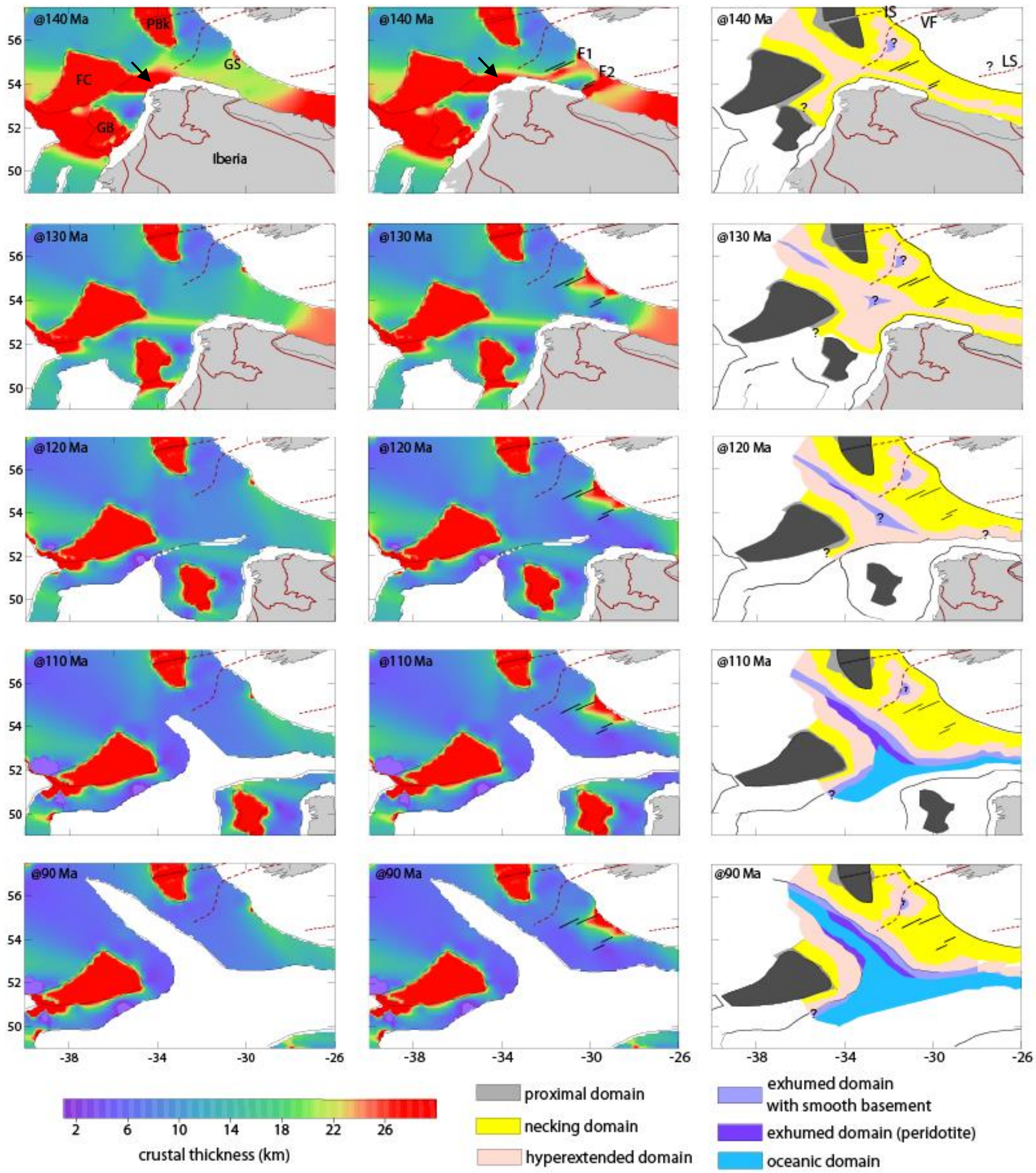

Figure 5.12: Evolution of crustal thickness (left two columns) and rift domain map (right column) during the Cretaceous (140 to 90 Ma), overlain by the major pre-existing fault zones (indicated by the red lines). The first column indicates the results from model 5d in Yang et al. (2021). The middle column shows the results from the locally updated model in this study. F1 and F2 indicate the new introduced faults in the Goban Spur. The interpreted rift domain map is mainly based on seismic reflection data interpretation in Yang et al. (2020) and Yang and Welford (2021). Abbreviations: FC, Flemish Cap; GB, Galicia Bank; GS, Goban Spur; PBk, Porcupine Bank; VF, Variscan Front; IS, Iapetus suture; LS, Lizard suture.

In the original model (see the first column in Fig. 5.12), crustal thickness of the Goban Spur also decreases from 140 Ma to 110 Ma due to the transtension between the Goban Spur and the Iberian margin (see the first column in Fig. 5. 12 and the red line in Fig. 5.13a), however, the model fails to generate thicknesses that are consistent with the results from gravity inversion (Fig. 5.10a). The comparison of crustal thicknesses from model 5d (Yang et al., 2021) and the locally updated model in this study clearly show that the two transfer faults (F1 and F2) play a dominant role in shaping the crustal thickness variations for the Goban Spur during the Jurassic to the earliest Cretaceous (200 -140 Ma).

From Figures 5.11 and 5.12, there is an evolving thick crustal belt between the Flemish Cap and the Iberian margin in the context of the North Atlantic opening during the Jurassic to the earliest Cretaceous (200-140 Ma) (indicated by the black arrows). Its formation is possibly related to the interaction between the faster southeastward rotation of the Flemish Cap and slower southeastward motion of the Iberian margin during the Jurassic (Fig. 5.13). This thick crustal belt disappears (observe the relative displacement between the Flemish Cap and the Iberian margin at 140 Ma and 130 Ma) in the Early Cretaceous, due to the relatively faster motion of the Iberian margin with respect to the Goban Spur during this period (Fig. 5.13a). The transtension (140 -130 Ma) between the Goban Spur and the Iberian margin has a governing effect on the crustal thickness change during the Early Cretaceous.

In the rift domain maps (see the third column in Figs. 5.11 and 5.12), the necking phase for the Goban Spur spans the Mid-to-Late Jurassic until the Early Cretaceous, forming a relatively wider necking zone. The crustal hyperextension on this Spur probably began in the Late Jurassic, and the serpentinized mantle exhumation is proposed to start in the Early Cretaceous outboard of the Goban Spur. In contrast, from the crustal thickness map (especially at

90 Ma in Fig. 5.12), the area of the necking zone for the Goban Spur margin appears to be smaller than that shown on the corresponding rift domain map. However, according to constraints from seismic reflection data (WAM line in Fig. 5.S1) and crustal thickness from gravity inversion (Welford et al., 2012), the areal extent of the necking zone should be relatively wide (Yang et al., 2020). This inconsistency may result from the faster motion of the Iberian margin during the Early Cretaceous, which directly leads to abrupt crustal thinning during this period in the locally updated deformable plate model (observe crustal thickness at 140 Ma and 130 Ma in Fig. 5.12).

It seems paradoxical to map the necking zone (see the third column in Figs. 5.11 and 5.12) between the Flemish Cap, the Iberian margin, and the Goban Spur margin during Mid-Jurassic to earliest Cretaceous (170-140 Ma) due to the presence of the thick crustal belt between the Flemish Cap and the Iberian margin and the thick crust along the fault (F1) in the Goban Spur region (see the middle column in Figs. 5.11 and 5.12). It should be noted that the crustal thickness from the locally updated deformable model is not the only criteria used to delimit the crustal domains over time. We map the distribution of the necking zone back through time here, primarily according to the general conceptual development of magma-poor rifted margins from continental stretching, necking, hyperextension, and/or mantle exhumation, and oceanization over time (Péron-Pinvidic et al., 2013). Local transpression may also occur due to compressional reactivation in the regions of overall extension (Tugend et al., 2014), which may explain the thickening crust in the deformable model. Although it is difficult to constrain the transfer fault (F2) in the southern Goban Spur region due to lacking seismic data constraints as compared with fault F1, the introduction of two transfer faults in the locally updated deformable model (model 4 in this study) plays an important role in generating realistic crustal thickness variations over time.

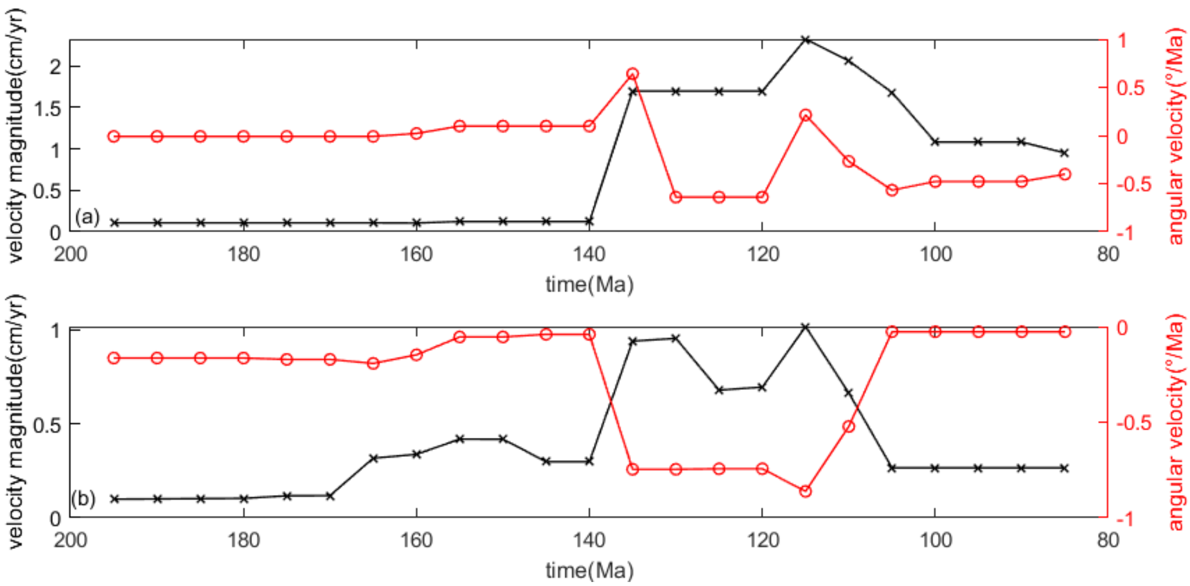

Figure 5.13: Motion velocity in the updated deformable plate model with Greenland fixed during the Jurassic to Cretaceous. (a) the Iberian margin with respect to the Goban Spur; (b) the Flemish Cap relative to the Goban Spur.

5.6 Discussion

5.6.1 Strong influence of pre-existing inheritance

The Goban Spur margin comprises the collapsed Variscan orogenic belt (Sibuet et al., 1985). From seismic data interpretation of four seismic reflection lines (X3-X6) on the continental crust of the Goban Spur margin (Figs. 5.2-5.8), extensional features (grabens), compressional features (inversion structures, folds, reverse faults), and transtensional features (flower structures) are also observed in the pre-rift and syn-rift sedimentary layers. The complexity of the imaged structures is suggestive of continued reactivation of both the Variscan basement terranes and inherited faults within this margin.

On the Goban Spur, the interpreted transfer fault (F1) is located closer to the offshore continuation of the Variscan Front, and fault F2 is situated closer to the westward continuation of the Lizard Suture (Fig. 5.1). The interpreted transfer faults correspond to basement discontinuities that can accommodate crustal extension and transtension between heterogenous basement terranes. These transverse structures may arise from the reactivation of the offshore continuations of the Variscan Front and Lizard Suture (Figs. 5.11 and 5.12), or inherited weaknesses in the Early Mesozoic basins in the continental crust (Scrutton, 1979). The evolving transfer faults also lead to strain localization along pre-existing structural weaknesses, compartmentalizing crustal thicknesses along the Goban Spur margin based on the locally updated deformable plate model (see the middle column in Figs. 5.11 and 5.12).

The broad necking zone for the Goban Spur interpreted by Yang et al. (2020) may have formed through episodic extensional tectonic processes throughout the necking stage from the Jurassic to Early Cretaceous, governed by reactivation of pre-existing heterogeneous basement terranes and/or inherited faults. Similar to how the hyperthinned domain is reactivated within the north-oriented thrust system along the northern Iberian margin (Tugend et al., 2014), the necking and hyperextended zones along the Goban Spur may have also been affected by a thrust system prior to the crustal breakup. Seismic sections across the necking region also record a protracted and polyphased rift process according to the structurally-rotated and erosionally-trimmed syn-rift depocenters (Fig. 5.2) The presence of mid-crustal reflectors may indicate decoupled deformation in the early necking stage. As the crust thins to the north along these seismic lines, deformation becomes coupled in the later necking and hyperextended stages. The timings of these crustal necking processes are diachronous. Meanwhile, the extension amount and orientation during different necking phases are different as well (Figs. 5.11-5.13), possibly leading to the complex structures in the wide necking zone on the margin.

The Goban Spur basins underwent long-lived influence of Variscan deformation in margin development during the Mesozoic according to the interpretation of the seismic profiles (X3-X6) and the locally updated deformable plate model. In comparison, on the NE Newfoundland side, the basement underlying the Orphan Basin is relatively uniform, despite the presence of a transfer zone along the Cumberland Fault (Enachescu et al., 2010) and multiple failed rifts (Lau et al., 2015; Welford et al., 2020). Further evidence from seismic reflection data needs to better capture the interplay between pre-existing structures and more recent structural features in the Orphan Basin. Along the rifted edge of the Flemish Cap, the basement features (Welford et al., 2010) and crustal architecture vary significantly along strike of the margin (Figs. 5.11 and 5.12). Since the Flemish Cap is considered as a continental microplate with strong crustal strength compared with the neighboring Orphan Basin areas, the along-strike variability in basement features along the eastern side of the Flemish Cap may be primarily associated with oblique rifting between the Cap and the Porcupine Bank (Yang et al., 2021), rather than inherited structures.

5.6.2 Significance of segmentation of the Goban Spur during oblique rifting

In the locally updated deformable plate model, the orientation and magnitude of crustal extension vary over time, resulting in the oblique rifting of the Goban Spur (Figs. 5.11 and 5.12). This obliquity challenges previous rift-perpendicular extension models and the conjugate relationship between the Flemish Cap and the Goban Spur (Keen et al., 1989; Gerlings et al., 2012). The Porcupine Atlantic rift system to the north of the Goban Spur is characterized by its segmentation along a series of Caledonian fault zones (Whiting et al., 2021; Yang et al., 2021).

Similarly, the Western Approaches – Armorican rift system to the south of the Goban Spur is segmented by NE-SW trending transfer faults (Tugend et al., 2014). In this study, the Goban Spur continental margin is also proposed to be offset by two NE-SW trending transfer faults in the locally updated deformable model. Compared with the crustal-scale faults that compartmentalize the Armorican – Irish Atlantic rift systems, the small-scale transfer faults proposed in the locally updated model in this study suggest that local strain partitioning during basin development within the Goban Spur may simply be associated with along-strike variability in rheology.

It should be stressed that there are still uncertainties in the orientations and locations of the two inferred transfer faults, despite the seismic constraints for the northern transfer fault (F1). We postulate the existence of a second transfer fault (F2) in the southern Goban Spur based on the needs of the deformable plate model, however, there is no supporting seismic evidence for the fault. In addition to the two proposed transfer faults, there may be additional cross-cutting features that further cut and offset the margin basement, for example, the NW-SE faults (Dingle and Scrutton, 1979), which may exert an influence on the crustal thickness evolution during the margin basin development. There may also exist more as-yet-undetected structures and tectonic events that compartmentalize the margin further and control crustal thickness variations, similar to the major NW-SE orientated strike-slip fault that bounds the Fastnet Basin to the south (Masson and Miles, 1986), and/or shear zones along the Armorican margin (Thinon et al., 2003).

Inevitably, there exist many uncertainties in the locally updated deformable plate model in addition to those intrinsic drawbacks of GPlates, such as the uniform initial crustal thickness assumption, and failure to consider depth-dependent stretching (Gurnis et al., 2018; Peace et al., 2019). First, the motion of the Iberian plate during the Mesozoic is still under debate (Tugend et al., 2014; Angrand et al., 2020). The rotation pole for the Iberian plate in the model from Nirrengarten et al. (2018), which is used herein, may introduce uncertainties in terms of the evolution of the Goban Spur. Second, the updated deformable model fails to consider the effect on the Goban Spur of compressional deformation along the northern Iberian margin during the Cenozoic (Ruiz et al., 2017). Third, regionally, the development of margin basins, offshore Ireland, is believed to initiate in the Triassic and/or earlier (Naylor and Shannon, 2005; O'Sullivan et al., 2021). However, the updated deformable plate model sets the initial rifting time at 200 Ma and fails to consider an extensional phase of basin initiation prior to the Jurassic. Fourth, in this study, we take the crustal thickness from gravity inversion as the measure of success for the updated deformable model, yet, there still exists some uncertainties in gravity inversion as to how the base of the crust is defined (Welford et al., 2012), possibly leading to some misfits where crust/mantle densities are anomalous.

5.6.3 Implications for basin evolution for the Goban Spur

Despite the uncertainties associated with the updated deformable model and the seismic data interpretation, this study still reveals more details than were previously available from vintage seismic data and provides insights into the basin development on the Goban Spur margin. Previous rigid plate reconstructions suggested that the Goban Spur basins had linkages with the Flemish Pass Basin during the Mesozoic (Masson and Miles, 1986). Since conjugate margins usually share similar tectono-stratigraphic features, the rifting history and petroleum prospectivity of the Flemish Pass Basin have usually been used as analogs to understand the underexplored Goban Spur basins (Keen et al., 1989; Gerlings et al., 2012; Grow et al., 2019). This implies that incorrect conjugate relationships may misguide petroleum exploration in underexplored conjugate basins. The locally updated deformable plate model in this study reveals that the Goban Spur basins likely have a closer connection with the northern Iberian basins (Figs. 5.11 and 5.12), consistent with the previous discussion of a continuous basin formed between the Porcupine and Galicia Interior basins during the Jurassic (Sandoval et al., 2019). This may be the main reason why the crustal architecture of the Flemish Cap margin is significantly different from that of the Goban Spur margin (Yang et al., 2020).

On the whole, the formation of the Goban Spur basins is complicated, as the continental crust comprising the Goban Spur margin experienced episodic extension, local compression, uplift, and segmentation, all following the collapse of the Variscan Orogeny. This tectonic complexity is mainly a result of the migration and intersection of propagating rift zones between the Porcupine Atlantic and NE Newfoundland margin pair, and the Iberia and Irish margins during the Mesozoic. In terms of prospectivity, the pronounced Jurassic and Cretaceous sequences in the discrete fault-bounded basins may be favourable to hydrocarbons for the Goban Spur basins. However, significantly more seismic coverage and drilling will be required, along with a reconsideration of appropriate basin analogs, to de-risk future exploration.

5.7 Summary

(1) Newly presented long-offset 2D seismic profiles across the Goban Spur margin provide a clear structural framework that enables the interpretation of rift-related mega-sequences and the identification of potential prospects.

(2) Sediment thickness in the Goban Spur basins is highly variable and is predominantly controlled by normal faults that mainly developed during Jurassic and Early Cretaceous extension.

(3) The crustal architecture and interpreted sedimentary basin fill represent a protracted and polyphase crustal necking process for the Goban Spur margin.

(4) The influence of transfer faults on the deformable plate modelling of the Goban Spur is tested, showing that they play a significant role in reshaping the evolution of crustal thickness of the continental crust. The modelling results imply that reactivation of Variscan orogenic structures and/or inherited faults occurred during the prolonged rifting stage, forming discrete basement zones along the Goban Spur margin, displaced along NE-SW-directed transfer faults.

(5) In the locally updated deformable plate model (model 4), the orientation and magnitude of crustal extension vary over time, resulting in the oblique rifting of the Goban Spur, relative to its neighbouring margins. This locally updated deformable plate model not only provides a more realistic depiction of the evolution of the Goban Spur, but also complements existing deformable plate models of the southern North Atlantic. Understanding the evolution of the Goban Spur and its basins has important implications for reducing exploration risk in the underexplored margin basins of the southern North Atlantic, particularly when it comes to defining basin connectivity prior to continental breakup.

5.8 Supplemental material

The supplemental WAM line shows the approximate location of the updated boundary between the proximal and necking domains on the Goban Spur (indicated by the dashed pink line in Fig. 5.S1). The updated border is also mentioned and used in section 5.5 for redefining the boundary of the deformable region.

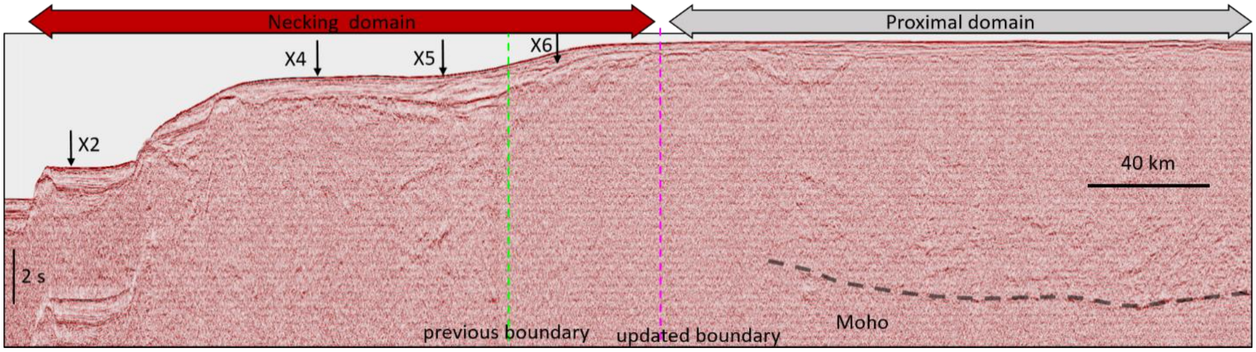

Figure 5.S1: Portion of WAM line in the time domain, which crosses seismic profiles X2, X4, X5, and X6. The previous boundary indicates the interpreted border between the proximal and necking domains based on crustal thickness from gravity inversion in Yang et al. (2020). The updated boundary shows the border between the two domains used in this study, mainly based on seismic data interpretation.

Acknowledgements

We are grateful to the Department of the Environment, Climate and Communications of Ireland for providing the multichannel seismic reflection data. We also acknowledge the Petroleum Infrastructure Programme (PIP) in Ireland for access to the technical studies and regional reports. Schlumberger are acknowledged for donating Petrel software to Memorial University. We would like to thank the members of the Memorial Applied Geophysics for Rift Tectonics (MAGRiT) group for providing suggestions for this research.

Chapter 6

6. Summary, conclusions, and future work

6.1 Summary

According to all of the information in previous chapters, we can see that rifting propagated progressively towards the triple junction between the Newfoundland-Iberia and Newfoundland-Irish rift systems during the Early Jurassic, following the collapse of the Caledonian and Variscan orogenies, forming proximal margin basins along the southern North Atlantic. During the same period, the Porcupine Basin experienced opening, forming the necking zone. Then, with the continued rotation of the Flemish Cap, rifting in the Porcupine Basin gradually shifted to the dominant rifting center between the Porcupine Bank and Flemish Cap in the Mid-to-Late Jurassic, forming the hyperextended domain in the Porcupine Basin. The Goban Spur was still undergoing the necking stage with gradual segmentation of the crust. As the oblique rifting continued during the earliest Cretaceous, serpentinized mantle may have been exhumed due to extreme crustal thinning. The obliquity of extension between the Goban Spur and Flemish Cap became more consistent in the Early Cretaceous, accompanied by the formation of the serpentinized peridotite ridges. Then, the rifting axis between the Goban Spur and Iberia plates continued to move eastward, leading to their final separation, involving relatively little magmatic activity. The northward rifting axis between the NE Newfoundland and Porcupine region arrived at the next triple junction close to the Rockall Basin until the final breakup, primarily triggered by voluminous magmatism.

During the polyphase and diachronous rifting of the southern North Atlantic, in addition to the strong structural inheritance and varying obliquity of extension, independent continental micro-plates also play a significant role in generating the complexity of the hyperextended rifted margins of the region. The kinematic geometries and locations of the micro-continent plates (e.g., the Flemish Cap, Porcupine Bank, Rockall Bank, and Galicia Bank) have been restored in previous deformable plate models (Peace et al., 2019; King et al., 2020). They are the key components to generate a better fit between the crustal thicknesses from deformable plate models and those from gravity inversion (Welford et al., 2012). Recently, a mechanism for rotation of the Flemish Cap has been elucidated using 3D numerical modelling (Neuharth et al., 2021). Therein, one extensional zone due to the hyperextension of the Orphan Basin interacts with another extensional zone due to northward rifting between the Newfoundland and Irish Atlantic margins, which together generate the forces that give rise to the rotation of the Flemish Cap, with an eventual eastward rift jump to the present-day margin. Just as the Orphan Basin, the Porcupine Basin is a failed rift system on the Irish Atlantic counterpart margin (Shannon, 2018). The Porcupine Bank is formed between the Porcupine Basin rifting zone and the oceanward rifting zone between the Newfoundland and Irish Atlantic margins. Although a similar mechanism for the rotation of the Porcupine Bank can be envisaged by analogy with that of the Flemish Cap, the Porcupine Basin and Bank are highly segmented based on seismic interpretation (Whiting et al., 2021; Yang and Welford, 2021). This leads to more complicated formation processes for the Porcupine Bank, wherein the rotation is likely to be coeval with segmentation that exploits inherited Caledonian fault zones. Just as with the Flemish Cap rotation mechanism, rift jump from the Porcupine Basin to the dominant North Atlantic ocean-forming rift is hypothesized. This study shows the influence of micro-plates on crustal thickness variation and rift propagation at the regional scale, but also implies that the segmentation within a micro-plate is of great importance at the local scale and should be carefully considered when performing plate reconstructions.

The Newfoundland-Irish Atlantic margins are often considered as one rift segment, just like the Newfoundland-Iberia margins are a separate rift segment further south (Reston, 2009; Enachescu et al., 2010). Based on this thesis work, the Newfoundland-Irish rift system can be described as highly segmented due to the Porcupine Bank being segmented by inherited Caledonian structural fabrics and the Goban Spur margin being offset by transfer faults related to Variscan structures. This can be shown by the along-strike variability in crustal thicknesses from the deformable plate model during the Jurassic and Early Cretaceous as observed along the NE Newfoundland and Porcupine Atlantic margins. Furthermore, the regional seismic lines (X1 and X2) on the Porcupine Atlantic margin cross distinct basement terranes (Variscan fold belts, Avalonian terrane, Proterozoic to early Paleozoic, and Proterozoic terranes from south to north) separated by major Caledonian fault zones and crustal sutures. The diversity of basement terranes is discerned by variations in basement reflectivity, magmatic components, and structural styles, and these can be associated with drastic changes in rheological behaviors during crustal extension and thinning. These present a more detailed segmentation of the North Atlantic than previously known.

In addition to the North Atlantic, the Red Sea is also a good target for examining transitional stages from continental rifting to the nascent ocean as the Arabian and African plates are pulling apart (Bonatti, 1985; Ligi et al., 2012). However, tectonic models of the Red Sea remain controversial (Augustin et al., 2021). The key factors such as segmentation, pre-exising inheritance, and oblique extension that contribute to the NE Newfoundland-Porcupine Atlantic rift system may also apply to the Red Sea but additional deformable plate modelling is required to obtain an enhanced understanding concerning its formation.

6.2 Conclusions

By comprehensively combining the newly acquired seismic reflection data with previous seismic refraction data, potential field data, and drilling borehole data, and using deformable plate reconstruction plate modelling in GPlates, an advanced understanding of the structural style and tectonic evolution of the NE Newfoundland-Porcupine Atlantic rift system is obtained, summarized as follows:

1. The rift system experienced polyphase, protracted, and diachronous rifting stages following the collapse of Variscan and Caledonian fold belts during the Mesozoic, leading to considerable variations in crustal architecture, orientation, infills, and segmentation within the rifted margin and associated basins. These rifting stages were linked to the North Atlantic rifting, opening of the Bay of Biscay, and/or stresses from mid-ocean ridge-push, and/or local tectonic events.

2. Along-strike variability in structural styles and crustal architecture along the NE Newfoundland-Porcupine Atlantic rift system is pronounced, associated with varying extension rates and obliquity, as well as the distribution of inherited Caledonian and Variscan basement terranes. In addition, variable serpentinization of the exhumed upper mantle and disappearance of the peridotite ridges are likely related to the variations in rheology and compositions of the crustal basement.

3. The main syn-rift stratigraphy across the Goban Spur and Porcupine Bank margins ranges from the Jurassic to the earliest Cretaceous, but the Porcupine Bank contains increasingly

abundant volcanic successions in the Jurassic-Cretaceous sedimentary layers and there may also exist some Triassic sediments in the Goban Spur basins.

4. There is a northward increase in magmatism from the Goban Spur to the southern Rockall Basin. The final breakup at the former margin is not magmatic, while it is magmatic at the latter margin. The timing of magmatic addition emplacement can be inferred from the distinct locations of interpreted sills. Some cut across the sediments in post-rift layers, while some interfere with basement reflectors.

5. Extensional fault types evolved during the formation of the Goban Spur - Porcupine Atlantic margin, with normal faults soling out at the middle crust level in the necking domain, detachment faults cutting the entire crust in the transition between the hyperextended and exhumed domains, and/or exhumation faults, implying detachment mechanisms in the magma-poor regions of the rift system.

6. The rifting between the Newfoundland margin and the Goban Spur-Porcupine Atlantic margin shows strong structural inheritance based on the results from this study. Caledonian and Variscan basement terranes, transfer faults on the Goban Spur, and inherited extensional faults that were subsequently reactivated during later episodic tectonic events, had a pronounced impact on the evolution of crustal thickness and on the formation of complex extensional, compressive, and transtensional features observed on seismic reflection data in the southern North Atlantic region.

7. The deformable plate model incorporates the segmentation of the Porcupine Bank and transfer faults on the continental crust of the Goban Spur, producing a better fit compared with previous plate reconstruction models. Crustal thickness is restored back through geologic time,

illustrating the extension obliquity and supporting the connection between the Goban Spur and the northern Iberian margin.

In total, this study advances our understanding of the tectonism of the NE Newfoundland-Porcupine Atlantic rift system. Restoration of margins along this rift system helps to unravel the complex evolution of the associated sedimentary basins and to compare their similarities and differences between margins, de-risking resource exploration in the southern North Atlantic.

6.3 Future work

There are still many unresolved ambiguities and challenges regarding the southern North Atlantic rifting and final breakup, which need to be addressed in the future.

1. We know little about numbers, geometries, and ages of faults during crustal hyperextension to initial oceanization because fault patterns formed during this time may be too complex due to being affected by the interplay of increasing magmatic additions, poly-phase faulting, and mantle exhumation. Nonetheless, it is worthwhile to do fault restoration in Move software to understand fault growth, by which the structures of the rifted margin basins can be better understood.

2. Crustal architecture along the Porcupine Atlantic region is well constrained by newly acquired seismic reflection data, however, it is less constrained on its Newfoundland counterpart, especially the East Orphan Basin and the Orphan Knoll and neighboring regions. Future work to establish an equally detailed crustal architecture of the Newfoundland side is needed, which will help to map the rift domains in this region and advance our understanding.

3. This study mainly focuses on the syn-rift and pre-rift sedimentary layers, ignoring post-rift layers in which uplift, erosion, compression, and extension may occur as well. The

Eocene motion incorporated into the deformable plate model may generate a better fit, resulting in a more accurate understanding of the evolution of the southern North Atlantic.

4. In this study, only crustal-scale inherited structures have been discussed. The influence of other scales of inherited structures (mantle-crust and fault-scale in the sedimentary layers) on the progressive deformation of the rifted margins along the southern North Atlantic remains unknown. Future work will focus on investigating the extent of influence of different scales of inherited structures on margin evolution.

5. The Orphan Knoll, a continental fragment with a pronounced topographic high, is overlooked to obtain a regionally reasonable crustal thickness from the deformable plate model. This micro-plate may play a role in improving our understanding of the kinematic linkage between the Irish and Newfoundland margins and deserves to be reconsidered in the deformable plate reconstruction model.

6. The motion of the Iberian plate in the deformable plate model in this study is directly cited from a previously published reconstruction model, despite the remaining fit discrepancy. Efforts to better constrain the pre-breakup movement of the Iberian margin by integrating geological and geophysical observations and modelling are needed. Then, a better fit for the deformable plate model can be obtained for the southern North Atlantic region. Furthermore, it is worthwhile to try varying initial crustal thickness in GPlates to obtain a more geologically realistic deformable plate model.

References

Ady, B., Whittaker, R., 2019. Examining the influence of tectonic inheritance on the evolution of the North Atlantic using a palinspastic deformable plate reconstruction. Geological Society, London, Special Publications, 470 (1), 245-264.

Albertz, M., Beaumont, C., Shimeld, J., Ings, S., Gradmann, S., 2010. An investigation of salt tectonic structural styles in the Scotia Basin, offshore Atlantic Canada: 1. Comparison of observations with geometrically simple numerical models. Tectonics 29, TC4017.

Angrand, P., Mouthereau, F., Masini, E. and Asti, R., 2020. A reconstruction of Iberia accounting for Western Tethys–North Atlantic kinematics since the late-Permian–Triassic. Solid Earth, 11(4), 1313-1332.

Auffret, G.A., Pastouret, L., Cassat, G., De Charpal, O., Cravatte, J., Guennoc, P., 1979. Dredged rocks from the Armorican and Celtic margins. Initial Reports of the Deep Sea Drilling Project, 68, 473-491.

Augustin, N., Van der Zwan, F.M., Devey, C.W., Brandsdóttir, B., 2021. 13 million years of seafloor spreading throughout the Red Sea Basin. Nature communications, 12(1), 1-10.

Barnett-Moore, N., Müller, D., Williams, S., Skogseid, J., & Seton, M., 2018. A reconstruction of the North Atlantic since the earliest Jurassic. Basin Research, 30, 160-185.

Bentley, P.A.D., Scrutton, R.A., 1987. Seismic investigations into the basement structure of southern Rockall Trough. In Conference on petroleum geology of North West Europe 3, 667-675.

Beslier, M.O., Ask, M., Boillot, G., 1993. Ocean-continent boundary in the Iberia Abyssal Plain from multichannel seismic data. Tectonophysics, 218(4), 383-393.

Boillot, G., Recq, M., Winterer, E.L., Meyer, A.W., Applegate, J., Baltuck, M., Bergen, J.A., Comas, M.C., Davies, T.A., Dunham, K. and Evans, C.A., 1987. Tectonic denudation of the upper mantle along passive margins: a model based on drilling results (ODP leg 103, western Galicia margin, Spain). Tectonophysics, 132(4), 335-342.

Bois, C., Lefort, J.P., Le Gall, B., Sibuet, J.C., Gariel, O., Pinet, B. and Cazes, M., 1990. Superimposed Variscan, Caledonian and Proterozoic features inferred from deep seismic profiles recorded between southern Ireland, southwestern Britain and western France. Tectonophysics, 177(1-3), 15-37.

Bonatti, E., 1985. Punctiform initiation of seafloor spreading in the Red Sea during transition from a continental to an oceanic rift. Nature, 316(6023), 33-37.

Bonvalot, S., Balmino, G., Briais, A., Kuhn, M., Peyrefitte, A., Vales, N., Biancale, R., Gabalda, G., Reinquin, F., Sarrailh, M., 2012. World Gravity Map. Commission for the Geological Map of the World. Eds. BGI-CGMW-CNES-IRD, Paris

Bradley, J., 1964. Intrusion of major dolerite sills: Royal Society of New Zealand Transactions 3, 27-54.

Brune, S., Heine, C., Clift, P.D. and Pérez-Gussinyé, M., 2017. Rifted margin architecture and crustal rheology: reviewing Iberia-Newfoundland, central South Atlantic, and South China Sea. Marine and Petroleum Geology, 79, 257-281.

Brune, S., Heine, C., Pérez-Gussinyé, M. and Sobolev, S.V., 2014. Rift migration explains continental margin asymmetry and crustal hyper-extension. Nature communications, 5(1), 1-9.

Brune, S., Williams, S., & Müller, R., 2018. Oblique rifting: the rule, not the exception. Solid Earth, 9 (5), 1187-1206.

Buiter, S.J., Torsvik, T.H., 2014. A review of Wilson Cycle plate margins: A role for mantle plumes in continental break-up along sutures? Gondwana Research 26, 627-653.

Bullock, A., Minshull, T., 2005. From continental extension to seafloor spreading: crustal structure of the Goban Spur rifted margin, southwest of the UK. Geophysical Journal International, 163 (2), 527-546.

Bulois, C., Pubellier, M., Chamot-Rooke, N., & Watremez, L., 2018. From orogenic collapse to rifting: A case study of the northern Porcupine Basin, offshore Ireland. Journal of Structural Geology, 114, 139-162.

Calvès, G., Torvela, T., Huuse, M., Dinkleman, M.G., 2012. New evidence for the origin of the Porcupine Median Volcanic Ridge: Early Cretaceous volcanism in the Porcupine Basin, Atlantic margin of Ireland. Geochemistry, Geophysics, Geosystems 13.

Cande, S.C., Kristoffersen, Y., 1977. Late Cretaceous magnetic anomalies in the North Atlantic. Earth and Planetary Science Letters 35, 215-224.

Causer, A., Pérez-Díaz, L., Adam, J., & Eagles, G., 2020. Uncertainties in break-up markers along the Iberia–Newfoundland margins illustrated by new seismic data. Solid Earth, 11 (2), 397-417.

Chen, C., Watremez, L., Prada, M., Minshull, T.A., Edwards, R.A., O'Reilly, B.M., Reston, T.J., Wagner, G., Gaw, V., Klaeschen, D. and Shannon, P.M., 2018. From continental hyperextension to seafloor spreading: New insights on the Porcupine Basin from wide-angle seismic data. Journal of Geophysical Research: Solid Earth, 123(10), 8312-8330.

Chenin, P., Beaumont. C., 2013, Influence of offset weak zones on the development of rift basins: Activation and abandonment during continental extension and breakup, Journal of Geophysical Research, Solid Earth, 118, 1698-1720.

Chenin, P., Manatschal, G., Lavier, L.L., Erratt, D., 2015. Assessing the impact of orogenic inheritance on the architecture, timing and magmatic budget of the North Atlantic rift system: a mapping approach. Journal of the Geological Society, 172(6), 711-720.

Chenin, P., Picazo, S., Jammes, S., Manatschal, G., Müntener, O. and Karner, G., 2019. Potential role of lithospheric mantle composition in the Wilson cycle: a North Atlantic perspective. Geological Society, London, Special Publications, 470(1), 157-172.

Christeson, G.L., Gulick, S.P., van Avendonk, H.J., Worthington, L.L., Reece, R.S., Pavlis, T.L., 2010. The Yakutat terrane: Dramatic change in crustal thickness across the Transition fault, Alaska. Geology, 38(10), 895-898.

Cole, J.E., Peachey, J., 1999. Evidence for pre-Cretaceous rifting in the Rockall Trough: an analysis using quantitative plate tectonic modelling. In Geological Society, London, Petroleum Geology Conference series (Vol. 5, No. 1, pp. 359-370). Geological Society of London.

Colin, J.P., Ioannides, N.S., Vining, B., 1992. Mesozoic stratigraphy of the Goban Spur, offshore south-west Ireland. Marine and Petroleum Geology, 9(5), 527-541.

Colin, J.P., Lehmann, R.A., Morgan, B.E., 1981. Cretaceous and Late Jurassic biostratigraphy of the North Celtic Sea basin, offshore southern Ireland. Microfossils from Recent and fossil shelf seas, 122-155.

Cook, D.R., 1987. The Goban Spur-exploration in a deep-water frontier basin. In Conference on petroleum geology of North West Europe 3, 623-632.

Copestake, P., Ainsworth, N. R., Bailey, H. W., Dominey, S. J., Donato, J. A., Farrimond, P. R., et al., 2017. A Biostratigraphic, Lithostratigraphic & Sequence Stratigraphic Framework of Offshore Ireland. Atlantic Ireland 2017 Conference. www.pip.ie

Croker, P.F., Shannon, P.M., 1987. The evolution and hydrocarbon prospectivity of the Porcupine Basin, offshore Ireland. In Conference on petroleum geology of North West Europe 3, 633-642.

Davy, R. G., Minshull, T. A., Bayrakci, G., Bull, J. M., Klaeschen, D., Papenberg, C., Reston, T. J., Sawyer, D. S., Zelt, C. A., 2016. Continental hyperextension, mantle exhumation, and thin oceanic crust at the continent-ocean transition, West Iberia: New insights from wide-angle seismic, Journal of Geophysical Research: Solid Earth 121, 3177-3199.

de Graciansky, P. C., Poag, C. W., 1985. Geologic history of Goban Spur, northwest Europe continental margin. Deep Sea Drilling Project Initial Reports 80, 1187-1216.

de Graciansky, P.C., Poag, C.W., Cunningham J.R, Loubere, P., Masson, D.G., Mazzullo, J.M., Montadert, L., Müller, C.A.R.L.A., Otsuka, K., Reynolds, L.A. and Sigal, J., 1985. The Goban Spur transect: Geologic evolution of a sediment-starved passive continental margin. Geological Society of America Bulletin, 96(1), 58-76.

Dean, S.L., Sawyer, D.S., Morgan, J.K., 2015. Galicia Bank ocean-continent transition zone: New seismic reflection constraints. Earth and Planetary Science Letters 413, 197-207.

Dean, S.M., Minshull, T.A., Whitmarsh, R.B., Louden, K.E., 2000. Deep structure of the ocean-continent transition in the southern Iberia Abyssal Plain frosm seismic refraction profiles: the IAM-9 transect at 40 20'N. Journal Geophysical Research 105, 5859-5886.

Dean, S.M., Murton, B.J., Minshull, T.A., Henstock, T.J., White, R.S., 2009. An integrated kinematic and geochemical model to determine lithospheric extension and mantle temperature from syn-rift volcanic compositions. Earth and Planetary Science Letters 278, 26-39.

Dingle, R. V., Scrutton, R. A., 1977. Continental margin fault pattern mapped south-west of Ireland. Nature 268, 720-722.

Dingle, R. V., Scrutton, R. A., 1979. Sedimentary succession and tectonic history of a marginal plateau (Goban Spur, southwest of Ireland). Marine Geology 33, 45-69.

Dingle, R.V., Megson, J.B., Scrutton, R.A., 1982. Acoustic stratigraphy of the sedimentary succession west of Porcupine bank, NE Atlantic Ocena: A preliminary account. Marine Geology, 47, 17-35.

Doré, A., Lundin, E., Jensen, L., Birkeland, Ø., Eliassen, P., Fichler, C., 1999. Principal tectonic events in the evolution of the northwest European Atlantic margin. Petroleum Geology Conference series, 5 (1), 41-61.

Doré, T., Lundin. E., 2015, Hyperextended continental margins -Knowns and unknowns, Geology, 43, 95-96.

Duclaux, G., Huismans, R., May, D., 2020. Impact of crustal rheology on oblique rift development and geometry: a numerical study. Paper presented at EGU General Assembly 2020, Online, 4–8 May 2020, EGU2020-17271.

Ebinger, C., 2005, Continental break-up: The East African perspective, Astronomy & Geophysics, 46,16-21.

Enachescu, M. E., Hogg, J. R., Fowler, M., Brown, D. E., Atkinson, I., 2010. Late Jurassic Source Rock Super-Highway on Conjugate Margins of the North and Central Atlantic (offshore East Coast Canada, Ireland, Portugal, Spain and Morocco). II Central & North Atlantic Conjugate Margins Conference, Lisbon.

Enachescu, M.E., 2006. Structural Setting and Petroleum Potential of the Orphan Basin, offshore Newfoundland and Labrador. Pan-Atlantic Petroleum System Consortium (PPSC) and Oil and Gas Development Program (OGDP), Recorder, 31, 5-13.

Enachescu, M.E., Kearsey, S., Hardy, V., Sibuet, J., Hogg, J., Srivastava, S., Fagan, A., Thompson, T., Ferguson, R., 2005. Evolution and petroleum potential of Orphan Basin, offshore Newfoundland, and its relation to the movement and rotation of Flemish Cap based on plate kinematics of the North Atlantic. In 25th annual Gulf Coast section SEPM Foundation, Bob F. Perkins research conference 25, 7-8.

Enachescu, M.E., Meyer, K., Hogg, J., 2004. East Orphan Basin: Structural setting and evolution with seismic and potential field arguments, in Canadian Society of Exploration Geophysicists (CSEG) Annual Convention, Expanded Abstracts.

Francis, E.H., 1982. Magma and sediment-I Emplacement mechanism of late Carboniferous tholeiite sills in northern Britain. Journal of the Geological Society 139, 1-20.

Franke, D., 2013, Rifting, lithosphere breakup and volcanism: Comparison of magma-poor and volcanic rifted margins, Marine and Petroleum Geology, 43, 63-87.

Funck, T., Erlendsson, Ö., Geissler, W.H., Gradmann, S., Kimbell, G.S., McDermott, K. and Petersen, U.K., 2017. A review of the NE Atlantic conjugate margins based on seismic refraction data. Geological Society, London, Special Publications 447, 171-205.

Funck, T., Hopper, J.R., Larsen, H.C., Louden, K.E., Tucholke, B.E., Holbrook, W.S., 2003. Crustal structure of the ocean-continent transition at Flemish Cap: seismic refraction results. Journal of Geophysical Research 108, B11, 2531.

Gagnevin, D., Haughton, P.D., Whiting, L. and Saqab, M.M., 2018. Geological and geophysical evidence for a mafic igneous origin of the Porcupine Arch, offshore Ireland. Journal of the Geological Society 175, 210-228.

Gee, D.G., Fossen, H., Henriksen, N., Higgins, A.K., 2008. From the early Paleozoic platforms of Baltica and Laurentia to the Caledonide Orogen of Scandinavia and Greenland. Episodes, 31(1), 44-51.

Gee, D.G., Janák, M., Majka, J., Robinson, P. and van Roermund, H., 2013. Subduction along and within the Baltoscandian margin during closing of the Iapetus Ocean and Baltica-Laurentia collision. Lithosphere 5, 169-178.

Geoffroy, L., Burov, E.B. and Werner, P., 2015. Volcanic passive margins: another way to break up continents. Scientific reports, 5(1), 1-12.

Gerlings, J., 2013. A deep seismic analysis of the Flemish Cap Continental Margin off Newfoundland, Canada (Doctoral dissertation). Dalhousie University, Halifax, NS.

Gerlings, J., Louden, K., Minshull, T., Nedimovic, M., 2012. Flemish Cap-Goban Spur conjugate margins: New evidence of asymmetry. Geology, 40 (12), 1107-1110.

Gerlings, J., Louden, K.E., & Jackson, H.R., 2011. Crustal structure of the Flemish Cap Continental Margin (eastern Canada): an analysis of a seismic refraction profile. Geophysics Journal International, 185, 30-48.

Gernigon, L., Shannon, P.M., Readman, P.W., O'Reilly, B.M., 2006. Geological interpretation and synthesis of the Irish Rockall and Hatton margins. Final report for the Hatton Deep Seismic, Project P2. https://www.pip.ie.

Gillard, M., Autin, J. and Manatschal, G., 2016. Fault systems at hyper-extended rifted margins and embryonic oceanic crust: Structural style, evolution and relation to magma. Marine and Petroleum Geology, 76, 51-67.

Gillard, M., Autin, J., Manatschal, G., Sauter, D., Munschy, M. and Schaming, M., 2015. Tectonomagmatic evolution of the final stages of rifting along the deep conjugate

Australian-Antarctic magma-poor rifted margins: Constraints from seismic observations. Tectonics, 34(4), 753-783.

Gillard, M., Tugend, J., Muntener, O., Manatschal, G., Karner, G.D., Autin, J., Sauter, D., Figueredo, P.H., Ulrich, M., 2019. The role of serpentinization and magmatism in the formation of decoupling interfaces at magma-poor rifted margins. Earth-Science Reviews 196, 102882.

Gouiza, M., Paton, D.A., 2019. The role of inherited lithospheric heterogeneities in defining the crustal architecture of rifted margins and the magmatic budget during continental breakup. Geochemistry, Geophysics, Geosystems 20, 1836-1853.

Grevemeyer, I., Hayman, N.W., Peirce, C., Schwardt, M., Van Avendonk, H.J., Dannowski, A. and Papenberg, C., 2018. Episodic magmatism and serpentinized mantle exhumation at an ultraslow-spreading centre. Nature Geoscience 11, 444.

Grow, T.J., Armstrong, R., Belopolsky, A., Derewetzky, A., Huber, N., Kilsdonk, B., & Wolters, J., 2019. Shearing and Stretching the Porcupine Basin–A Tectonic Model Based on Integrated Geophysical Analysis. Paper presented at Atlantic Ireland 2019 Conference, Dublin. https://www.pip.ie.

Gurnis, M., Turner, M., Zahirovic, S., DiCaprio, L., Spasojevic, S., Müller, R.D., Boyden, J., Seton, M., Manea, V.C. and Bower, D.J., 2012. Plate tectonic reconstructions with continuously closing plates. Computers & Geosciences, 38(1), 35-42.

Gurnis, M., Yang, T., Cannon, J., Turner, M., Williams, S., Flament, N., & Müller, R., 2018. Global tectonic reconstructions with continuously deforming and evolving rigid plates. Computers & Geosciences, 116, 32-41.

Haughton, P., Praeg, D., Shannon, P., Harrington, G., Higgs, K., Amy, L., Tyrrell, S. and Morrissey, T., 2005. First results from shallow stratigraphic boreholes on the eastern flank of the Rockall Basin, offshore western Ireland. In Geological Society, London, Petroleum Geology Conference series 6, 1077-1094.

Hauser, F., O'Reilly, B.M., Jacob, A.B., Shannon, P.M., Makris, J. and Vogt, U., 1995. The crustal structure of the Rockall Trough: differential stretching without underplating. Journal of Geophysical Research: Solid Earth 100, 4097-4116.

Hawkes, P., Thomas, R., Mackay, H., 2019.The Jurassic and Cretaceous Petroleum System of the East Flank of the Porcupine Basin: Implications for Prospectivity in Licences FEL 1/17 and FEL 3/13. Paper presented at Atlantic Ireland 2019 Conference, Dublin. www.pip.ie.

Healy, D., Kusznir, N.J., 2007. Early kinematic history of the Goban Spur rifted margin derived from a new model of continental breakup and sea-floor spreading initiation. Geological Society, London, Special Publications 282, 199-215.

Holdsworth, R.E., Imber, J., McCaffrey, K., et al., 2013. Tectonic inheritance during extension in rifts and passive margins: a review. GSA annual meeting in Denver-Abstract Paper No. 217-1. https://gsa.confex.com/gsa/2013AM/finalprogram/abstract_222758.htm.

Hopper, J., Funck, T., Tucholke, B., Louden, K., Holbrook, W. & Larsen, H.C., 2006. A deep seismic investigation of the Flemish Cap margin: implications for the origin of deep reflectivity and evidence for asymmetric break-up between Newfoundland and Iberia. Geophysics Journal International 164, 501-515.

Horsefield, S.J., Whitmarsh, R.B., White, R.S., Sibuet, J. C., 1994. Crustal structure of the Goban Spur rifted continental margin, NE Atlantic. Geophysics Journal International 119, 1-19.

Huismans, R., Beaumont, C., 2007, Roles of lithospheric strain softening and heterogeneity in determining the geometry of rifts and continental margins, Geological Society of London, Special Publication, 282, 111-138.

Huismans, R., Beaumont, C., 2011, Depth-dependent extension, two-stage breakup, and cratonic underplating at rifted margins, Nature, 473, 74-78.

Jackson, M.P., Talbot, C.J., 1986. External shapes, strain rates, and dynamics of salt structures. Geological Society of America Bulletin 97, 305-323.

Jacobi, R.D., Kristoffersen, Y., 1981. Transatlantic correlations of geophysical anomalies on Newfoundland, British Isles, France and adjacent continental shelves. 1981, 197-229.

Johnson, H., Ritchie, J.D., Gatliff, R.W., Williamson, J.P., Cavill, J. and Bulat, J., 2001. Aspects of the structure of the Porcupine and Porcupine Seabight basins as revealed from gravity modelling of regional seismic transects. Geological Society, London, Special Publications 188, 265-274.

Johnson, H., Ritchie, J.D., Gatliff, R.W., Williamson, J.P., Cavill, J. and Bulat, J., 2001. Aspects of the structure of the Porcupine and Porcupine Seabight basins as revealed from gravity modelling of regional seismic transects. Geological Society, London, Special Publications, 188(1), 265-274.

Jones, D., Underhill, J., 2011. Structural and stratigraphic evolution of the Connemara discovery, Northern Porcupine Basin: significance for basin development and petroleum prospectivity along the Irish Atlantic Margin. Petroleum Geoscience, 17 (4), 365-384.

Jones, S.M., White, N. and Lovell, B., 2001. Cenozoic and Cretaceous transient uplift in the Porcupine Basin and its relationship to a mantle plume. Geological Society, London, Special Publications 188, 345-360.

Jourdon, A., Le Pourhiet, L., Mouthereau, F. and May, D., 2020. Modes of Propagation of Continental Breakup and Associated Oblique Rift Structures. Journal of Geophysical Research: Solid Earth 125, p.e2020JB019906.

Keen, C.E., Dafoe, L.T., Dickie, K., 2014. A volcanic province near the Western termination of the Charlie-Gibbs Fracture Zone at the rifted margin, offshore northeast Newfoundland. Tectonics, 33, 1133-1153

Keen, C.E., de Voogd, B., 1988. The continent-ocean boundary at the rifted margin off eastern Canada: New results from deep seismic reflection studies. Tectonics 7, 107-124.

Keen, C.E., Peddy, C., deVoogd, B., Mathews, D., 1989. Conjugate margins of Canada and Europe: Results from deep reflection profiling. Geology 17, 173-176.

Kimbell, G.S., Ritchie, J.D. and Henderson, A.F., 2010. Three-dimensional gravity and magnetic modelling of the Irish sector of the NE Atlantic margin. Tectonophysics 486, 36-54.

King, L., Fader, G., Poole, W., Wanless, R., 1985. Geological setting and age of the Flemish Cap granodiorite, east of the Grand Banks of Newfoundland, Canadian Journal Earth Sciences 22, 1286-1298.

King, M.T., Welford, J.K., Cadenas, P., Tugend, J., 2021. Investigating the plate kinematics of the Bay of Biscay using deformable plate tectonic models. Tectonics, 40(7), 2020TC006467.

King, M.T., Welford, J.K. and Peace, A.L., 2020. Investigating the role of the Galicia Bank on the formation of the North West Iberian margin using deformable plate tectonic models. Tectonophysics, 789, 228537.

Kroner, U., Romer, R.L., 2013. Two plates-many subduction zones: the Variscan orogeny reconsidered. Gondwana Research, 24(1), 298-329.

Kusznir, N., Karner, G., 2007. Continental lithospheric thinning and breakup in response to upwelling divergent mantle flow: application to the Woodlark, Newfoundland and Iberia margins, Geological Society of London, Special Publication, 282, 389-419.

Landes, M., O'Reilly, B.M., Readman, P.W., Shannon, P.M. and Prodehl, C., 2003. VARNET-96: three-dimensional upper crustal velocity structure of SW Ireland. Geophysical Journal International, 153(2), 424-442.

Lau, K.W.H., Watremez, L., Louden, K.E., Nedimovíć, M.R., 2015. Structure of thinned continental crust across the Orphan Basin from a dense wide-angle seismic profile and gravity data. Geophysical Journal International, 202, 1969-1992.

Li, Y., Oldenburg, D.W., 1998. 3-D inversion of gravity data. Geophysics, 63, 109-119.

Li,Y., Oldenburg, D.W., 1996. 3-D inversion of magnetic data. Geophysics, 61, 394-408.

Ligi, M., Bonatti, E., Bortoluzzi, G., Cipriani, A., Cocchi, L., Caratori Tontini, F., Carminati, E., Ottolini, L. and Schettino, A., 2012. Birth of an ocean in the Red Sea: initial pangs. Geochemistry, Geophysics, Geosystems, 13(8).

Lister, G. S., Etheridge, M. A., Symonds, P. A., 1986. Detachment faulting and the evolution of passive continental margins, Geology, 14, 246-250.

Louvel, V., Dyment, J., Sibuet, J., 1997. Thinning of the Goban Spur continental margin and formation of early oceanic crust: constraints from forward modelling and inversion of marine magnetic anomalies. Geophysics Journal International, 128,188-196.

Lymer, G., Roche, V., Saqab, M., Childs, C., & Walsh, J., 2020. Multi-phase development of the Porcupine Basin during the rifting of the North-Atlantic. Paper presented at EGU General Assembly 2020, Online, 4-8 May 2020, EGU2020-5065.

Mackay, H., 2018. Europa Oil & Gas in Ireland Progress and Prospects 2018. Paper presented at Atlantic Ireland 2018 Conference, Dublin. https://www.pip.ie.

Mackenzie, G.D., Shannon, P.M., Jacob, A.W.B., Morewood, N.C., Makris, J., Gaye, M. and Egloff, F., 2002. The velocity structure of the sediments in the southern Rockall Basin: results from new wide-angle seismic modelling. Marine and Petroleum Geology 19, 989-1003.

Magee, C., Muirhead, J.D., Karvelas, A., Holford, S.P., Jackson, C.A.L., Bastow, I.D., Schofield, N., Stevenson, C.T.E., McLean, C., McCarthy, W., Shtukert, O., 2016. Lateral magma flow in mafic sill complexes. Geosphere, 12.

Makris, J., Egloff, R., Jacob, A.W.B., Mohr, P., Murphy, T., & Ryan, P., 1988. Continental crust under the southern Porcupine Seabight west of Ireland. Earth and Planetary Science Letters, 89, 387-397.

Manatschal, G., Lavier, L., Chenin, P., 2015. The role of inheritance in structuring hyperextended rift systems: Some considerations based on observations and numerical modeling. Gondwana Research, 27 (1), 140-164.

Masini, M., Mojonero, C.G., Welsink, H., Cortes, N.A. and Ceballos, C.G., 2013. Structural Style of Continental Rifting in Goban Spur and Porcupine Basins, Irish Atlantic Margin. Abstract presented in 75th EAGE Conference.

Masson, D., Montadert, L., Scruiton, R., 1985. Regional geology of the Goban Spur continental margin. Initial Reports of the Deep Sea Drilling Project 80, 1115-1139.

Masson, D.G., Dobson, M.R., Auzende, J.M., Cousin, M., Coutelle, A., Rolet, J., & Vaillant, P., 1989. Geology of Porcupine Bank and Goban Spur, Northeastern Atlantic—Preliminary results of the Cyaporc submersible cruise. Marine Geology, 87, 105-119.

Masson, D.G., Miles, P.R., 1986. Development and hydrocarbon potential of Mesozoic sedimentary basins around margins of North Atlantic. AAPG bulletin, 70(6), 721-729.

Masson, F., Jacob, A.W.B., Prodehl, C., Readman, P.W., Shannon, P.M., Schulze, A. and Enderle, U., 1998. A wide-angle seismic traverse through the Variscan of southwest Ireland. Geophysical Journal International, 134(3), 689-705.

Matte, P., 2001. The Variscan collage and orogeny (480–290 Ma) and the tectonic definition of the Armorica microplate: a review. Terra nova 13, 122-128.

Matthews, K. J., Maloney, K. T., Zahirovic, S., Williams, S. E., Seton, M., Müller, R. D., 2016. Global plate boundary evolution and kinematics since the late Paleozoic. Global and Planetary Change 146, 226-250.

McCann, T., Shannon, P.M., Moore, J., 1995. Fault patterns in the cretaceous and tertiary (end syn-rift, thermal subsidence) succession of the Porcupine Basin, offshore Ireland. Journal of Structural Geology 17, 201-214.

McDermott, K., Reston, T., 2015. To see, or not to see? Rifted margin extension. Geology, 43(11), 967-970.

McDonnell, A., Shannon, P.M., 2001. Comparative Tertiary stratigraphic evolution of the Porcupine and Rockall basins. Geological Society, London, Special Publications 188, 323-344.

McGrane, K., Readman, P.W. and O'Reilly, B.M., 2001. Interpretation of transverse gravity lineaments in the Rockall Basin. Geological Society, London, Special Publications 188, 393-399.

McKenzie, D., 1978. Some remarks on the development of sedimentary basins, Earth and Planetary Science Letters, 40, 25-32.

Merle, O., 2011. A simple continental rift classification, Tectonophysics, 513, 88-95.

Minshull, T.A., 2009. Geophysical characterisation of the ocean-continent transition at magma-poor rifted margins. Comptes Rendus Geoscience 341, 382-393.

Minshull, T.A., Muller, M.R., Robinson, C.J., White, R.S., Bickle, M.J., 1998. Is the oceanic Moho a serpentinization front?. Geological Society, London, Special Publications, 148(1), 71-80.

Mjelde, R., Breivik, A.J., Raum, T., Mittelstaedt, E., Ito, G., Faleide, J.I., 2008. Magmatic and tectonic evolution of the North Atlantic. Journal of the Geological Society, 165, 31-42.

Mohn, G., Manatschal, G., Beltrando, M., Masini, E., Kusznir, N., 2012. Necking of continental crust in magma-poor rifted margins: evidence from the fossil Alpine Tethys margins. Tectonics, 31, 1-28.

Montadert, L., Roberts, D. G., de Charpal, O., Guennoc, P., 1979. Rifting and subsidence of the Northern Continental Margin of the Bay of Biscay. Initial Reports of the Deep Sea Drilling Project 48, 1025-1060.

Moore, J. G., 1992. A syn-rift to post-rift transition sequence in the Main Porcupine Basin, offshore western Ireland. Geological Society Special Publication, 62, 333-349.

Morewood, N., Mackenzie, G., Shannon, P., O’Reilly, B., Readman, P., Makris, J., 2005. The crustal structure and regional development of the Irish Atlantic margin region. Petroleum Geology Conference series, 6 (1), 1023-1033.

Morewood, N.C., Shannon, P.M., Mackenzie, G.D., O'Reilly, B.M., Jacob, A.B. and Makris, J., 2003. Deep seismic experiments investigate crustal development at continental margin. Eos, Transactions American Geophysical Union 84, 225-228.

Morgan, C., 2016. Status of Exploration Offshore Ireland. Paper presented at Atlantic Ireland 2016 Conference, Dublin. https://www.pip.ie.

Morgan, W.J., 1968. Rises, trenches, great faults, and crustal blocks. Journal of Geophysical Research, 73, 1959-1982.

Morley, C.K., Haranya, C., Phoosongsee, W., Pongwapee, S., Kornsawan, A. and Wonganan, N., 2004. Activation of rift oblique and rift parallel pre-existing fabrics during extension and their effect on deformation style: examples from the rifts of Thailand. Journal of Structural Geology, 26, 1803-1829.

Müller, R.D., Cannon, J., Qin, X., Watson, R.J., Gurnis, M., Williams, S., Pfaffelmoser, T., Seton, M., Russell, S.H. and Zahirovic, S., 2018. GPlates: building a virtual Earth through deep time. Geochemistry, Geophysics, Geosystems, 19(7), 2243-2261.

Müller, R.D., Seton, M., Zahirovic, S., Williams, S.E., Matthews, K.J., Wright, N.M., Shephard, G.E., Maloney, K.T., Barnett-Moore, N., Hosseinpour, M., Bower, D.J., Cannon, J., 2016. Ocean Basin Evolution and Global-Scale Plate Reorganization Events Since Pangea Breakup. Annual Review of Earth and Planetary Sciences 44, (1), 107-138.

Müller, R.D., Zahirovic, S., Williams, S.E., Cannon, J., Seton, M., Bower, D.J., Tetley, M.G., Heine, C., Le Breton, E., Liu, S. and Russell, S.H., 2019. A global plate model including lithospheric deformation along major rifts and orogens since the Triassic. Tectonics, 38(6), 1884-1907.

Müntener, O., Manatschal, G., 2006. High degrees of melt extraction recorded by spinel harzburgite of the Newfoundland margin: The role of inheritance and consequences for the evolution of the southern North Atlantic. Earth and Planetary Science Letters, 252, 437-452.

Murillas, J., Mougenot, D., Boillot, G., Comas, M.C., Banda, E., Mauffret, A., 1990. Structure and evolution of the Galicia Interior Basin (Atlantic western Iberian continental margin). Tectonophysics, 184, 297-319.

Murphy, J.B., van Staal, C.R. and Collins, W.J., 2011. A comparison of the evolution of arc complexes in Paleozoic interior and peripheral orogens: speculations on geodynamic correlations. Gondwana Research, 19(3), 812-827.

Naylor, D., Shannon, P.M., 2009. Geology of offshore Ireland. In: Holland, C.H. and Sanders, I.S. (eds) The Geology of Ireland. Dunedin Academic Press, Edinburgh, 405-460.

Naylor, D., Shannon, P.W., 2005. The structural framework of the Irish Atlantic Margin. In: Doré, A.G., and Vining, B., Eds.) Petroleum Geology: North-West Europe and Global Perspectives - Proceedings of the 6th Petroleum Geology Conference, 6, 1009-1022.

Naylor, D., Shannon, P.W., Murphy, N., 2002. Porcupine-Goban region – a standard structural nomenclature system. Dublin, Ireland: Petroleum Affairs Division.

Neuharth, D., Brune, S., Glerum, A., Heine, C. and Welford, J.K., 2021. Formation of continental microplates through rift linkage: Numerical modeling and its application to the Flemish Cap and Sao Paulo Plateau. Geochemistry, Geophysics, Geosystems, 22(4), 2020GC009615.

Nirrengarten, M., Manatschal, G., Tugend, J., Kusznir, N., & Sauter, D., 2018. Kinematic Evolution of the Southern North Atlantic: Implications for the Formation of Hyperextended Rift Systems. Tectonics, 37, 89-118.Norton, M.G., 2002. Tectonic evolution of the Porcupine Basin. The final report by Porcupine Studies Group. https://www.pip.ie.

O'Sullivan, C.M., Childs, C.J., Saqab, M.M., Walsh, J.J., Shannon, P.M., 2021. The influence of multiple salt layers on rift-basin development; The Slyne and Erris basins, offshore NW Ireland. Basin Research, 33(3), 2018-2048.

O'Sullivan, P.T., Ebbing, J., 2008. Styles of extension offshore mid-Norway and implications for mechanisms of crustal thinning at passive margins. Tectonics, 27, TC6016.

O'Reilly, B.M., Hauser, F., Jacob, A.B., Shannon, P.M., 1996. The lithosphere below the Rockall Trough: wide-angle seismic evidence for extensive serpentinisation. Tectonophysics, 255, 1-23.

O'Reilly, B.M., Hauser, F., Ravaut, C., Shannon, P.M. and Readman, P.W., 2006. Crustal thinning, mantle exhumation and serpentinization in the Porcupine Basin, offshore Ireland: evidence from wide-angle seismic data. Journal of the Geological Society, 163, 775-787.

Peace, A.L., Welford, J.K., Ball, P.J. and Nirrengarten, M., 2019. Deformable plate tectonic models of the southern North Atlantic. Journal of Geodynamics, 128, 11-37.

Peace, A.L., Welford, J.K., 2020. Conjugate margins - An oversimplification of the complex southern North Atlantic rift and spreading system? Interpretation, 8, 33-49.

Peddy C., Pinet, B., Masson, D., Scrutton, R., Sibuet, J.C., Warner, M.R., Lefort, J.P., Shroeder, I.J., 1989. Crustal structure of the Goban Spur continental margin Northeast Atlantic, from deep seismic reflection profiling. Journal of the Geological Society, 146, 427-437.

Pérez-Gussinyé, M., Andrés-Martínez, M., Araújo, M., Xin, Y., Armitage, J., Morgan, J.P., 2020. Lithospheric Strength and Rift Migration Controls on Synrift Stratigraphy and Breakup Unconformities at Rifted Margins: Examples from Numerical Models, the Atlantic and South China Sea Margins. Tectonics, 39, 2020TC006255.

Pérez-Gussinyé, M., Ranero, C.R., Reston, T.J. and Sawyer, D., 2003. Mechanisms of extension at nonvolcanic margins: Evidence from the Galicia interior basin, west of Iberia. Journal of Geophysical Research: Solid Earth, 108(B5).

Pérez-Gussinyé, M., Reston, T.J., 2001, Rheological evolution during extension at passive non-volcanic margins: onset of serpentinization and development of detachments to continental break-up, Journal of Geophysical Research, 106, 3691-3975.

Péron-Pinvidic, G., Manatschal, G. and Osmundsen, P.T., 2013. Structural comparison of archetypal Atlantic rifted margins: A review of observations and concepts. Marine and petroleum geology, 43, 21-47.

Péron-Pinvidic, G. and Manatschal, G., 2009. The final rifting evolution at deep magma-poor passive margins from Iberia-Newfoundland: a new point of view. International Journal of Earth Sciences, 98(7), 1581-1597.

Petersen, K.D., Schiffer, C., 2016. Wilson cycle passive margins: Control of orogenic inheritance on continental breakup. Gondwana Research, 39, 131-144.

Phillips, T.B., Jackson, C.A., Bell, R.E., Duffy, O.B. and Fossen, H., 2016. Reactivation of intrabasement structures during rifting: A case study from offshore southern Norway. Journal of Structural Geology, 91, 54-73.

Phillips, T.B., McCaffrey, K.J., 2019. Terrane boundary reactivation, barriers to lateral fault propagation and reactivated fabrics - Rifting across the Median Batholith Zone, Great South Basin, New Zealand. Tectonics, 38(11), 4027-4053.

Pickup, S. L. B., Whitmarsh, R. B., Fowler, C.M.R., Reston, T. J., 1996. Insight into the nature of the ocean-continent transition off West Iberia from a deep multichannel seismic reflection profile. Geology, 24, 1079-1082.

Planke, S., Rasmussen, T., Rey, S.S., Myklebust, R., 2005. Seismic characteristics and distribution of volcanic intrusions and hydrothermal vent complexes in the Vøring and Møre basins. In Geological Society, London, Petroleum Geology Conference series 6, 833-844.

Prada, M., Lavoué, F., Saqab, M.M., O'Reilly, B.M., Lebedev, S., Walsh, J.J., Childs, C., 2019. Across-axis variations in petrophysical properties of the North Porcupine Basin, offshore Ireland: New insights from long-streamer traveltime tomography. Basin Research, 31(1), 59-76.

Prada, M., Watremez, L., Chen, C., O'Reilly, B.M., Minshull, T.A., Reston, T.J., Shannon, P.M., Klaeschen, D., Wagner, G. and Gaw, V., 2017. Crustal strain-dependent serpentinisation in the Porcupine Basin, offshore Ireland. Earth and Planetary Science Letters, 474, 148-159.

Praeg, D., Stoker, M.S., Shannon, P.M., Ceramicola, S., Hjelstuen, B., Laberg, J.S., Mathiesen, A., 2005. Episodic Cenozoic tectonism and the development of the NW European ‘passive’continental margin. Marine and Petroleum Geology, 22(9-10), 1007-1030.

Ranero, C.R., Pérez-Gussinyé, M., 2010. Sequential faulting explains the asymmetry and extension discrepancy of conjugate margins. Nature 468, 294-299.

Readman, P., O’Reilly, B., Shannon, P., Naylor, D., 2005. The deep structure of the Porcupine Basin, offshore Ireland, from gravity and magnetic studies. Petroleum Geology Conference series, 6 (1), 1047-1056.

Readman, P.W., O’Reilly, B.M., Edwards, J.W.F., Sankey, M.J., 1995. A gravity map of Ireland and surrounding waters. Geological Society, London, Special Publications 93, 9-16.

Reston, T.J., 2005. Polyphase faulting during the development of the west Galicia rifted margin. Earth and Planetary Science Letters 237, 561-576.

Reston, T.J., 2007. The formation of non-volcanic rifted margins by the progressive extension of the lithosphere: the example of the west Iberian margin, in: Karner, G., Manatschal, G. & Pinheiro, L. (Ed.), Imaging, Mapping and Modeling Continental Lithosphere Extension and Breakup. Geological Society, London, Special Publications, 282, 77-110.

Reston, T.J., 2009. The structure, evolution and symmetry of the magma-poor rifted margins of the North and Central Atlantic: A synthesis. Tectonophysics, 468 (1-4), 6-27.

Reston, T.J., Gaw, V., Pennell, J., Klaeschen, D., Stubenrauch, A., Walker, I., 2004. Extreme crustal thinning in the south Porcupine Basin and the nature of the Porcupine Median High: implications for the formation of non-volcanic rifted margins. Journal of the Geological Society, 161 (5), 783-798.

Reston, T.J., Krawczyk, C.M., Klaeschen, D., 1996. The S reflector west of Galicia (Spain): Evidence from prestack depth migration for detachment faulting during continental breakup. Journal of Geophysical Research: Solid Earth 101, 8075-8091.

Roberts, D.G., Masson, D.G., Montadert, L., De Charpal, O., 1981. Continental margin from the Porcupine Seabight to the Armorican Basin. In: Petroleum Geology of the Continental Shelf of NW Europe (Eds L. V. Illing and G. D. Hobson), Heyden, London, 455-473.

Ruiz, M., Díaz, J., Pedreira, D., Gallart, J., Pulgar, J.A., 2017. Crustal structure of the North Iberian continental margin from seismic refraction/wide-angle reflection profiles. Tectonophysics, 717, 65-82.

Russell, S.M., Whitmarsh, R.B., 2003, Magmatism at the west Iberia non-volcanic rifted continental margin: evidence from analyses of magnetic anomalies, Geophysical Journal International, 154, 706-730.

Sandoval, L., Welford, J.K., MacMahon, H. and Peace, A.L., 2019. Determining continuous basins across conjugate margins: The East Orphan, Porcupine, and Galicia Interior basins of the southern North Atlantic Ocean. Marine and Petroleum Geology, 110, 138-161.

Saqab, M.M., Childs, C., Walsh, J.J., Delogkos, E., 2021. Multiphase deformation history of the Porcupine Basin, offshore west Ireland. Basin Research, 33(3), 1776-1797.

Sauter, D., Tugend, J., Gillard, M., Nirrengarten, M., Autin, J., Manatschal, G., Cannat, M., Leroy, S., Schaming, M., 2018. Oceanic basement roughness alongside magma-poor rifted margins: insight into initial seafloor spreading. Geophysical Journal International, 212, 900-915.

Sawyer, D. S., Whitmarsh, R. B., Klaus, A., et al., 1994. Proceedings of the Ocean Drilling Program, Initial Reports 149, College Station, TX (Ocean Drilling Program).

Schiffer, C., Doré, A., Foulger, G., Franke, D., Geoffroy, L., Gernigon, L. et al., 2020. Structural inheritance in the North Atlantic. Earth-Science Reviews, 206, 102975.

Sclater, J.G., Christie, P.A., 1980. Continental stretching: An explanation of the post-Mid-Cretaceous subsidence of the central North Sea Basin. Journal of Geophysical Research: Solid Earth 85, 3711-3739.

Scrutton, R.A., 1979. Structure of the crust and upper mantle at Goban Spur, southwest of the British Isles—some implications for margin studies. Tectonophysics, 59(1-4), 201-215.

Seton, M., Müller, R.D., Zahirovic, S., Gaina, C., Torsvik, T., Shephard, G., Talsma, A., Gurnis, M., Turner, M., Maus, S. and Chandler, M., 2012. Global continental and ocean basin reconstructions since 200 Ma. Earth-Science Reviews, 113(3-4), 212-270.

Shannon, P.M., 1991. The development of Irish offshore sedimentary basins. Journal of the Geological Society, 1481, 181-189.

Shannon, P.M., 2018. Old challenges, new developments and new plays in Irish offshore exploration. Petroleum Geology Conference series, 8 (1), 171-185.

Shannon, P.M., Jacob, A.W.B., Makris, J., O'Reilly, B., Hauser, F. and Vogt, U., 1994. Basin evolution in the Rockall region, North Atlantic. First Break 12, 515-522.

Shannon, P.M., Jacob, A.W.B., O'Reilly, B.M., Hauser, F., Readman, P.W. and Makris, J., 1999. Structural setting, geological development and basin modelling in the Rockall Trough. In Geological Society, London, Petroleum Geology Conference series 5, 421-431.

Shannon, P.M., Moore, J.G., Jacob, A.W.B., Makris, J., 1993. Cretaceous and Tertiary basin development west of Ireland. Geological Society, London, Petroleum Geology Conference series, 4, 1057-1066.

Shannon, P.M., Williams, B. P. J., Sinclair, I. K., 1995. Tectonic controls on Upper Jurassic to Lower Cretaceous reservoir architecture in the Jeanne d'Arc Basin, with some comparisons from the Porcupine and Moray Firth Basins. Geological Society, London, Special Publications, 93(1), 467-490.

Sharp, I., Higgins, S., Scott, M., Freitag, U., Allsop, C., Kane, K., Sultan, A., Doubleday, P., et al., 2017. Rift to Drift Evolution and Hyperextension in the North Atlantic – Insights from a Super-Regional Approach. Abstract presented at Atlantic Ireland 2017 Conference, Dublin. https://www.pip.ie.

Shillington, D. J., Holbrook, W. S., Van Avendonk, H. J. A., Tucholke, B. E., Hopper, J. R., Larsen, H. C., Nunes, G. T., 2006. Evidence for asymmetric nonvolcanic rifting and slow incipient oceanic accretion from seismic reflection data on the Newfoundland margin. Journal of Geophysical Research, 111, B09403.

Sibuet, J. C., Collette, B.J. 1991. Triple junctions of Bay of Biscay and North Atlantic: New constraints on the kinematic evolution. Geology, 19, 522-525.

Sibuet, J.C., Mathis, B., Pastouret, L., Auzende, J.M., Foucher, J.P., Hunter, P.M., Guennoc, P., de Graciansky, P.C., Montadert, L., Masson, D.G., 1985. Morphology and basement structure of the Goban Spur continental margin (northeastern Atlantic) and the role of the Pyrenean orogeny. Initial Reports of the Deep Sea Drilling Project 80, 1153-1165.

Sibuet, J.C., Rouzo, S., Srivastava, S., 2012. Plate tectonic reconstructions and paleogeographic maps of the central and North Atlantic oceans. Canadian Journal of Earth Sciences 49, 1395-1415.

Sibuet, J.C., Srivastava, S., Enachescu, M.E., Karner, G., 2007. Early Cretaceous motion of Flemish Cap with respect to North America: implications on the formation of Orphan Basin and SE Flemish Cap-Galicia Bank conjugate margins, in: Karner, G., Manatschal, G. & Pinheiro, L. (Ed.), Imaging, Mapping and Modeling Continental Lithosphere Extension and Breakup. Geological Society, London, Special Publications, 282, 63-76.

Sibuet, J.C., Tucholke, B.E., 2012. The geodynamic province of transitional lithosphere adjacent to magma-poor continental margins. Geological Society, London, Special Publications 369, 429-452.

Simon, K., Huismans, R.S. and Beaumont, C., 2009. Dynamical modelling of lithospheric extension and small-scale convection: implications for magmatism during the formation of volcanic rifted margins. Geophysical Journal International 176, 327-350.

Sinclair, I.K., Shannon, P.M., Williams, B.P.J., Harker, S.D., Mooren, J.G., 1994. Tectonic control on sedimentary evolution of three North Atlantic borderland Mesozoic basins 1. Basin Research, 6, 193-217.

Srivastava, S., Verhoef, J., 1992. Evolution of Mesozoic sedimentary basins around the North Central Atlantic: a preliminary plate kinematic solution. Geological Society, London, Special Publications, 62 (1), 397-420.

Srivastava, S., Verhoef, J., Macnab, R., 1988. Results from a detailed aeromagnetic survey across the northeast Newfoundland margin, part ii: Early opening of the North Atlantic between the British Isles and Newfoundland. Marine and Petroleum Geology, 5, 324-337.

Stampfli, G.M., Borel, G.D., 2002. A plate tectonic model for the Paleozoic and Mesozoic constrained by dynamic plate boundaries and restored synthetic oceanic isochrons. Earth and Planetary Science Letters, 196, 17-33.

Stoker, M.S., Stewart, M.A., Shannon, P.M., Bjerager, M., Nielsen, T., Blischke, A., Hjelstuen, B.O., Gaina, C., McDermott, K. and Ólavsdóttir, J., 2017. An overview of the Upper Paleozoic–Mesozoic stratigraphy of the NE Atlantic region. Geological Society, London, Special Publications 447, 11-68.

Štolfová, K., Shannon, P.M., 2009. Permo-Triassic development from Ireland to Norway: basin architecture and regional controls. Geological Journal, 44 (6), 652-676.

Štolfová, K., Whittaker, R.C., & Shannon, P.M., 2012a. A regional stratigraphic and structural synthesis of Mesozoic/Cenozoic basins, offshore Ireland. Paper presented at Central Atlantic Conjugate Margins Conference, Dublin.

Štolfová, K., Whittaker, R.C., & Shannon, P.M., 2012b. New insights into regional Mesozoic and Cenozoic evolution of the Irish offshore continental margin. Paper presented at Central Atlantic Conjugate Margins Conference, Dublin.

Sutra, E., Manatschal, G., Mohn, G., Unternehr, P., 2013. Quantification and restoration of extensional deformation along the Western Iberia and Newfoundland rifted margins. Geochemisty, Geophysics, Geosystems, 14, 2575-2597.

Tate, M., 1993. Structural framework and tectono-stratigraphic evolution of the Porcupine Seabight Basin, offshore Western Ireland. Marine and Petroleum Geology, 10 (2), 95-123.

Tate, M.P., 1992. The Clare Lineament: a relic transform fault west of Ireland. Geological Society, London, Special Publications 62, 375-384.

Tate, M.P., Dobson, M.R., 1988. Syn-and post-rift igneous activity in the Porcupine Seabight Basin and adjacent continental margin W of Ireland. Geological Society, London, Special Publications 39, 309-334.

Tate, M.P., White, N., Conroy, J.J., 1993. Lithospheric extension and magmatism in the Porcupine Basin west of Ireland. Journal of Geophysical Research: Solid Earth, 98, 13905-13923.

Tetreault, J.L., Buiter, S.J.H., 2018. The influence of extension rate and crustal rheology on the evolution of passive margins from rifting to break-up. Tectonophysics 746,155-172.

Thinon, I., Matias, L., Réhault, J.P., Hirn, A., Fidalgo-González, L. and Avedik, F., 2003. Deep structure of the Armorican Basin (Bay of Biscay): a review of Norgasis seismic reflection and refraction data. Journal of the Geological Society, 160(1), 99-116.

Thomson, A., McWilliam, A., 2001. The structural style and evolution of the Bróna Basin. Geological Society, London, Special Publications 188, 401-410.

Thomson, K., Schofield, N., 2008. Lithological and structural controls on the emplacement and morphology of sills in sedimentary basins. Geological Society, London, Special Publications 302, 31-44.

Tomsett, B., Jones, N., Slater, L., Jones, G., 2017. Evolution and prospectivity potential of Jurassic pre- to syn-rift sequences of the western Porcupine Basin margin. Atlantic Ireland 2017 Conference. www.pip.ie.

Torsvik, T.H., Rehnström, E.F., 2003. The Tornquist Sea and Baltica–Avalonia docking. Tectonophysics, 362, 67-82.

Tucholke, B. E., Sibuet, J.C., Klaus, A., et al., 2004. Proceedings of the Ocean Drilling Program, Initial Reports 210, College Station, TX (Ocean Drilling Program).

Tucholke, B., Austin, J., Uchupi, E., 1989. Crustal structure and rift-drift evolution of the Newfoundland basin, in Extensional Tectonics and Stratigraphy of the North Atlantic Margins, Vol. 46, Chapter 16, pp. 247-263, eds Tankard, A. & Balkwill, H., AAPG Memoir.

Tugend, J., Gillard, M., Manatschal, G., Nirrengarten, M., Harkin, C., Epin, M.E., Sauter, D., Autin, J., Kusznir, N., Mcdermott, K., 2020. Reappraisal of the magma-rich versus magma-poor rifted margin archetypes. Geological Society, London, Special Publications, 476(1), 23-47.

Tugend, J., Manatschal, G., Kusznir, N. J., Masini, E., Mohn, G., Thinon, I., 2014. Formation and deformation of hyperextended rift systems: Insights from rift domain mapping in the Bay of Biscay- Pyrenees. Tectonics 33, 1239-1276.

Tugend, J., Manatschal, G., Kusznir, N., Masini, E., 2015. Characterizing and identifying structural domains at rifted continental margins: application to the Bay of Biscay margins and its Western Pyrenean fossil remnants. Geological Society, London, Special Publications, 413 (1), 171-203.

Tyrrell, S., Haughton, P.D.W., Daly, J., 2007. Drainage reorganization during breakup of Pangea revealed by in-situ Pb isotopic analysis of detrital K-feldspar. Geology, 35 (11), 971-974.

Tyrrell, S., Souders, A., Haughton, P., Daly, J., Shannon, P., 2010. Sedimentology, sandstone provenance and palaeodrainage on the eastern Rockall Basin margin: evidence from the Pb isotopic composition of detrital K-feldspar. Petroleum Geology Conference series, 7 (1), 937-952.

Van Avendonk, H.J., Holbrook, W.S., Nunes, G.T., Shillington, D.J., Tucholke, B.E., Louden, K.E., Larsen, H.C. and Hopper, J.R., 2006. Seismic velocity structure of the rifted margin of the eastern Grand Banks of Newfoundland, Canada. Journal of Geophysical Research: Solid Earth, 111(B11).

Van Avendonk, H.J., Davis, J.K., Harding, J.L., Lawver, L.A., 2017. Decrease in oceanic crustal thickness since the breakup of Pangaea. Nature Geoscience 10, 58.

von Raumer, J., Stampfli, G., Bussy, F., 2003. Gondwana-derived microcontinents — the constituents of the Variscan and Alpine collisional orogens. Tectonophysics, 365 (1-4), 7-22.

Waldron, J.W., Schofield, D.I., Murphy, J.B., 2019. Diachronous Paleozoic accretion of peri-Gondwanan terranes at the Laurentian margin. Geological Society, London, Special Publications, 470, 289-310.

Watremez, L., Prada, M., Minshull, T., O'Reilly, B., Chen, C., Reston, T. et al., 2018. Deep structure of the Porcupine Basin from wide-angle seismic data. Petroleum Geology Conference series, 8 (1), 199-209.

Welford, J.K., Dehler, S.A., Funck, T., 2020. Crustal velocity structure across the Orphan Basin and Orphan Knoll to the continent–ocean transition, offshore Newfoundland, Canada. Geophysical Journal International, 221 (1), 37-59.

Welford, J.K., Hall, J., Sibuet, J.C., Srivastava, S.P., 2010b. Structure across the northeastern margin of Flemish Cap, offshore Newfoundland from Erable multichannel seismic reflection profiles: evidence for a transtensional rifting environment. Geophysical Journal International 183, 572-586.

Welford, J.K., Peace, A.L., Geng, M., Dehler, S.A., & Dickie, K., 2018. Crustal structure of Baffin Bay from constrained three-dimensional gravity inversion and deformable plate tectonic models. Geophysical Journal International, 214 (2), 1281-1300.

Welford, J.K., Shannon, P.M., O'Reilly, B.M., Hall, J., 2012. Comparison of lithosphere structure across the Orphan Basin–Flemish Cap and Irish Atlantic conjugate continental margins from constrained 3D gravity inversions. Journal of the Geological Society, 169 (4), 405-420.

Welford, J.K., Shannon, P.M., O'Relly, B.M., Hall, J., 2010c. Lithospheric density variations and Moho structure of the Irish Atlantic continental margin from constrained 3-D gravity inversion. Geophysical Journal International 183, 79-95.

Welford, J.K., Smith, J.A., Hall, J., Deemer, S., Srivastava, S.P., Sibuet, J.C., 2010a. Structure and rifting evolution of the northern Newfoundland Basin from Erable multichannel seismic reflection profiles across the southeastern margin of Flemish Cap. Geophysical Journal International 180, 976-998.

Wernicke, B., 1985, Uniform-sense normal simple shear of the continental lithosphere, Canada Journal of Earth Science, 22, 108-125.

White R., Mckenzie, D., 1989, Magmatism at rift zones: the generation of volcanic continental margins and flood basalts, Journal of Geophysical Research, 94, 7685-7729.

White, N., Tate, M., Conroy, J.J., 1992. Lithospheric stretching in the Porcupine Basin, west of Ireland. Geological Society, London, Special Publications, 62 (1), 327-331.

White, R.S., Minshull, T.A., Bickle, M.J., Robinson, C.J., 2001. Melt generation at very slow-spreading oceanic ridges: Constraints from geochemical and geophysical data. Journal of Petrology 42, 1171-1196.

White, R.S., Spence, G.D., Fowler, S.R., McKenzie, D.P., Westbrook, G.K. and Bowen, A.N., 1987. Magmatism at rifted continental margins. Nature, 330(6147), 439-444.

Whiting, L., Haughton, P., Shannon P.M, 2016. The evolution of hyperextended basins: Lower Cretaceous tectono-stratigraphy of the Porcupine Basin. Paper presented at Atlantic Ireland 2016 Conference, Dublin. www.pip.ie.

Whiting, L., Haughton, P.D., Shannon, P.M., 2021. From rifting to hyperextension: Upper Jurassic–Lower Cretaceous tectono-stratigraphy of the Porcupine Basin, Irish Atlantic Margin. Basin Research, 33(2), 1662-1696.

Whitmarsh, R. B., Beslier, M.O., Wallace, P. J., et al., 1998. Proceedings of the Ocean Drilling Program, Initial Reports 173, College Station, TX (Ocean Drilling Program).

Whitmarsh, R.B., Langford, J.J., Buckley, J.S., Bailey, R.J., Blundell, D.J., 1974. The crustal structure beneath Porcupine Ridge as determined by explosion seismology. Earth and Planetary Science Letters, 22, 197-204.

Whitmarsh, R.B., Manatschal, G., Minshull, T.A., 2001. Evolution of magma-poor continental margins from rifting to seafloor spreading. Nature, 413, 150-154.

Whittaker, R.C., Štolfová, K., Shannon, P.M., 2012. A regional stratigraphic and structural interpretation of the Newfoundland and Ireland conjugate margins. Paper presented at Central Atlantic Conjugate Margins Conference, Dublin.

Wilson, J.T., 1966. Did the Atlantic close and then re-open? Nature, 211, 676-681.

Yang, P., Welford, J.K. and King, M.T., 2021. Assessing the rotation and segmentation of the Porcupine Bank, Irish Atlantic margin, during oblique rifting using deformable plate reconstruction (No. EGU21-3043). Copernicus Meetings.

Yang, P., Welford, J.K., 2021. Investigating the Porcupine Atlantic margin, offshore Ireland, through integration of new seismic reflection and gravity data. Tectonophysics, 807, 228809.

Yang, P., Welford, J.K., Peace, A.L., Hobbs, R., 2020. Investigating the Goban Spur rifted continental margin, offshore Ireland, through integration of new seismic reflection and potential field data. Tectonophysics, 777, 228364.

Zalán, P.V., 2015, Similarities and Differences between Magma-Poor and Volcanic Passive Margins- Applications to the Brazilian Marginal Basins, International Congress of the Brazilian Geophysical Society, 1-6.

Zhu, Y., Liu, S., Zhang, B., Gurnis, M., Ma, P., 2021. Reconstruction of the Cenozoic deformation of the Bohai Bay Basin, North China. Basin Research, 33(1), 364-381.

Zwaan, F., Schreurs, G., Naliboff, J., Buiter, S., 2016, Insights into the effects of oblique extension on continental rift interaction from 3D analogue and numerical models, Tectonophysics, 693, 239-260.

Appendices

A Seismic reflection lines used in Chapter 2

In Chapter 2, seismic data reprocessing is carried out to obtain a higher-quality image. The data processing workflow involves geometry definition, amplitude compensation, bandpass filtering, predictive deconvolution, noise attenuation, velocity analysis, pre-stack time migration, and coherency filtering. The reprocessed seismic sections (Lines L2, L3, L4, X1, and X2) are compared with those originally processed by the company Geotrace for Eni Ireland, shown in Figures A.1-A.6. The reprocessed profiles show no significant improvement from those provided by Eni Ireland for the Department of Communications, Climate Action & Environment of Ireland. This is the reason why the seismic lines provided by Ireland are directly used for interpretation in Chapters 3 and 5.

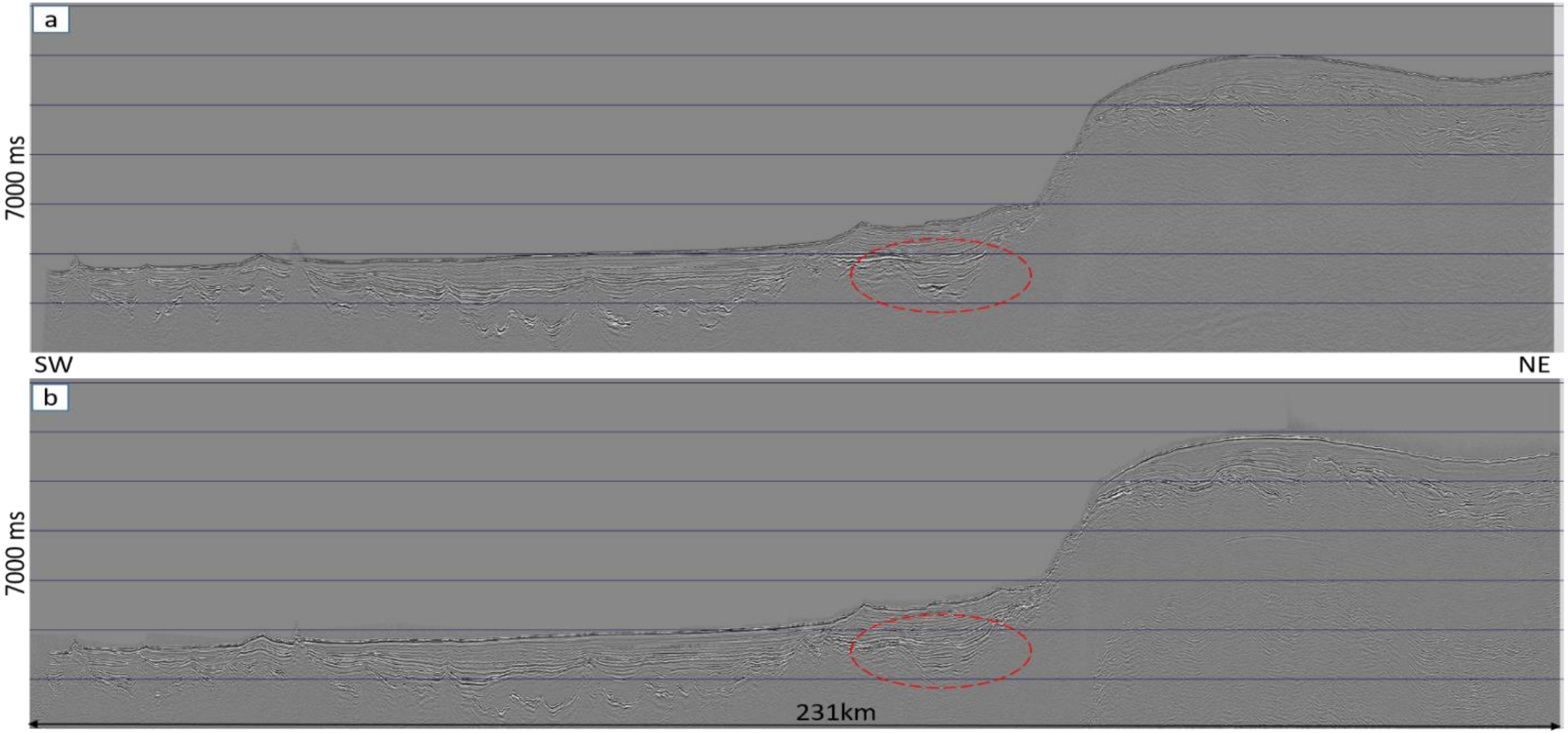

Figure A.1: (a) Seismic profile L2 processed by Geotrace. (b) Reprocessed profile L2. In the lower panel, the seismic image in the red circle shows a higher resolution character.

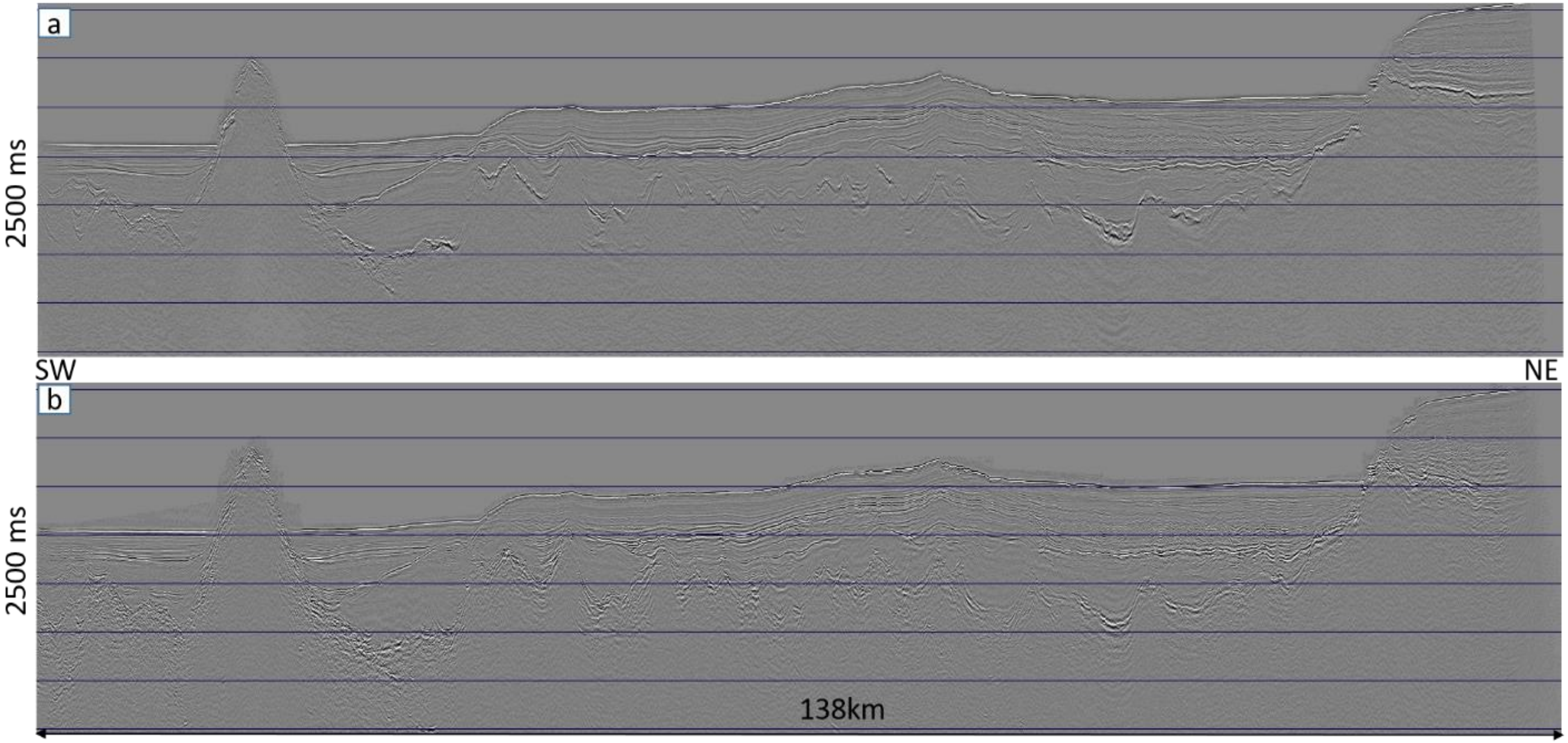

Figure A.2: (a) Seismic profile L3 processed by Geotrace. (b) Reprocessed seismic profile L3.

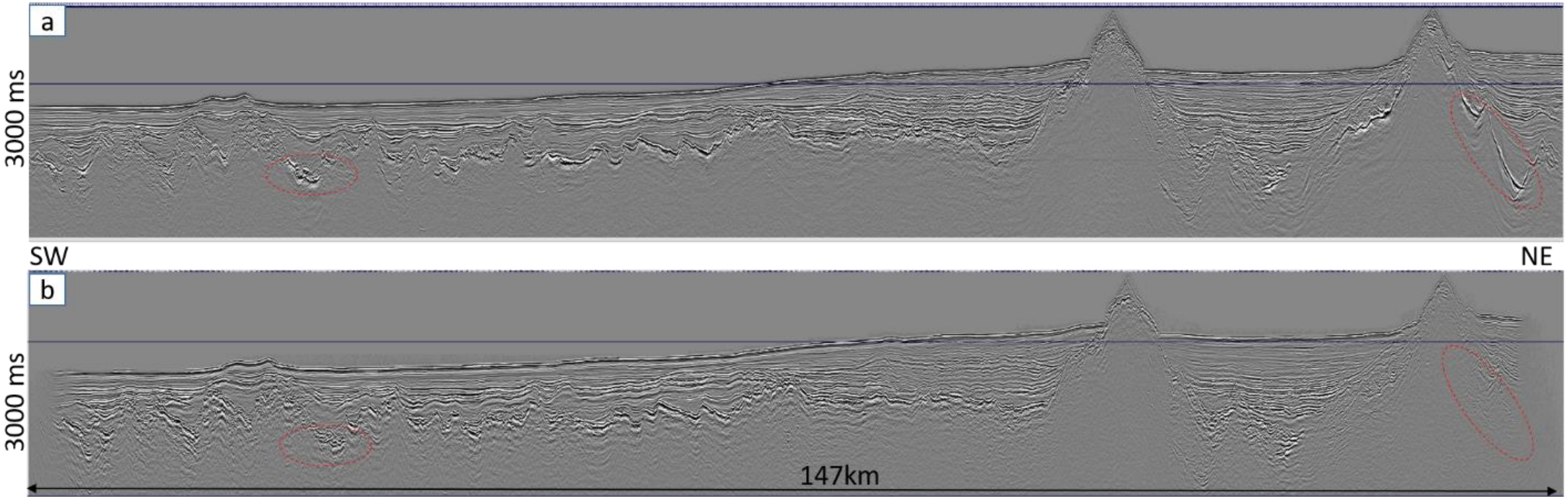

Figure A.3: (a) Seismic profile L4 processed by Geotrace. (b) Reprocessed seismic profile L4. In the lower panel, the seismic image in the red circle on the left shows a higher resolution character, while the weaker reflectivity in the red circle on the right may be due to the low data fold on the edge.

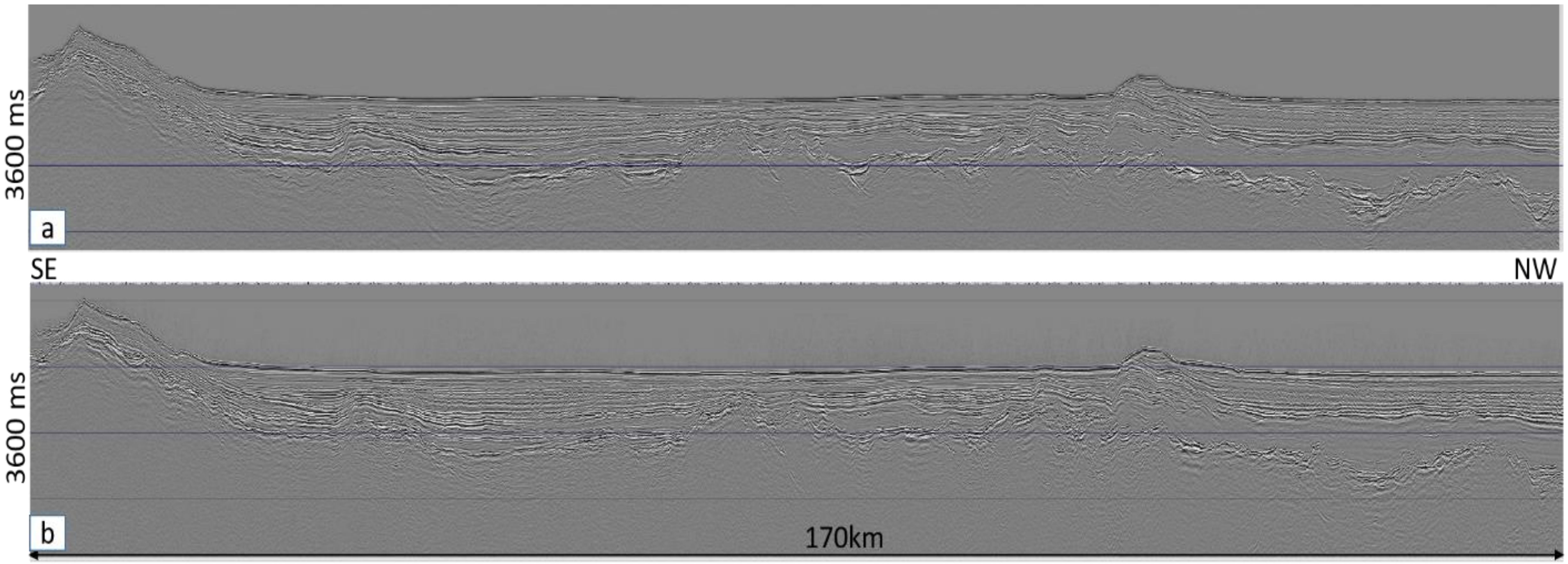

Figure A.4: (a) A segment of seismic profile X1 processed by Geotrace. (b) The reprocessed segment of seismic profile X1.

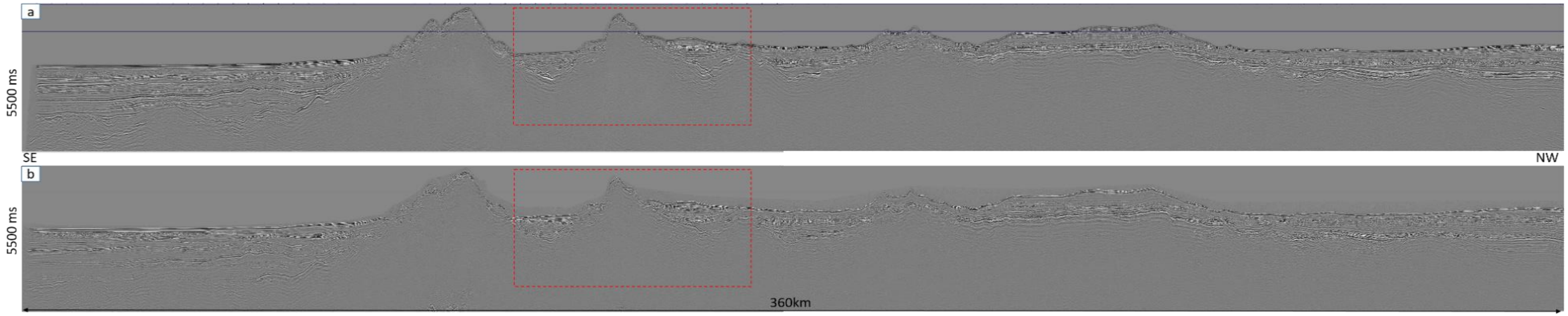

Figure A.5: (a) Seismic profile X2 processed by Geotrace. (b) Reprocessed seismic profile X2.

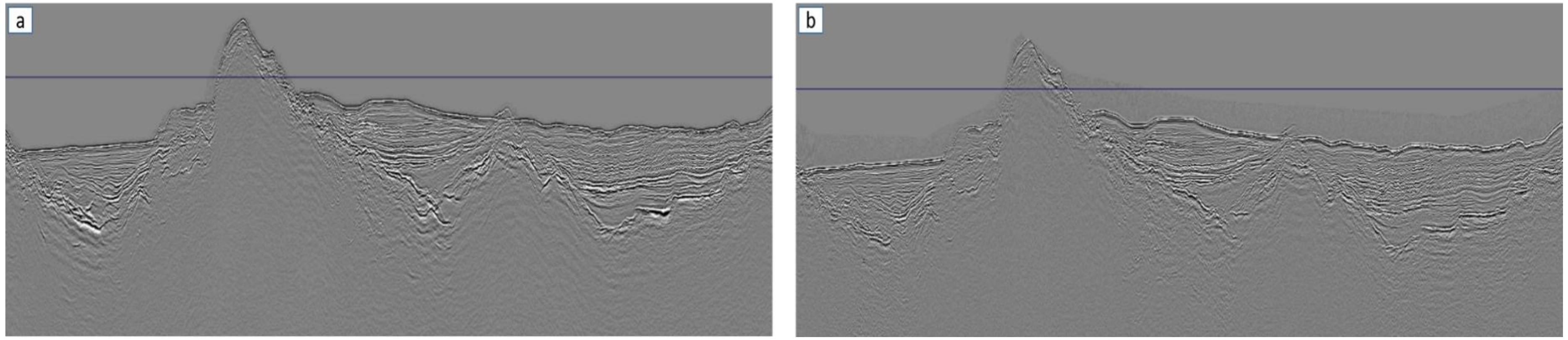

Figure A 6: (a) Expansion of a portion of seismic profile X2 processed by Geotrace, indicated by red box in Figure A.5(a). (b) Expansion of a portion of reprocessed seismic profile X2, denoted by red box in Figure A.5 (b)

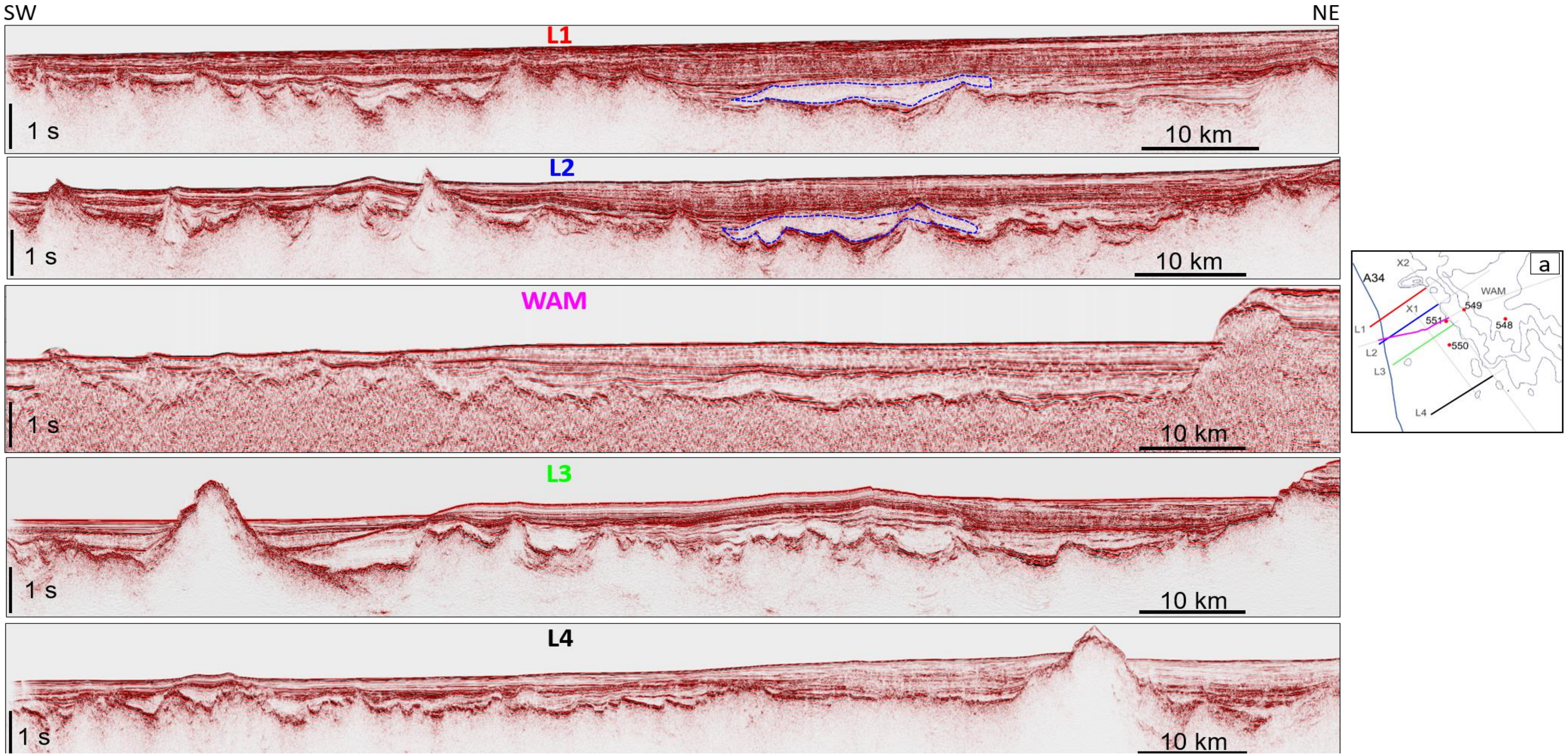

Figure A.7: The portions of uninterpreted seismic profiles L1-L4 in the time domain

B Seismic reflection lines interpreted in Chapter 3

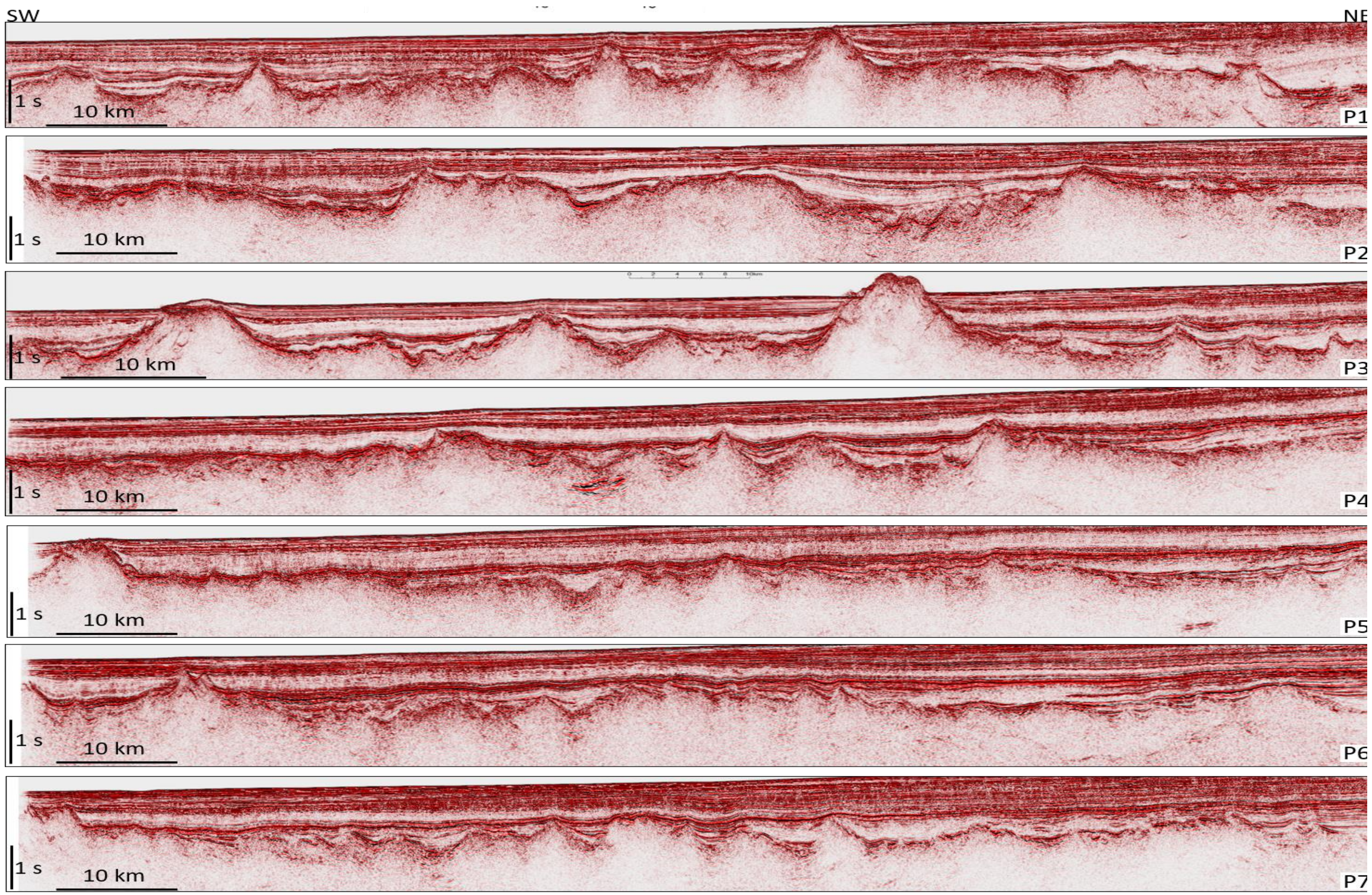

Figure B.1: The portions of uninterpreted seismic profiles P1-P7 in the time domain, corresponding to seismic lines in Fig. 3.5.

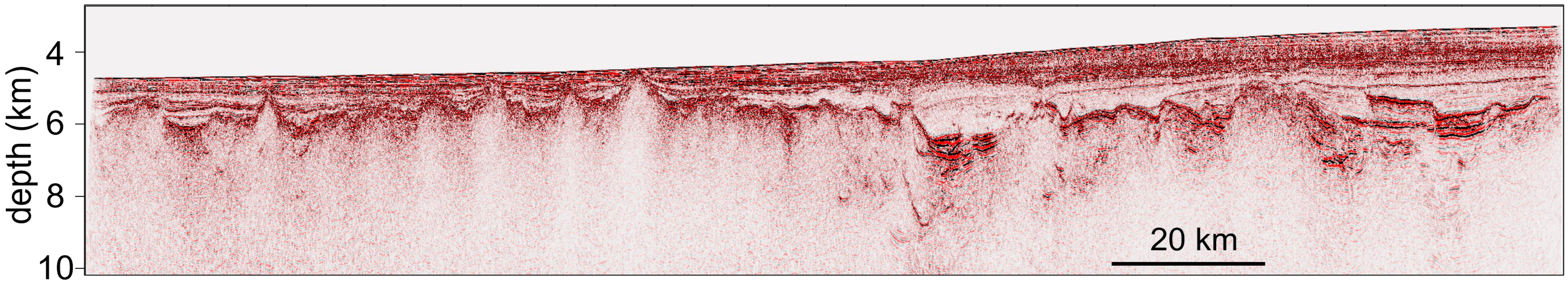

Figure B.2: The uninterpreted seismic profile P1 in the depth domain.

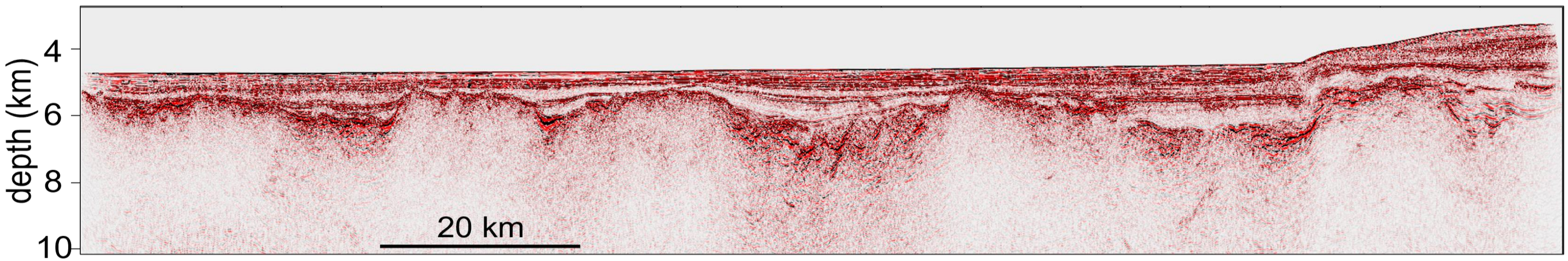

Figure B.3: The uninterpreted seismic profile P2 in the depth domain.

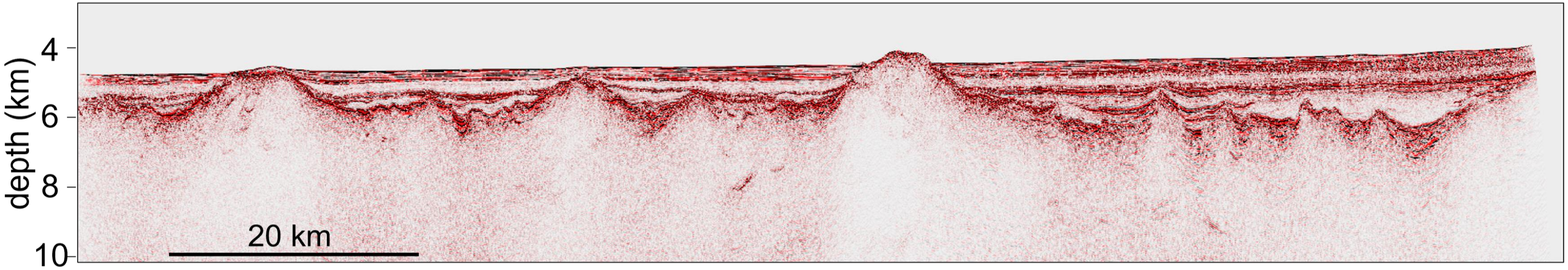

Figure B.4: The uninterpreted seismic profile P3 in the depth domain.

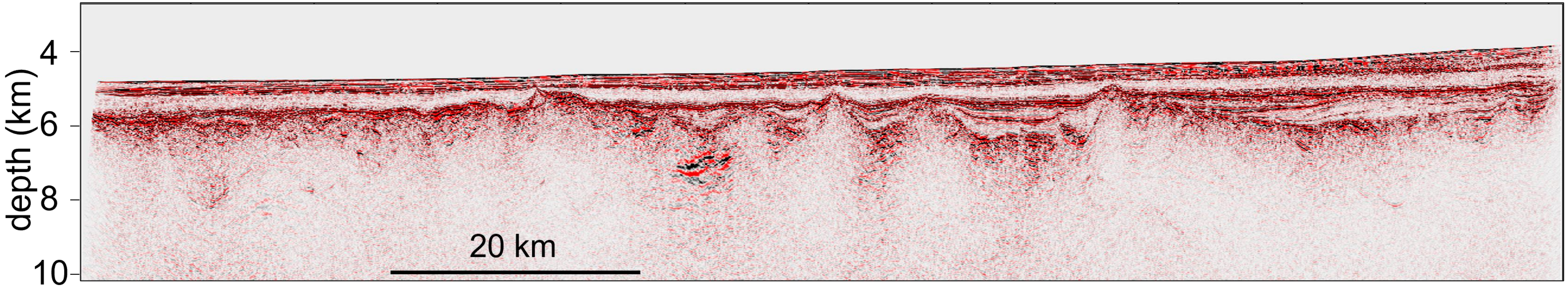

Figure B.5: The uninterpreted seismic profile P4 in the depth domain.

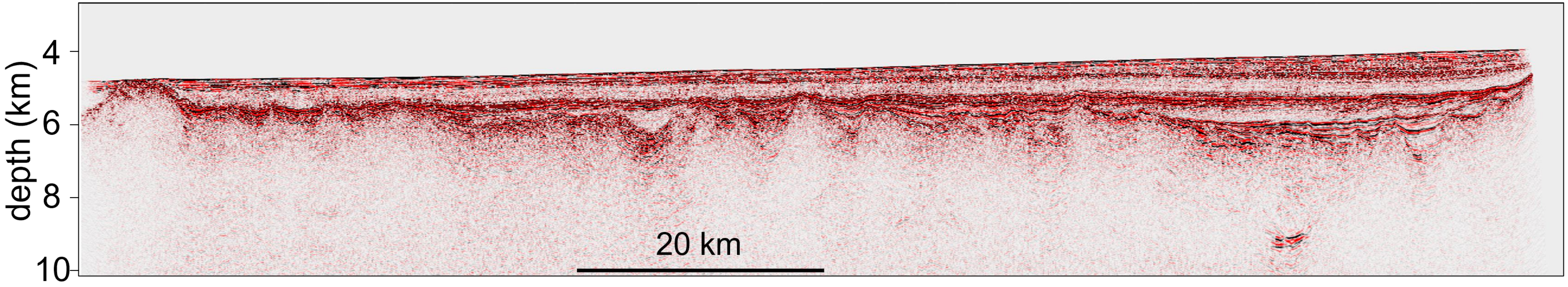

Figure B.6: The uninterpreted seismic profile P5 in the depth domain.

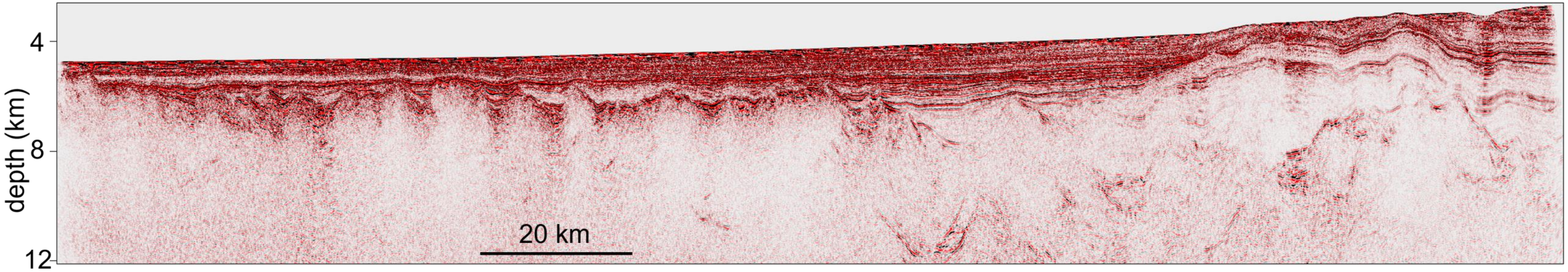

Figure B.7: The uninterpreted seismic profile P7 in the depth domain.

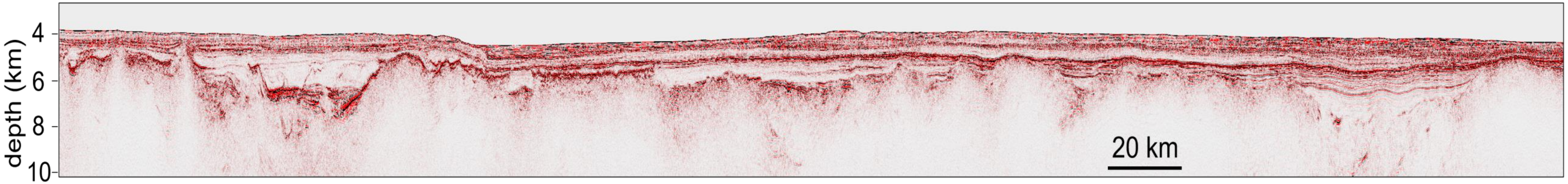

Figure B.8: The uninterpreted seismic profile X2-1 in the depth domain.

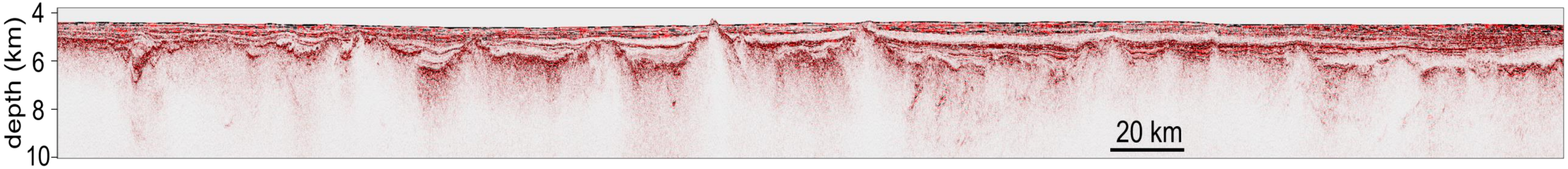

Figure B.9: The uninterpreted seismic profile X1-1 in the depth domain.

C Seismic reflection lines interpreted in Chapter 5

The corresponding uninterpreted seismic lines X6-X3 shown in Figure 5.2.

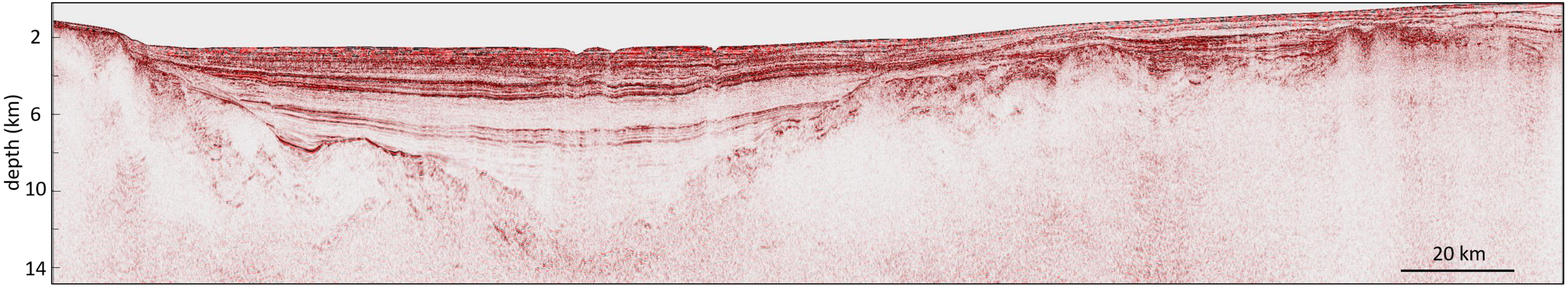

Figure C.1: The uninterpreted seismic profile X6 in the depth domain.

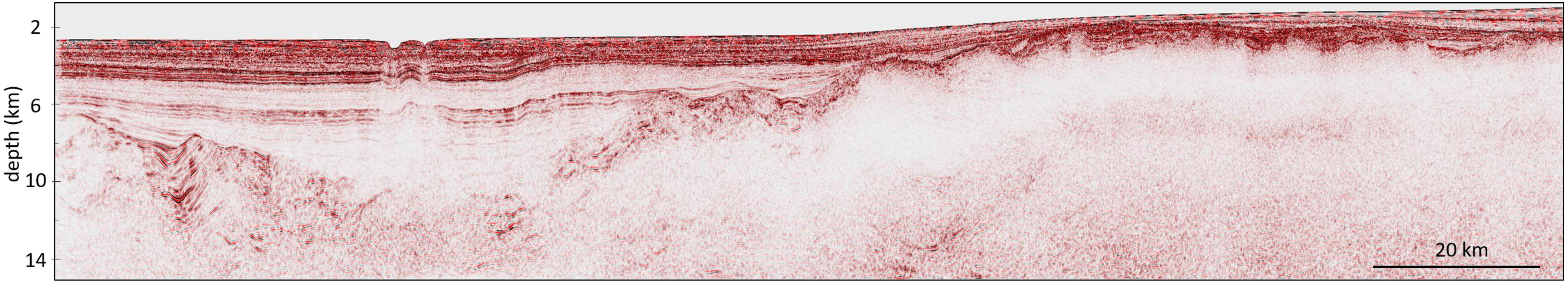

Figure C.2: The uninterpreted seismic profile X5 in the depth domain.

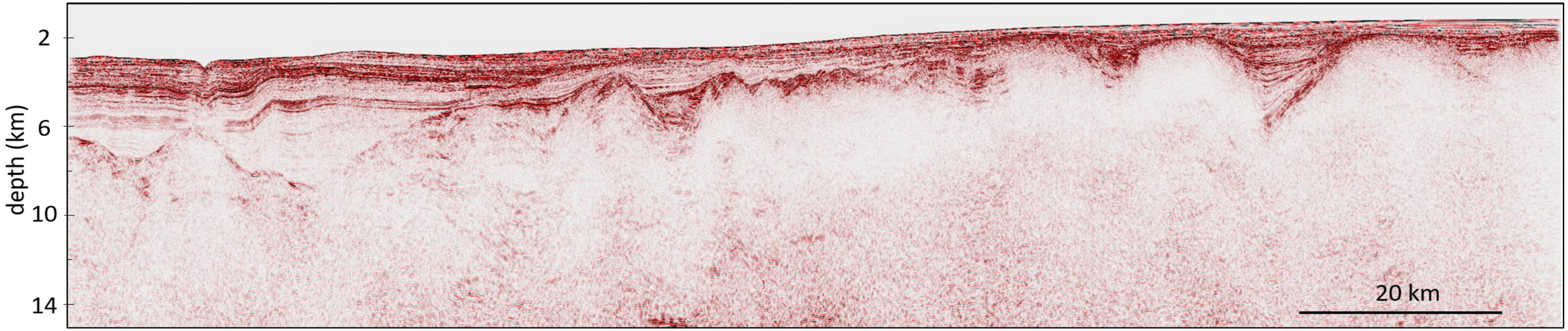

Figure C.3: The uninterpreted seismic profile X4 in the depth domain.

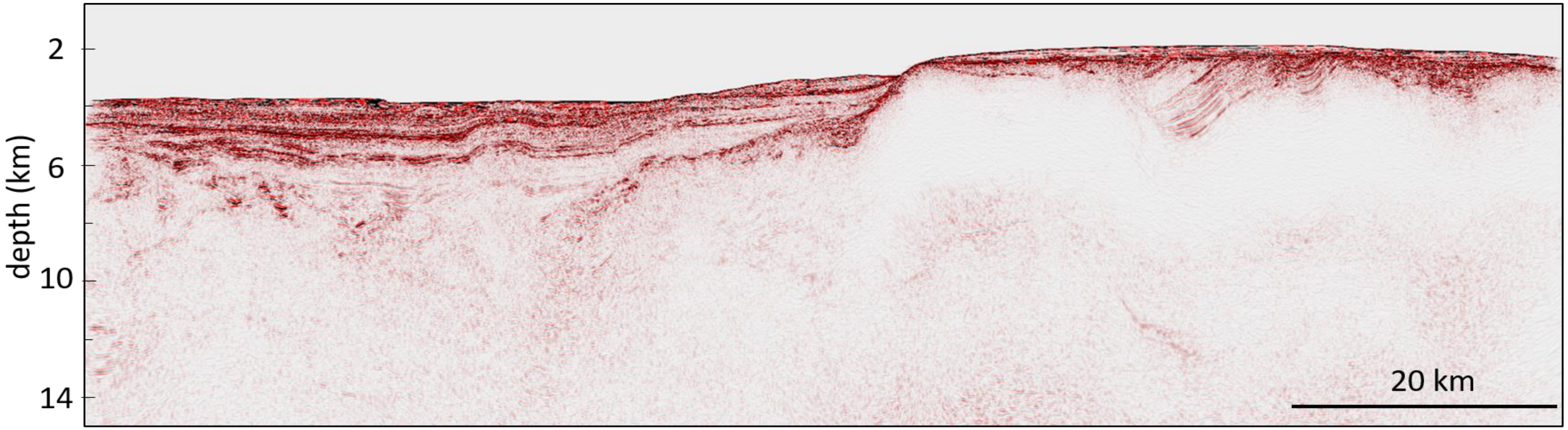

Figure C.4: The uninterpreted seismic profile X3 in the depth domain.